UNIVERSITÀ
DEGLI STUDI
FIRENZE

DOTTORATO DI RICERCA IN SCIENZE DELLA TERRA

CICLO XXIX

COORDINATORE Prof. LORENZO ROOK

Combining remote sensing techniques with numerical modeling for the runout analysis of shallow rapid landslides

Settore Scientifico Disciplinare GEO/05

Dottorando

Dott. Salvatici Teresa

Tutore

Prof. Nicola Casagli

Coordinatore

Prof. Lorenzo Rook

Anni 2013/2016

Table of contents

ABSTRACT **2**

RIASSUNTO **4**

1. INTRODUCTION **6**

2. LANDSLIDE CLASSIFICATION **11**

2.1 CLASSIFICATION OF SHALLOW RAPID LANDSLIDE 15

2.2 RHEOLOGICAL CLASSIFICATION OF SHALLOW RAPID LANDSLIDE 18

3. MODELS FOR LANDSLIDE RUNOUT PREDICTION **22**

3.1 EMPIRICAL METHODS 22

3.2 DYNAMIC METHODS 24

3.3 NUMERICAL MODELLING DAN-W AND DAN-3D 28

3.3.1 Equivalent fluid theory *28*

3.3.2 DAN-W *29*

3.3.3 DAN-W program framework *31*

3.3.4 DAN-3D *32*

3.3.5 Material entrainment *35*

3.3.6 Basal rheologies *37*

3.3.7 DAN-3D program framework *41*

4. REMOTE SENSING MONITORING TECHNIQUES **42**

4.1 GROUND BASED INTERFEROMETRIC SAR (GB-INSAR) 42

4.1.1 Radar Data *43*

4.1.2 The system GB-InSAR LISA *44*

4.1.3 SAR images *46*

4.2 LASER SCANNING TECHNIQUE 47

4.2.1 Airborne Laser Scanning (ALS) *49*

4.2.2 Terrestrial Laser Scanner (TLS) *50*

4.2.3 Laser scanning data *52*

5. COMBINING NUMERICAL MODELLING WITH REMOTE SENSING TECHNIQUES **54**

5.1 BACK ANALYSIS PROCEDURE 55

5.1.1 Pre-event and post-event topography *56*

5.1.2 Volume *57*

5.1.3 Velocity ... 58
5.1.4 Deposits thickness ... 60
5.1.5 Runout distance and impact area ... 60
5.2 FORECAST ANALYSIS PROCEDURE ... 61
5.2.1 Possible new source areas ... 61
5.2.2 Possible new source thickness and volume ... 62
5.2.3 Runout prediction ... 64
6. CASE STUDIES ... 67
6.1 STROMBOLI GRAVITY-INDUCED PYROCLASTIC DENSITY CURRENTS (GIPDCS) ... 67
6.1.1 Events descriptions ... 69
6.1.2 Model calibration ... 70
6.1.3 Back analysis results ... 73
6.1.4 Forecaster analysis ... 76
6.1.5 Mobility of basaltic gravity-induced PDCs ... 78
6.1.6 Implication for hazards ... 80
6.1.7 Discussions ... 83
6.1.8 Conclusion ... 85
6.2 MONTE ROTOLON DEBRIS FLOW ... 86
6.2.1 Rotolon landslide description ... 87
6.2.2 Geological setting ... 88
6.2.3 GB-InSAR system ... 89
6.2.4 Rotolon debris flow back analysis ... 92
6.2.5 Velocity analysis ... 97
6.2.6 Rotolon debris flow forecast analysis ... 99
6.2.7 Conclusion ... 102
6.2.8 Gessi – Mazzalasino (Scandiano) landslide ... 103
6.2.9 Geological setting ... 104
6.2.10 Geotechnical characterization ... 106
6.2.11 Velocity analysis ... 110
6.2.12 Laser scanning survey ... 111
6.2.13 Gessi-Mazzalasino landslide back analysis ... 113
6.2.14 Empirical prediction methods ... 115
6.2.15 Forecast analysis ... 116
6.2.16 Conclusion ... 117
6.3 SANTA TRADA LANDSLIDE ... 119

6.3.1 Geological setting 121

6.3.2 Santa Trada GB-InSAR 122

6.3.3 Santa Trada landslide back analysis 126

6.3.4 Model forecast 128

6.3.5 Conclusion 133

7. DISCUSSION OF RESULTS 134

8. REFERENCE 140

9. PUBLICATIONS 159

Abstract

The aim of this research project is to improve the ability to forecast the propagation of shallow and rapid landslides through the combination of remote sensing and advanced methods of numerical modelling techniques.

The activities carried out during the PhD have been done in order to achieve three objectives:

- to define the procedures and methods of numerical analysis of the propagation of shallow rapid landslides, through the use of existing codes that allow to model the post-failure behaviour dynamic;
- to use remote sensing data derived from LiDAR images (aerial or terrestrial) or radar monitoring data (in particular GB-InSAR), to obtain information about the geometric and geomorphological features of the landslides and to find new future sources areas that can be used with numerical models in order to obtain new risk scenarios;
- to use abovementioned the new procedure on case studies of high-risk landslide.

Two numerical modelling DAN-W and DAN-3D (Hungr, 1995 McDougall, 2006) are used, based on Lagrangian numerical method to solve the equations of St. Venant. Consider the mass as an "equivalent fluid", governed by an internal frictional rheology and basal rheology that must be chosen with back analysis by trial-and-error procedure. These parameters are then used to forecast analysis using new source areas with new volumes obtained by LiDAR and GB-InSAR monitoring data analysis. The latter, in particular, are processed through a numerical code developed in the MATLAB language. The MATLAB code uses the cumulative displacement maps relative to a selected time interval, to calculate possible sources areas according to a threshold and finally analysed the frequency of movement occurrence.

This procedure has been applied at four case studies: gravity induced-Pyroclastic Density Currents (gi-PDC) that take place on the side of Stromboli volcanic island; Mount Rotolon debris flow; Gessi-Mazzalasino debris slide and Santa Trada rock/debris slide.

Riassunto

L'obiettivo della ricerca è il miglioramento delle capacità di previsione dell'innesco e della propagazione di frane superficiali a cinematica rapida, per la definizione operativa e preventiva di scenari di rischio e di misure di salvaguardia e prevenzione.

Le attività svolte durante il dottorato di ricerca sono state finalizzate, in particolare, a realizzare i seguenti tre obiettivi specifici:

- definire le procedure e i metodi di analisi numerica della propagazione di frane superficiali a cinematica rapida, attraverso l'impiego di codici numerici che consentono di modellare il comportamento post-rottura dei pendii in terra;
- utilizzare i dati di telerilevamento derivanti da rilievi LiDAR (di tipo aereo o terrestre) o da monitoraggio radar (in particolare GB-InSAR), per ottenere informazioni quantitative sulle caratteristiche geometriche e geomorfologiche delle aree in frana nonché per individuare possibili aree sorgenti di eventi futuri da integrare nei modelli numerici;
- sperimentare le procedure sopra definite sul campo in casi applicativi di frane ad alto rischio riguardanti centri abitati e infrastrutture.

Per raggiungere tali obiettivi sono stati utilizzati due codici numerici di modellazione: DAN-W e DAN-3D (Hungr, 1995, McDougall, 2006), basati sull'analisi lagrangiana per risolvere le equazioni di St. Venant. I modelli considerano la massa come un "fluido equivalente", governato da una reologia interna attritiva e da una reologia basale che scelta tramite *back analysis* seguendo una procedura di *trial-and-error* per ottenere i parametri reologici più adeguati al caso in esame. Tali parametri sono poi utilizzati per la *forecast analysis* utilizzando nuove aree sorgenti con nuovi volumi ottenuti tramite l'analisi di dati LiDAR e di monitoraggio GB-InSAR. Questi ultimi sono elaborati attraverso un codice numerico originale, sviluppato in linguaggio MATLAB, che utilizza le mappe di spostamento cumulato relative ad un intervallo di tempo scelto, per calcolare possibili aree sorgenti in base ad una soglia di spostamento significativo e ne analizza in seguito la frequenza di accadimento.

I casi di studio scelti sono stati: i flussi piroclastici indotti dalla gravità (gi-PDC) che avvengono sull'isola vulcanica di Stromboli, il *debris flow* del Monte Rotolon, il *debris slide* di Gessi-Mazzalasino (Scandiano) e la r*ock/debris slide* di Santa Trada.

1. Introduction

In the last few years the continuum dynamic modelling of landslide motion has developed as critical component of hazard assessment to estimate the impact area, landslide velocity, flow depth and depth of deposits (Hungr 1997). Whit the aim to improve the knowledge about landslide runout prediction, in this thesis an integrated procedure of numerical modelling and remote sensing techniques has been developed.

In particular, shallow rapid landslides as debris flows, debris avalanches, rock avalanches and some types of planar slides are discussed. These landslides are extremely rapid and can cause significant destruction, often far from their point of origin posing a risk to human lives and infrastructures. The main causes and predisposing factors of slope instability are gravity, soil or rock geo-mechanical properties; slope gradient, aspect and land cover characteristics (Cruden and Varnes, 1996). These mass movements are triggered by different natural phenomena as intense or prolonged rainfall, snowmelt, earthquakes, volcanic eruptions etc..

Prediction of possible impact areas, flow velocities and thickness, is essential for efficient actions towards risk reduction and hazard assessment (McDougall and Hungr, 2004). Various definitions of risk have been proposed in the literature: Varnes and the IAEG Commission on Landslides and other Mass-Movements (1984) proposed the definition of risk adopted by UNDRO (Office of the United Nations Disaster Relief Coordinator) for all natural hazards, which refers to the combined vulnerability of the community to potential damage caused by a particular hazard within a specified future time period; it can be expressed as follows:

[1] $$R_s = H_L \times W_L \times E$$

Where:

- R_s *(Risk*) is the expected degree of loss due to a particular landslide phenomenon;
- H_L (*Hazard*) is the probability of occurrence within a specified period of time and within a given area of a potentially damaging phenomenon;the definition incorporates the concepts of location, time and size (Guzzetti et al., 2005) as follow:

[2] $H_L = P_{AL} \times P_N \times S$

where P_{AL} is the probability of occurrence of a landslide with a specific size; P_N is the probability of a landslide occurrence in an established period *t*; S is the spatial probability of a landslide occurrence *S*.

- W_L (*vulnerability*) is the potential degree of loss (damage) to a given element or set of elements at risk resulting from the occurrence of a landslide of a given magnitude (Varnes, 1984);
- *E* (*elements at risk*) includes the population, properties, economic activities, including public services exposure (Fell, 1994).

Italy is one of the countries in the world which is most affected by hydrogeological hazards: the estimated landslide losses range from 1 to 2 billion of dollars annually, corresponding to about 0.15% of the national domestic product (Canuti et al., 2004). The IFFI project (*Inventario dei Fenomeni Franosi in Italy*), carried out by ISPRA, has recorded 614.799 landslides that cover an area of about 23000 km^2. In the 58-year period, between 1950 and 2008, 2204 landslide events have caused 4077 deaths, 26 missing persons and at least 2019 injured people and 177.376 evacuees and homeless people (Salvati et al., 2010).

Landslide mapping, hazard assessment and risk evaluation are important goals for scientists, planners, decision makers and land developers (Guzzetti, 2003).

In this thesis is proposed an innovative approach for hazard assessment of shallow rapid landslides through a combination of numerical modelling and active remote sensing techniques for the runout analysis.

To predict the landslide motion and its effects, the runout analysis methods have been developed. The main quantitative methods can be classified as either empirical or analytical. Empirical methods operate on observational data correlations to calculate the extent of the runout zone. Analytical methods try to predict the motion of the landslide mass from initiation to deposition, providing estimates of hazard extent and intensity. The latter models perform the time-wise numerical solution of the equations of motion and advance the location of the simulated landslide incrementally, computing the spatial distribution of landslide hazard intensity parameters, such as flow velocity and depth (Hungr, 1997). A large number of dynamic models exist; within this thesis two continuum models, developed at the University of British Columbia (UBC), Vancouver, Canada, have been used: DAN-W (Hungr, 1995) and DAN-3D (McDougall and Hungr, 2004). The models describe the motion along a path (2D or 3D,

respectively) starting from several features of shallow rapid landslides, such as the effect of internal strength, material entrainment and variation in rheology. The models are based on Lagrangian numerical solution of depth-average equations of the motion, considering an "equivalent fluid" theory (Hungr, 1995), which allows to simulate the landslide mass as a hypothetical material governed by simple rheological relationships, a fixed internal frictional and a basal that must be calibrated through back analysis and trial and error procedure.

The developments of remote sensing technologies give the possibility of acquiring data over wide areas with high accuracy, high spatial resolution, good data visualization, management and reproducibility, allowing new ways of investigating the landslide phenomena. The two major remote sensing techniques that are exponentially developing for landslides characterization and monitoring are interferometric synthetic aperture radar (InSAR) (Fruneau et al., 1996; Colesanti et al., 2003; Squarzoni et al., 2003), in particular Ground Based Radar Interferometry (GB-InSAR), and light detection and ranging (LiDAR) (Carter et al., 2001; Slob et al., 2002; Haugerud et al., 2003; Slob and Hack, 2004).

The GB-InSAR is a method widely used in landslide monitoring applications, for its capability to detect with high spatial and temporal accuracy structures and ground displacements (Antonello et al., 2004; 2008; Atzeni et al., 2001a; 2004; Casagli et al., 2002, 2009, 2010; Del Ventisette et al., 2011a, 2011b; Gigli et al., 2011; Luzi et al., 2004; Pieraccini et al., 2002; Tarchi et al., 1998, 2002, 2003). GB-InSAR represents a versatile and flexible technology, allowing the production of near-real time displacement maps of areas overall several square kilometres. It is able to observe the scenario twenty-four hours per day in all wheatear conditions.

The LiDAR technique (Slob et al., 2002; Slob and Hack, 2004; Lombardi et al., 2006; Rahman et al., 2006; Turner et al., 2006; Slob and Hack, 2007; Oppikofer et al., 2008; Jaboyedoff et al. 2009-2012; Fanti et al., 2011; Fanti et al., 2012; Gigli et al., 2009; Gigli et al., 2012; Gigli et al.,2013) can provide in a short time a high detailed and accurate 3D geometrical representation of the investigated slope, it is mainly used for landslide investigation to create accurate and precise high resolution digital elevation models (HRDEM), or point clouds with a high density of information.

This thesis represents the main outcome of three years-long activity at the Earth Sciences Department of the University of Firenze (Centre of Competence of the Italian Civil Protection for geo-hazards). The main objective of this PhD program was to test the potential and applicability of LiDAR and GB-InSAR techniques as novel support tools for landslide runout numerical

modelling. In particular, an integrated approach between numerical models with remote sensing techniques, such as LiDAR and GB-InSAR, was employed in order to detect criticalities in unstable slopes and evaluate, with DAN-W and DAN-3D, the possible hazardous scenarios in emergency management. This approach could represent a valid support for local authorities in the framework of the post-disaster initiatives, led by the Italian National Department of Civil Protection (DPC). Within this work, a research period was carried out in Vancouver (Canada) at the University of British Columbia (UBC) (Department of Earth, Ocean & Atmospheric Sciences), to improve the knowledge of numerical modelling DAN-W and DAN-3D.

Besides the Introduction (Chapter 1)**,** this thesis includes a total of seven chapters, structured as follows (Fig. 1):

Chapter 2 *s*ummarizes the fundamentals of landslides classification with special regards to shallow rapid landslides;

Chapter 3 is a review of the current status of models for landslide runout predictions, focusing on continuum numerical models DAN-W and DAN-3D;

Chapter 4 describes general applications and the methodology applied in this study for landslide characterization and monitoring, including a brief description of Ground based interferometry and LiDAR techniques;

Chapter 5 mainly deals with discussions regarding the potential, applicability, limitations of the combination procedures between remote sensing techniques and numerical models DAN-W and DAN-3D, in particular it regards the methods to calculate the simulated back analysis parameters and the innovative procedure to forecast new possible event scenarios;

Chapter 6 presents the analyses and results of the procedure applied at different types of shallow rapid landslides case studies;

Chapter 7 presents the discussion of results drawn out of the study.

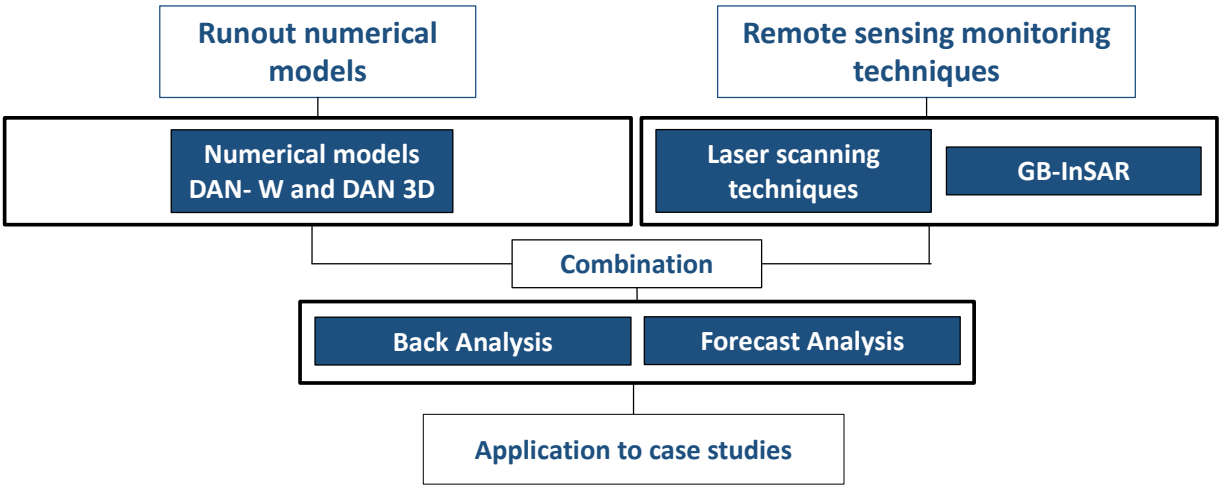

Fig. 1. Work flow.

2. Landslide classification

A landslide is a rapid downward movement of a mass, which mobility is the result of the gravity force (Cruden and Varnes, 1993). The involved materials are rocks, sediments, earths and a mixture of these ones. The geomorphological evidence consists of a steep area, which represent the upper limit of detachment, with an accumulation deposit area below. A landslide, of which kinematic can be very complex, is a physical system that develops in the time through several stage (Terzaghi, 1950).

Many authors have classified these phenomena, according both to morphological and mechanical criteria. The first classification, ascribable to Skempton (1953), divides the landslides according to the ratio *D/L*, where *D* is the maximum deposits thickness and L the length in the maximum slope direction. The most widely used system is the Varnes' (1954-1978) classification, which has been modified by Cruden and Varnes (1996), which introduces a rate of movement (velocity). Another important classification is the Hutchinson' (1988) classification based primarily on the landslide morphological characteristics and evolutionary features. A more recent classification suggests a new division of landslide materials, based on a geotechnical approach to describe the movement mechanisms and material properties (Hungr et al., 2014).

The landslide classification of Varnes (1954, 1978) and Cruden and Varnes (1996) is based on two main factors (Table 1):

- type of movement: fundamental term that define the mechanism, it is possible to discern five types of movements fall, topples, slide, lateral spread and flow;
- type of material: rocks, earths and debris are the terms generally used to distinguish the materials involved in the landslide process. For example, the distinction between earth and debris is made by comparing the percentage of coarse grain size fraction. The earth are materials with a weight percentage of lower 2 mm particles greater or equal to 80%, the debris are characterized by a weight percentage between 20% and 80% of particles with diameter greater than 2 mm.

Table 1. Varnes' (1978) classification (modified).

Type of movement	Material		
	Bedrock	Debris	Earth
Fall	rock fall	debris fall	earth fall
Topple	rock topple	debris topple	earth topple
Rotational slide	rock slump	debris slump	earth slump
Transitional slide	rock slide	debris slide	earth slide
Lateral spread	rock spread	debris spread	earth spread
Flow	rock flow	debris flow	earth flow
Complex	combination of different mechanisms		

The classification of Cruden and Varnes (1996) introduced the body velocity and the damage caused to the infrastructures (Table 2). The velocity, indeed, has a great importance in the risk evaluation. Cruden and Varnes (1996) propose also other useful features relative to the post-failure activity index. A landslide can be called *active* if is currently in motion, *reactivated* if is reactivated after an inactivity period, *suspended* if is moved in the last seasonal cycle. A landslide that does not move for over a seasonal cycle is defined generally *inactive* or *dormant* in the case it might have a possible reactivation. If a possible reactivation is not possible the landslide is *stabilized.* The latter category belongs to the landslides called *relict*: a phenomenon which it has developed in the geomorphological and climatic conditions considerably different from the present.

Table 2. Intensity scale of the landslide based on the velocity and damage (Cruden and Varnes, 1996).

Velocity class	Description	Damages	Velocity [mm/s]	Typical velocity
7	Extremely rapid	Catastrophe of major violence; building destroyed by impact of displaced material. Many deaths and escape unlikely.	5×10^{3}	5 m/sec
6	Very rapid	Some lives lost. Escape unlikely.	5×10^{1}	3 m/min
5	Rapid	Escape evacuation possible. Structures, possessions and equipment destroyed.	5×10^{-1}	1.8 m/h
4	Moderate	Some temporary and insensitive structures can be maintained.	5×10^{-3}	13 m/month
3	Slow	Remedial 13cceleration can be undertaken during movement.	5×10^{-5}	1.6 m/year
2	Very slow	Some permanent structures undamaged by movement.	5×10^{-7}	16 mm/year
1	Extremely slow	Imperceptible whiteout instrument. Construction possible with precautions.	$< 5 \times 10^{-7}$	<16 mm/year

A recent classification developed by Hungr et al. (2014), represent an update of the Varnes classification and it based on the type of materials and mechanical properties of the landslide. The main aim of Hungr et al. (2014) classification is a review of material classes from a geotechnical point of view. In particular, the classification separates: rock, clay, mud, earth, silt, sand, gravel, boulders, debris, peat and ice. The main characteristic of these materials are based on the granular or plastic behaviour and on the plasticity and liquidity indexes. For example, the term "mud" can be used to indicate a plastic mixture of clayey soil with a sand and finer matrix, which a Plasticity Index > 0.05 and liquidity Index > 0.5, instead, the word earth indicates a cohesive, plastic and clayey soil which plasticity Index > 0.05 and liquidity Index < 0.5. On the contrary debris can be unsorted or mixed material with low plasticity (plasticity Index< 0.05) (Hungr et al. 2001). In additional Hungr et al. 2014 add geomorphological information to the landslide name: Rock or Soil. The modified classification by Hungr et al. (2014) has 32 landslide types as show in Table 3.

Table 3. Classification proposed by Hung et al. (2014). The blue cells are the rapid shallow landslide.

Type of movement	Rock	Soil
Fall	1. Rock/ice fall	2. Boulder/debris/silt fall
Topple	3. Rock block topple	5. Gravel/sand/silt topple
	4. Rock flexural topple	
Slide	6. Rock rotational slide	11. Clay/silt rotational slide
	7. Rock planar slide	12. Clay/silt planar slide
	8. Rock wedge slide	13. Gravel/sand/debris slide
	9. Rock compound slide	14. Clay/silt compound slid
	10. Rock irregular slide	
Spread	15. Rock slope spread	16. Sand/silt liquefaction spread
		17. Sensitive clay spread
Flow	18. Rock/ice avalanches	19. Sand/silt/debris dry flow
		20. Sand/silt/debris flowslide
		21. Sensitive clay flowslide
		22. Debris flow
		23. Mud flow
		24. Debris flood
		25. Debris avalanches
		26. Earth flow
		27. Peat flow
Slope deformation	28. Mountain slope deformation	30. Soil slope deformation
	29. Rock slope deformation	31. Soil creep
		32. Solifluction

2.1 Classification of shallow rapid landslide

Of particular interest, for this work, are some type of slide and flows. In general, the first are mass movements characterized by a distinct zone of weakness that separates the slide material from more stable underlying material while the second are slope movements whose behaviour resembles that of a viscous liquid.

In the slide the mass sometime remains semi-coherent (Hendron and Patton, 1985), but more often it disintegrates producing a rock avalanche. I particular the Hungr et al. (2014) show two types of slide that can be classified in the shallow rapid landslide:

- 7. Rock planar slide: Sliding of a mass of rock on a planar rupture surface. The surface may be stepped forward. Little or no internal deformation. The slide head may be separating from stable rock along a deep tension crack (Hungr et al. 2014). This type of landslide can take place in sedimentary, metamorphic and magmatic intrusive rocks, due to the fault planes, schistosity or exfoliation. Planar slides can be of different in scale and develop in a dip slopes that have been undercut by erosion or excavation.
- 13. Gravel/sand/debris slide: Sliding of a mass of granular material on a shallow, planar surface parallel with the ground. Usually, the sliding mass is a veneer of colluviums, weathered soil, or pyroclastic deposits sliding over a stronger substrate. Many debris slides become flow-like after moving a short distance and transform into extremely rapid debris avalanches (Hungr et al. 2014). This type of landslide occurs when homogeneous soil covering developed on steep slope usually in hill or mountain regions, tends to fails as a thin layer. The major triggered factors are the intense rainfalls. The mechanism of failure involves loss of cohesion and often also partial or full spontaneous liquefaction, the slides usually have a brittle behaviour, with the progressive acceleration start a loss of coherence and the slide change downslope in a flow-like debris avalanches. Most debris slides begin or end as a mechanism classified a debris avalanches or debris flows.

Differently to the slide in the flows the particles travel separately within the mass and are characterized by internal differential movements (Cruden and Varnes, 1996). In the new classification by Hungr et al. (2014) there many categories of flow that differ from one another in some features:

- 18. Rock avalanches: extremely rapid, massive, flow-like motion of fragment rock from a large rock slide or rock fall. The extensive mass fragmentation makes this type of

landslide very dry, due to the large pore space, which during the rapid motion are waterless. Along the path of the flow, however, a saturated entrained layer may liquefy under the weight of rock avalanches (Hungr and Evans, 2004b);

- 19. Sand/silt/debris dry flow: slow or rapid flow-like movement of loose dry, moist or subaqueous, sorted or unsorted granular material, without excess pore pressure (Hungr et al., 2001). These landslides are generally small and slow and in absence of excess pore pressure the movement is shallow and planar;
- 20. Sand/silt/debris flowslide: very rapid to extremely rapid flow of sorted or unsorted sutured granular material on moderate slope, involving excess pore-pressure or liquefaction of material originating from the landslide source. Usually originates as a multiple retrogressive failure. May occur subaerial or under water. In these landslides the loose saturated granular materials are full or partially liquefy causing rapid and very dangerous mass movements. The main characteristic of these flow is the spontaneously liquefaction at the source. The liquefaction phenomenon can affect all source mass or only certain horizons in subaerial or underwater conditions. The material involved are common loose sand or gravel under water, loose glacial-fluvial silts or loess with basal saturation, loose man. Made fills, mining waste or mining tailing or fall pyroclastic soils (Hungr et al., 2002; Blight, 1997; Picarelli et al., 2008);
- 21. Sensitive clay flowslide: very rapid to extremely rapid flow of liquefied sensitive clay, due to remoulding during a multiple retrogressive slide failure at, or close to the original water content. These landslides occur in quick clays or in leached marine clay. These movements start as a retrogressive multiple rotational failures or as sudden liquefaction (Bjerrum, 1995; Mitchell and Markell, 1974);
- 22. Debris flow: very rapid to extremely rapid surging flow of saturated debris in a steep channel with strong entrainment of material and water from the flow path. The particular behaviour of a debris flow is that the flow is channelled in an established drainage channel or gully where the process can be occurred periodically. The velocity can be ranging from 0.05 m/sec to 20 m/sec. The presence of a laterally confined path is an important as allows increasing the debris water content, collecting the water come from the surface runoff, maintains fairly large flow depth and longitudinal sorting and defining a different hazard assessment for debris flow. Debris flow deposits consist in heterogeneous size sediments, from sand to very large boulders with varying

proportions of silt and clay, which are arranged in an inverse gradient in the vertical clasts distribution with the boulders close to the flow surface. A similar gradation is present, also, in the longitudinal direction where can be a coarse surge front (called peak of discharges) (Pierson, 1986; Iverson, 1997; Hungr, 2000, Fig. 2). Behind the front is located a fluid and generally saturated body, characterized by a free surface parallel to the channel bottom (Davies, 1986).

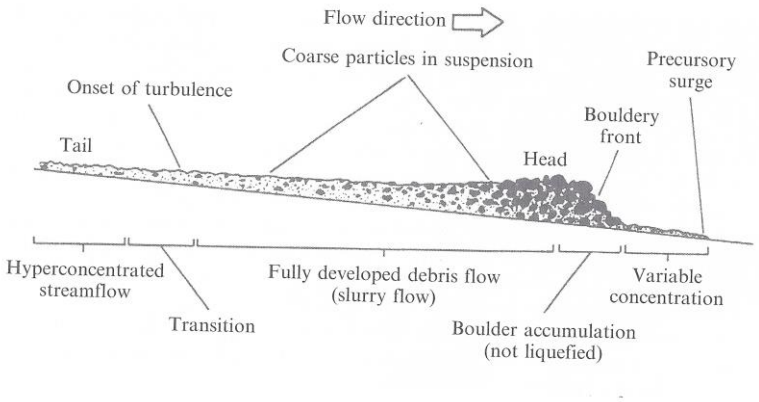

Fig. 2. Schematic representation of a debris flow (Pierson, 1986).

The debris flow path can be divided into a source, a main track and a depositional area. Generally, the source area has a steep slope, ranging between 20° - 45°, flow may be initiated by a slide, debris avalanches or rock fall. Some of them initiate in low-order streams due to intense runoff (both in riverbeds and over bank deposits), or to overland flow mobilizing sediment without slope instability phenomena (Brayshaw and Hassan, 2009). Others debris flows types are related to slope failures which rush down mountainsides, subsequently funnelling into stream channels and forming thick deposits on valley floors (Iverson, 1997). The latter type is usually associated with intense erosion along their path, which can lead to a substantial increase in magnitude (volume), runout distance and disruptive energy.

In the main track the flow can travel along a not erodible or erodible channel. In the latter case the entrainment of material lead to a considerable increase in the initial volume of the flow. During the process of surge formations, debris flows have an increase in the drag forces and further enhancement of the entrainment intensity.

The flow end in the depositional area usually occurs as a result of slope reduction and a loss of confinement as a debris fan or colluvial fan or cone.

- 23. Mud flow: very rapid to extremely rapid surging flow of saturated plastic soil in a steep channel, involving significantly greater water content relative to the source material. The mud flows are different from debris flow because have significant content of fines clay fraction that can become dilute beyond liquid limit. Usually they can attain long runout distance due to the clay content that retards the dilution by water and the drainage;
- 24. Debris flood: very rapid flow with water heavily charged with debris, in a steep channel;
- 25. Debris avalanches: very rapid to extremely rapid shallow flow of partially or fully saturated debris on steep slope, whiteout confinement in an established channel. Like debris flows the debris avalanches can be initiates as a debris slide, however the mass movement flows in a steep slope one time. The depositional area is unconstrained and difficult to construe. The debris avalanches have a lesser degree of saturation and the absence of longitudinal sorting and a front composed by coarse granular sediment. If a rock avalanche joining a channel may incorporate surface water and become debris flow.

2.2 Rheological classification of shallow rapid landslide

Rheology is the study of fluid deformation properties subjected to an applied stress. Consider two parallel planes at an infinitesimal distance *dy*, among which moves a horizontally viscous fluid. The shear stress (τ, Pa) is the ratio between applied strength (*F*) and the area (*A*) of the planes, which causes the sliding of the flow surface. This upper part moves most rapid that the lower one. The rate of shear strain (du/dy, s^{-1}) will therefore be defined as the change of velocity along the orthogonal direction to the velocity vector. The relationship between and the rate of shear strain and the shear stress is called rheological equation and its graphic representation is called rheogram (Fig. 3).

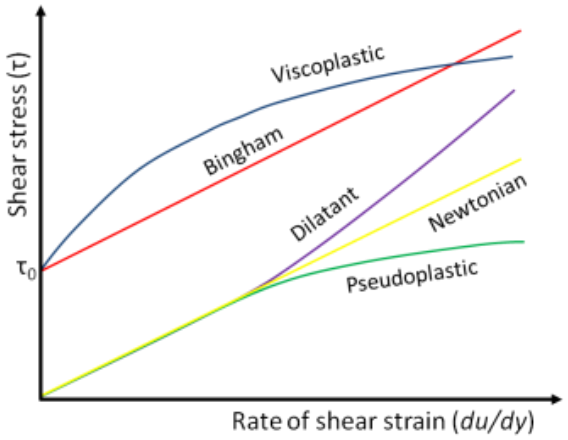

Fig. 3. Graphical representation of the rheograms of different types of fluid.

On the basis of the rheogram, the fluids can be divided in Newtonian and non-Newtonian.

A fluid is called Newtonian if the relationship between applied stress and shear rate is linear:

$$[3] \qquad \tau = \mu \frac{du}{dy}$$

where μ is a constant called dynamic viscosity defined as the inclination of the equation that links the rate of shear strain at the shear stress, increases with the increase of sediment concentration (Thomas, 1963; Happel and Brenner, 1965).

A fluid characterized by a variable viscosity is called non-Newtonian. This happens when the link between the shear stress and the strain rate is no longer linear, for that reason, the non-Newtonian rheological equations are generally described as:

$$[4] \qquad \tau = f\left(\frac{du}{dy}\right)$$

with these characteristics there are different types of fluids:

pseudoplastic (shear thinning), fluids having viscosity that decreases with increasing rate of share. For these fluids, the viscosity is constant for very high and very low values of strain rate. Their behaviour can be described by the power law equation by Ostwald (1925);

$$[5] \qquad \tau = k\left(\frac{du}{dy}\right)^{n_c}$$

where k is a constant called flow consistency index and n_c is the flow behaviour index.

If $n_c < 1$ the fluid is pseudoplastic, if $n_c > 1$ the fluid is dilatants, while, if $n_c = 1$ and $k = \mu$ the fluid is Newtonian;

dilatants (shear thickening), fluids having a viscosity that increase with and decreasing rate of share ($n_c > 1$);

viscoplastic, fluids that require an initial stress in order for movement to take place. There are several empirical rheological models to describe the behaviour of viscoplastic materials, however, constitutive equations do not exist with general validity for the whole class of such materials. The rheological behaviour of viscoplastic fluids is described by the simplest and most often used Bingham model (Bingham and Green, 1919), initially proposed for debris flows by Johnson (1970) and Daido (1971):

$$[6] \qquad \tau = \tau_0 + \mu_B \frac{du}{dy}$$

where τ_0 is the yield stress, represents the critical value above which the material starts to flow, μ_B is the Bingham plastic viscosity.

A general relationship that provides for description of all fluids is represented by Herschel and Bulkley (1926) model:

$$[7] \qquad \tau = \tau_0 + k\gamma^n$$

where τ and γ are the shear stress and the shear strain rate, τ_0 is the yield stress, k is the consistency index and n is the power-law index. The Herschel-Bulkley model is for viscoplastic fluids a combination of the Bingham model with the power law model.

There are numerous classifications defined over the years by various researchers to describe the rheological behaviour of the flows based on their rheological relationship.

Pierson and Costa (1987) proposed a classification on rheological fluids behaviours separating the flows according to the deformation rate (mean velocity) and sediment concentration (Fig. 4). They observed that moving from left to right in the graph, increasing therefore the solid concentration between 0% and 100%, at the first is obtained an increase of yield stress (hyperconcentrated streamflow) with the subsequent appearance of liquefaction behaviours (slurry flow) and after the loss of the ability to liquefy (granular flow). In the graph, the first red line (on the left) represents the yield stress, moving to the right, the second red line represents the rapidly increase of the yield stress and the beginning of fluidization which then ends at the third red line. The second red line, also, divides the flows between fluid mixture (streamflow and hyperconcentrated streamflow) and plastic fluid mixtures (viscos slurry and granular flows and inertial slurry and granular flows) If the flow contains a high amount of cohesive materials,

the vertical lines are shifted to the left, if the flow contain mostly coarse grains, the vertical lines are shifted to the right (Lorenzini and Mazza, 2004). These rheological behaviours can be associated to the names uses by Varnes (1954, 1978), Cruden and Varnes (1996), Hungr et al. (2014) for the classification of the landslide flow type.

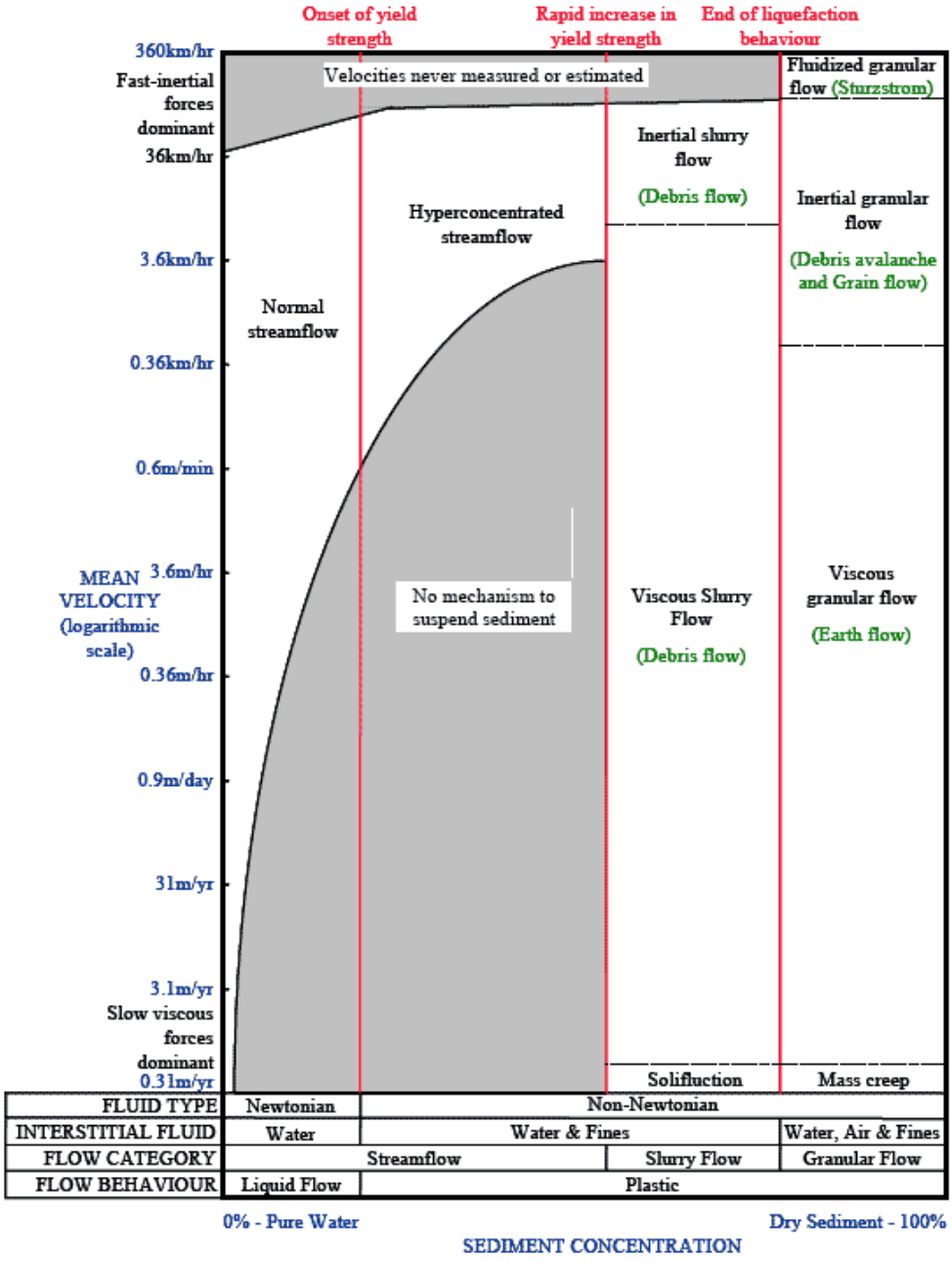

Fig. 4. Rheological classification of sediment-water flows. Vertical boundaries are rheological thresholds function of grain-size distribution and sediment concentration. Moving from the left to the right it is possible to observe an increasing of yield strength that permits static suspension of gravel and onset of liquefaction behaviour and finally a cessation of liquefaction behaviour. Horizontal velocity boundaries are determined by how stress is transmitted between particles during flow (Pierson and Costa, 1987).

Another rheological classification developed by Coussot (1992) and Coussot and Munier (1996) divided the water-debris mixture on the basis of total solid volume fraction and the ratio of silt-and-clay to total solid fraction (Fig. 5). In this classification the flows are distinguished on content of fine fraction. If a greater amount of 10% in volume of particles at a grain size less than 40 µm is present the flow is called "muddy debris flow", if the amount of fine particle is low the flow is called "granular debris flows".

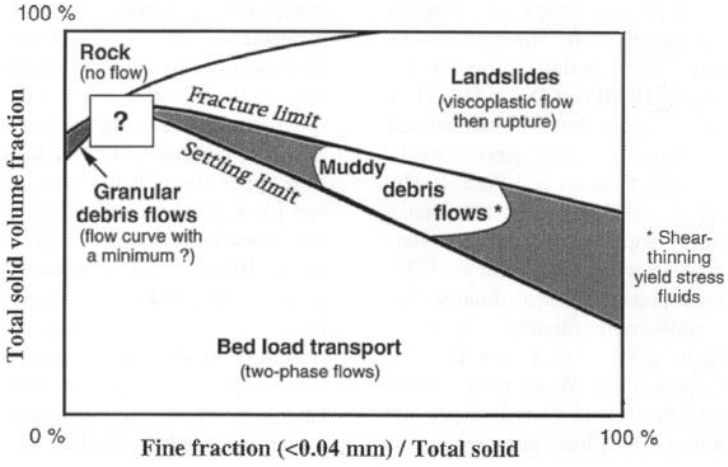

Fig. 5. Coussot's classification (Coussot, 1992).

3. Models for Landslide runout prediction

3.1 Empirical methods

Empirical models correlate physical properties of the landslide with the area of the runout zone (McDougall and Hungr, 2004). In the statistical analysis of empirical observations it is necessary to have a good knowledge of initial conditions of the landslide to establish the runout behaviour. For this reason such analysis are subject to a high degree of approximation (Crosta et al., 2006). The empirical methods are based on correlation between pairs of physical parameters and are very easy and fast to use, but they do not allow to determine the complex dynamic of landslides in detail. The output is a probability correlation which depends on the entered input parameters. As a matter of fact, it is important comparing similar cases to obtain good results.

Empirical models have been created to understand the runout characteristics, including the impact of mechanism, material, morphology, and to predicting average or maximum runout velocity (Hsu¨, 1975; Evans and Clague, 1988; Nicoletti and Sorriso-Valvo, 1991; Legros, 2002).

The models can be applied quickly to establish initial hazard characteristics for preliminary runout analysis, which may be later refined by other prediction models.

The empirical predictive equations involving different parameters such as volume (*V*) (Rickenmann, 1994; Rickenmann, 1999), the inundated area (*A*) (Zimmermann et al., 1997), the vertical height (*H*) and the horizontal length (*L*). They can be subdivided into: 1) heuristic methods and 2) the angle of reach method.

Heuristic methods are based on the mapping the extent of ancient and recent landslide deposits to understand future travel distances. The most widely used methods are the field investigation and photo interpretation. The margin of the landslide deposits give an indication of the maximum reach that a landslide is able to reach in the present landscape (Hungr et al., 2005).

The angle of reach method is used as an index of efficiency for the dissipation of energy. The ratio between *H/L* is considered an important mobility index and can be expressed, also as:

fahrböschung angle (α) the vertical angle between the crest of the crown and the tip of the toe (Heim, 1932) (very easy to measure in field);

$$[8] \qquad tan\alpha = \frac{H}{L}$$

the travel angle (*α'*) that depend on centre of mass, measuring the angle between the source and deposits centres of mass (calculate mathematically) (Fig. 6).

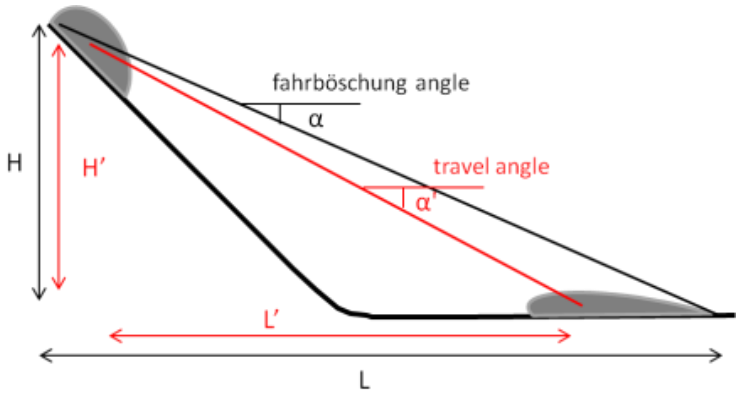

Fig. 6. *H* is the vertical maximum height, *L* the horizontal maximum length and α the fahrböschung angle. *H'* is the vertical center of mass height, *L'* the horizontal center of mass length and α' the travel angle.

These angles are inversely related to mobility and usually are used in the relationship with the landslide volume. In particular, Corominas (1996) analysed 204 landslides using correlation

coefficient of a linear regression to recognized relationship between the log(V) and the log (tanα).

Similar to the Corominas (1996), Iverson (1998) proposed a method for the debris flow involving pyroclastic materials (lahar), that provide to estimate the inundate area (*A*) and the planimetric area (*B*) on the base of a relationship between volume (*V*) and coefficients of mobility (*C* and *c*) (Scheidl and Rickenmann, 2009) established with statistical calibrations on cases of historical study. For example, Griswold and Iverson (2008), using field data acquired from different sources, define the mobility coefficients for lahar, rock avalanche and debris flows:

[9] $$A = 0.1\, V^{2/3}$$

[10] $$B = 20V^{2/3}$$

Later these equations were implemented within the program LAHARZ (Schilling, 1998), which assumes a constant cross-section area and a confined flow. The model is capable of providing a hazard map in which are delineated all possible flow paths, in addition to the area inundated on the alluvial fan. Berti and Simoni (2007) with the application Dflowz, modified LAHARZ to simulate, also, unconfined flow. The model expected that the flows are propagated on the fan according to a preferred direction entered as input file; the maximum deposit thickness is constant and depending only on the volume.

Subsequently Scheidle and Rickenmann (2009), proposed a model (TopRunDF) that allows, instead, the mapping of the potential flow paths according to the topography of the fun in the direction of maximum slope. Firstly, multiple flow paths are identified with the D8 model associated with the Monte Carlo technique; then the probability, of flow associated with 8 possible directions, is calculated, in order to obtain a final direction.

3.2 Dynamic methods

Dynamic methods take into account the solution of a governing system of equations of motion (conservation the mass, momentum and energy) and a rheological model to describe the material behaviour of landslide (O'Brien et al., 1993; Hungr, 1995; Iverson and Denlinger, 2001; Laigle et al., 2003; McDougall and Hungr, 2003). These may be used to predict a complete description of the landslide motion and use physical and mathematical relationships, but must be verified against empirical observations to determine, when making a prediction, the

appropriate input parameters (Hungr, 1995; Iverson, 1997; Rickenmann, 2005). One of the advantages of these methods is that they have a good ability of computing the movement of the flow over irregular topographic terrains. Besides this, they give the intensity factors of the landslides directly, as the volume involved and the travel distance, which can be coupled directly to vulnerability.

The dynamic methods can be grouped into two main categories: distinct element methods (Cundall and Strack, 1979, Asmar et al., 2003; Miyazawa et al., 2003; Cleary and Prakash, 2004) and the continuum methods (O'Brien et al., 1993; Hungr, 1995; Iverson and Denlinger, 2001; Laigle et al., 2003; McDougall and Hungr, 2003). In the first case the mass is modelled as collection of distinct elements that interact with each other and may be different shape and size, to simulate the large deformation. A famous model is the Particle Flow Code (PFC) developed HCItasca (Cleary and Prakash, 2004) for a dry flow. The second category is continuum methods are considered a potentially powerful tool for landslide runout analysis. They commonly use the depth-average form to simulate the large scale internal deformation based on hydrodynamic theory. Continuum models are simplified by integrating the internal stresses in either vertical or bed-normal directions to obtain a form of the Saint-Venant or Navier-Stokes equations (shallow water assumption) (Iverson, 2005). Most models are based either on the Hutter and Savage (1988), which has been modified in Savage and Hutter (1991) theory of frictional grain flow or on the Iverson 1997, revisited by Iverson and Denlinger (2001) theory of mixture flow.

The dynamic models can be divided in 2D or 3D and in Eulerian and Lagrangian. The models that use the 2D terrain are referred to depth-average 1D, while the 3D terrains are referred to a depth-averaged 2D. Another major distinction is between Eulerian approach, where the reference frame is fixed in the space and we observed the particles changing behaviour from inlet to outlet in the observation space. This framework requires the solution of a more complex form of the governing equations using a dense, fixed computational grid.

The Lagrangian used a reference frame moving along the path, with the local velocity. In this second case a particle is chosen and followed to observe what happens along the way. Been doing this for all system particles, it is possible to obtain govern the dynamics equations of the whole system. This method simplifies the governing equations and does not sacrifice computational resources in empty zones.

Summary rapid shallow landslide numerical models are show in 2D (Table 4) and in in 3D (0). These models have evolved from simple hydrodynamic models to more complex models that include various methods accounting for internal strength, entrainment and rheology variations. The classification is based on solution dimension (1D or 2D), solution reference frame (Eulerian or Lagrangian) and basal rheology.

Table 4. Existing 2D dynamic models with main characteristics.

Authors	**Model name**	**Reference frame**	**Rheology**	**Model description**
Lang et al. (1979)	AVALNCH	Eulerian hydrodynamic model	Frictional	Simulate the fast-stops observed during the avalanche deposition
Dent and Lang (1980), Dent and Lang (1983)	BVSMAC	Eulerian hydrodynamic model	Biviscous resistance similar to the Bingham	Used to back-analysed the same series of debris avalanches
Jayapalan (1981), Jayapalan et al. (1983a)	TFLOW	Eulerian model	Bingham	Used to back-analysed mine waste flow slide
Hutter and Savage (1988)		Eulerian and Lagrangian models	Frictional	The model separates the internal and basal rheologies. Using the Rankine earth pressure theory.
Savage and Hutter (1991)		Lagrangian model	Frictional	Add the centripetal acceleration due to the curvature of the path, which influences the magnitudes of the internal and basall stress.
Thaaìkahashi (1991)		Eulerian models	Dilatant	Solid-fluid mixture is modelled ad a dilatant fluid, using a semi-empirical relationship for erosion e deposition rate.
Hungr (1995)	DAN-W	Lagrangian model	Frictional Bingham Voellmy Newtonian ecc.	Equivalent fluid governed by simple internal and basal rheology
Laigle and Coussot (1997)		Eulerian model	Herschel-Bulkley	Used for mud flows.
Iverson (1997)		Lagrangian model	Frictional	Based on grain-fluis mixture theory, with the effects of viscous pore varying pressure

Table 5. Existing 3D dynamic models with main characteristics.

Authors	Model name	Reference frame	Rheology	Model description
Sassa (1988)		Eulerian model	Frictional	Use to back-analysed of rock avalanches
O'Brien et al. (1993)	FLO-2D	Eulerian model	Quadratic	Used in a full scale mudflow
Greve et al. (1994), Koch et al. (1994)		Lagrangian model	Frictional	Using modified the Savage-Hutter theory.
Gray et al. (1999)		Lagrangian model	Frictional	Using modified the Savage-Hutter theory.
Crosta et al. (2003)	TOCHNOG	Differential	Frictional	
Pitman et al. (2003)	TITAN2D	Eulerian model	Frictional	Based on Savage-Hutter theory for dry granular flow
McDougall and Hungr (2004); McDougall (2006)	DAN 3D	Lagrangian model	Frictional Voellmy Bingham	Used equivalent fluid theory to simulate a different internal and basal rheology. Used a meshless SPH.
Pirulli (2005)	RASH3D	Eulerian model	Frictional Voellmy Quadratic	Used to simulate dry granular flows using a kinetic scheme.
Kwan and Sun (2007)	3dDMM	Eulerian model	Frictional Voellmy	Used a numerical strategy called Particle-in-cell
Chen and Lee (2007)	MADFLOW	Lagrangian model	Frictional Voellmy Bingham	
Medina et al. (2008)	FLATMODEL	Eulerian model	Frictional Voellmy	Uses the finite volume method with the numerical implementation of the Godunov scheme.
Pastor et al. (2009)	Pastor Model	Lagrangian model	Frictional Voellmy Bingham	Used a meshless SPH.
Beguería et al. (2009)	MassMov2D	Eulerian model	Voellmy Bingham	Mass movements can be defined as gravity- driven flows of a mixture of rocks, soil, and water, with a behavior exhibiting properties of viscous and turbulent flows.
Christen et al. (2010)	RAMMS	Eulerian model	Voellmy	uses the total variation diminishing (TVD) finite volume scheme (FVM) applied on 3D terrain

3.3 Numerical modelling DAN-W and DAN-3D

DAN-W (Dynamic Analysis) (Hungr, 1995) and DAN-3D (McDougal, 2006) are the two models chosen in this thesis. These, are dynamics models developed to predict the runout parameters of shallow rapid landslide, including maximum distance reached, flow velocity, thickness and distribution of deposits and behaviours in bends and obstacles in flow path. These models are calibrated by back-analysis procedure of known cases and afterwards, used to predict the behaviour of new events. Previous works suggest that the models have similar parameters during back-analysis of the historical case studies (Hungr, 1995; Hungr and Evans, 1996; McDougall and Hungr, 2003, 2004, 2005; Hungr and McDougall, 2009; McKinnon et al., 2008; among others).

Both models focus on external features of landslides behaviour, ignoring internal micro-mechanics. DAN-W and DAN-3D using simplified concept of "equivalent fluid" proposed by Hungr (1995) and shall the following principles:

- they are controlled by an internal rheology different from the basal rheology;
- the basal rheology and the material parameters may be changed with position along the path;
- they have the possibility to impose an entrainment along the slide path;
- they are user-friendly and permit a rapidly and efficient back-analysis on the observed behaviour of historical events.

3.3.1 Equivalent fluid theory

DAN-W and DAN-3D use a simpler semi-empirical method based on the concept of "equivalent fluid" (Hungr, 1995). In this approach the heterogeneous and complex landslide material is represented in a schematic form. The landslide is represented with a hypothetical material governed by two simple rheologies, internal and basal, which may be different one from each other. The "equivalent fluid" method comes from idea of Chow (1957) of shallow flow assumption where a variety of viscous and turbulent relationships can be used to determine basal friction forces, while the internal stress is assumed to be hydrostatic. A similar division was implemented by Savage and Hutter (1989), who detect an internal stress frictional and capable to sustaining strain-dependent in a deforming granular mass together with basal shear strength. In the Savage-Hutter theory, the internal and basal rheologies are frictional but could be

governed by distinct frictions angles. DAN-W and DAN-3D extend the Savage-Hutter theory by replacing the frictional basal rheology term by an open rheological kernel, which can be assigned in different zone along the path and has to be selected based on trial-and-error back analysis.

The internal rheology is assumed frictional and governed by one parameter the internal friction angle ϕ_i.

The basal rheology and its associated parameters (one or two), are selected based on empirical calibration procedure, in which the results are evaluated in terms to reproduce the historical landslides behaviours as: the travel distance, the duration, the velocity and the flow and deposits thickness.

3.3.2 DAN-W

Hungr (1995) presented a 2D Lagrangian numerical model called DAN-W that includes some of models behaviours in Table 4. The model is based Lagrangian solution of the depth-averaged equations of the motion in one dimensional form. These equations are integrated between bed and free surface by the St. Venant shallow water equation. The conservation of momentum is used to derive the St. Venant equation to thin layers perpendicular to the base of the flow called "boundary blocks" numbered *I = 1* to *n*. These divided the mass in *j = 1* to *n – 1* "mass blocks" with constant volume. The dimension of each boundary blocks is measured perpendicular to the flow direction; H_i is the height and B_i the width (Fig. 7).

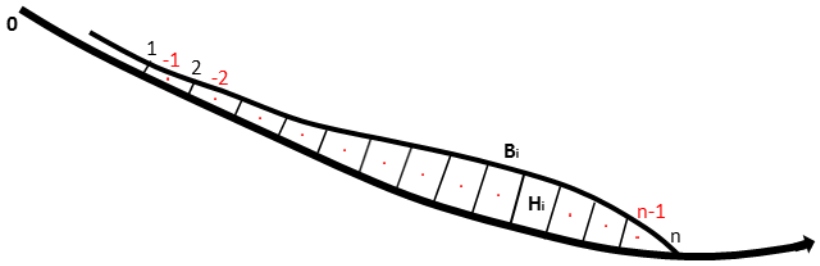

Fig. 7. The Lagrangian mesh, the Boundary blocks are numbered I = 1 to n (in black), the mass blocks j = 1 to n – 1.

On these blocks act a net driving force (*F*):

$$[11] \quad F = \gamma H_i B_{\,i} ds \sin\alpha + P - T$$

where *γ* is the unit weight, *ds* the infinitesimal length of boundary block, *α* the angle of base from horizontal, *T* resistance force and *P* tangential internal pressure.

The solution of equations occurs for successive time steps start from initial at-rest condition.

The velocity to a given period of time *Δt* and a unit of length *ds* is obtained by:

$$[12] \quad \Delta v = g \frac{F\,\Delta t - M}{\gamma H_i B_{\,i}}$$

M is the momentum flux caused from deposition or material entrainment. To find the new position of boundary blocks and volume between them is possible integrate the velocity equation in:

$$[13] \quad S_i = S_{i,old} + \frac{\Delta t}{2(v_i + v_{\,i,old})}$$

where S_i is the curvilinear displacement. Is possible now found a new height of each boundary blocks calculated as the mean of the adjacent mass blocks depth:

$$[14] \quad H_i = \frac{h_{j-1} + h_j}{2}$$

The term *P* in the eq. [11] is the longitudinal pressure and is calculated assumed that the flow lines are approximately parallel to the bed and increases linearly with the depth.

The *T* term is the basal resistance and is governed by the basal rheology of the material, which must be chosen by trial and error procedure of back analysis (Hungr, 1995), as discussed below (chapter 3.3.6).

3.3.3 DAN-W program framework

DAN-W works with four input screens; the *Control Parameters*, the *Material Proprieties*, the *Material Location* and the *Edit Geometry* path, top and width (Fig. 8).

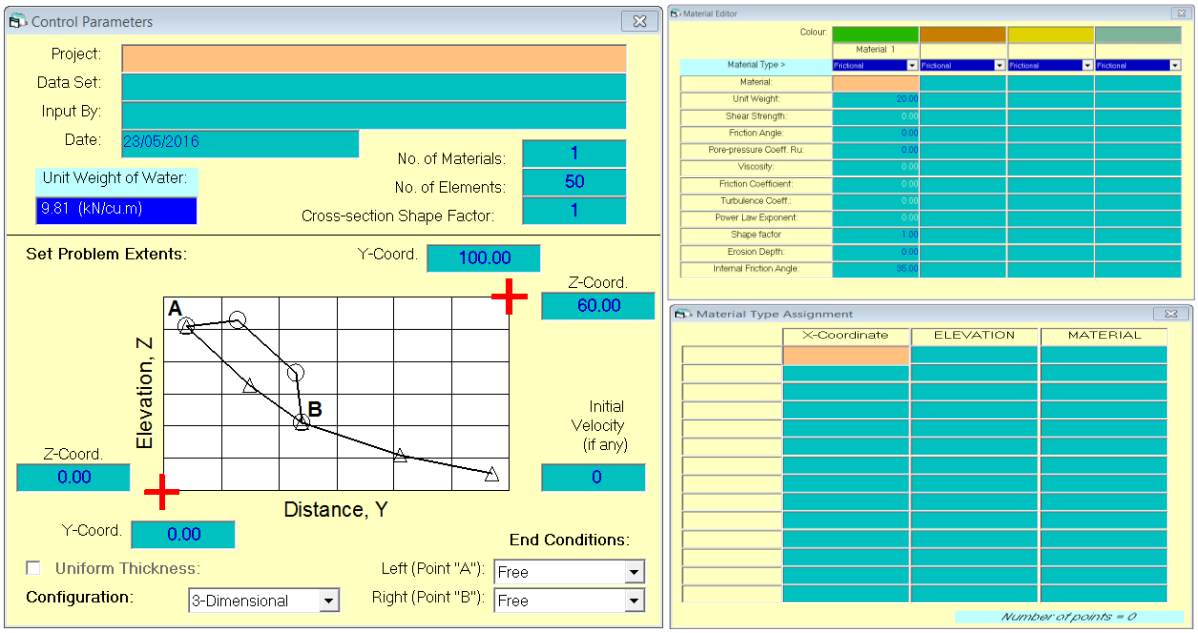

Fig. 8. The three inputs screens of DAN-W.

The *Control Parameters* allow defining the numbers of boundary blocks and rheological materials, to select the type of cross-section shape factor and the geometry extents.

In particular the cross-section shape factor define the shape of the flow channel, is calculated with the ratio between the hydraulic depth and the maximum depth of the channel and ranges between 1 rectangular cross-section to 0.5 triangular cross section.

The *Material Proprieties* is used to input the material rheologies and properties, while the *Material Locations* screen allows us to determine the position of each material along the path. After defining the fundamental parameters of the model, is necessary to add the slope profile, the sliding mass profile and the slope width of the case study (*Edit Geometry*).

Two important considerations can be done before the insertion of the path and top data files: first the input profile should be made reasonably smooth to avoid the instability. This means that the path shall not have many points and details such a minor step. Second the front and rear of the slide mass should coincide with points of the path file.

More information can be obtained from DAN-W Manual (Hungr, 2004).

3.3.4 DAN-3D

McDougall (2006) presents a 3D Lagrangian numerical model called DAN-3D that includes some of models behaviours in 0. The model is based on Lagrangian forms of depth-integrated St. Venant equations adapted for Smoothed Particle Hydrodynamics (SPH). It begins from mass and momentum conservation laws governing the mechanism of continuum (Hungr and McDougal, 2009). The continuum approach is based on the assumption that the particles size of the landslide materials are small than the landslide depth. This is appropriate if is considered the fine-grained landslide materials. The laws governing the continuum can be expressed as followed:

$$[15] \quad \frac{\partial \rho}{\partial t} + \nabla \cdot \rho v = 0$$

$$[16] \quad \frac{\partial (\rho v)}{\partial t} + \nabla \cdot \rho v \tau \otimes v = -\nabla \cdot T + \rho g$$

where ρ in the bulk density, t is time, v velocity, T the stress tensor, g the gravitational acceleration vector, ∇ is gradient operator. After some assumptions the equations can be expanding for x, y and z directions. The rapid landslides are generally well-bounded by the top with the atmosphere and at the base with the bed interface.

The best orientation of the reference coordinates system is that one where the z direction corresponds at the depth of the flow h and the x direction is aligned with the direction of the motion. The top surface is assumed to be stress free. Moreover the model assumes that no material enter or leave the landslide at the free surface. In DAN-3D the entrainment material, with the same bulk density of the landslide, is eroded only from the bed. The time-dependent rate at which the material enters in the landslide is known as the "erosion velocity" and must be positive (Takahashi, 1991). The kinematic boundary condition at the bed is:

$$[17] \quad \frac{\partial b}{\partial t} + v_x \frac{\partial b}{\partial x} + v_y \frac{\partial b}{\partial y} - v_z = -E_t$$

After the applying boundary condition and depth-averaging with the use of the Leibniz's rule, and converting the equations to a Lagrangian coordinate system. The final form of the continuity mass balance equation and momentum balance equations is:

[18] $$\frac{Dh}{Dt} + h\left(\frac{\partial v_x}{\partial x} + \frac{\partial v_y}{\partial y}\right) = E_t$$

[19] $$\rho h \frac{Dv_x}{\partial t} = -\frac{\partial(\sigma_x h)}{\partial x} - \frac{\partial(\tau_{yx} h)}{\partial y} + \tau_{zx} + \rho h g_x - \rho v_x E_t$$

[20] $$\rho h \frac{Dv_y}{\partial t} = -\frac{\partial(\sigma_{xy} h)}{\partial x} - \frac{\partial(\tau_y h)}{\partial y} + \rho h g_y$$

[21] $$\rho h \frac{Dv_z}{\partial t} = -\frac{\partial(\sigma_{xz} h)}{\partial x} - \frac{\partial(\tau_{yz} h)}{\partial y} + \sigma_z + \rho h g_z$$

The Lagrangian approach allows us to simplify the convective acceleration terms from the momentum balance therefore facilitates subsequent numerical integration improving the efficiency. Furthermore, the computational resources are focused within the simulated slide mass leads to the higher resolution possible.

Following the theories of Savage and Hutter (1989) and Gray et al. (1999), according to which the depth varies gradually and is smaller than the landslide length and width, the terms τ_{xz} and τ_{yz} are small relative to σ_z and can be neglected. This is the assumption of Chow (1959) where the flow lines are parallel to the path. Lagrangian derivative of v_z is equal to the centripetal acceleration of the flow:

[22] $$\frac{Dv_z}{\partial t} = \frac{v_x^2}{R}$$

where *R* is the bed-normal radius of curvature of the path, positive if is concave. The *z* direction on gravity is:

[23] $$g_z = -g\cos\alpha$$

where *g* is the acceleration of gravity and *α* in the inclination of the bat from horizontal.

Substituting the equation [22] and [23] in the equation of motion is possible to find the total bed-normal stress at the base:

[24] $$\sigma_z = \rho h\left(g\cos\alpha + \frac{v_x^2}{R}\right)$$

The model is simplified with the classical soil mechanics techniques, using classical Rankine earth pressure theory (Savage and Hutter, 1989; Terzaghi and Peck, 1967) that is useful to normalize the stress state with respect to the total bed-normal stress.

Further, neglected the spatial variations in the normalized stress state and the terms containing the derivative of stress coefficients, the Lagrangian forms of the depth-averaged momentum balance equations in *x* and *y* directions are:

$$[25] \quad \rho h \frac{Dv_x}{Dt} = \rho h g_x - k_x \sigma_z \frac{\partial h}{\partial x} - k_{yx} \sigma_z \frac{\partial h}{\partial y} + \tau_{zx} + -\rho v_x E_t$$

$$[26] \quad \rho h \frac{Dv_y}{Dt} = \rho h g_y - k_y \sigma_z \frac{\partial h}{\partial x} - k_{xy} \sigma_z \frac{\partial h}{\partial y}$$

D/D is the Lagrangian differential operator.

The terms on the left side of the equations [25] and [26] represent local depth-averaged accelerations of a moving reference column of material. The first term on the right side is the gravity force, the second and third are the pressure terms. The equation [25] presents two additional terms, due to the direction of the motion, the fourth represents the motion-resisting basal shear described in chapter (3.3.6), the fifth term represent the momentum flux due to entrainment of path material, described in chapter (3.3.5).

The numerical method used in DAN3D is a meshless Lagrangian method called Smoothed Particle Hydrodynamics (SPH). This method was originally developed by Lucy (1977) and Gingold and Monaghan (1977) for simulation of stellar evolution and astrophysical phenomena and subsequently reviews by Benz (1989) and Monaghan (1992). The SPH start from a known distribution of the reference masses that is afterwards interpolated at any given time. Following this approach, the total volume of the landslide is divided among a number of particles with a finite volume which remains cantered at one of the reference columns. The volume may only increase due to the entrainment. The depth and local depth gradient can be estimated whereas the material density constant and that the flow depth is proportional to the volume of material in the area given by the proximity of nearby particles.

The method uses a Gaussian interpolating kernel Fig. 9:

$$[27] \quad W_{ij} = \frac{1}{\pi \ell^2} exp\left[-\left(\frac{s_{ij}}{\ell}\right)^2\right]$$

where ℓ is the smoothing length measures of the kernel width and defines the influence radius of each particles (Benz, 1990). In particular, DAN-3D use:

[28] $$\ell = \frac{B}{\sqrt{\frac{\sum_{i=1}^{N} \frac{h_i}{V_i}}{N}}}$$

where *B* is a dimensionless smoothing coefficient and *N* the total number of particles.

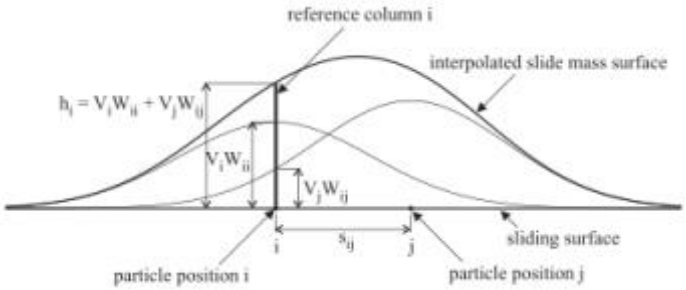

Fig. 9. A physical interpretation of SPH. A bell-shaped control volume defined by Gaussian kernel. The total depth and depth gradient at any location are determined by superposition of the particles (from McDougal and Hungr, 2004).

3.3.5 Material entrainment

The dynamics models DAN-W and DAN-3D have the possibility to include material entrainment. Entrainment may be due to destabilization of the path bed and margins under a change of stress conditions, may occur, also, at the front by "ploughing" (Sovilla et al., 2006). The erosion of the path implies an increase of the landslide volume, which correlate with a higher peak discharge and an enlargement of impact area (Rickenmann, 1999; Iverson et al., 1998). To understand and quantify the entrainment Hungr and Evans (2004a) defined a simple index called "entrainment ratio":

[29] $$ER = \frac{V_{Entrainment}}{V_{Fragmented}} = \frac{V_E}{V_R(1+F_F)'}$$

where V_E is the volume of the entrained material, V_R is the volume of the initial rockslide and F_F is the fractional amount of volume expansion due to fragmentation (0.25). The total volume of the landslide deposits equals $V_R(1+F_F) + V_E$. In case of debris flow and debris avalanches the volume change is a dominant feature and must be accounted for numerical models. While in the cases of rock slide and avalanches the entrainment may be neglected, due to the volume of erodible path material is small compared to the initial volume of the landslide.

In DAN-W model (Hungr,1995) the erosion amount is defined by a single value "erosion depth" which define the entire moving volume after that the slide has crossed the specific entrainment

zone, defined by the user. In DAN-W the erosion rate increases in proportion of the flow depth and, resulting in a depth-proportional distribution on entrainment material and natural growth of the landslide with displacement (McDougall and Hungr, 2005; Hung and McDougall, 2009).

In DAN-3D model (McDougall and Hungr, 2005; McDougall, 2006) used a similar empirical approach based on user-prescribed parameter *E*, which represents the bed-normal depth eroded per unit flow depth and unit displacement or, the displacement-dependent natural exponential growth rate. In DAN-3D the entrainment occurs only in material specified with a maximum erosion depth established a priori by a geological, geomorphological a field analysis.

[30] $E_t = E_s h v$

this latter equation represents the relationship between erosion velocity and the growth rate. The momentum balance equation in *x* direction [25] becomes:

[31] $\rho h \frac{Dv_x}{Dt} = \rho h g_x - k_x \sigma_z \frac{\partial h}{\partial x} - k_{yx} \sigma_z \frac{\partial h}{\partial y} + \tau_{zx} + -\rho h v_x^2 E_s$

Entrainment is then function of the flow depth and the square of the flow velocity.

The SPH numerical solution method allows the mass transfer from the erodible bed to the landslide mass. The area covers by particle *I* is:

[32] $A_i = \frac{V_i}{h_i}$

The volume of each particle increase due to the entrainment along the travel in a time step:

[33] $\Delta V_i = E_s h_i A_i \Delta s_i$

And so is possible obtain substituting:

[34] $\Delta V_i = E_s V_i \Delta s_i$

To simulate the entrainment, the program integrates the change of volume in all points of a fixed reference grid choice by the user, until the available material is spent or the landslide passes. The material added to each particle is detached from the local path. DAN-3D uses an average growth rate $\overline{E_s}$ or erosion rate, which gives a preliminary estimation of the average growth rate in the entrainment zone choice:

[35] $$\bar{E}_s = \frac{ln(V_f/V_0)}{\bar{S}}$$

where V_f is the final volume of the landslide as the sum of V_0 the source volume and the total volume of the untrainable material in the entrainment zone, and $\bar{S}$ is the average path length of the zone.

3.3.6 Basal rheologies

The terms T in DAN-W and τ_{zx} in DAN-3D, the basal flow resistance and the basal shear stress respectively, are governed by the basal rheology of the "equivalent fluid" theory. Some basal rheological relationship are implemented in DAN-W and in DAN-3D which can be change along the path or within the slide mass, according to the type of rheological material behaviour. All different type of rheological relationships, have usually one or two parameters which must be calibrated to a trial and error back analysis procedure. The results are judged in terms of ability to reproduce the landslide prototype event as the travel distance, duration, spatial distribution, velocity and deposits thickness. The main rheological functions use in DAN-W and in DAN-3D, are:

Laminar flow, is useful for granular and clayey fully liquefied flow whit a Newtonian behaviour and low Reynolds number. It is implemented in DAN-3D where:

[36] $$\tau_{zx} = -\frac{3\mu v_x}{h}$$

where μ is the dynamic viscosity.

Turbulent flow, is used to simulate the movement of water and granular flow with low solid concentration. The term of basal resistance is proportional to the square of depth-average flow velocity, follow the Manning equation or Chézy equation:

[37] $$\tau_{zx} = -\frac{\rho g n^2 v_x^2}{h^{\frac{1}{3}}}$$

[38] $$\tau_{zx} = -\frac{\rho g v_x^2}{C^2}$$

where n is the Mannign coeficent and C is the Chézy coefficient. This rheology is implemented both in DAN-W both in DAN-3D.

Plastic flow, relative to pseudo-static motion of liquefied solid. The basal shear strength is assumed as constant:

[39] $\tau_{zx} = -c$

Newtonian flow, is used where τ_{zx} is linear function of velocity with a dynamic viscosity μ. The rheological law is determined by the Poiseuille equation.

[40] $\tau_{zx} = -\frac{3\rho g v_x \mu}{H^{\frac{1}{3}}}$

Bingham flow, combine plastic and viscous behaviour. The body is rigid until threshold yield strength, after which the body behaves as a viscous material (Fig. 10).

[41] $\tau^3{}_{zx} + 3\left(\frac{\tau_{yield}}{2} + \frac{\mu_{Bingham}}{h}\right)\tau^2{}_{zx} - \frac{\tau^3{}_{zyieldx}}{2} = 0$

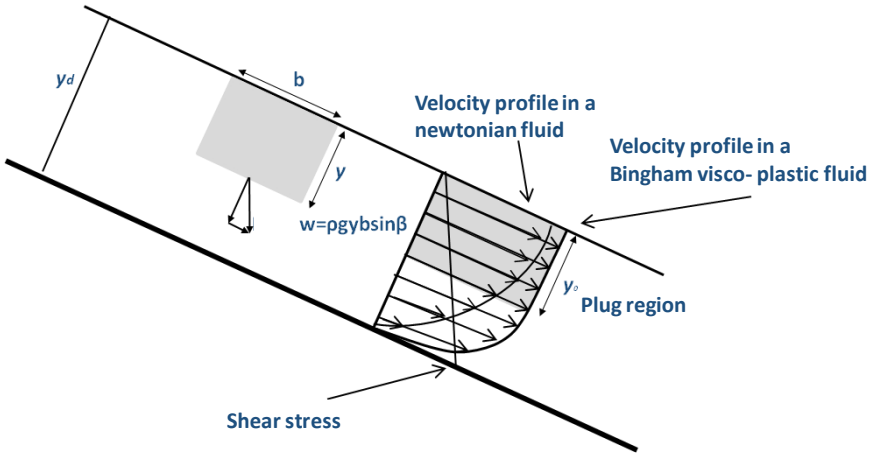

Fig. 10. Schematic velocity and stress distribution for laminar flow of a Bingham plastic fluid.

Frictional flow, the basal resistance is proportional to the effective bed-normal stress at the base, σ_z' which is the difference between the total stress σ_z and the pore pressure u.

[42] $\tau_{zx} = -(\sigma_z - u)tan\phi = -\sigma_z' \tan\phi$

where ϕ is the dynamic basal friction angle.

The pore pressure is very difficult to estimate, therefore, in geotechnical slope stability analysis is commonly assumed that the pore pressure is related to a pore pressure ratio, $r_u = u/\sigma_z$, in which case:

[43] $\tau_{zx} = -\sigma_z(1 - r_u)tan\phi$

this equation can be simplified considering only one independent variable ϕ_b a bulk basal friction angle:

[44] $tan\phi_b = (1 - r_u)tan\phi$

[45] $\tau_{zx} = -\sigma_z tan\phi_b$

The frictional rheological model often overestimates the velocity and the proximal-thickening of deposits.

The loading pressure is intermediate between drained and un-drained response. The relationships between the various frictional parameters are shown in Fig. 11.

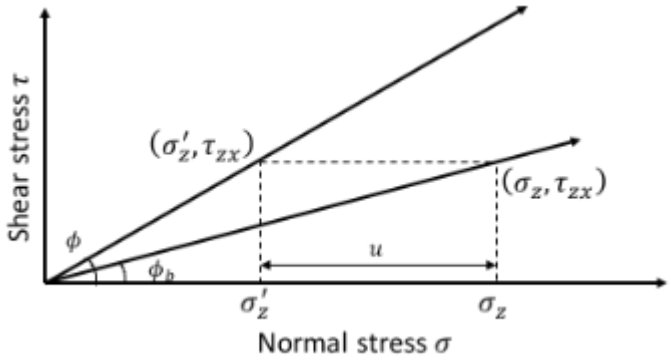

Fig. 11. Relationships between the various frictional parameters.

Voellmy, this rheological model combines frictional and turbulent features:

[46] $\tau_{zx} = -\left(\sigma_z f + \frac{\rho g v_x^2}{\xi}\right)$

where f is the friction coefficient and ξ the turbulence. The equation is divided in two terms: the first one represents the frictional component of resistance and is the same of the ϕ_b of the equation [45].

The second term was originally introduced by Voellmy (1955) to account for the velocity-dependent influence of air drag on snow avalanche; it is represented by the turbulence as the square of Chezy coefficient. This term in the landslide dynamics represents all possible sources of velocity-dependent resistance. As suggested by Bagnold (1954) a landslide moving on a thin undrained layer, where the low initial frictional resistance increases with the square of velocity.

The Voellmy model typically produces distal thickening of the deposit, and better simulations of velocity than frictional rheology (Koerner, 1976; Hungr et al., 2005; McDougall, 2006). That rheology matched the frictional and turbulent behaviours and provides for a better description of the complex dynamics of the avalanche and its long travel distance.

For DAN-W and DAN-3D is also, now available a database of inputs basal rheology parameters that can be used for prediction for many type of landslides, the frictional and Voellmy are the most used rheologies (Table 6).

Table 6. Ranges of values for the rheological parameters, adopted in the literature for the frictional and Voellmy rheologies (Hungr and Evans, 1996; Ayotte and Hungr, 2000; Chen and Lee, 2003; Pirulli et al., 2004; McDougall, 2006; Crosta et al., 2006b).

	Internal rheology	**Frictional rheology**	**Voellmy rheology**	
	Friction angle ϕ_i (°)	Bulk basal friction Angle ϕ_b (°)	Frictional coefficient *f (-)*	Turbulent coefficient ξ (ms^{-2})
Rock avalanches	35-40	10-30	0.1-0.025	450-1000
Debris avalanches	35	23-30	0.07-0.1	200-250
Rockslide-debris avalanches	35	8-31	0.05-0.2	200-400
Ice-rock avalanches	20-35	10-20	0.03-0.1	1000
Debris flows	35	27-29	0.05-0.2	200-500
Volcanik-rock avalanches	30-35	9-13	0.05-0.1	100-140

3.3.7 DAN-3D program framework

As DAN-W the software DAN-3D shows a similar framework structured in tree main steps: step 1, *Control Parameters*; step 2 *Grid File Assignment*; and step 3 *Material Editor* (Fig. 12).

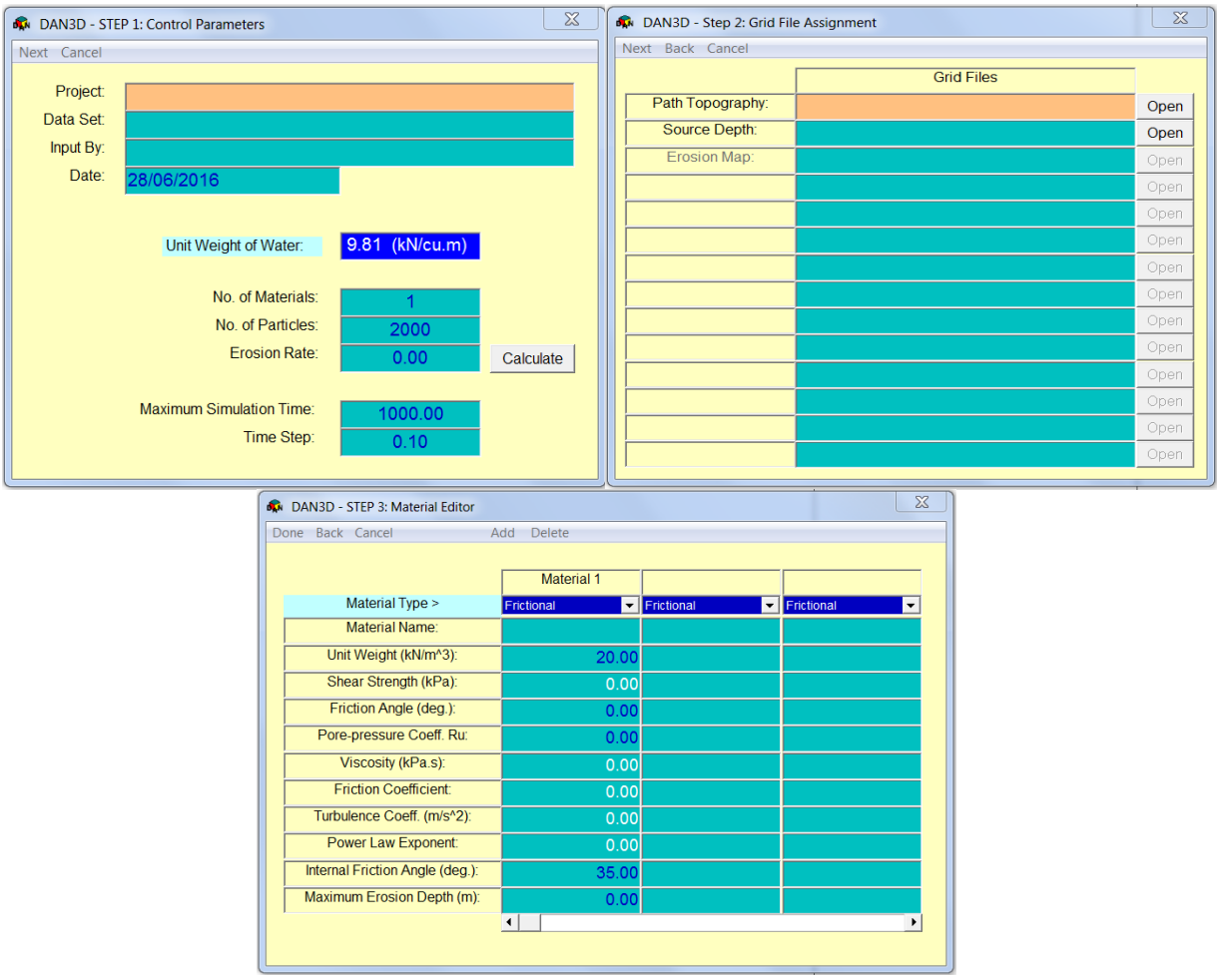

Fig. 12. Three main screens of DAN-3D.

The *Control Parameters* screen allow us to insert the primarily parameters of the model as the number of material and particles and the erosion rate.

The second step provide to assign at the model the grid files, in particular the path topography file, the source depth file and the erosion map file if is necessary (*Grid file Assignment*). The last screen is the *Material Properties* where, as in DAN-W, the user chooses among five rheology the materials properties. More information can be obtained from DAN-3D Manual (Hungr, 2010).

4. Remote sensing monitoring techniques

Remote sensing refers to the science aimed at collecting Earth Observations (EO) without physical contact with the object investigated. According to this general definition, a variety of different sensors are available today, which may be implemented on ground-based, airborne and spaceborne platforms. Remote sensing techniques for landslides investigations are undergoing rapid developments. The main applications are categorized into three main groups by Mantovani et al. (1996):

- landslide detection, classification, and post-event analysis;
- landslide monitoring;
- landslide susceptibility and hazard assessment.

In recent years, the possibility of acquiring 3D information of the terrain with high accuracy and high spatial resolution has advanced the investigation of landslide phenomena in the exploitation of High Resolution Digital Elevation Models (HRDEM), automation of feature extraction and analysis of images, including panchromatic, multispectral, hyperspectral, and synthetic aperture radar (*SAR*) data; and integration of different kinds of Remote sensing data. In particular, in this work, two major remote sensing techniques are discussed: the interferometric synthetic aperture radar (InSAR) (Fruneau et al. 1996; Colesanti et al. 2003; Squarzoni et al. 2003), and Light Detection And Ranging (LiDAR) (Carter et al. 2001; Slob et al. 2002; Haugerud et al. 2003; Slob and Hack 2004). Nowadays, advanced techniques are available for obtaining high resolution 3-D representations of land surface, such as digital photogrammetry (Chandler, 1999; Lane et al., 2000) and laser scanning (both terrestrial and aerial) (Kraus and Pfeiffer, 1998; Frohlich and Mettenleiter, 2004).

4.1 Ground Based Interferometric SAR (GB-InSAR)

The system Ground Based Interferometric SAR (GB-InSAR) allow the use the SAR technique (synthetic aperture radar) generating high spatial resolution images measured in much shorter time intervals (minutes rather than several days) (Casagli et al., 2010).

The radar is an active system that uses the microwave to observe the scenario. In particular, in the SAR system the electromagnetic wave are emitted by a radar antenna along a linear direction and recorded after their reflection on the objects in the scene. Backscattered waves are recorded and used to measure the time necessary for the signals to travel from the source

to the scene and back. In the radar technique are used the microwave, a portion of the electromagnetic spectrum ranging between 1 m and 3 mm of wavelength (frequency range: 100GHz – 300MHz), because allows to penetrate clouds and have a lightly interact with the atmosphere.

In the radar geometrical configuration, the sensor moves along a direction call along-trak (*azimuth*), while the signal is sent laterally towards the scene forming an angle with the vertical (off-nadir, ϑ). The emitted radar impulses are issued orthogonally to the azimuth, cross-track (*range*). This brings to different problem:

- *foreshortening:* occurs when the slope of the terrain is perpendicular to the line sensor-target. In these cases, the contribution of more points is concentrated in a few cells producing very bright pixels in the image;
- *layover:* occurs when the slope of the terrain is greater than the angle ϑ, this produces a strong image distortion;
- *shadowing:* occurs when some areas are not illuminated by the radar signals.

4.1.1 Radar Data

Each pixel of a radar images is represented by the reflectivity of the objects in the scene, by a phase which represent the distance between sensor and objects and by its dielectric characteristics. Usually, is used the Interferometry SAR (InSAR) technique, based on the comparison of the phase matrixes of two SAR images, acquired at different times from the same position (zero baseline). The result is an image containing information on the variation of the distance, which can be represented by an interferogram or by a displacement map. These last have the following characteristics: the displacements are recorded along the line of sight (LOS), define as the line from the antenna to the scene; the spatial resolution is the same of the original SAR image; the precision is amounts to a fraction of the used wavelength, typically centimetric or millimetric.

The interferograms and the displacement maps are represented in a colour scale, the negative values are equivalent to movements towards the sensor and positive values represented the movements away from the sensor.

The phase assumes values between $-\pi$ and $+\pi$ ($-\lambda/4$ and $+\lambda/4$) therefore, if the phase of a pixel exceeds that range (corresponding to 2π) the problem is recognized a "phase ambiguity". In this case, the interferogram is characterized by a series of coloured bands, called interferometric

fringes cycles. To derive a deformation pattern is necessary to apply special algorithms, said phase unwrapping that allows the phase to "unroll" and correct interpreter the displacements greater than n λ/2. To understand the validity of interferometric results the coherence value is estimated, that ranges between 0 (minimum coherence) and 1 (maximum coherence). Coherence values are represented on two-dimensional map where can be different pixel by pixel. Therefore, is possible to neglect the pixels that present coherence values lower than a specific threshold.

To obtain the radars results is possible compare SAR images following two procedures:

- Rolling: each image is compared to the next image in a given time interval. In this way it calculates the displacement occurred between the two images while maintaining constant the time interval which separates them. Rolling procedures allows highlighting the acceleration;
- Incremental: a SAR image is taken as a reference and interferograms are made by comparing the images acquired at different incremental time intervals always with the same image. In this case, if the time interval becomes too large, you can easily avoid in the "ambiguity problem" of phase and in loss of coherence.

4.1.2 The system GB-InSAR LISA

The first prototype of a GB-InSAR named LISA (Linear SAR) was developed by the Joint Research Centre (JRC) of the European Commission.

The microwave part of the radar system consists of a scatterometer, which acts as a synthesizer of the microwave signal sent to the transmitting antenna. A second antenna, identical to the first, is used to receive the reflected signal and convey it to perform the measurements. The synthetic aperture is made by moving the system of the two antennas, along a linear rail. The system is computer controlled and is capable of synthesizing a linear aperture along the azimuth direction. One of the main advantages of this approach is the possibility to choose the time of single acquisition according to the movements velocity to be detected (minimum technical time is around a few minutes). The acquisitions are obtained step by step during the radar motion along the rail. The rail length ranges between 1 and 4 m; and the minimum vertex aperture of the observed cone varies between 30° and 60° (Bardi 2014) (Fig. 13).

The instrument use a continuous wave step frequency (cw-sf) radar, that operates in Ku, C or L microwave bands covering an interval between 14.5 and 18 GHz with a polarization "VV".

The resolution of the GB-InSAR LISA images depend on the measurements parameters chosen, on the installation characteristics and on the distance of the sensor from the scene. The resolution in *range* (distance, *r*) and in *azimuth* (parallel to the radar acquisition movement, r_x) are given by:

[47] $$r = \frac{c}{2B}$$

[48] $$r_x = \frac{cR}{2Lf_c}$$

where *L* is the rail length, f_c is the central frequency of the signal transmitted, *B* is the bandwide and *c* and *R* represent respectively the speed of light and the distance in range. The term *L* and f_c are inverse proportional to the resolution in *azimuth* while *B* influence only the resolution in *range*.

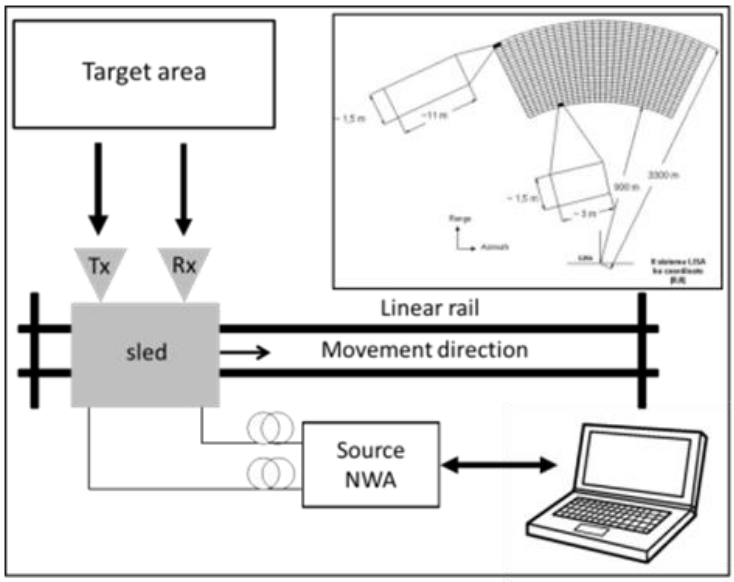

Fig. 13. Principal componentes of GB-InSAR instrument and resolutionof a GB-InSAR in a typical configuration.

The main advantages are:

- high operatively flexibility, versatility and transportability;
- near real-time measurements (every few minutes);
- very high precision;
- fast acquisition time, 5-15 minutes;
- long working distance, 3-4 km.

The main limitations are:

- bad acquisition in the vegetated areas;
- the displacement is recorded only long the LOS;
- possibility to detect a limited range of velocity;
- visible area;
- atmospheric distortions;
- Power supply.

4.1.3 SAR images

The first SAR image (Fig. 14a) is a map of the energy reflected by the objects in the scene observed. The values are visualized in logarithmic scale and usually the yellow colour represent the best reflectivity regions while the blue ones the lowest. The reflectivity depends of the acquisition system geometry compare to the observed scene or by the nature of the observed objects. The black areas are characterized by a low signal or represented the masked areas due to the shadowing phenomenal.

Using a two radar acquisition precisely to the same position (zero baseline condition) is possible to derive from the obtained interferograms a map of the displacements that occurred along the sensor LOS with millimetre accuracy (Tarchi et al., 1997, 2000) (Fig. 14b, c). The displacement maps are projected on a horizontal plane and are referred to a local Cartesian coordinate system in which the origin is placed in the central point of the scan (centre of the rail), the x-axis is the scan direction (*azimuth*) and the y-axis is the wave propagation direction (*range*). The displacement maps main feature is that they do not exhibit the phase ambiguity due to the appropriate algorithms that allows the phase extraction (phase unwrapping). The displacement maps scale expresses the cumulative movement from the beginning of the sequence.

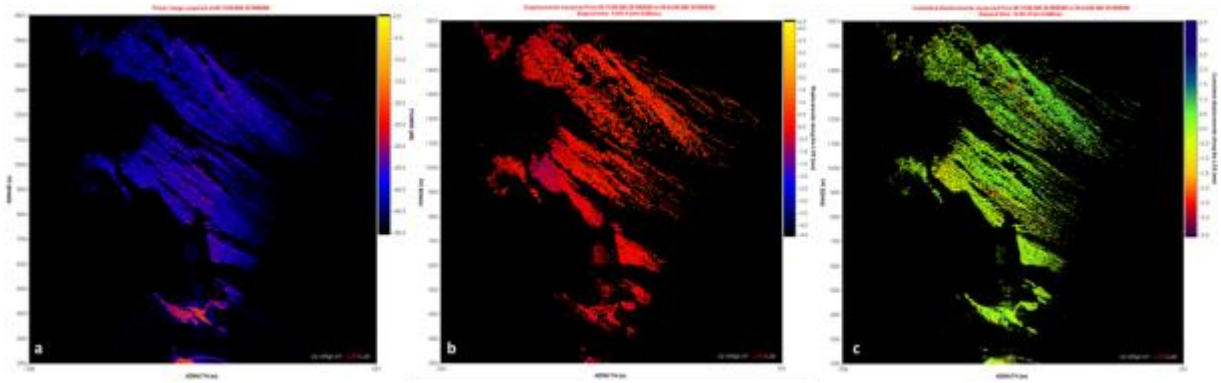

Fig. 14. The GB-InSAR thecnique data a) power map, b) Interferograms and c) cumulative desplacemnt map.

4.2 Laser scanning technique

LiDAR (or laser scanning) is a remote sensing system based on the LASER technology (Light Amplification by the Stimulated Emission of Radiation). A laser is active optical sensor that produces and emits a beam (or a pulse series) of directional, collimated by a lens and mirrors system, coherent and in-phase electromagnetic radiation with a wavelength in the NIR range (0.8-1.6 µm) sometimes in the VIR (0.5 µm) (Gomarasca, 2004), make it possible to determine the three-dimensional coordinates of scattered points by means of the distance measurement between the sensor and the scene observed.

The LiDAR data is a high-resolution point cloud of the observed scene in particular. In geological contexts it show several applications that range from mapping (Ardizzone et al., 2007; Jaboyedoff et al., 2008a) to monitoring deformation (Gordon et al., 2001), landslides or rockfall displacements (Teza et al., 2007; Oppikofer et al., 2008; Abellan et al., 2010) to landslide in soils (Jaboyedoff et al., 2009a).

Two type of sensor can be used: the airborne-based for ALS (Airborne Laser Scanner) and ground-based for TLS (Terrestrial Laser Scanner) (Wehr and Lohr, 1999; Baltsavias, 1999; Petrie and Toth, 2008) usually they use the pulse methods.

There are two methods for range determination: phase and pulse method, the second is the most used and measures the range (*D*) based on the Time Of Flight (TOF) of the laser pulse, as follow:

$$[49] \quad D = \left(\frac{\Delta t}{2}\right) c$$

where *c* is the velocity of light (*c* ≈ 3·108 m/s).

The laser bream is directed towards the scanning mirror which, in turn, directs the generated laser pulses to objects on the ground, without any artificial reflectors, and subsequently receives the return signals. The laser's spot dimension (or breamwidth projected on the topography) increases with the distance due to the laser beam divergence. This is crucial to exploit some characteristics of LiDAR systems, as the possibility to investigate different surface thank to the phenomenon of multiple echoes. In fact, the first laser pulse returning in wooded areas, in most cases corresponds to the trees crown (Lim et al., 2005), while the information obtained from the last return pulse, with high probability, will match to the ground surface, but will need to be cleaned from errors in the processing phase to create the Digital Terrain Model (DTM), using different mathematical and statistical techniques (Kraus and Pfeifer, 1998)(Fig. 15).

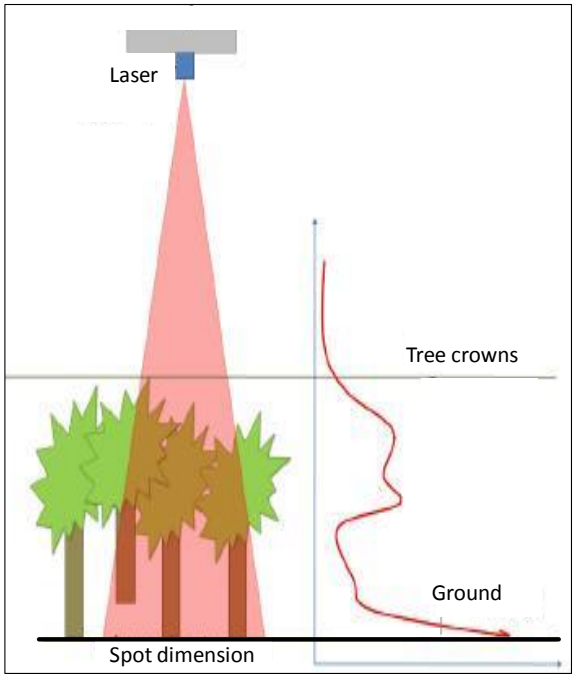

Fig. 15. The Laser scanning technique.

The parameters that change in different laser scanning techniques are the accuracy, resolution and point density.

The accuracy may be different due to some factors as: poorly reflecting very rough surfaces, parallel incident angles, bad weather conditions, very bright ambient conditions, excessive range, etc. However the typical accuracy of the laser is ±1.5 cm, within maximum distances of about 800 – 1000 m (Manetti and Steinmann 2007). The resolution is calculated in range and angular, the first is the ability of a rangefinder to resolve two objects on the same LOS; the second is the ability to resolve two objects on adjacent LOS (Jaboyedoff et al., 2012). Another

important factor is the point density that range between 0.5 to 100 pts/m^2 for the ALS and range between 50 to 10000 pts/m^2 for the TLS.

4.2.1 Airborne Laser Scanning (ALS)

The Airborne Laser Scanning system (ALS) allows us to have 3D coordinates of millions of points with decimetre-level accuracy. This instrument is widely used for the generation of High Resolution Digital Elevation Models (HRDEM) and is typically composed by:

- A distance meter (or rangefinder) laser, which records the time taken from the moment of transmission to signal reception;
- A GPS receiver (Global Positioning System) kinematic, which allows determining the coordinates of the transmitter during the phase of flight;
- A GPS receiver master, fixed to the ground on a point with known coordinates, useful for relative positioning (differential correction);
- An INS (Inertial Navigation System) electronic system which uses an Inertial Measurement System (IMU) containing an Inertial Sensors Array ISA, composed of a computer and a platform with accelerometers and gyroscopes, capable of measuring the specific strength and the rotational movements;
- Service equipment, for the power supply the control of the sensors and the registration of data service.

The transmitting and receiving apertures of the ALS system is range approximately 8 - 15 cm diameter and the first is always smaller than the second. This guarantees that object surface points illuminated by the laser are always in the Field Of View (FOV) of the receiver. The laser beam divergence ranges from 0.3 mrad to 2 mrad and define Instantaneous Field Of View (IFOV) depends on the following factors:

[50] $$IFOV_{diff} = 2.44\frac{\lambda}{A}$$

where A is the transmitting aperture and λ wavelength.

While the airplane moves forwards the laser beam moves across the flight direction in order to obtain area coverage required for surveying.

For a given flying height h, the laser footprint (f) mainly depends on the divergence of the laser beam γ (IFOV), and the swath width (SW) on the scan angle θ (FOV).

[51] $$f = \frac{h}{cos^2(\theta_{ist})}\gamma$$

[52] $$SW = 2h\,tan\left(\frac{\theta}{2}\right)$$

Normal flying heights range from 1 to 3 km.

The scanning mechanism, composed to optical elements, directs a laser beam at known angles, in the direction cross-track relative to the flight direction, allowing the sequential measurements of the ranges and angles to successive points along this line. The acquisition cross-track, while aircraft is travelling along-track, makes possible to determine of ground elevations and of the objects in the scene, for a large swath width.

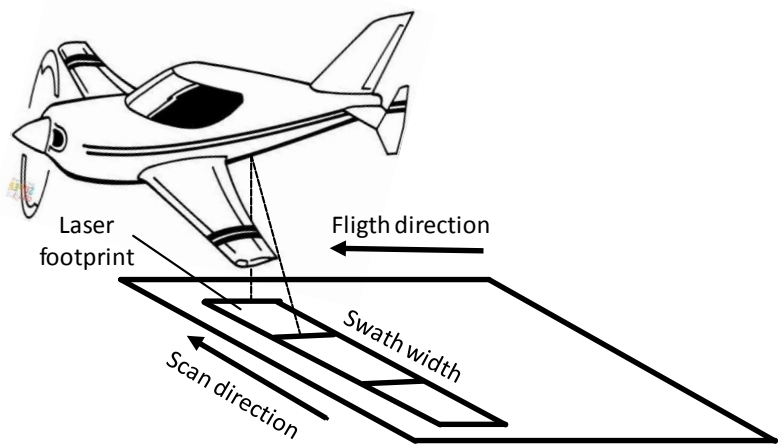

Fig. 16. LiDAR system- airborne and ground segment (Modified by, Wehr, 2008).

The accuracy of ALS system usually ranges from 10 to 30 cm. This variation of the values is due to the great number of parameters that influence in the final accuracy (Baltsavias, 1999) as: laser rangefinder, scanning device, Inertial Measurement System (IMU), GPS and the time offsets. The resolution of a point cloud is controlled by the flying height and the ratio between flying velocity and scanning speed. ALS systems allow the acquisition of a high density of information (1 point per 5 or 10 m^2) over wide areas. In bibliography some basic formulas for the calculation of this parameter are presented (Shan and Toth, 2009).

4.2.2 Terrestrial Laser Scanner (TLS)

When LiDAR is fixed over a ground- based platform, is known as a Terrestrial Laser Scanner (TLS) or ground- based LiDAR. This technology system acquires dense 3D information of the terrain

with high accuracy, high resolution (mm to cm order) and very high data acquisition speeds. The instrument is composed of:

- a transmitter/receiver of infrared laser pulses for distance calculation;
- a scanning device, formed by an internal system of rotating mirrors and rotating instruments.

The TLS technique uses a small laser beam to scan an object under a default solid angle and with a regular scanning pattern. The scan result is a point cloud, which is the 3D digital model of the object scanned, whose position is defined in polar coordinates relative to the centre of the instrument range(r), horizontal (θ) and the vertical (ϕ) angles. The instrument a long range 3D laser scanner of RIEGL LMSZ410-i (Fig. 17), use the time of flight technique and have the following characteristics:

- Distance: 2-1000 m;
- Accuracy: ± 10 mm;
- Scan velocity: maximum 12000 pt/sec;
- Wavelength: near infrared;
- Beam divergence: 0.25 mrad;
- Vertical scan angle: from 0° to 80°;
- Horizontal scan angle: from 0° to 360°.

Fig. 17. 3D laser scanner of RIEGL LMSZ410-i.

The accuracy of this instrument depends on many factors:

- the distance in range, higher the range, lower the accuracy is;
- the reflectivity of the material, lower the reflectivity, lower the accuracy is;
- the surface complexity, a high complexity of the material correspond to a lower accuracy (Abellán et al., 2009);
- the incident angle, higher the obliquity is, lower the accuracy is (Lichti, 2007; Ingensand et al., 2006).

4.2.3 Laser scanning data

The data results is a point cloud consisting of millions of *x*,*y*,*z* points, initially acquired in relation to a reference system corresponding to the centre of the laser instrument. The acquired data had to be edited following some procedures as:

- Alignment and georeferencing;
- Filtering;
- Union.

The first procedure is called "alignment". Often during a laser survey, it is necessary carried out several scans to completely covering the area of interest. Each point could be obtained, initially will be referred to a system of instrumental coordinates and coincides with the position of the laser scanner at the time of acquisition. To obtain a uniform representation, all the point clouds must be roto-traslate in a reference system. The tie-points is the most used technique for alignment. These points don't have ground coordinates known, but are visually recognizable in the overlap area between two or more scans. The alignment operation, performed by applying the Iterative Closest Point algorithm (ICP), requires at least three tie-points simultaneously present in two neighbouring scans.

After the alignment, the scans are transformation from a local reference system into a real world coordinate system, in the georeferencing phase. Georeferencing is usually performed using the DGPS and calibrated using ground control points.

The second operation, the filtering, means the elimination of all the "noise", namely all those points which do not belong to the detected surface. Different procedures for the detection of these not ground points can be used, based on a visual inspection and manual filtering, on

geometrical aspects, on the intensity of returned signal or on the detection of multiple returns. The last operation is the union of all scans in one point cloud.

The 3D coordinates of million points of the ground surface are obtained at the end of these three editing operations. These points can be resampled to obtain more uniform and manageable data.

The final product is a High Resolution DEM (HRDEM) obtained by rasterizing and interpolation the point cloud. Assuming homogeneous point coverage over the study area, the minimum recommended HRDEM cell size *d*, is given by:

$$d = \sqrt{\frac{A}{n}} \quad [53]$$

where *A* is the surface covered by point cloud and *n* is the total number of ground points.

To obtain a DTM can be used in two different procedures: by means of a regular grid or by Triangulated Irregular Network (TIN), a grid of irregular triangular mesh nodes that are able to better describe the trend of natural surfaces.

Main applications of derived HRDEM are focused on detection, mapping, characterization, monitoring and modelling of mass movements such as landslides, debris flows, rock falls and deep-seated gravitational slope deformations (DSGSD).

5. Combining numerical modelling with remote sensing techniques

The aim of this thesis is the combination between monitoring remote sensing data and runout numerical models, to provide landslide hazard assessment. Based on this aim a procedure, comprising two steps, has been designed as shown in Fig. 18.

The numerical models work on the relationship between a set of fixed parameters and a set of variables. A first phase regards model calibration using back analysis to validate the model output results on different necessary parameters as: pre-event topography; event volume; velocity; deposits thickness; runout distance and impact area.

This phase mainly requires the use of monitoring techniques as ALS or TLS LiDAR data. In particular, the HRDEM is useful to create the pre-event topography defining the sliding surface over which the slide flows and it is useful to calculate all geometrics and behavioural parameters for model validation. The rheological parameters are selected through trial-and-error procedure. The outputs of each run are evaluated for all real event characteristics described and the rheological input parameters are adjusted and re-ran the model using an iterative process. The validation procedure was carried out through expert judgement and calculating the quantitative difference between the modelled and observed values. When the outputs were validated is possible to start with forecast event phase.

In forecast analysis the combination between numerical model and monitoring techniques is a fundamental step. The LiDAR data are useful to implement in the model post-event topography and to calculate possible new source thickness. Furthermore, an innovative technique has been developed using GB-InSAR data, especially the cumulative displacement maps, to define new possible events source areas by means of automatic MATLAB code. These source areas are combined with source thickness to find new event source volumes. The numerical model with these two new input data and the rheological parameters found with back analysis is used to simulate future hazard scenarios.

In the following paragraphs, the main methods and techniques used in this thesis to perform the back analysis, forecast analysis and the necessary parameters to validate the model output results are described. The selection of the most appropriate methods depends on the specific case study and on the available data; therefore the applied methods are described in detail in the paragraphs related to the case studies description.

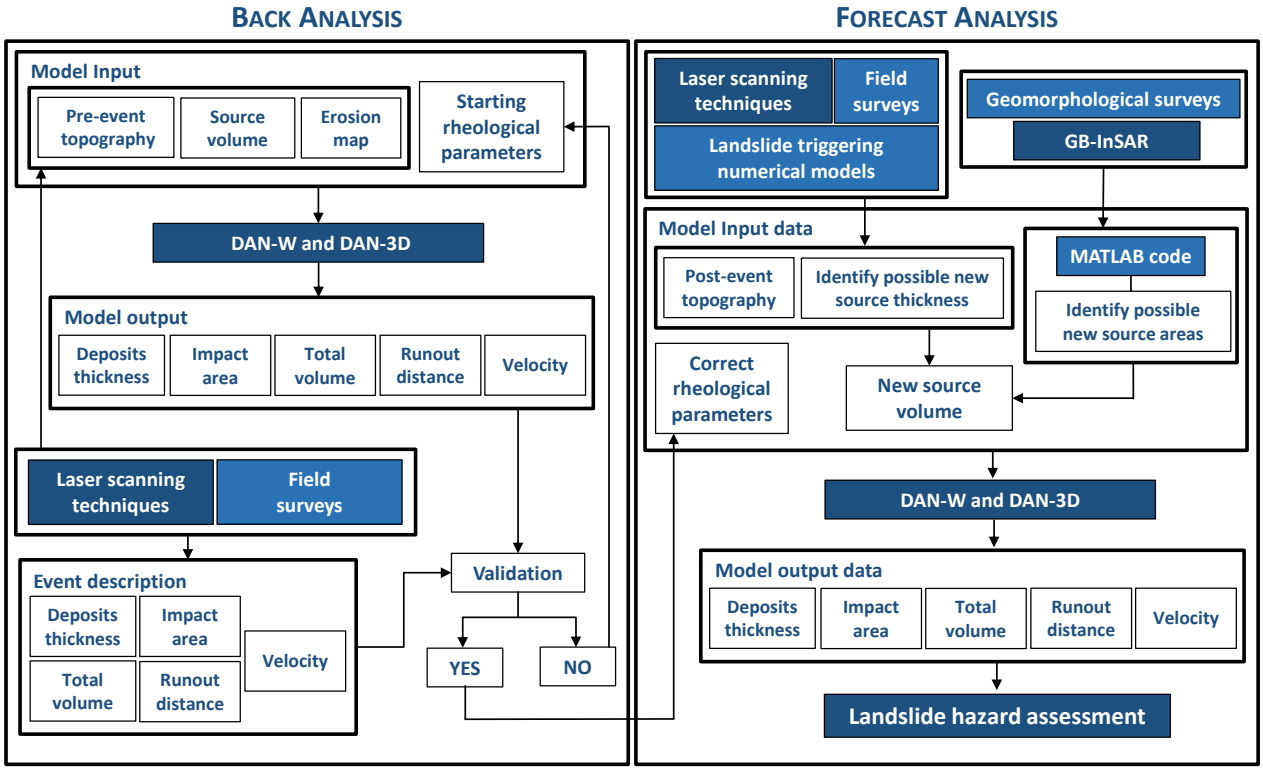

Fig. 18. Shematic approch of new procedure of landslide hazard assessment, the left block concerns the back analysis and its validation to find the better rheological parameters of event, the right block exaplains the forcast analysis starting from the rheological parametres fuond with back analysis and the new methods to find new source area, thickness and volume of possible future events. This procedure take to account the combining of numerical modeling and remote sensing tecnhiques.

5.1 Back Analysis procedure

Before performing forecast modelling of a possible future event, similar historical events must be back analysed to establish a range of applicable model parameters. The back analysis is an important step for the analysis of past events and it is often carried out to improve knowledge on runout dynamic parameters, which may characterize different types of landslides. The fundamental of runout back analysis is the choice of a suitable rheology and its rheological parameters. The higher number of parameters required by a certain rheology is, the grater will be the difficulty of calibrating these parameters (Pirulli and Mangeney, 2008).

For landslide runout numerical models it is important the knowledge of the measurable characteristics of runout as: runout distance, deposits thickness, velocities and time duration of the motion with the identification of the triggering area, the geometry of the source volume, the runout path, the deposit shape.

Back analysis is a process by which the input rheology and rheological parameters are changed using a trial-and-error procedure until to obtain modelled landslide runout results that best represent the propagation in the path and all description parameters of the real event.

However, there are numerous uncertainties in the back analysis approach that can be improved with information combined from all possible sources and experiences.

The most important information, are:

- the better possible geometry of the slope;
- the location and volume of the source area;
- the velocity of mass movement;
- the deposit thickness;
- the runout distance and impact area.

5.1.1 Pre-event and post-event topography

The topography has a fundamental effect on landslide dynamics. The construction period and resolution of the DEM are important issues when testing the accuracy of any terrain-dependent model. A better solution is represented by the new remote sensing techniques, as light detection and ranging (LiDAR), which give the possibility of acquiring 3D information of topography with high spatial resolution and accuracy. Landslide characterization (i.e. landslide magnitudes, conditioning factors such as slope angle, landslide confinement or not….) can be carried out on a HRDEM. The new techniques also lead to time series DEM acquired rapidly. The time series DEM datasets allow the comparison of the topographic relief at different periods and the determination of already fallen source area volume.

Pre- and post-event topography are increasingly instrumental in identifying of landslide event. It is not always possible to get a pre-event DEM but only old contour maps with low spatial resolution, in these cases the best procedure consists in digitalize the contour lines and change them with the recent topographic information from the field investigations (example in paragraph 6.2.8).

The topography effect is an important factor for the numerical runout analysis. The different confinement of the path can change the flow behaviours. For example, on the slope unconfined flow could have or lateral spreading or branching, these phenomena cause the energy dissipation and reducing of the travel distance. In contrast, channelization typically decreases

the slope angles at which landslides begin to deposit and increases their travel distance (Hungr et al., 1984).

It is important that the simulation of an event should be based on a reasonably accurate representation of the topography on which the landslide event occurred. For this reason, the DEM must be modified for modelling.

If pre- and post-event topography are available, it is possible to calculate the real event source thickness by subtracting the post from the pre-event DEM. To obtain the topography file for numerical simulation it is necessary to subtracted from the pre-event path the thickness of the landslide event source area (as example in paragraphs 6.1, 6.2 and 6.4). If only the contour map is available it is possible to use the digitalized file as topography path (as example in paragraph 6.3).

The depth-integrated dynamics models such as DAN-3D usually may not work correctly with a path grid that is excessively detailed and rough. Sudden redirections due to abrupt changes in slope angle or orientation, even by minor surface irregularities, result in momentum and energy losses. The better solution is use a smooth grid with one or two cycles of Gaussian smoothing (McDougall, 2006).

5.1.2 Volume

The landslide volume is one of the most important parameters for the evaluation of: the landslide deposits, the erosion rate, the morphological evolution of the slope and the potential hazard. The volume of landslides determination is not simple; the problem requires the availability of information on shallow and deep landslides geometry.

It is important to make a clear distinction between the landslide source volume and the landslide total volume as result of landslide runout and erosion along the path. While the first one is a main input data for DAN-W and DAN-3D numerical models, the second is important parameter for the model results calibration.

In this work the landslide source volume as an input data for the back analysis was calculated using the LiDAR data, were they are available. In particular, the difference between pre- and post-event DTMs allows us to identify the source area and to establish the landslide source volume (example in paragraph 6.2). In other cases, where the per- and post-event LiDAR data are not available, the source volume was chosen through field investigation, considering the behaviours and thicknesses of deposits (example in paragraphs 6.1, 6.3 and 6.4).

The landslide total volume was found considering the difference between post and pre-event DTMs, in this case if the total volume was different from start volume, the erosion rate was calculated. The total volume was estimated by adding the volume of soil in the deposit area and the volume of scoured material. Both values were calculated by combining the measured thickness and the area of the failed/scoured portion, assessed through field survey, DEM analysis.

When the source volume and total volume was not evaluable with precision a different empirical approaches, to estimate the volume were needed (example in paragraph 6.3).

Famous method to estimate the landslide source volume is based on landslide dimensions; *The International Geotechnical Societies UNESCO Working Party on World Landslide Inventory (*WP/WLI, 1990) for example has suggested this equation for the volume calculation:

[54] $$V = \frac{1}{4}\left(\frac{3}{4} p D_d \frac{W_d}{2} \frac{L_d}{2}\right)$$

the volume is calculated approximating the source area to a quarter of an ellipsoid and measuring the size: Wd_2 is the maximum width of the mass moved measured perpendicular to the its length L_d measured at the distance between the summit point and the lower point of the mass moved and D_d is the maximum depth of the failure surface. The parameters Wd_2 and L_d could be obtained graphically on the maps, while D_d could be obtained from geognostic surveys or triggering numerical model simulations.

5.1.3 Velocity

In order to describe the shallow rapid landslide behaviour another important parameter is the velocity. Most of the equations for the velocity are based on empirical data of mean flow parameters of prototype flows or measured velocity profiles in laboratory flows, in which simplified material mixtures have been used to simulate debris flows (Rikenmann, 1999).

The main approaches to predict the landslide velocity are three, based on: the experience and precedents events, empirical equations and analytical methods. The first one depends on material properties, motion mechanisms and characteristics of the path. For example some lithologies are expected to produce extremely rapid movements and in many case steep slopes help to the acceleration of the movements.

The main empirical methods, used in this thesis, are described below. These may represent a useful instrument to calculate the velocity to validate the numerical model simulation results.

Most equations available in literature estimate the mean translation velocity of the frontal part or the maximum (mean cross-sectional) velocity along the debris flow surge (Hungr et al. 1984) as:

- the back-calculation method of Forced Vortex Equation for superelevation, which requires an estimate of the bend's radius of curvature (Chow 1959; Hungr et al. 1984; Revellino et al. 2004; Zanchetta et al. 2004; Prochaska et al. 2008):

[55] $$v = \left(\frac{gR_c\Delta h}{w}\right)^{0.5}$$

where *g* is the acceleration of gravity, Δh is the superelevation of the debris wave in the channel bends, *w* is the channel width and R_c is the curvature radius. The radius of curvature can be calculated in the field using the relation between the two cross-section arc lengths and their angular (azimuth) difference or taken from the topographic map (example in paragraphs 6.2 and 6.3);

- the Johnson and Rondine (1984) relationship, another superlevation method, based on the difference of the splash heights on the internal and the external side of the bends of the flow path (Nocentini et al. (2015):

[56] $$v = \sqrt{gR_c \cos\delta \tan\beta}$$

were β is the angle between the line connecting the top of the deposits in both bend sides and the horizontal line, δ is the slope angle of the flow path, R_c is the curvature radius of the channel, and *g* is the gravity acceleration (example in paragraph 6.3);

- the Poiseuille equation that enables connection between the velocity of the flow to the gradient and geometry of a channel and to the dynamic viscosity and unit weight of the debris flow:

[57] $$v = \frac{\gamma \sin\delta H^2}{l\,\upsilon}$$

where γ is the unit weight of the debris mass of landslides, δ is the channel slope, *H* is the flow depth, *l* is a constant based on the cross-sectional shape of the channel and ν the flow viscosity (example in paragraph 6.2);

- the method of velocity prediction, based on the maximum discharge (Rickenmann 1999, Zanchetta et al. 2004):

[58] $v = 2.1{Q_p}^{0.33}S^{0.33}$

where Q_p is the maximum discharge, S is the channel bed slope (example in paragraph 6.2).

5.1.4 Deposits thickness

Important parameter for back analysis validation is the knowledge of deposits thickness along the travel path. This information can be obtained by means of LiDAR HRDEMs data or by field survey.

The LiDAR surveys carried out before and after the event can be used to calculate the event magnitude, the deposit thickness and distribution of materials along the path, by simply subtracting the two topographic surfaces. Thanks to this technique it is possible to draw cross sections across the landslide body, with thickness representation that can be used as control points on simulated landslide deposits thickness (example in paragraph 6.2). The reconstruction of local deposit thickness can be estimated with field investigation and explorative borehole surveys (example in 6.1, 6.3, and 6.4). The field investigation is the decisive part of a study of landslides and landslide-prone areas, to define features and environmental factors involved in an existing slide and to identify areas subject to sliding when future construction is being planned as discussed below.

5.1.5 Runout distance and impact area

Runout distance is an important factor to know the potentially affected areas, which are essential elements for producing hazard maps (Petrasscheck and Kienholz, 2003).

As just described in paragraph 3.1, the geometrical characteristics of the landslide as the vertical height (*H*) and horizontal length (*L*), allow evaluating some important mobility parameters as fahrboschung angle (Heim, 1932) or the travel angle. Other methods use the area (*A*) and the volume (*V*) to forecast new events. All these parameters are simple to calculate and can be a useful method to compare the results of the runout modelling analysis with the field investigation (example in paragraph 6.1).

If pre- and post-event DEM or/and the field information are available, it is possible to know the exact runout distance of the past event and use this information as a further parameters to validate the back analysis results (example in paragraphs 6.2, 6.3 and 6.4).

5.2 Forecast analysis procedure

Predicting the spatial occurrence and runout of landslides represents an important scientific and operational issue due to the high threat that they pose to human life and property. The forecast analysis can be applied when information of the past event is available and it is reasonable to assume that some aspects of the past behaviors will recur into the future.

The post-event DEM and the possible new area, source thickness and volume are fed into the new model for forward modelling runout distribution and intensity. Increased use of accurate prediction for landslide runout and anticipated intensity, would lead to improved mitigation, reduced risk and a decrease in the loss of life associated with landslides. The forecast analysis is the second part of the procedure described in this thesis. The main difficult to forecast new possible events is the identification of new source areas and volumes.

In this work some methods are proposed using the remote sensing instruments and advanced numerical models. These methods will be described in detail for each case study, according to available data.

5.2.1 Possible new source areas

To obtain a good forecast event it is important to establish a new source area to assess the risk scenarios. A more common method is based on the field surveys. Geomorphology assessments enable to identify the past and present landslide processes and through which it is possible to establish new possible areas at risk of landslides.

To identify possible new source areas we decide to use an innovative technique using the GB-InSAR monitoring data, where these were available. The best radar data for this type of analysis are the cumulative displacement maps, where the cumulative movements are represented from the beginning of the sequence.

In order to automatically extract from radar displacement maps, the areas affected by movements higher than a selected threshold value, a MATLAB code was developed during PhD course.

After loading the cumulative displacement maps the code calculates the maximum cumulative displacement (calculated in the direction of the radar, negative values) for each map and use the minimum value found among them as a threshold. The result is the same number of displacement maps used in input but representing only the areas with significant movements.

The second operation of MATLAB code consists in the calculation of maps of the frequency of displacement occurrence, the code computes how many times each pixel has recorded a significant displacement during the monitoring period. The scheme of the MATLAB code routine is shows in Fig. 19.

The extracted areas were overlapped and compared in an ArcGIS™ and Golden Software SURFER™ environment in order to obtain the new critical sectors, which could be the potential source areas of future possible events, in a format compatible with DAN-3D.

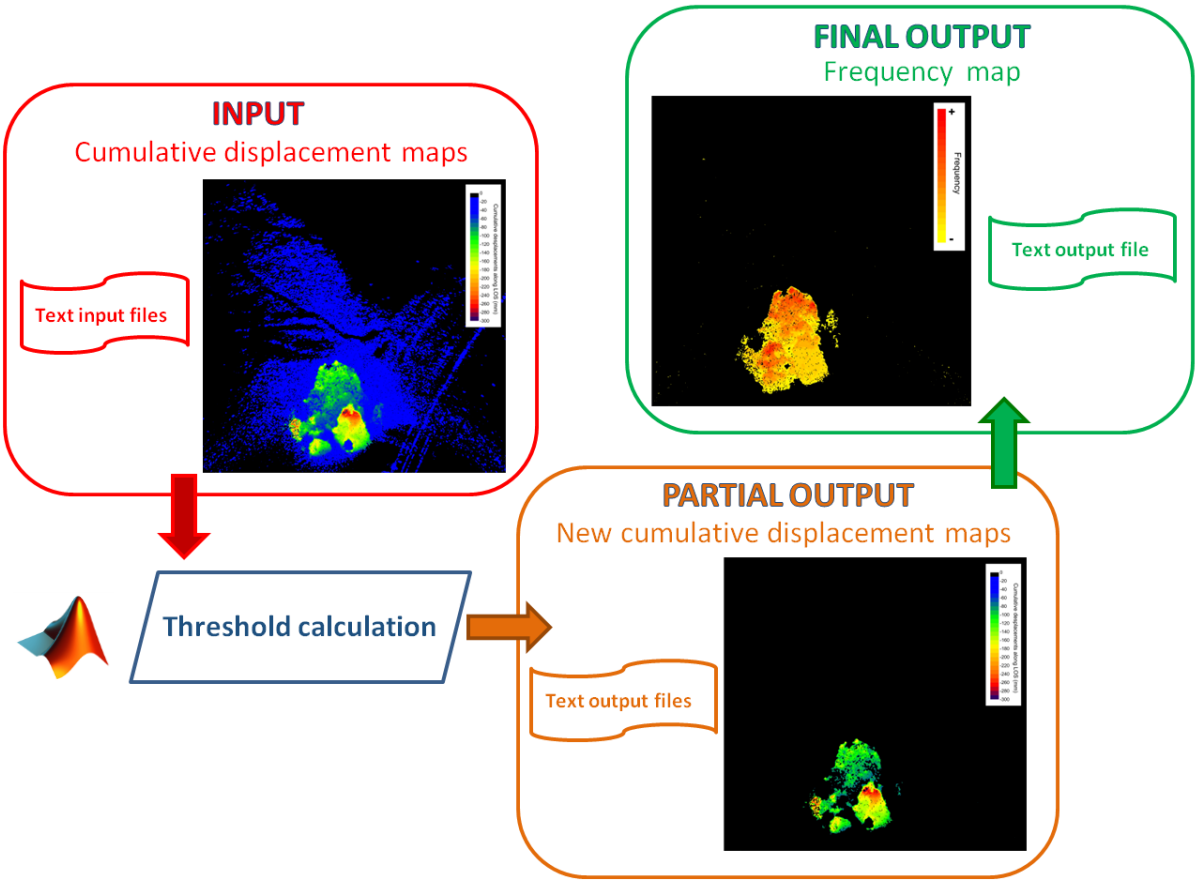

Fig. 19. Schematic approach of MATLAT code rutine.

5.2.2 Possible new source thickness and volume

An important parameter for the forecast analysis is the new source thickness, which applied in the area found from MATLAB code provides a new volume, of a possible future event. In this thesis the new source thickness determination was carried out following three methods:

- based on field investigation;
- based on the pre-event experience;
- based on the landslide triggering numerical models.

The field investigation is usually necessary in the study of landslide. In addition to the field geological surveys with an analysis of geometric behaviours of the landslide, a valuable support to evaluate material thicknesses could also be the geognostic surveys (example in paragraph 6.3).

The second method may be applied if the source deposits of the new event have the same emplacement of the old deposits. In this case it is possible to use the same thickness of the past event. With the pre- and post-DEMs available it is possible to carry out a statistical analysis on the deposits thickness using the data from difference of DEMs. The method considered the deposits thickness frequency distribution by a histogram, then it is possible to use the minimum, maximum and average thickness values of the pre-event source deposits (Fig. 20) (example in paragraphs 6.2, 6.3 and 6.4).

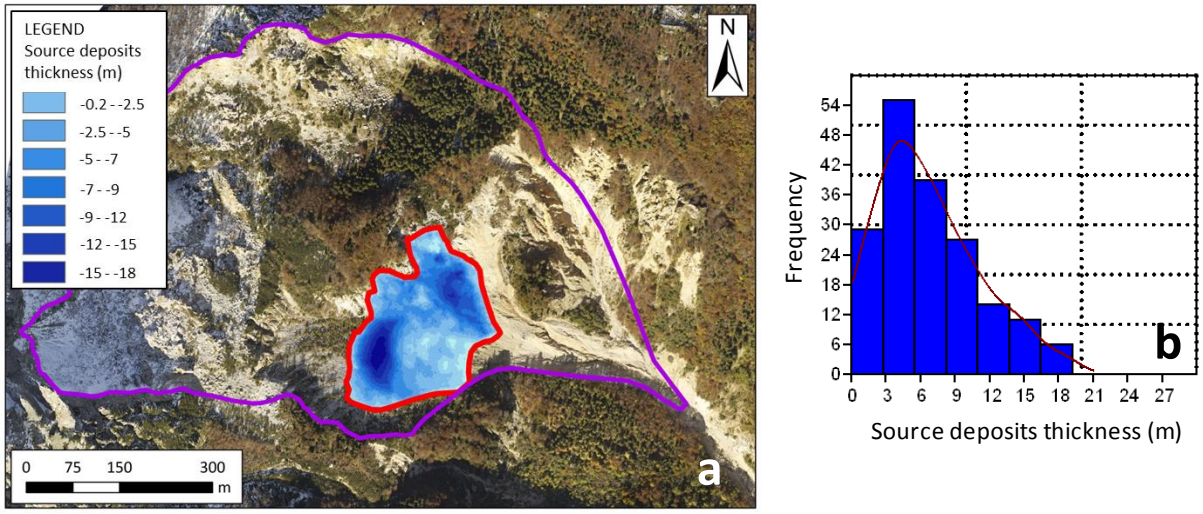

Fig. 20. a) deposits thikness by difference of DEMs, b) histogram of source thickness frequency.

The last method uses the landslide triggering numerical models (for example Fast Lagrangian Analysis of Continua, FLAC, ITASCA, 2005 or the three-dimensional methods of columns approach) to calculate the failure surface depth. Slope stability modelling adopting a continuum approach (Stead et al., 2006) can be performed to help constrain the mobilized volume used in the runout analysis. This approach requires that the rapture surface location and shape are modelled as a function of the shear stress distribution in the slope and resulting elasto-plastic yielding of elements (Eberhardt et al. 2004) (example in paragraph 6.4).

5.2.3 Runout prediction

The run out prediction is a method that can be used to compare the simulated results of forecast analysis. There are several empirical methods which connect use the geometric parameters of characterization of landslides, for example In Hungr et al., (1984), Iverson et al. (1988), Corominas (1996), Rickenmann (1999), Hunter and Fell (2003), Crosta et al. (2003) etc., to calibrate the numerical model results of back analysis (example in paragraph 6.3).

As show the work of Rikenmann (2005), the runout prediction methods can be divided in three major categories: methods based on total travel distance (entire path length), methods based on the runout length (indicate the depositional part of flow) and methods based on runout distance (entire path or depositional part of flow).

One of the most famous relations is to Corominas (1996) which examined the mobility for a given landslide volume and developed an empirical equation:

$$[59] \quad Log\frac{H}{L} = BlogV + A$$

where *A* and *B* are constant dependent on the type of landslide. The Corominas (1996) analysis result is show in the Fig. 21a. From general trend is possible note that increasing the volume the ratio *H/L* decreases, but for the data with small volume landslide there is a considerable scatter. In fact, no correlation exists between *H/L* and volume for the confined landslide of less than 1 million cubic meters, and for the unconfined landslide.

Considering the data of Ricknemann (1999) from a regression analysis which includes 160 debris flow from 300 t0 12,600 m, *V* from $7x10^2$ to 10^6 m^3 and *H* from 110 to 1.820 m data (Fig. 21):

$$[60] \quad L = 1.9V^{0.16}H^{0.83}$$

The results are show in Fig. 21b, in this graph is represented also the rock avalanches that have a similar trend with shorter travel distances.

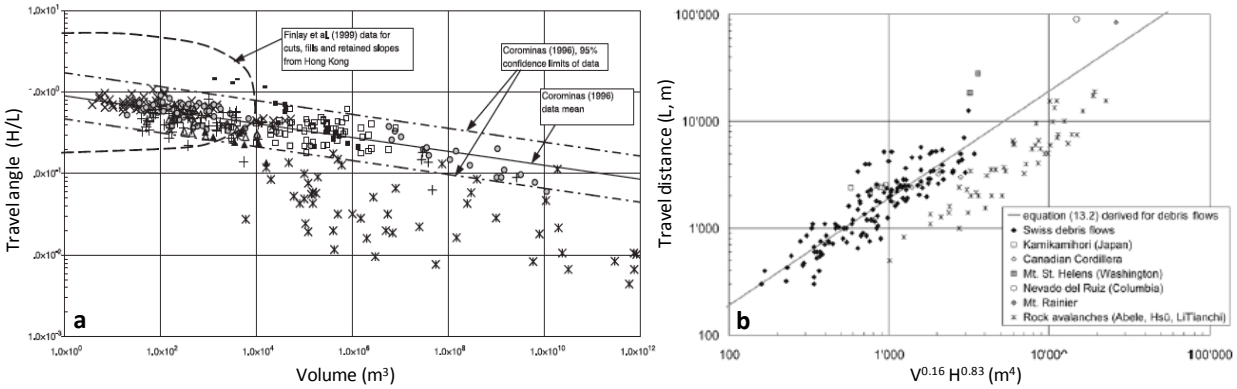

Fig. 21. a) Travel angle vs Volume (Hunter and Fell,2003) b) observed runout distance from data source of Rickenmann 1999.

Another interest relationship to find the total travel distance was proposed by Hutter and Fell (2003), which considers the slide in colluvial and residual soil, classifying as silty sands and sandy silts with gravel and boulders. Hutter and Fell (2003) equations correlate the travel distance angle *H/L* with downslope angle α_2, considering three classes of confinement degree:

[61] $$\frac{H}{L} = 0.77 tan\alpha_2 + 0.087$$

[62] $$\frac{H}{L} = 0.69 tan\alpha_2 + 0.086$$

[63] $$\frac{H}{L} = 0.54 tan\alpha_2 + 0.147$$

the equation [61] is for unconfined landslide with a standard error of *SE*=0.095 and an angular coefficient r^2=0.71, the equation [62] is for partly confined landslide with a *SE*=0.11 and r^2=0.52, the last equation [63] is for confined landslide with a *SE*=0.027 and r^2=0.85 (Fig. 22).

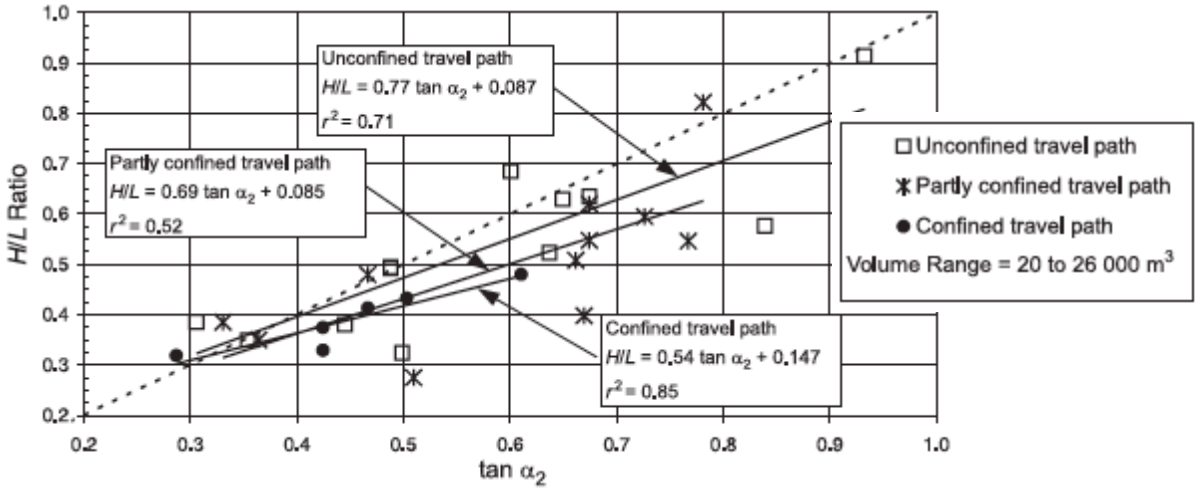

Fig. 22. *H/L* versus tangent of the downslope angle below the source area, α_2.

The volumes considered range from 20 to 26000 m^3. The results show that the difference of the cases around the trend line, are not dependent on the slide volume. The main conclusion are that the landslides with small volumes in unconfined path deposit the debris along the entire travel, regardless of the downslope angle, while landslides with large volumes, in the same path, move for significant distance. The landslides along confined path move long distance than landslides in unconfined path, due to the entrainment and water within the flow. The causes of the flow stop are mainly the obstructions along the travel of the slide and the flow behaviour, water content and entrainment (Hutter and Fell, 2003).

These methods may be applied in preliminary hazard assessments and they may be comparing with dynamic analysis results (example in paragraph 6.3).

6. Case studies

The procedure described in chapter 5 was applied to four case studies: Stromboli volcano gravity-induced Pyroclastic Density Currents (gi-PDC), Monte Rotolon debris flow, Gessi-Mazzalasino landslide and Santa Trada landslide.

All case studies analyzed in this thesis represent a different type of rapid shallow landslides, with several failure and runout mechanisms analyzed with different remote sensing techniques.

A full landslide description was included assessing all available data, including pre- and post-event topography, runout distance, deposits thickness, flow velocity, source volume, total volume and impact area. Descriptions preferably include the use of LiDAR data and field investigation, when this data were not available the literature description was used.

In all case studies a back analysis was carried out ranging the input rheology parameters for a landslide model until the modelled landslide runout (the output) is judged to be an adequate representation of the described runout. After the rheology parameters were used for forecast analysis with the aid of input parameters found with the remote sensing techniques integration and additional observation on geomorphological field investigation.

6.1 Stromboli gravity-induced Pyroclastic Density Currents (giPDCs)

Stromboli is the northernmost volcanic island of the Aeolian archipelago, in the southern Tyrrhenian Sea. The island is the subaerial part of a rather regular volcanic edifice that rises to 924 m above sea level (a.s.l.) from a base that lies at a water depth between 1300 and 2300 m. Volcanic activity on Stromboli has been continuous since the III–VII centuries A.D. and consists of mild- to low-energy intermittent explosions (Strombolian activity), which are occasionally interrupted by effusive events and violent explosions that are commonly called paroxysms (Barberi et al., 1993; Rosi et al., 2000). The active vents are located in the crater terrace at approximately 750 m a.s.l. on the upper part of the Sciara del Fuoco (SdF), which is a horseshoe-shaped depression on the NW uninhabited flank of the volcano (Fig. 23).

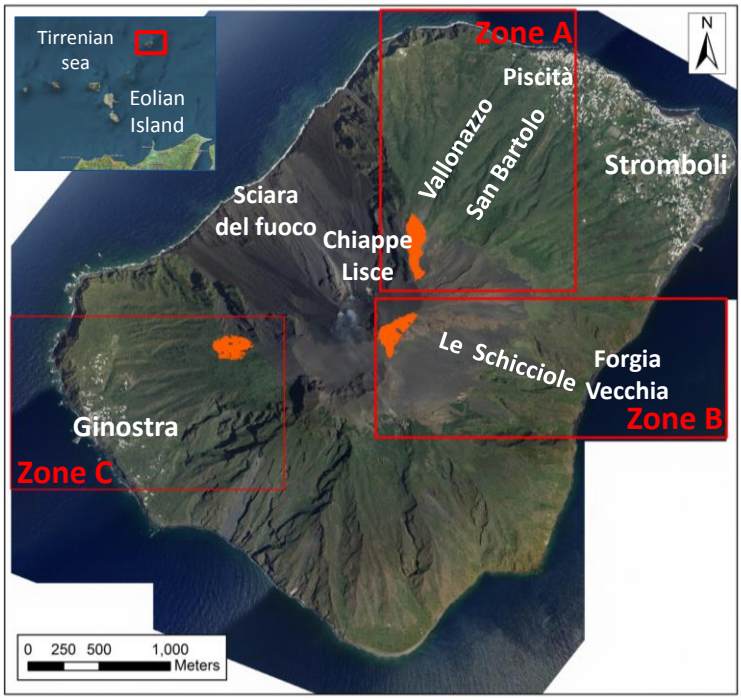

Fig. 23. Orthoimage of the study area, Stromboli volcano with the primary toponyms (from the QuickBird Satellite Sensor). The three red rectangular areas cover the volcanic sectors involved in the gravity-induced PDCs of 1930 (zone A), 1944 (zone B) and 1906 (zone C). These zones were used for numerical modelling with DAN-3D. The source areas of the three events are shown by orange.

The formation of gravity-induced Pyroclastic flows has been reported several times. The flows occurred as a direct result of explosive and effusive volcanic activities such as those on 6 December 1985, (De Fino et al., 1988), 5 April 2003, (Rosi et al., 2006, 2013; Pistolesi et al., 2008) and 12 January 2013 (Di Traglia et al., 2014; Calvari et al., 2016) or of the sliding of incandescent pyroclastic fall deposits accumulated over steep slopes such as during the 1930 and 1944 paroxysms (Di Roberto et al., 2014) and the eruptive activity of 28 and 29 December 2002 (Pioli et al., 2008). Gravity-induced PDCs usually occur in the SdF depression and therefore do not represent a serious threat to the population of Stromboli (Barberi et al., 1993; Rosi et al., 2013). However, in 1906, 1930 and 1944, gravity-induced PDCs occurred outside the SdF, and in the latter two cases they reached the coast of the island. In particular, the 1930 PDCs reached the village of Stromboli on the NE part of the island, causing extensive damage and four casualties (Rittmann, 1931). These phenomena begins with instability in the lower part of the slope on which material accumulates which results in a remobilization of the deposited material in a landslide. This mechanism for generating gravity-induced PDCs is consistent with the model proposed by Ui et al. (1999) and Takahashi and Tsujimoto (2000) for the dome collapse-induced

block and ash flows (Merapi-type) during the 1991–1995 eruption of Unzen Volcano, Japan. Failures of crater-rims or pyroclastic piles develop into rockslides, dry gravel/debris flows or avalanches (Hazlett et al., 1991; Cole et al., 2005; Di Traglia et al., 2014), which have been described as the "extremely rapid, massive, flow-like motion of fragmented rock from a large rock slide or rock fall" (Hungr et al., 2014). Rockslides attain a degree of mobility that far exceeds what would be expected from a frictional flow of dry, angular, broken rock, and the mobility is increased with the volume of an event (Heim, 1932; Hayashi and Self, 1992; Dade and Huppert, 1998; Calder et al., 1999).

6.1.1 Events descriptions

The event of gravity-induced PDCs during the 1930 paroxysm was described by Rittmann (1931) and Abbruzzese (1935). Rittmann (1931) reports that the event was triggered by the sliding of an approximately 1 m-thick source deposit with an estimated volume of at least 45000 m^3 and consisting of metre-sized spatters, decimetre-sized bombs, lapilli, and ash. The deposit had accumulated over an area of more than 60000 m^2 on the steep cliff side of Chiappe Lisce during an extremely violent paroxysm (Bertagnini et al., 2011) channeling inside the Vallonazzo valley reaching a speed of 15-20 m/s. Rittmann(1931) racounts also that the chanbeled flow in the Vallonazzo reached the shore close to Piscità village while a second flow was stopped by topographic barriers in the top most part of the volcano. Vice versa, the historical accounts and field data (Abbruzzese, 1935) revealed that during the 1930 event "… flows of incandescent material were sliding into the S. Bartolo and Piscità (Vallonazzo) valleys. The first one stopped within tens of metres from the church of S. Bartolo (where the slope change from 25° to 15°), whereas the second one reached the sea".

The most complete outcrop of the 1930 PDC occurs at the opening of the S. Bartolo Valley, at approximately 420 m a.s.l. The thickness of the PDC deposits there is >4.5 m, and the base is not exposed. The deposit rapidly thins downslope, and 75 m away from the main outcrop it is ca. 2 m-thick. This order of magnitude of the thickness (approximately 1.5 m) remains to the end of the Vallonazzo where the PDC stopped (Fig. 24).

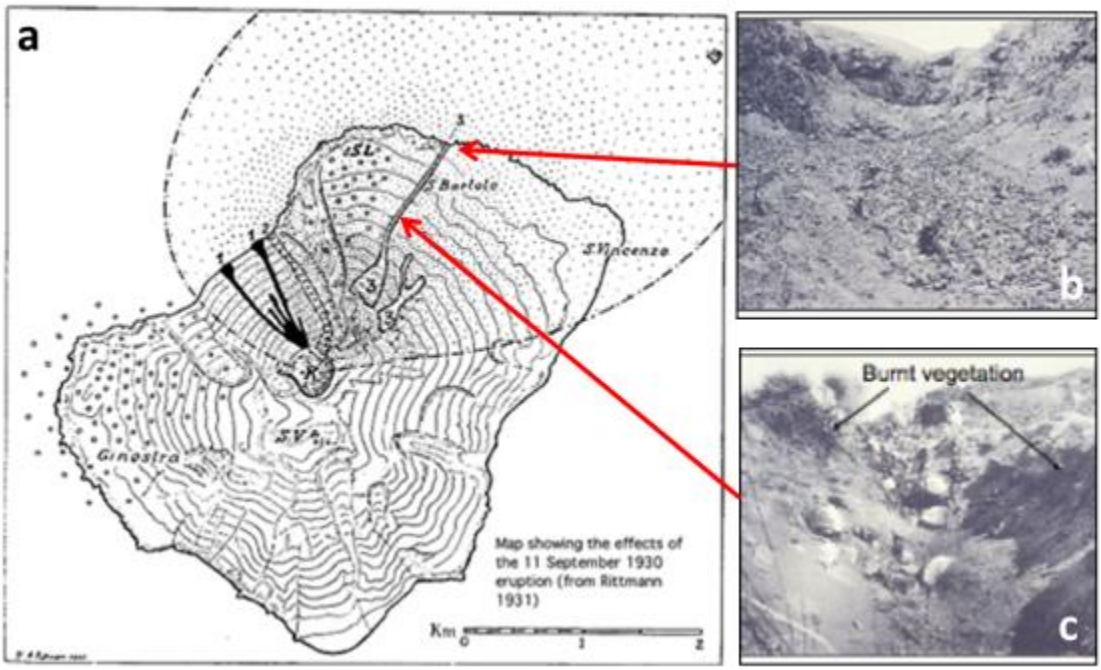

Fig. 24. a) The paths of the 1930 PDC as reportet by Rittmann (1931), b) gi-PDCs deposits in the Vallonazzo valley near the sea, c) gi-PDCs deposits in the middle of Vallonazzo valley.

The Little information was reported on the PDCs on 15 July 1906 and 20 August 1944. Riccò (1907) reported that during the late afternoon of 15 July 1906 a very large eruption of incandescent material hit the area of Forgia Vecchia on the ESE side of the island and was preceded by a loud and long-lasting rumble. A column of incandescent material flowed in the direction of the village of Ginostra, WSW from the vent, burning the vegetation. Similarly, Ponte (1948) described that on 20 August 1944 a large amount of incandescent material consisting of large blocks and ash that had accumulated on the summit of the volcano and on the Forgia Vecchia flowed downslope, reached the shore and formed a ca. 100-m-long delta in the sea. The delta was rapidly eroded by the action of sea waves.

6.1.2 Model calibration

Simulations were performed on three areas corresponding to those affected by the gravity-induced PDCs of 1930 (zone A), 1944 (zone B) and the area possibly affected in the 1906 event (zone C). Zone A was used as a test area because information on the distributions and thickness of deposits, the velocity of the 1930 glowing avalanche, the event duration and the total travel distance are known from the literature (Rittmann, 1931; Abbruzzese, 1935; Di Roberto et al., 2014). The materials involved in 1906 and 1944 gravity-induced PDCs were assumed to be

similar to that of 1930 (for example, see Bertagnini et al., 2011). Thus, the parameters obtained for zone A were used to calibrate the model by back-analysis and to find the input rheological parameters that were later applied to the simulations in zones B and C. The main characteristics of the three events under consideration are shown in Table 7.

Table 7. Table xx: Main characteristics of the three events. Zones A, B, and C are from Rittmann (1931), Abbruzzese (1935) and Di Roberto et al. (2014).

	Zone A	Zone B	Zone C
Eruption	1930	1944	1906
Date	Sept 11	Jun 15 (uncertain)	Aug 20
Area of interest	NE flank	WSW flank	ESE flank
Source elevation (m a.s.l.)	790	920	600
Volume source (m^3)	42000	35000	33000
Entrainment (Mm^3)	Unspecified	Unspecified	Unspecified
Travel distance (km)	1.6	1.5	-
Thickness (m)	0.1–4	0.1–0.6	-
Velocity ($m\ s^{-1}$)	15–20	-	-
H/*L* (height/run out distance)	<0.4	<0.5	-

The modelling was performed on a high resolution (50 cm) Digital Elevation Model (DEM) of the current volcanic flank. The DEM was obtained by elaborating the 3D data (8 points m^{-2}) acquired during the airborne laser scanning survey on 04 May 2012 to 18 May 2012 carried out by the BLOM Compagnia Generale Ripreseaeree S.P.A. (www.blomasa.com). The construction period and resolution of the DEM are important issues when testing the accuracy of any terrain-dependent model, and, in this case, the exact reconstruction of the pre-event topography is difficult. We used the current topography assuming that it well approximates the topography before the avalanche. Most of the materials deposited by the pyroclastic flow have been eroded, and only limited portions are preserved in sheltered areas, and, therefore, the topography is largely unchanged compared to that of 1930. Because DAN-3D does not work correctly with path grids that are excessively detailed, the path grid file was resampled to a

spatial resolution of 5 m and repeatedly filtered using Gaussian smoothing (3×3), the excessive roughness cause an a decrease in the mobility of the model landslide (McDougall, 2006). The use of the Smoothed Particle Hydrodynamics (SPH) numerical technique allowed the slide materials to spread, branch and join without problems due to the mesh and flow boundaries (McDougall and Hungr, 2003). The area where accumulations of spatter and fallout deposits were observed (Rittmann, 1931) was assumed to be the source area of the 1930 gravity-induced PDC, whereas for the 1906 and 1944 eruptions, the source areas were identified as the regions upslope of the flow path where the slope exceeds 29° (Di Roberto et al., 2014). This value is usually assumed to be the lowermost value of the angle of repose for dry pyroclastic deposits (Apuani et al., 2005b; Miyabuchi et al., 2005). The initial value of 1 m for the thickness of the sliding material was defined according to the observations by Rittmann (1931) regarding the material accumulated on the summit of the volcano shortly before the 1930 PDC. The value was then applied to the other two events. The source volumes reconstructed using those areas and material thicknesses are reported in Table 7. Erosion was not considered because a very low degree of substrate erosion and entrainment was observed in the field and defined by a sedimentological study of the 1930 event deposits (Di Roberto et al., 2014). Because DAN-3D does not implement a routine for automatically stopping the simulation, we decided to interrupt the simulation when the flow reached sea level. If the flow never reached the coastline, the simulation was manually stopped when the flow velocity decreased to zero.

Afterwards, the same analysis were used in DAN-W. In 2D dimension the simulation automatically stops when the flow arrives at the end of the established path profile or when the mass stops. The topographic and geometrical input data (path and top files) were directly extrapolated by the results obtained with DAN-3D. The channel width was calculated on DEM. In fact, the 2D analysis was performed along profiles representing the lines connecting the source regions with the most distal extension of the deposits previously modeled with the 3D tool. For the zone A two separate models were performed along the two principal line of flow described by Abruzzese (1935): one in Vallonazzo valley and the other in San Bartolo valley. For the zone B and zone C the models were executed along the main flow path.

6.1.3 Back analysis results

In accordance with the failure mechanism and motion of the Stromboli PDCs, the suitability of the DAN-W and DAN-3D depth-averaged numerical codes (Hungr, 1995; McDougall and Hungr, 2004; Hungr and McDougall, 2009) was tested. The simulations relative to the 1930 PDC were performed with Voellmy rheologie by a trial-and-error procedure (Morelli et al., 2010; Sosio et al., 2012a, b). This method was used to obtain values of the runout, velocity, and duration of the flow that will match those derived from the literature and the available field data. The simulation that best reproduced the path, extension, and thickness order of magnitude of the 1930 gravity-induced PDC deposit (zone A) was obtained using a Voellmy rheological model with a frictional coefficient of f = 0.19, a turbulence parameter ξ = 1000 m s^{-2}, a unit weight of 14.71 and an internal friction angle of ϕ_i = 20° (Apuani et al., 2005b). Simulations using the Voellmy rheological model displayed a strong topographic control, which allowed the 1930-like gravity-induced PDCs to flow inside the Vallonazzo valley with little overbank deposition. The simulation using the Voellmy rheological model was able to reproduce the two main gravity-induced PDCs reported in the literature (Rittmann, 1931; Abbruzzese, 1935; Di Roberto et al., 2014); the first flow extended along the Vallonazzo valley and reached the sea close to Piscità after 135 s, and the second flow moved in the San Bartolo valley and stopped near the church of San Bartolo after approximately 120 s. The Voellmy rheological model also simulated the 1930 PDC deposits' thicknesses, matching the order of magnitude of those measured in the field by Di Roberto et al. (2014). At approximately 418 m a.s.l. in the San Bartolo valley (Site 1 of Di Roberto et al., 2014) the measured thickness was approximately 4.5 m, and the simulated thickness was 1.6 m. In the NE rim of the Vallonazzo valley, at approximately 370 m a.s.l. (Site 2 of Di Roberto et al., 2014), the measured and simulated thicknesses were comparable and had accuracies of 30–40 cm, whereas close to the outlet of Vallonazzo valley (Site 3 of Di Roberto et al., 2014), the measured thickness was approximately 100 cm, and the simulated thickness was 60 cm. The areas hit by the gravity-induced PDC and covered by the deposit were 3.6×10^5 and 0.8×10^5 m^2, respectively (Fig. 25a). The outcomes of DAN-W code along the considered sections in Vallonazzo valley and in San Bartolo valley show a good correspondence with the 3D simulation (Fig. 25b, c).

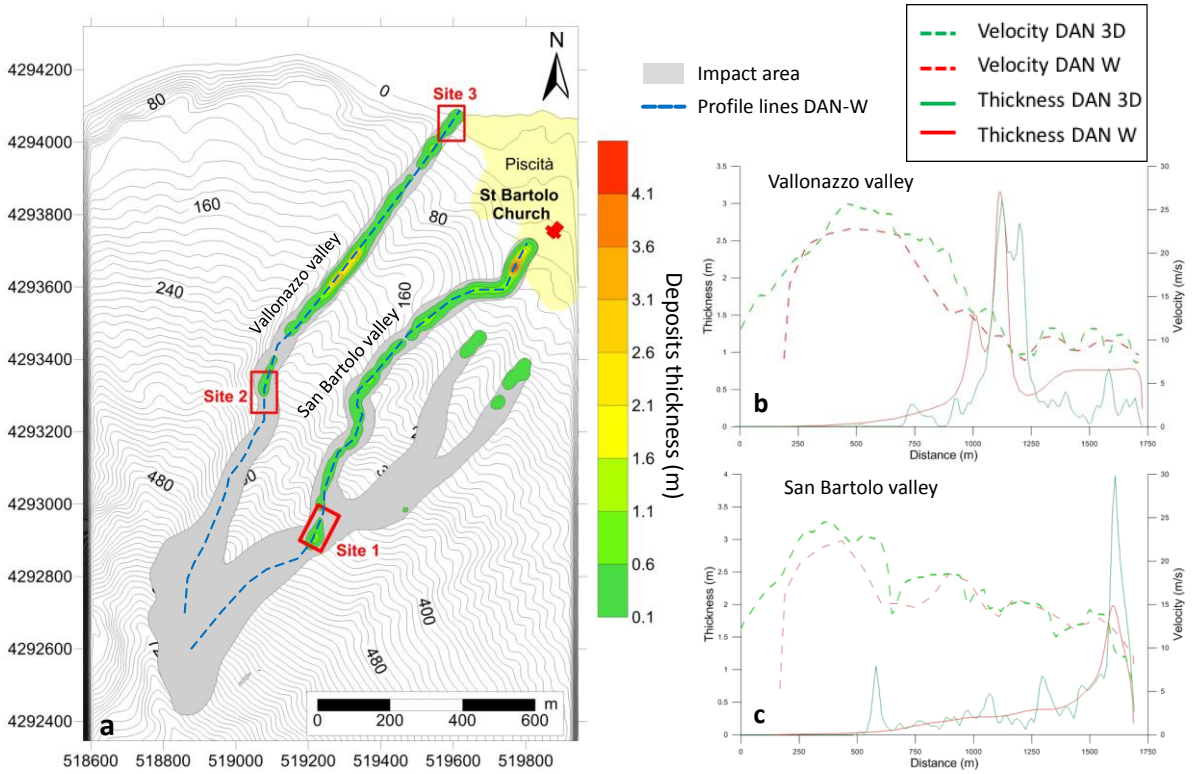

Fig. 25. Results of DAN-3D simulation of a) deposit thickness for the zone A (1930-like event); comparison between the DAN-W and DAN-3D for the b) Vallonazzo and c) San Bartolo valleys.

The rheological parameters obtained using this procedure for the 1930 PDC were then used in the simulation of the gravity-induced PDCs events in zones B (in 1944) and C (in 1906).

The results for zone B show that the flow moved into the "Le Schicciole" valley (Forgia Vecchia) and reached the sea in 88 s. In this case, the simulated deposit thickness of 60 cm matched the field measurement (Di Roberto et al., 2014). The areas impacted by the PDC and covered by the deposit in zone B were 3.1×10^5 and 0.8×10^5 m^2, respectively (Fig. 26a). Also in this case, DAN-W results show a very good correlation with the DAN-3D simulations (Fig. 26b).

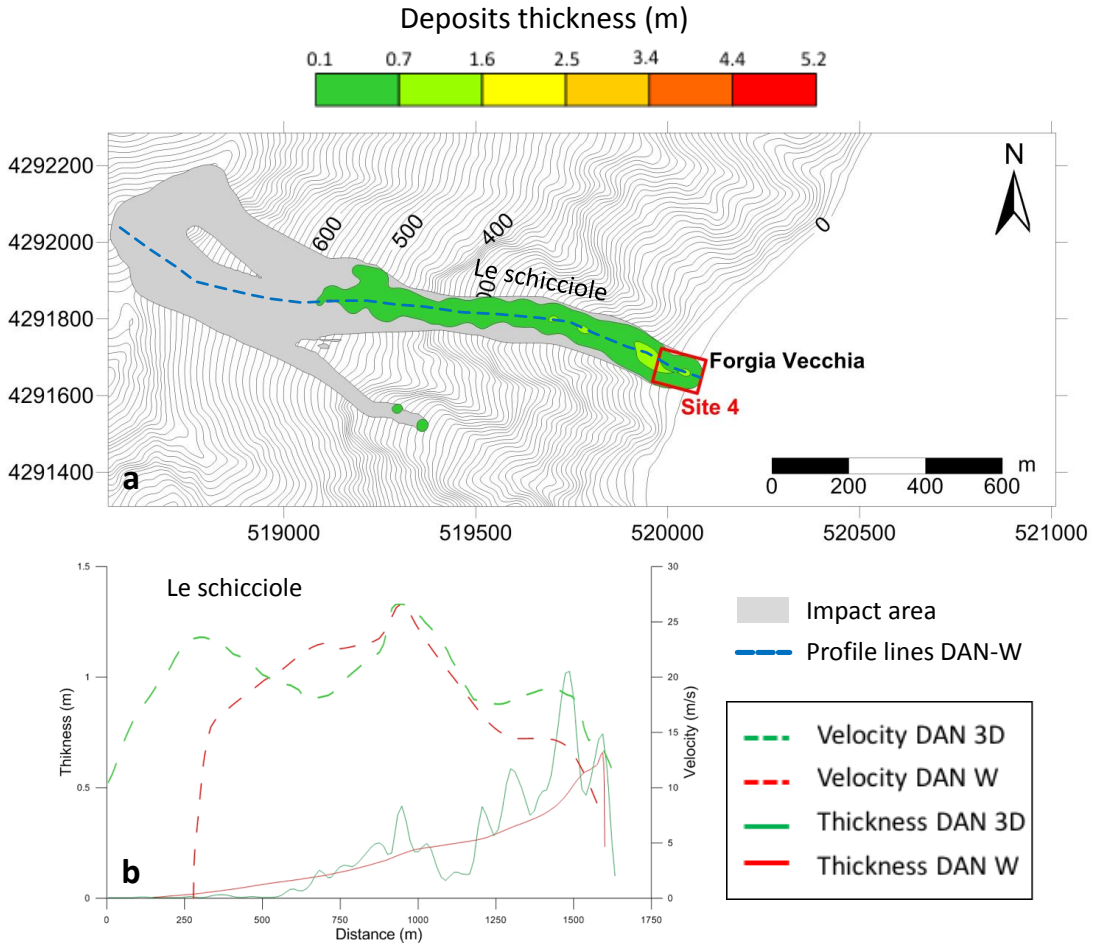

Fig. 26. Results of DAN-3D simulation of a) deposit thickness for the zone B; comparison between the DAN-W and DAN-3D for the b) Le schiocciole.

The simulation in zone C showed that the flow never reached the sea. After an initial phase of spreading on the flat area above the village of Ginostra, the flow channelized inside the village and stopped after approximately 180 s. In this case, no data in the literature describe the flow dynamics and runout or the deposit's thickness, and a direct comparison between the results of the simulation and field evidence was impossible. In zone C, the areas impacted by the PDC and covered by the deposit were 1.5×10^5 and 0.3×10^5 m^2, respectively (Fig. 27a). The results obtained by DAN-W show a very good correlation with the DAN-3D simulations (Fig. 27b).

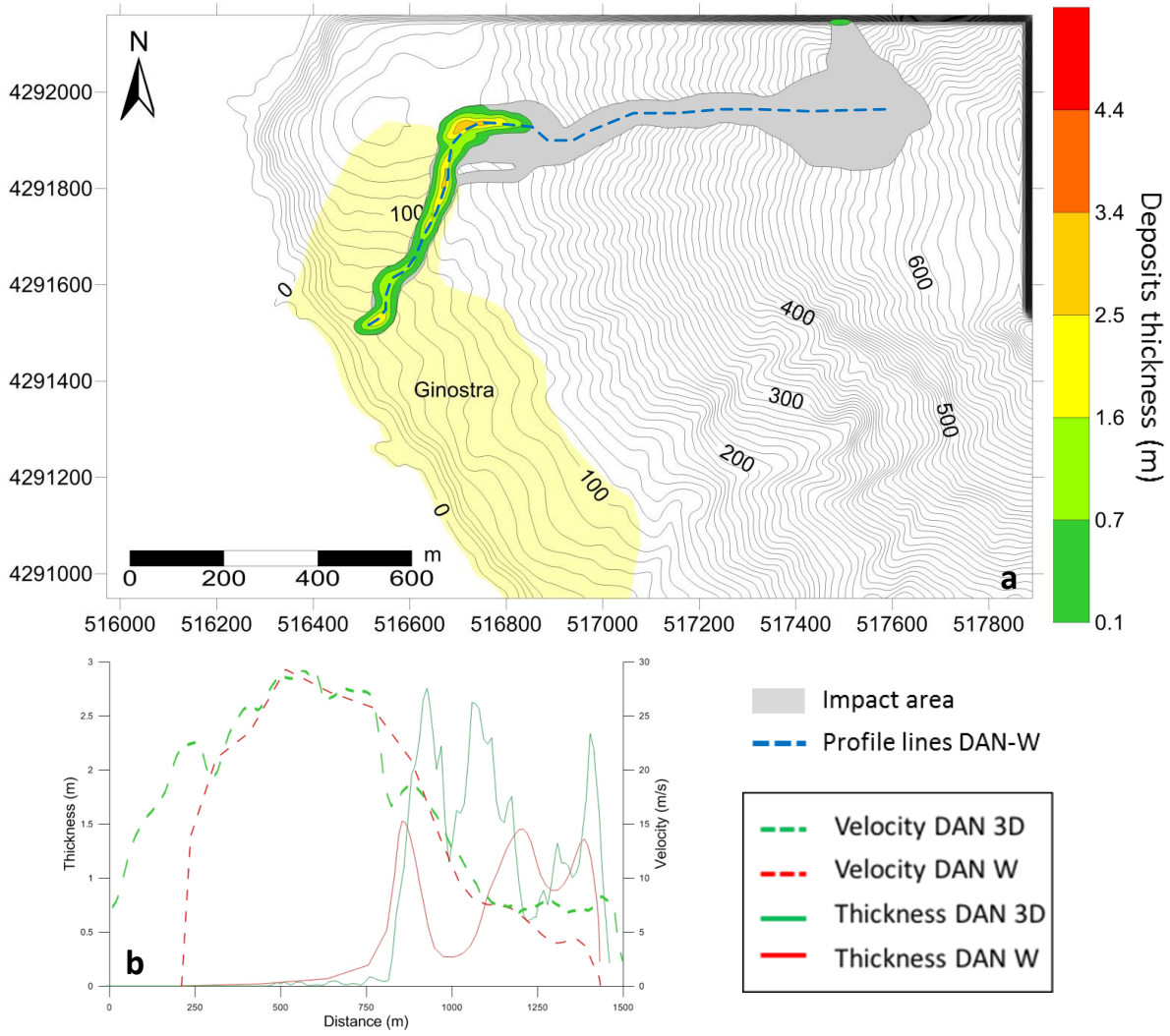

Fig. 27. Results of DAN-3D simulation of a) deposit thickness for the zone C; b) comparison between the DAN-W and DAN-3D.

The outcomes of DAN-W code along the considered sections show a very good correspondence in terms of total runout distance, flow thickness and velocity, with the 3D simulation. In the tree zones A, B and C the front displacement and thickness of deposits are similar in both models. This means that the model predictions of the simulated deposits thickness is mached with the measuraments in the field.

6.1.4 Forecaster analysis

To obtain a forcast analysis a second set of simulations was performed in the same areas. In these simulations we arbitrarily used a source deposit with double thickness compared to previous simulations and so a double volume of materials involved in the flow. A paroxysm able to emplace a thick-ness of deposit double respect to those emplaced in 1930 possibly

represents the worst scenario for the generation of a gravity-induced PDC on the Stromboli volcano. The results show that areas impacted by double volume PDCs are larger than those affected during the first simulation.

In particular, in zone A, the flow reached the Piscità locality after approximately 90 s and moved into the San Bartolo valley and adjacent valleys, depositing material along its path. The deposits were more distributed and reached a maximum thickness of 3.8 m in the Vallonazzo valley. The areas impact-ed by the gravity-induced PDC and covered by the deposit in the simulation with the double initial thickness were 5.6×10^5 and 1.3×10^5 m^2, respectively.

The simulation in zone B showed that deposition still occurred in the "Le Schicciole" valley (Forgia Vecchia), but it also occurred in the adjacent valley. In this case, the flow front reached the coastline after approximately 70 s. The areas impacted by the gravity- induced PDC and covered by the deposit in the simulation with a double initial thickness in zone B were 4.1×10^5 and 1.6×10^5 m^2, respectively.

In zone C, the flow ran through Ginostra village and reached sea level after approximately 100 s, with little lateral expansion in the urbanized areas. The deposit's maximum thickness was 4.4 m. The areas impacted by the PDC and covered by the deposit according to the simu- lation with the double initial thickness were 1.9×10^5 and 0.5×10^5 m^2, respectively.

In the simulation with double volume, the travel times of the flows in areas A, B and C decreased by 30%, 20% and 44%, respectively. The increase in volume caused consistent increase in the flow velocity and a greater impact force of the flow. In the Fig. 28 are show the comparison between the results obtaion using the volume for the back analysis and the resuls obtained using a double volume, on three areas A, B and C.

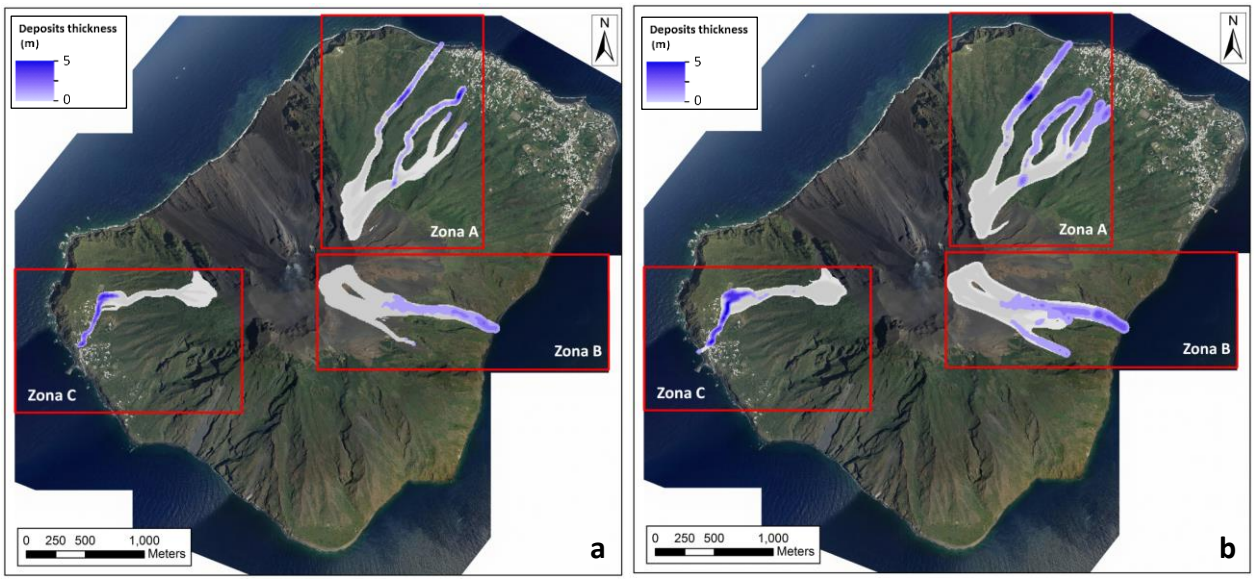

Fig. 28. Comparison between the results obtaion using a) the volume for the back analysis and b) using a double volume, on three areas A, B and C.

6.1.5 Mobility of basaltic gravity-induced PDCs

Gravity-induced PDCs are well known for their ability to travel long distances, so their mobility is critical to evaluate the areas at risk from future events (Davis et al., 1978). The morphometric parameters that best describe their mobility are: the total height of vertical drop (*H*), the runout distance (*L*), the volume (*V*) and the inundated area (*A*). Hayashi and Self (1992), Calder et al. (1999) and Saucedo et al. (2005) used different relationship between the four above mentioned parameters to explain the mobility of PDCs. In particular Hayashi and Self (1992) asserted that different material properties rather than different emplacement mechanisms appear to be the best explanation in the Log (*V*) versus Log (*H/L*) plot, where the historical data of PDCs and volcanic avalanches are compared. The plot shows an inverse correlation with a coincident regression lines for the two types of deposits (Fig. 29a):

[64] $$y = -0.1239x - 0.97228 \; R = 0.465B$$

indicating that material properties are similar for both phenomena.

The major difference is represented by the position in the graph. In fact, by plotting the data of PDCs found by Calder et al. (1999) and Saucedo et al. (2005), it is easily noticeable that the PDCs commonly have smaller volumes and higher *H/L* ratios than volcanic avalanches. This is in good agreement with the general results obtained from the work of Corominas (1996). This author shows a general inverse trend in reduction of *H/L* with increase of landslides volumes (*V*) and

H/L values less of 0.6 for landslides volumes below 10-4 km3. The *H/L* ratios resulting from the analysis of the gravity-induced PDCs of Stromboli are 0.42, 0.57 and 0.39 for A, B and C zones respectively (Fig. 29b).

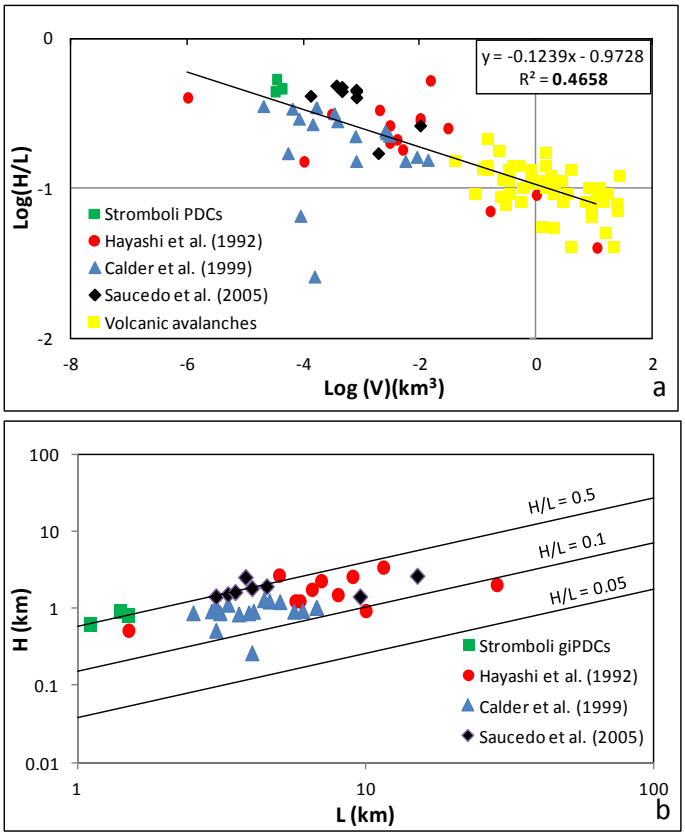

Fig. 29. a) Log(*V*) vs Log(*H/L*), b) *H/L* ratio of the Stromboli gravity-induced PDCs compared with world-wide PDCs (data from Hayashi and Self, 1992; Calder et al., 1999; Suacedo et al., 2005).

Further analysis of the mobility of Stromboli gravity-induced PDCs was performed considering the parameter $A/V^{2/3}$ suggested by Dade and Huppert (1998) for the runout of rockfalls and used later by Calder et al. (1999) to discriminate between the mobility of PDCs at Soufriere Hills Volcano (Montserrat). The Stromboli gravity-induced PDCs deposits show that the $A/V^{2/3}$ factor varies between 60 (zone A) and 117 (zone B), being comparable to what measured by Calder et al. (1999) at Soufriere Hills Volcano for small volume PDCs (Fig. 30a, b).

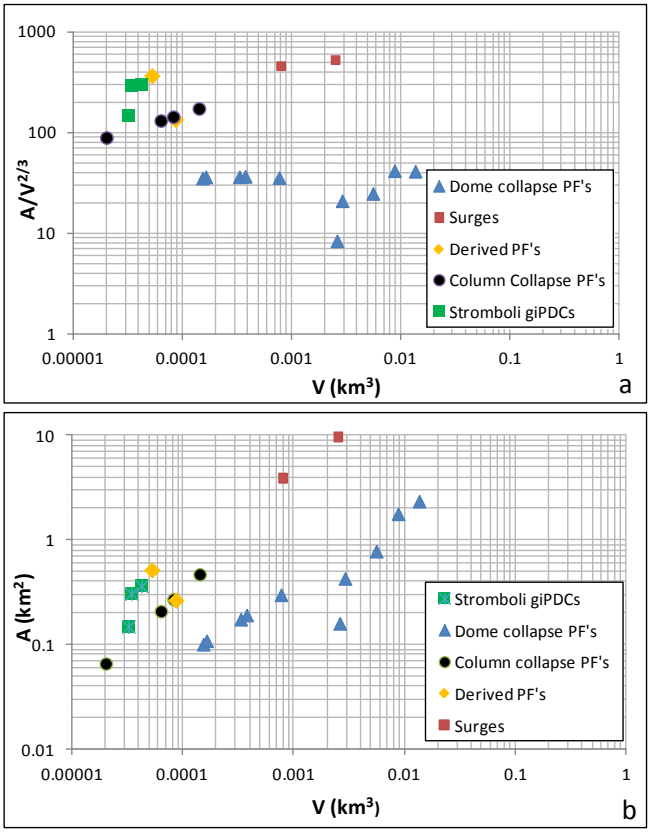

Fig. 30. a) $A/V^{2/3}$ vs V b) A vs V of the Stromboli gravity-induced PDCs compared with different kinds of PDCs (data from Calder et al., 1999).

DAN-3D was previously used by Morelli et al. (2010) and Sosio et al. (2012) to constrain the flow parameters of large volcanic debris avalanches, considered the large-volume end-members of gravity-induced mass-flow in volcanic areas. Combining the good results obtained using DAN-3D for both small-volume (this work) and large-volume (Morelli et al., 2010 and Sosio et al., 2012) mass-flows, in particular considering the mobility parameters (H/L and $A/V^{2/3}$ factor), allowed us to speculate that DAN-3D can be profitably used for modeling mass-flows with dominated by grain-collisions (granular flows).

6.1.6 Implication for hazards

As mentioned, gravity-induced PDCs are usually confined to the Sciara del Fuoco depression and are produced by the remobilization of significant thicknesses of tephra on steep slopes during paroxysmal explosions, the collapse of the crater rims or by lava breaking off the sides and fronts of advancing lava flows (Pioli et al., 2008; Rosi et al., 2013; Di Roberto et al., 2014; Di Traglia et al., 2014). Otherwise, small-volume gravity-induced PDCs were produced on the ESE side of the island in 1944, and on the inhabited NE part of the island in 1930 where they caused

four casualties. Hazard maps at the Stromboli volcano have been proposed by Barberi et al. (1993), Nave et al. (2010) and Rosi et al. (2013) and mainly focused on ballistic ejection and tsunamis, whereas threats associated with gravity-induced PDCs have not been examined in detail. This study represents the first contribution to a hazard assessment related to gravity-induced PDCs on Stromboli Island. The potential damage from PDCs interacting with buildings in the villages of Stromboli and Ginostra was evaluated using the method proposed by Jakob et al. (2011), which has been applied to the evaluation of debris flow impacts. The method determines the potential building damage using an intensity index (I_{DF}; a sort of impact force):

$$I_{DF} = dv^2 \quad [65]$$

where d is the maximum expected flow depth, and v is the maximum flow velocity.

The potential building damage was then estimated by classifying the calculated I_{DF} index, using the four classes proposed by Jakob et al. (2011), which range from some sedimentation (I) to complete destruction (IV). This classification is derived from back-analyses using building damage data from several case studies (Jakob et al., 2011; Corominas et al., 2014).

The modelling results in zone A were employed to evaluate the potential hazard in the Piscità zone of the village of Stromboli (Fig. 31a). The simulations showed serious threats due to the flows channelled into the St. Bartolo and Vallonazzo valleys. The first flow could destroy and inflict structural damage to buildings in the village near the St. Bartolo Church, whereas the second flow could inflict major structural damage on two edifices on the Vallonazzo rims. The simulation carried out for zone C also revealed a potential hazard in the village of Ginostra. The simulated path of the gravity-induced PDC, which travelled from the southwestern part of the summit area, could interact with the present day urbanization of the village and result in some structural damage or the complete destruction of several buildings in the central part of Ginostra (Fig. 31b).

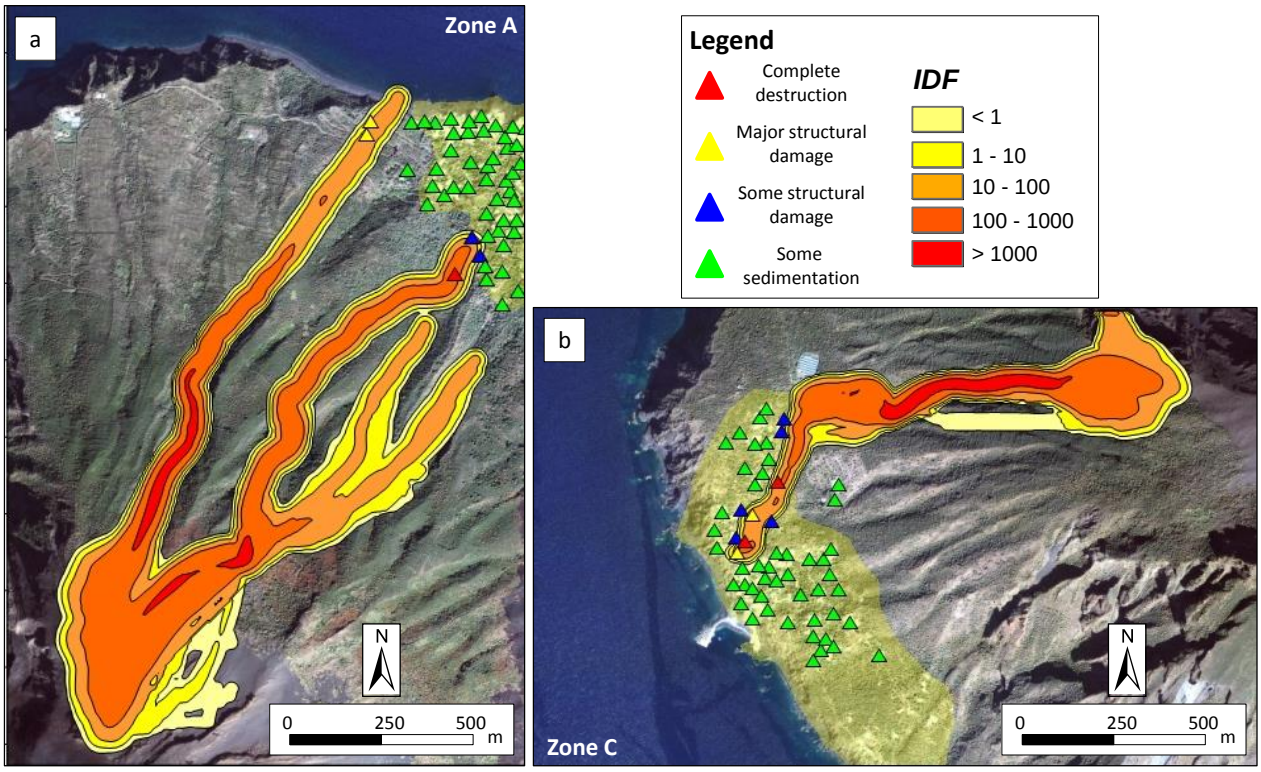

Fig. 31. Hazard evaluation for gravity-induced PDCs showing the potential intensity index (*IDF*) and a) effect on the building in the Stromboli village, Piscità (zone A) and b) in the Ginostra village (zone C).

The simulations with double initial thicknesses of the sliding masses in zones A and C show that in the case of gravity-induced PDCs, the areas with higher I_{DF} would greatly increase (). This implies that the greater spatter accumulation in the upper part of the island is related to directed paroxysmal explosions, which could produce serious threats to the inhabited areas of the island. Zone B is free of human settlement and was not considered for this type of evaluation. The results of the simulations with double initial thicknesses suggest that the performance of DAN-3D for simulating events primarily depends on calibration using field-based data such as deposit distributions (locations and areas of initial piles) and volumes (single or multiple volumes), and direct observations (i.e., travel times) (Fig. 32a, b).

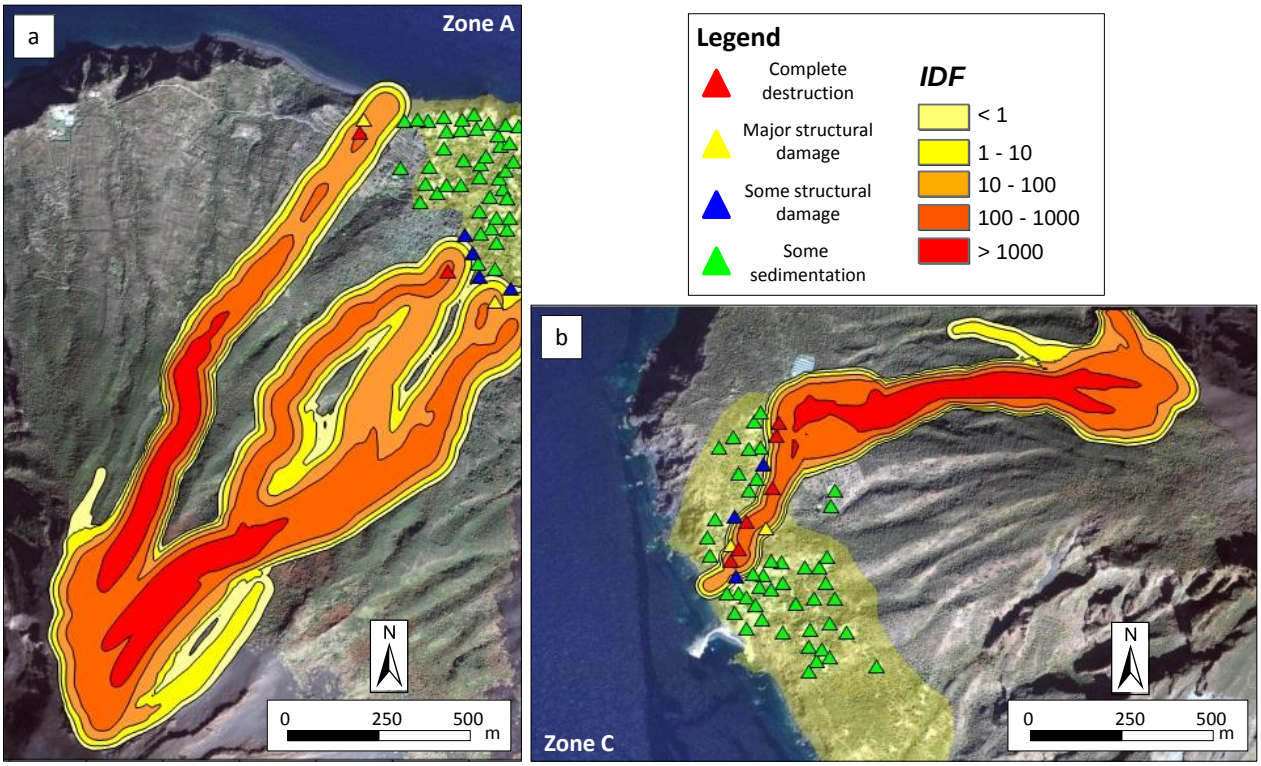

Fig. 32. Hazard evaluation for gravity-induced PDCs with double volume showing the potential intensity index (IDF) and effect on the building in the Stromboli village, Piscità (zone A) and in the Ginostra village (zone C).

6.1.7 Discussions

The best fit rheology is the Voellmy by using an internal friction angle of ϕ_i = 20° (Apuani et al., 2005b), f = 0.19 and ξ = 1000 m s^{-2} (internal friction and basal friction/turbulent) that well explained the 1930 PDC deposits, especially in the upper part of the deposit, which consists of a "blocks/bombs-and-ash-flow" (Miyabuchi et al., 2006) with metre to centimetre-sized clasts supported by a poorly sorted, massive, coarse ash matrix. This deposit is similar to the small-volume block-and-ash flows and rockfalls during the Soufriere Hills eruption (Cole et al., 2002) and the small-volume PDCs during the 1975 eruption at Ngauruhoe (Nairn and Self, 1978), which were interpreted as inertial granular flows (Lube et al., 2007). The lower unit consists of tens of cm-thick, well-sorted, medium ash deposit that often exhibit parallel to low-angle cross-laminations and short alignments of centimetric lapilli.

Since the work of Hayashi and Self (1992), the assumption of a pure frictional internal rheology has been questioned based on observations of high mobility PDCs and volcanic debris avalanches. Long run-out rockfalls, debris avalanches and PDCs exhibit horizontal runout distances (L) that can be 5–20 times the vertical fall height (H), depending on the magnitude of

the event. Several explanations for the scale dependence of *H/L* have been offered (Hungr, 1990), including mechanical fluidization (Hayashi and Self, 1992), acoustic fluidization (Melosh, 1979), and self-lubrication (Campbell, 1989). In particular, self-lubrification implies that most of the flowing mass moves over a thin, dilute layer of very agitated particles, where the energy dissipation is much smaller than in the mechanical fluidization (Hayashi and Self, 1992). Because this assumption was confirmed by the presence of a basal layer in the PDCs' deposits and the similarity of the basic physical processes that characterize dry granular avalanches and granular-flow dominated volcaniclastic flows (dense PDCs and debris avalanches), numerical codes that separate internal and basal frictions (i.e., Titan2D; Patra et al., 2005) have been increasingly used for reproducing past flows and hazard mapping (Saucedo et al., 2005; Norini et al., 2009; Widiwijayanti et al., 2009; Procter et al., 2010; Sulpizio et al., 2010b; Charbonnier and Gertisser, 2012).

DAN-3D was previously used by Morelli et al. (2010) and Sosio et al. (2012a) to constrain the flow parameters of large volcanic debris avalanches. Good results were obtained using DAN-3D for the large volume mass flows as well as the small-volume mass-flows investigated in this study. DAN-3D can be successfully used for modelling mass granular flows that are dominated by grain-collisions.

The main limitation of DAN-3D is the unchangeable internal rheology. Motion and field-based observations of dense PDCs and volcanic debris avalanche deposits have sometimes been explained using a plastic rheology (constant retarding stress or a Bingham rheology with no viscosity), in which the shear stress is constant regardless of the thickness or velocity of the flow (Dade and Huppert, 1998). Kelfoun and Druitt (2005) and Kelfoun et al. (2009, 2011) showed that the plastic rheology allows the morphology, lithology distribution and extension of volcanic debris avalanches and PDCs, even if Bingham behaviour with a minor viscous response cannot be excluded.

Charbonnier and Gertisser (2012) compared the hazard mapping of PDCs using both Titan2D (internal-basal frictional rheology) and VolcFlow (constant retarding stress). Their results evidenced the main limitation of using internal-basal frictional rheology for reproducing PDC velocities and travel times. Using a constant retarding stress, the resulting simulations reproduced the morphologies and distributions of the natural deposits as well as the times of emplacement and velocities of the PDCs. Further investigations of the suitability of different internal rheologies will be performed.

6.1.8 Conclusion

Gravity-induced PDC at Stromboli volcano were analyzed through the use of DAN-W and DAN-3D numerical codes developed by Hungr (1995), McDougall and Hungr (2004) and Hungr and McDougall, (2009), generally used for landslides modeling, using as test case the 1906, 1944 and 1930 events.The models were able to reproduce the extension and the order of magnitude of the thickness of three gravity-induced PDCs reported in the literature. The best modeling results on the 1930 PDC were obtained using a Voellmy model with frictional coefficient of f = 0.19 and a turbulence parameter ξ = 1000 m/s.

Simulations allowed studying the mobility of the simulated gravity-induced PDCs. The *H/L* index values are respectively 0.42, 0.57 and 0.39 for the three zones, and are in good agreement with the inverse trend in reduction of *H/L* with increase of landslides volumes (*V*) and *H/L* values less of 0.6 for landslides volumes below 10^{-4} km^3 (Corominas, 1996). The estimated $A/V^{2/3}$ factor for Stromboli gravity-induced PDCs varies between 60 and 117, being comparable with that of small volume PDCs (Calder et al., 1999).

Using DAN-3D is possible to generate hazard maps. The potential damage of the gravity-induced PDCs was evaluated using the intensity index (IDF) proposed by Jakob et al. (2011). For intensity index calculations, only parameters derived from the modeling results were used, therefore no other assumptions were made. Modeling results that PCDs will represent serious threats, potentially producing destruction and make some structural damage in all the inhabited area of the Island of Stromboli. Further investigation of the effect of this kind of mass-wasting entering into the sea are necessary to evaluate the tsunamigenic potential of the Stromboli gravity-induced PDCs.

6.2 Monte Rotolon debris flow

The study area is located in the Recoaro Terme municipality in the western sector of the Veneto region (Northern Italy), nearby the border with the Trentino Alto Adige region (Fig. 33), in the Vicentine Prealps, on the south-eastern flank of the Little Dolomites chain, which are part of the Agno river basin (Frodella et al. 2014).

The landslide is delimited on the NW by the ridge of the Mount Obante group and covers an area of about 626.000 m^2 and developing from about 1700 m to 1100 m a.s.l. (Frodella et al. 2014; 2015; Fidolini et al. 2015), where the waters of some natural springs give rise to a close valley of the Rotolon creek, along which all the mobilized material is channelled to reach the villages of Maltaure, Turcati and Parlati (about 700 m s.l.m.).

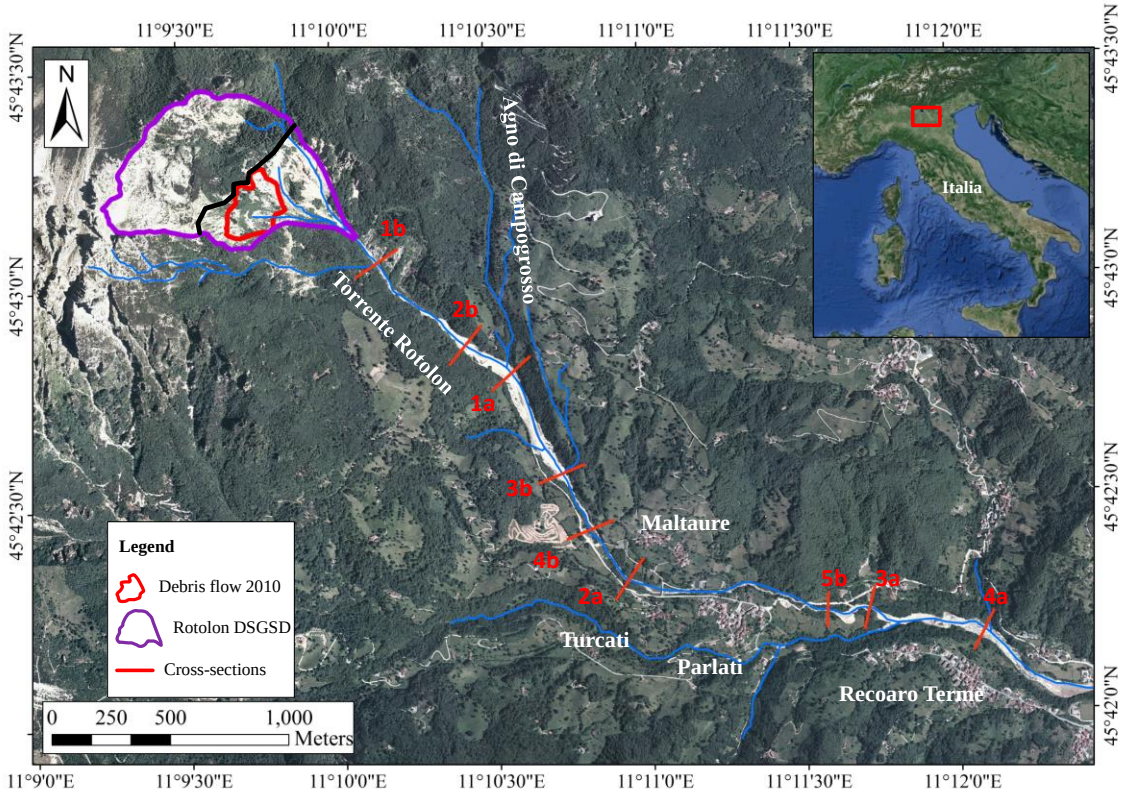

Fig. 33. Overview of the study area a) the Rotolon DSGSD landslide (violet line), with the local hydrographic network (blue lines) and all the main villages in the valley. In red is highlighted the November 4th, 2010 debris flow source area. In yellow is indicated the Detachment sector and in orange the Dismantling sector (according to Fidolini at al. 2015). Numbered red lines are the analysed cross-section.

6.2.1 Rotolon landslide description

The Rotolon landslide is a gravitational mass movement characterized by a complex activity (Cruden and Varnes, 1996) that leads to a very irregular physiography (Fidolini et al. 2015) (Fig. 34).

The morpho-structural characteristics (presence of trenches, counterslope scarps, sub-horizontal fractures in correspondence of the landslide toe, accessory instability phenomena, kinematic very slow displacement of large fractured rock masses) (Agliardi et al. 2009), this landslide presents the features of a "*Sackung*" type (according to Zischinsky, 1969) Deep Seated Gravitational Slope Deformation (DSGSD).

The landslide area can be divided into two sectors (Fig. 34a): i) an upper Detachment sector (red) and ii) a lower Dismantling sector (green) (Frodella et al. 2014). The Detachment sector has a mean slope of about 30° and is located nearby the landslide crown: it is characterized by tensional fractures, trenches and crests, and is largely constituted by colluvial, rockfall and rock avalanche deposits, very coarse and heterometric clasts, with scattered boulders. The Dismantling sector has a slope mean angle of about 34° and is characterized by mainly cobble-sized blocks and scattered boulders in coarse sandy matrix, coming from the Detachment sector rock slopes. This area is particularly prone to debris flow as documented by recent bibliography (Trivelli 1991; Altieri et al., 1994; Bossi et al. 2015b) and historical documentation available since 1573 (Schneuwly-Bollschweiler et al. 2012), which channelize downstream within the Rotolon Creek. The soil erosion, slope waste deposition and detrital cover failures are the main surficial processes that affected this area.

The 2010 debris flow event took place in correspondence to the right bank sector of the Rotolon landslide detrital cover, at about 1400 m a.s.l., and settled at about 550 m a.s.l., with adopt height of about 850 m. The collapsed material, characterized by a source volume of about 320000 m^3 (Bossi et al., 2015b), was formed by very coarse and heterometric clasts, ranging from cobbles to boulders with scattered blocks (decimetric to decametric in size) in a coarse sandy matrix.

This event, with a more of 3 km of runout distance, damaged several hydraulic works (such as weirs, fords and bank protections) putting at high risk the infrastructures (e.g. bridges and roads alongside the watercourse), and especially four villages situated along the creek banks (Maltaure, Turcati, Parlati and Recoaro Terme)(Fig. 34b, c) (Frodella et al., 2014).

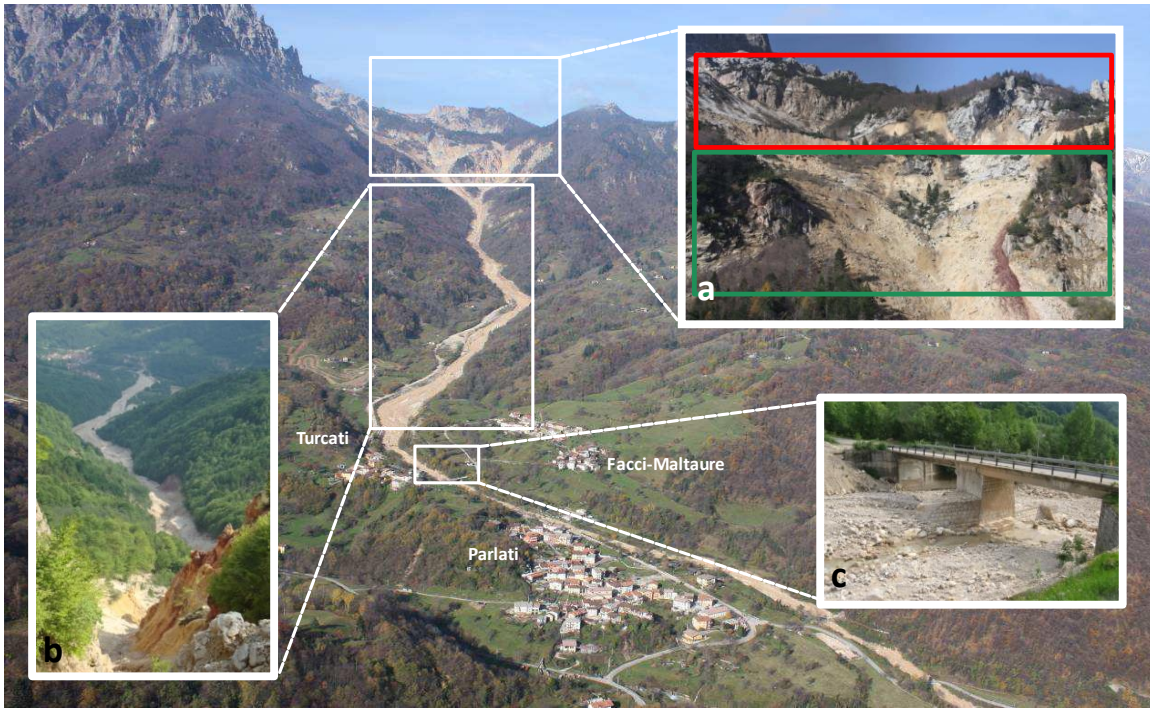

Fig. 34. Panoramic photo of the Monte Rotolon landslide, a) the source area. In red the Detachment sector and in green Dismantling sector, b) the 2010 debris flow event, c) the bridge situated along the Rotolon creek.

6.2.2 Geological setting

Rotolon landslide affects limestone and dolomitic formations belonging to the South Alpine Domain, from middle Triassic to lower Jurassic in age (Barbieri et al. 1980, De Zanche and Mietto 1981). The geological formations are, from top to bottom (Fig. 35):

- Dolomia Principale, dolostones and dolomitic limestones (Rhaetian – Carnian sup.);
- Raibl Formation, a sequence of volcanic conglomerates, sandstones, marls and dolomitic evaporates, showing at the bottom a discontinuous level of riolitic-dacitic phorphyrites (Carnian med.-Inf.);
- Ladinian Vulcanites, massive or scoriaceous rhyolites and dacites (Ladinian);
- Mt. Spitz Limestone, massive and locally layered limestones (Ladinian sup.);
- Conglomerate of Tretto, layered dolostones, sandstones and polygenic conglomerates (Ladinian med.);
- Recoaro Limestone, limestones, marly limestones and dolomite (Ladinian inf.);
- Formation of Gracilis, marly limestone, marl, siltstone and argillite with extensive gypsum deposits (Anisian).

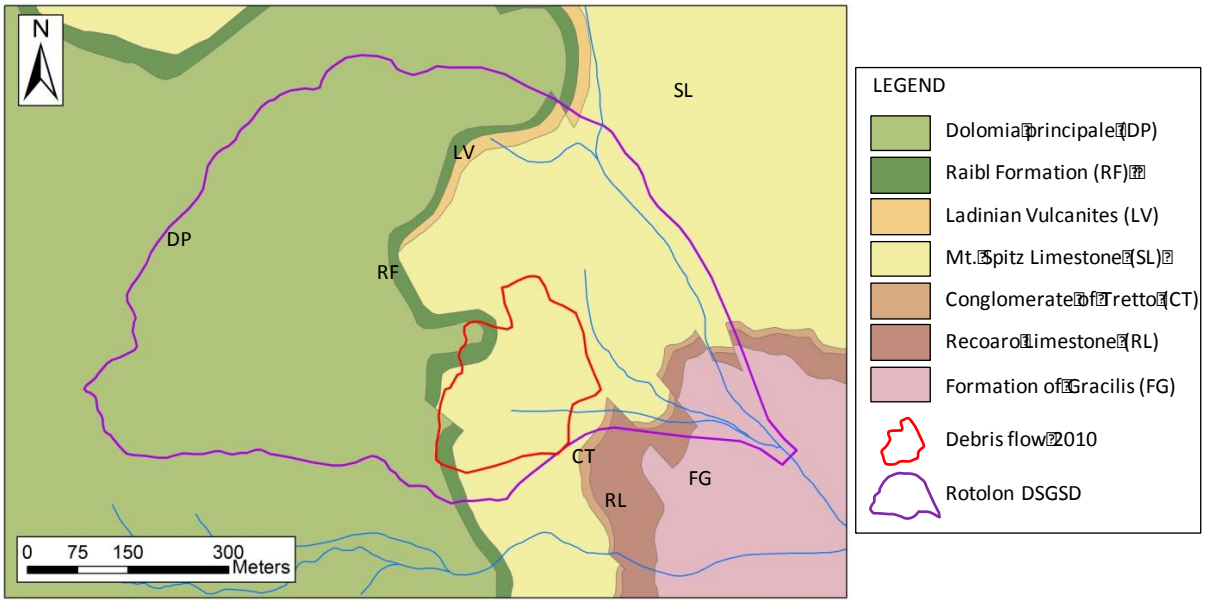

Fig. 35. Geological map of the Rotolon landslide and 2010 debris flow source area.

The area is intersected by two main fault systems, one NE-SW oriented and one NNW-SSE oriented (Barbieri et al., 1980; Castellarin et al., 1968a, 1968b; De Zanche and Mietto, 1981). An E-W-oriented fault system is also reported.

6.2.3 GB-InSAR system

In order to monitor the source area of the 2010 landslide a GB-InSAR system was located in the village of Maltaure, on 6 Dicember 2010, at an average distance of 3 km with respect to the debris flow source area and the surrounding debris cover. The antenna moved on a 2.7 m rail and the SAR image range resolution (spatial resolution along the direction perpendicular to the rail) was about of 3 m, while the azimuth resolution (spatial resolution parallel to the synthetic aperture) was between 1.6 m and 9.3 m (at a 500 m and 2900 m sensor-target distance respectively). The landslide monitoring activity was carried out from December 8th, 2010 to March 31st, 2013 (Fidolini et al. 2015). The Fig. 36 shows the radar and its resolution grid.

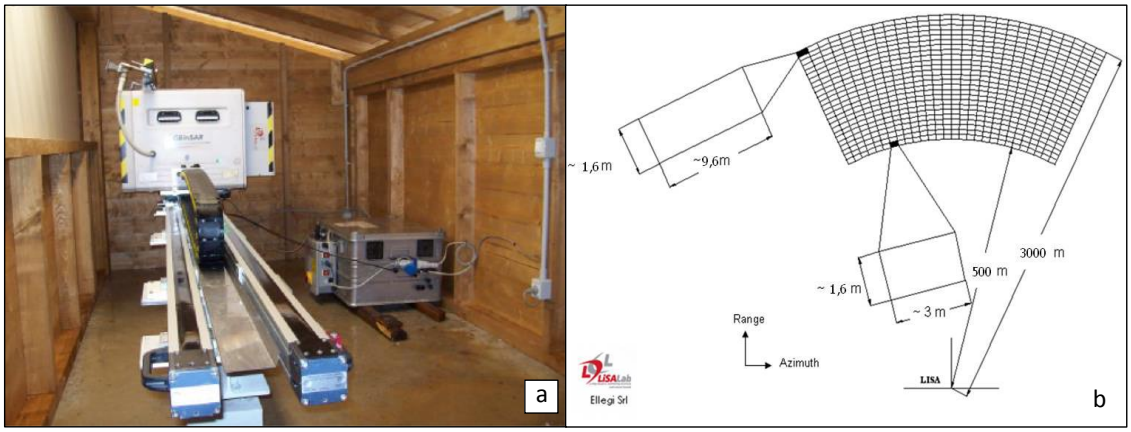

Fig. 36. a) GB-InSAR instrumet and b) resolution grid size used during the monitoring campaign.

The radar images are produced every 10 min and are elaborated to generate the 2D displacement maps, the more visible areas include much of the Detachment sector and the easternmost part of the Dismantling sector. Furthermore, based on the landslide physiographic, 10 control points (8 inside and 2 outside the landslide area) were selected to draw the displacements and velocities time series.

During the whole monitoring period four significant displacement acceleration events were recorded:

- on 19 March 2011 the SAR system recorded an acceleration in a landslide portion located to the right of the debris flow 2010 source area, which corresponds exactly to the apex of the detrital accumulation located at the main spring of Rotolon Creek. This portion suffered a reactivation on 7 April 2011 with a maximum speed of about 8 mm/h (Fig. 37a, b);
- during the period between November 8th and 12th, 2011, in a wider sector, always located in the area affected by the events in March and April 2011, has been recorded a maximum speed of about 2 mm/h (Fig. 37c);
- in November 2012 a new event of displacement was recorded in particular between November 2nd and 4th, 2012 and on November 10th, 2012 (Fig. 37d).

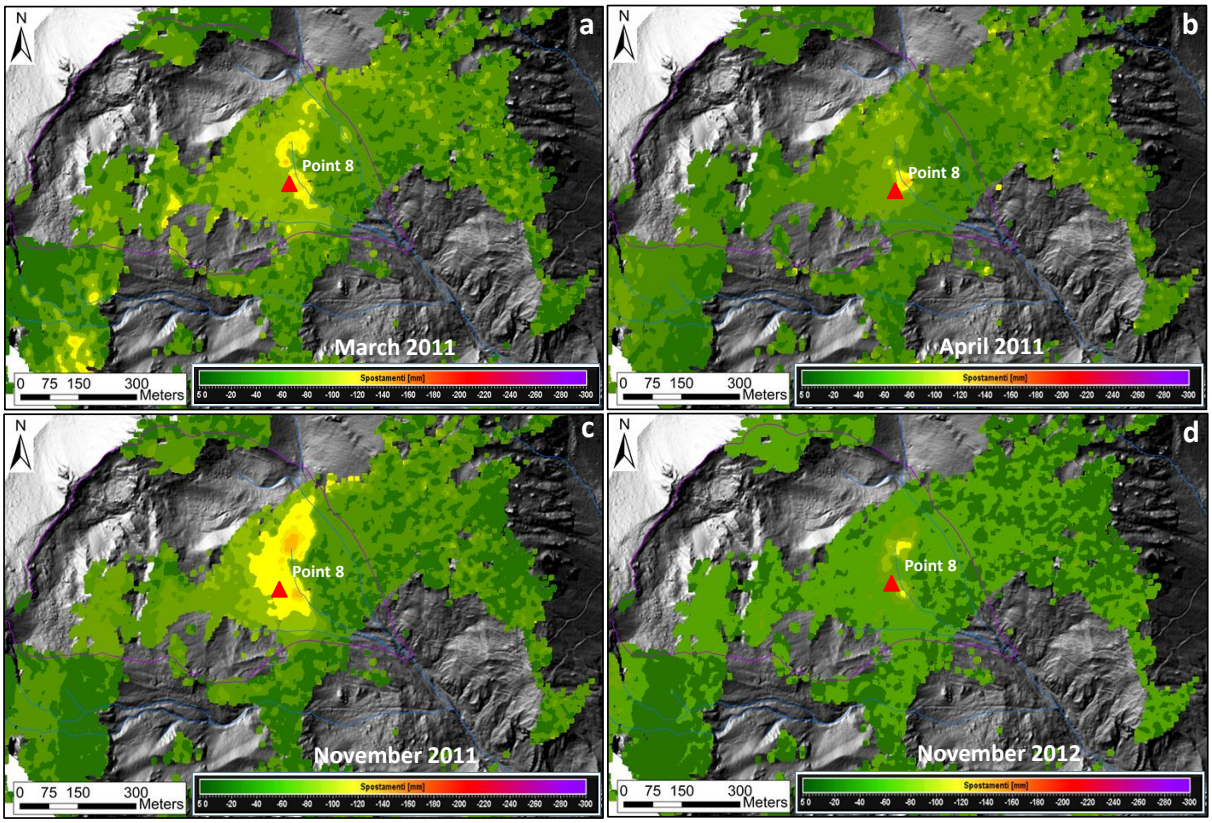

Fig. 37. Cumulative monthly desplacements masp of four significant displacement acceleration events a) March 2011, b) April 2011, c) November 2011 and d) November 2012.

During these event the control point 8, located in the eastern sector of the landslide body (Dismantling sector) in debris cover, near the source of Rotolon creek, has recorded some displacement phases. The kinematics of this control point shows periods of acceleration and deceleration associated to the precipitation accumulated exceeding a threshold value (estimated to be 100 mm at least three to four consecutive days). This correlation appears evident due to the heavy rainfall between November 8th and 12th, 2011 (cumulative precipitation of 500 mm in 5 days (Fig. 38). Due to water infiltration, the pore pressure increases and drastically reduces the shear stresses, such dynamics may develop rapid debris flow.

The Fig. 39 is shown the cumulative displacement map of entire monitoring period from December 8th, 2010 to March 31st, 2013.

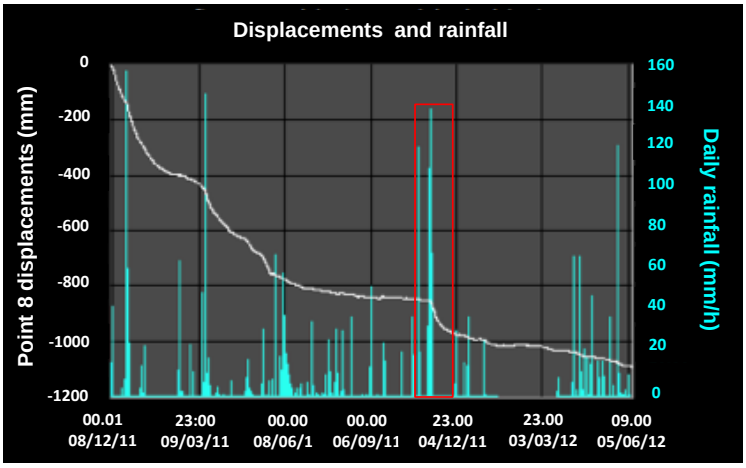

Fig. 38. Cumulative precipitation of 500 mm in 5 days between November 8th and 12th, 2011.

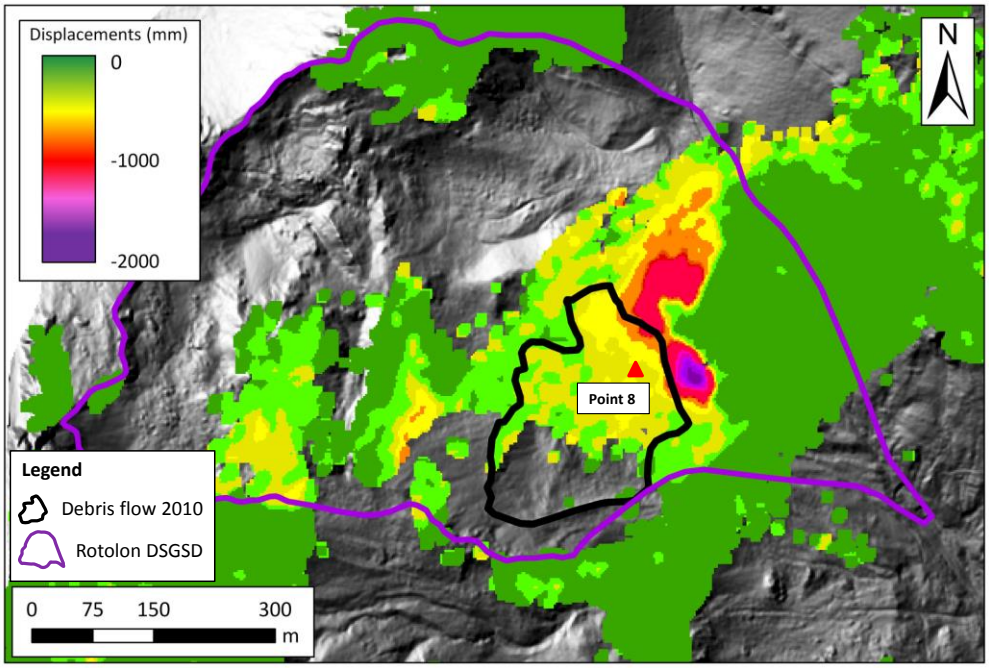

Fig. 39. Cumulative displacement map recorded between December 2010 and November 2012 (time interval 726gg 15h 18min, from 0:04 of 08/12/2010 to 09:45 29/11/2012) projected on hillshade, with the evidence of 2010 event source area in blak and the Monte Rotolon DSGSD in violet.

6.2.4 Rotolon debris flow back analysis

The back analysis modelling was performed with DAN-3D on high-resolution digital terrain models (DTMs). The DTM was obtained by elaborating light detection and ranging (LiDAR) acquired by the Soil Defence Department of the Veneto region, during two airborne laser scanning survey. The first was carried out on 21 October 2010 by the regional authority just 13 days before the event, and the second with the same characteristics (i.e. sensors, flight parameters, average point density) was carried out on 23 November. The average point density

for both surveys was about 8 pts m^{-2} while the vertical accuracy (root mean square error) of laser data was 0.072 and 0.044 m for the October and November surveys, respectively (Bossi et al., 2015). Having two DTMs pre- and post event, is important for two main reasons, it allows to have the path for back analysis and the path for the forecast analysis and it provides the magnitude and the erosion or deposition by simply subtracting the two topographic surfaces, that may be useful both for the model calibration and to have a real debris flow source volume.

For back analysis the pre-event DTM was resampled to a spatial resolution of 5 m and filtered using Gaussian smoothing (3×3). The considered model has an erosion rate of 1.1×10^{-4} and a maximum erosion depth of 5 m only in the upper part of the creek.

The simulation materials were chosen based on some main elements, that most influenced the flow complex dynamics (and therefore the choice of different rheological parameters along the track): i) the high plano-altimetric changes in the riverbed and the consequent variability of hydraulic sections; ii) the presence of two weirs at about 940 m a.s.l., that intercept the natural distribution of sediments; iii) the presence of the confluence of an ephemeral tributary of the Rotolon Creek (Agno di Campogrosso Creek) located at about 900 m a.s.l., which, during periods of intense rainfalls, is characterized by a high river discharge contributing to the debris transport and fluidification (Bossi et al. 2015b) (here the changing between Material 1 and 2); iv) the persistence of bank protections for a significant stretch upstream from the villages of Turcati and Maltaure and v) the presence of a narrowing section (i.e., a road bridge with a reinforced pylon in the middle of the riverbed (Fig. 33c) (here the changing between the Materia 2 and 3). The exposed build-up of sediments around this bridge following the 2010 debris flow event, suggested that its shape and dimension contributed to slowing down and stopping much of the coarser clast and boulder flow portions, while the remaining finer sediments flowed downstream along the creek bed for about two kilometres. Therefore, this bridge was considered a key element also for the terminal stages of the new simulations.

The best results were obtained using three types of materials with different frictional coefficient (f) and turbulence parameters (ξ) (Table 8) in the Voellmy kernel.

Table 8. Parameters of each material the erosion rate and Voellmy rheology parameters: friction (*f*) and turbulence (ξ).

	Range of altitude (m a.s.l.)	*E*	*f*	ξ (m/s^2)
Material 1	1420 - 920	0.0001	0.18	500
Material 2	920 - 780	-	0.12	1000
Material 3	780 - 560	-	0.01	1000

The parameters used in the Voellmy rheology successfully simulated the deposit thicknesses and the areal distribution of the 2010 event, matching positively the order of magnitude of those measured with the differences between pre- and post-event DTMs (Fig. 40a). In particular, the modelled flow in the sector upstream the Agno di Campogrosso confluence (Fig. 40b) shows a good accordance with the maximum thickness of about 10 m was reached by the debris flow (Fig. 40a).

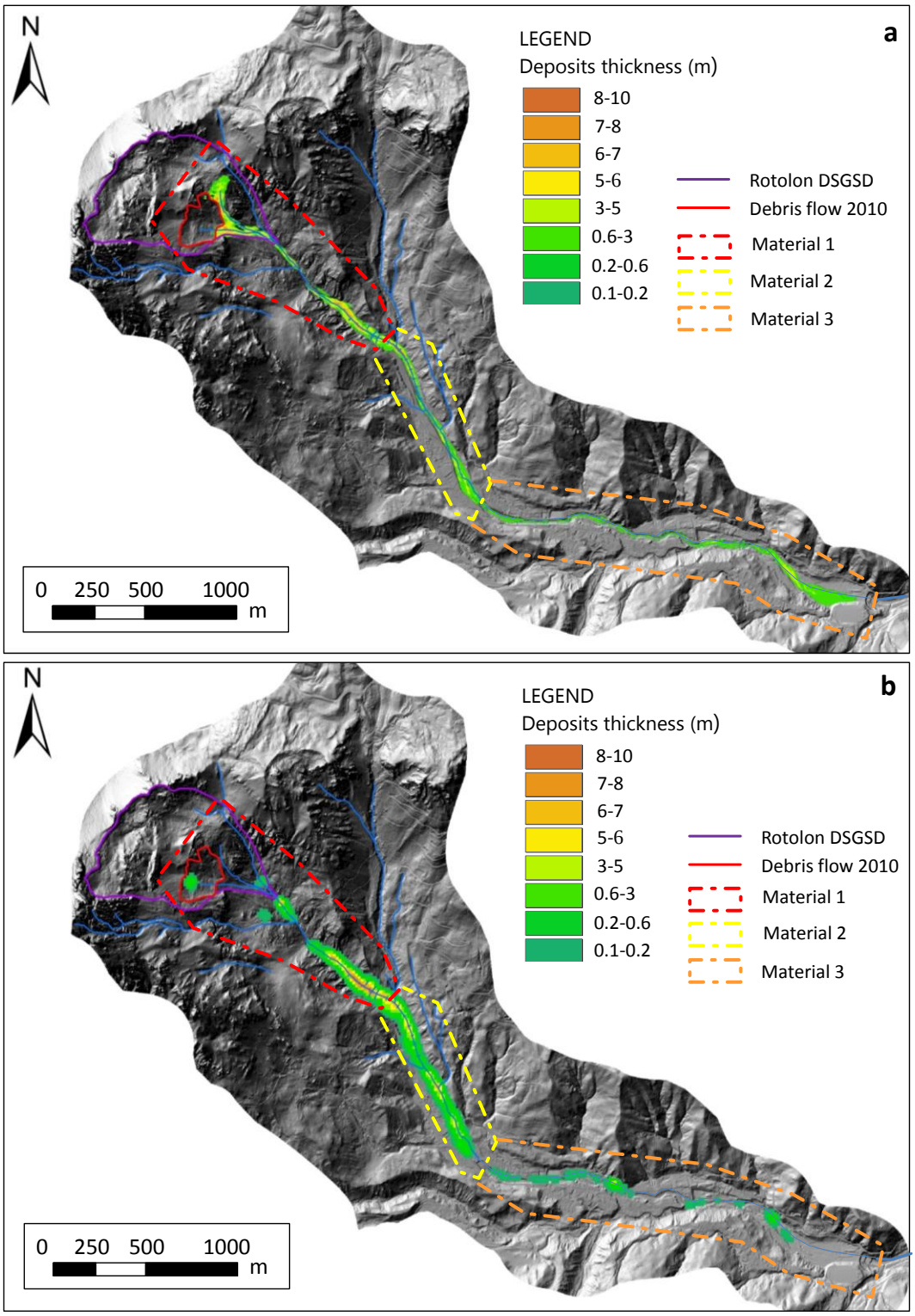

Fig. 40. Comparison between a) the deposits thickness resulting from the deference of two DTMs (pre- and post-event), b) the deposits thickness resulting from the back analysis with DAN-3D. The violet line is the Rotolon landslide DSGSD and the red one is the source area of the 2010 debris flow.

The comparison between the debris flow thickness and DAN-3D results was weighed also in other key locations along the creek bed, especially in correspondence the same cross-sections used for the velocity estimation (Fig. 33). The maximum obtained thickness difference was about 1.5 m, as shown in the cross-section 3b (Fig. 41).

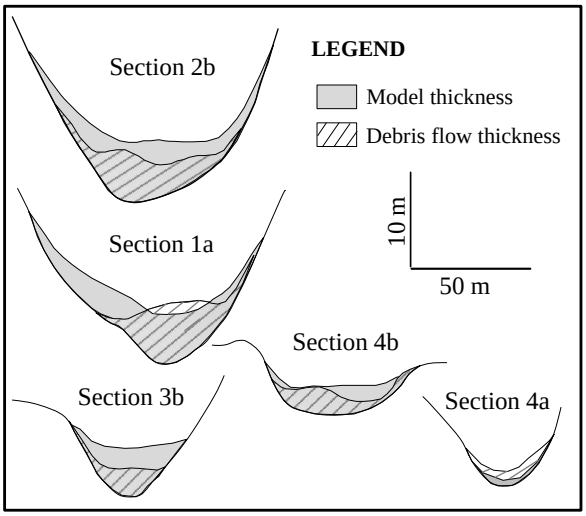

Fig. 41. Comparison between deposits thickness along some cross sections: in grey striped for the real debris flow thickness; in grey for the modelled thickness (for their map localization refer to Fig. 33).

The calculated debris flow impact area was about 245000 m^2, while the area covered by the modelled deposits was 250000 m^2. A good correlation was found between the calculated volume through the difference of DTMs (DoD analysis) by Bossi et al. (2015b) and that found with the DAN-3D modelling. The volume obtained by means of the DoD procedure was about 372000 m^3, whereas the DAN-3D volume was about 371000 m^3. A very good accordance was obtained between the modelled results and the DTMs analysis; nevertheless, localized differences between the above mentioned results were generated, mainly due to the input data and particularly to the model path processing stages (Table 9).

Table 9. Correlation between the calculated volume through the difference of DTMs (DoD analysis) by Bossi et al. (2015b) and that found with the DAN-3D modelling.

	DoD Analysis (Bossi et al., 2015)	DAN3D results
Source volume (m^3)	320022	318951
Erosion (m^3)	36021	51870
Debris flow volume (m^3) deposited before Agno di Campogrosso (1420 - 920 m a.s.l.)	186523	205590
Debris flow volume (m^3) deposited after Agno di Campogrosso (920-560 m a.s.l.)	149247	165231
Total volume (m^3)	371791	370821

6.2.5 Velocity analysis

The colmplex dynamic of the Monte Rotolon debris flow can be described also analyzing the velocity. The sliding movement starts with high velocity and an erosion depth of up to 27 m in the source area (with 27° slope). After the slide enter in confined creek, erodes the bed cover and grows considerably in volume. After that, the velocity decrease due to the change of channel slope (from 15° to 7°) and the majority of the sediments are deposited. The flow stops in the distal part of the path until a Giorgetti check dam, located near the Recoaro Terme village entrance.

In the latter framework the velocity of the Rotolon event was estimated using two different equations (described in the paragraph 5.1.3): the method of Forced Vortex Equation for superelevation (Chow 1959; Revellino et al. 2004; Zanchetta et al. 2004; Prochaska et al. 2008) and the method based on the maximum discharge (Rickenmann 1999).

The flow's radius of the central streamline was calculated where debris flow travels around a bends (cross-sections 1a-4a, Fig. 33). The result was obtained both from a graphical processing using a 1:5000 topographic map and from the application of Prochaska et al. (2008) method and its empirical equations. On the other hand, in the cross-sections from 1b to 5b (Fig. 33), the velocity estimation was based on the Rikenmann's (1999) flow equations considering the approximate maximum discharge (Q_p) assessed using two empirical relationships between peak discharge and volume of the debris flow (Mizuyama et al. 1992; Rickenmann 1999).

The resulting velocity estimations are show in Table 10 Here these values were also compared with the results of the numerical model velocity in the same cross-section (Fig. 33). This was possible because the DAN-3D code is able to calculate the maximum velocity at each grid node. The velocities calculated with DAN-3D were in good agreement with all the values obtained using the equation by Rickenmann (1999) and Mizuyama et al. (1992), ranging from 32.0 m/s (section 1b) to 6.6 m/s (section 4a). By comparing the flow velocity profilesobtained through the above mentioned equations and the modelled results (Fig. 42), it was possible to observe a similar trend along the overall debris flow travel distance, with an initial exponential deceleration and a decrease of velocity in the final section.

This is in accord with Pierson (1994), the peak flow velocities of the large debris flows is highest on the steep flanks and decreased with distance away from the source areas.

The higher velocities were recorded in the first two sections (1b, 2b) falling within the Material 1 of the runout model, where erosion takes place. The major difference between the calculated and modelled velocities were evident in the upstream part of the debris flow sector, while in the middle and lower flow sectors the obtained velocities showed similar values (sometimes almost coincident) (Table 10).

Table 10. Mean flow velocity measured in correspondence of selected cross-sections (for their map location refers to Fig. 1a).

	v (m/s) (Chow, 1959)	v (m/s) (Rickenmann 1999)	v (m/s) (Mizuyama et al. 1992)	v (m/s) (DAN 3D, maximum velocity)
Section 1b		21.2	18.7	32.1
Section 2b		18.4	16.3	22.5
Section 1a	14.1			17.3
Section 3b		17.1	15	16.6
Section 4b		15.6	13.8	14.2
Section 2a	11.8			13.5
Section 5b		13.6	12	8.4
Section 3a	11.5			8.2
Section 4a	5.6			6.6

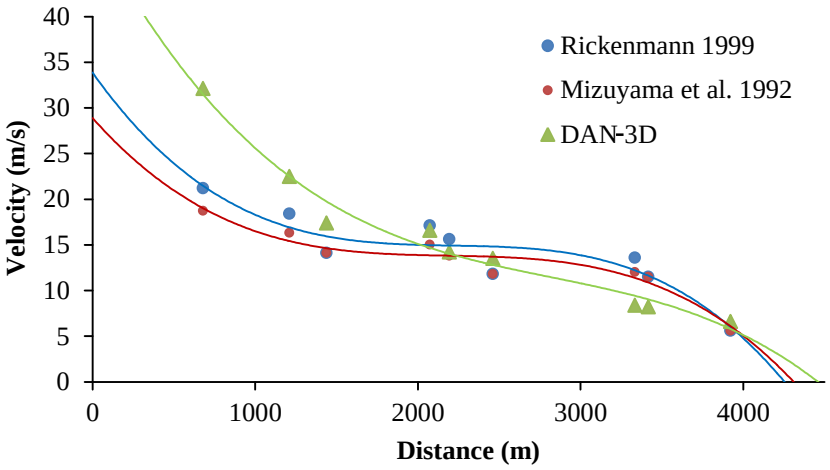

Fig. 42. Velocity profiles calculated by Ricknmann (1999) equations (blue points), Mizuyama et al. (1992) equation (red points) and DAN 3D simulation (green triangles).

6.2.6 Rotolon debris flow forecast analysis

In order to assess the Rotolon valley exposure to possible future debris flow events, new DAN-3D simulations were carried out combining the extension of the area established by means of the GB-InSAR displacement map analysis and the rheological parameters obtained by means of the 2010 event back analysis. The radar monthly displacement maps were elaborated in the MATLAB code in order to automatically extract from the cumulated displacement maps all the areas affected by movements and calculate the frequency of occurrence with which the movements take place during the monitoring period chosen. This analysis highlighted that the extracted areas were located in a landslide debris cover sector located just NW of the 2010 detachment zone (Fig. 43).

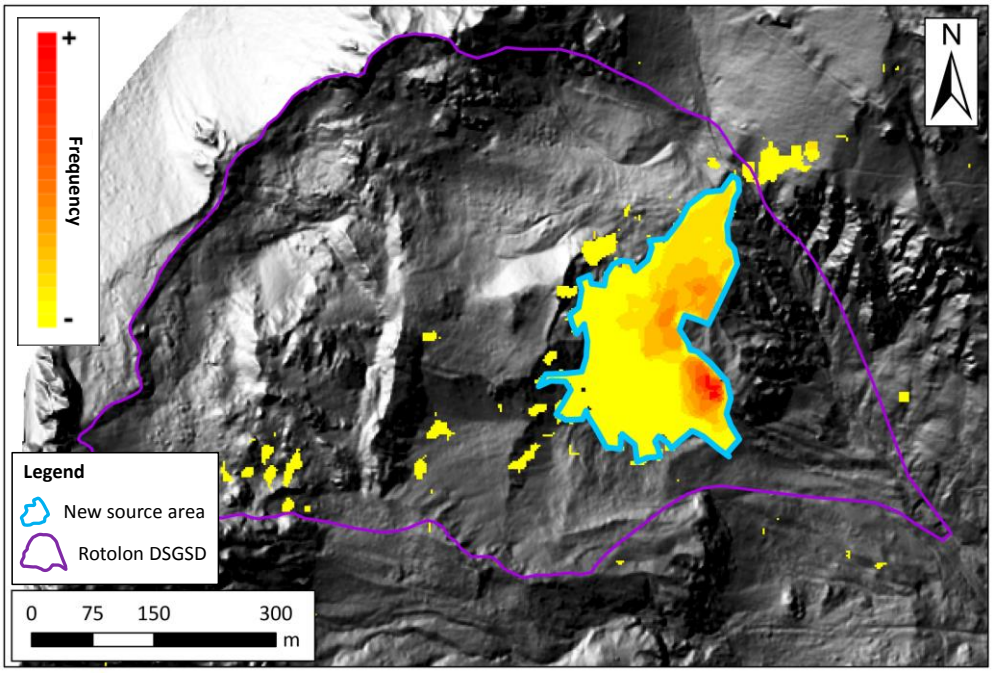

Fig. 43. Frquency map calculeted by MATLAB code from cumulative desplacements maps of GB-InSAR, in ligth blue the new source area for forecast analysis.

Usually, the estimate of a hypothetical volume potentially prone to collapse represents a difficult task, even in case of accurate field measurements. Therefore, in order to overcome this problem, three credible volumes were estimated considering the possible new source area extension and three different thickness values (average, modal and maximum), derived from a statistical analysis carried out in correspondence of the 2010 event source area (Fig. 44).

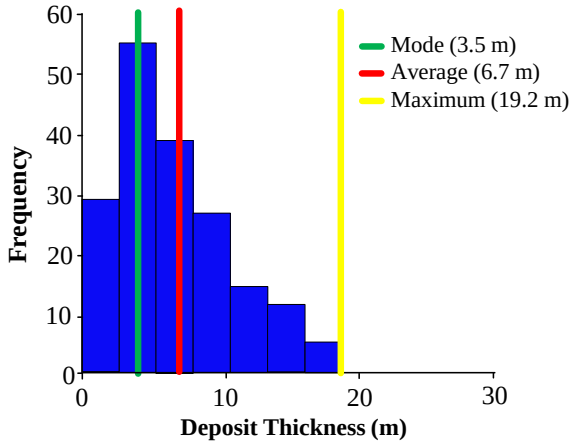

Fig. 44. Statistical analysis on 2010 event source area deposits thickness.

In this context three simulations were performed using different volume values: i) modal (165000 m^3), ii) average (304000 m^3), maximum (894000 m^3), respectively. The runout outcomes showed that by using the modal and average values the modelled debris flow stops in

any case upstream of the villages of Turcati and Maltaure (Fig. 45a, b). On the other hand by using the maximum volume value the resulting debris flow shows highly mobile and very rapid features, and capable of reaching the village of Recoaro Terme, even overflowing the riverbanks with dangerous implications for the inhabitants (Fig. 45c). Furthermore, a critical debris flow volume assessment was performed on the basis possible future events capable of reaching the villages of Turcati and Maltaure. The obtained critical volume is 373000 m^3 (slightly more than the statistically calculated average value and less than half of the maximum value), while the average thickness of its source area is about 8 m (Fig. 45d).

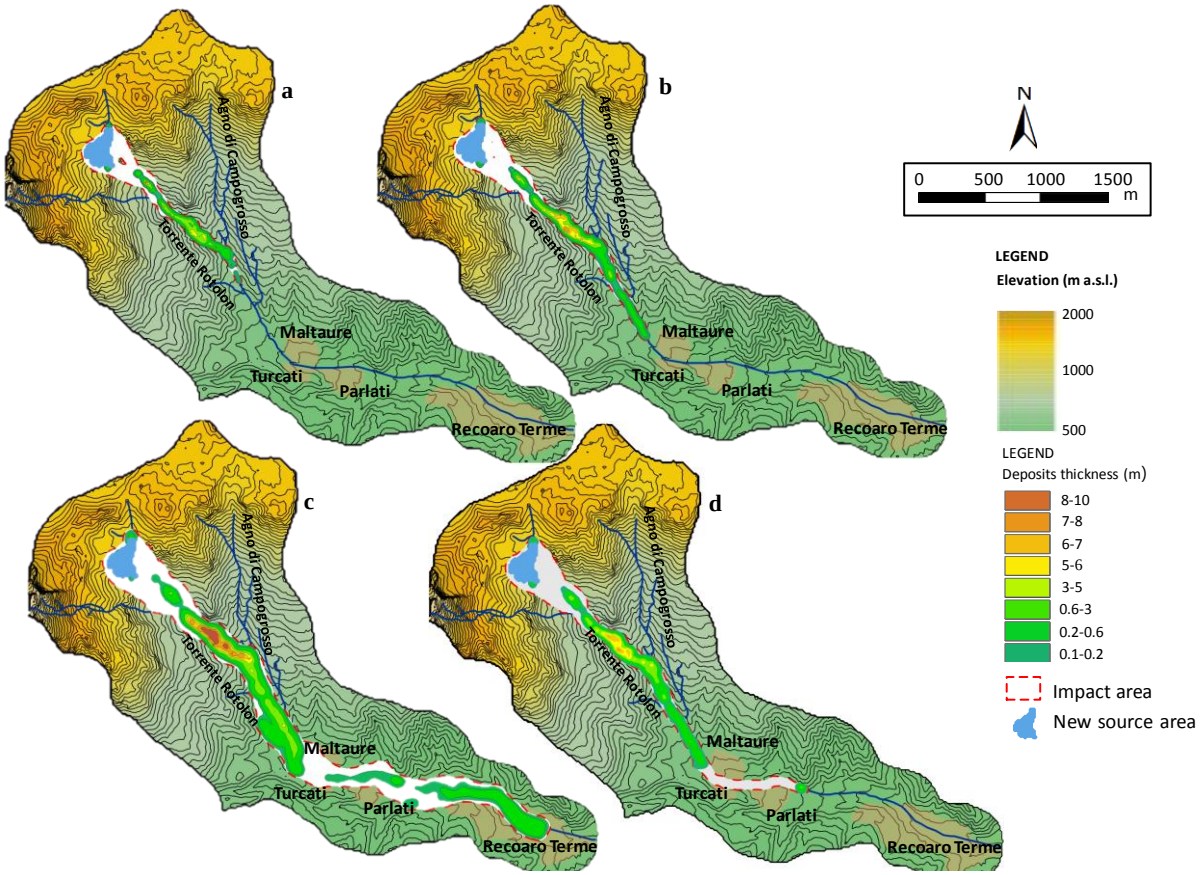

Fig. 45. Forecast analysis of future possible events with different values of collapsing volumes; a) modal (165000 m^3), b) average (304000 m^3), c) maximum (894000 m^3) and d) critical (373000 m^3). The considered source area (blue) is the new area show in Fig. 43. In white dashed red the impact area of the simulated debris flows.

6.2.7 Conclusion

The November 4th 2010 debris flow event detached from the Rotolon DSGSD detrital cover was modelled by means of DAN-3D numerical code and its results were discussed. The runout simulation shows that amongst the available rheological kernels the best rheology in the used model is the Voellmy type. The latter was applied to each of the three materials in which the path of the landslide was conventionally subdivided. After some attempts made by varying the rheological reference parameters, the 2010 event back analysis was able to reproduce with high accuracy: i) the debris flow impact area; ii) deposit thickness; ii) velocity, and iv) the final flow erosion volume. In order to assess the Rotolon valley exposure to possible future debris flow events, based on the back analysis results, a forecasting analysis was performed. This analysis was obtained by means of DAN-3D simulations, considering: a) the same input data of the back analysis; b) a new possible source area detected by means of GB-InSAR displacement data analysis; c) different hypothesized thicknesses by means of statistical considerations based on the differences between the pre- and post-2010 debris flow event DTMs. These simulations produced impact area maps useful for evaluating the different future debris flow scenarios within the Rotolon valley. The obtained results show that the integration of the modelling technique with ancillary data (such as geomorphological and topographic maps, location and characteristics of the hydraulic works along the creek bed), together with the GB-InSAR derived displacement maps, can be a very useful tool for the scientific community and local administrations in order to manage the problem related to debris flow events in the examined area. This working method could represent a standard procedure in case of areas prone to different type of debris flows, in case of GB-InSAR displacement monitoring. Nevertheless, the accuracy of the proposed method lies also in the skill of expert operators in the choice of reliable volumes of possible future debris flow events.

6.2.8 Gessi – Mazzalasino (Scandiano) landslide

On March 27th 2015 at about 08.00 PM, a rapid landslide triggered in upstream to the village of Gessi - Mazzalasino. The mass movement is situated on western slope of the Tresinaro creek valley, behind the Gessi-Mazzalasino village in the Scandiano Municipality (Reggio Emilia province, Emilia Romagna region) (Fig. 46).

From a geomorphological point of view, the Tresinaro creek valley is characterized in north-central sector by the presence of flat areas stopped by flood terraces and paleochannel, while in the southern sector by low hills and the average steep slopes of Mount Evangelo to the east and of the locality La Vedetta to the west at least 400 m s.l.m.. The landslide slope is characterized by high average gradient, about 17-20°.

The source area of the landslide is located at an elevation raging between 230 and 215 m a.s.l.. The cause that triggered the collapse was the rain fell throughout the days before the events. The Cà de Caroli weather station, located at 1 km north-east of the study area, recorded more than 100 mm of rainfall in 10 days, the annual average rainfall of the area is about 580 mm.

The triggering area shows an irregular shape and cover an area of 1700 m^2, approximately. The flow, after an initial spreading in a flat area, located in the middle of the slope, moves in an existing impluvium until reaching, after 450 m, the inhabited area at the foot of the hill.

The thickness of the deposits is between a few decimetres up to 2-3 m in the most significant accumulations area. The source volume, of about 10000 m^3 and the planimetric area, of the landslide have been identified according to field observation and aerial images surveys, taken after the event.

According to the classification system described by Hungr et al. (2014), the phenomenon would belong to the debris slide. Mass movements that start as sliding mass involving the surface layers and evolve in a rapid debris flow.

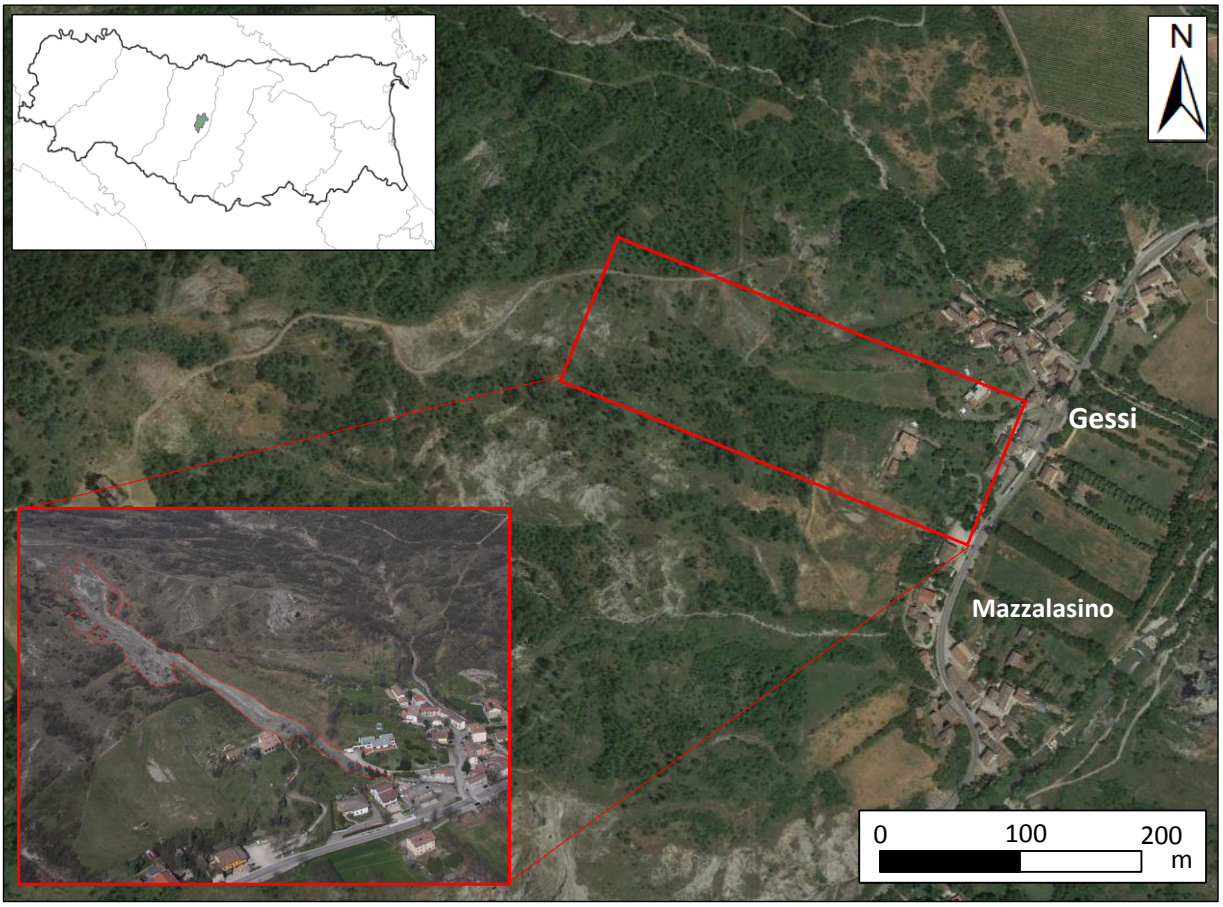

Fig. 46. Location of the study area and aircraft image of the Gessi-Mazzalasino landslide.

6.2.9 Geological setting

From the geological point of view the area is characterized by the External Liguride domain units and to the Neogene-Quaternary succession of the Northern Apennines (Fig. 47). The Liguride are represented by the unit "pre-flysch", deposited before the turbidite succession of the Upper Cretaceous and Paleocene, known as "Flysch Helminthoid". In the study area are found the outcrops of Clays of Varicolori di Casso and Palombini Clays.

- Palombini Clays (APA), constituted by an alternation of layers of clays and calcilutites. They have a dark gray or blackish color, and are massive or laminated. In many cases, however, they are very much deformed and appear as an indistinct clay mass, in which the original layers of calcilutite appear in blocks of various shapes and sizes.
- Clays of Varicolori di Cassio (AVV), heterogeneous formation, consisting of alternating red clays, gray, greenish and blackish and fissile very thin layers. The argillaceous layers are interbedded with sandstones and microconglomerati. The presence of carbonate breccias elements (calcilutites whitish siliceous) in blackish clay matrix, derived from

underwater debris and mud flows. The depositional environment is to flat mail submarine, below the carbonate compensation depth. Santonian-Campanian.

Over the latter is possible to find the most recent formations belonging to Neogene and Quaternary. The series corresponds to a new sedimentary cycle, which it develops on the edge of the mountain range, above the Ligurian territory. The pliocene and quaternary deposits give evidence of a regressive state, with switching from grading environments to transition environments. They represent the innermost portion of the south-western edge of Adriatic Avanfossa adjacent to the Apennines.

- Gessoso-solfifera formation (GES), consisting in selenitic gypsum in metric layers, with layers of debris gypsum and marl deposited in brackish lagoon environment. The formation is intensely tectonised, with variable thickness, due to the deformation. It was formed through alternating cycles of marine transgressions and regressions occurred during the Messinian (Upper Miocene).
- Quaternary continental soil, are represented by river deposits intravallivi, of piedmont alluvial fan and alluvial plain. They are defined as follows, from the oldest to the most recent: Sintema Emiliano-Romagnolo Lower (AEI) and Sintema Emiliano-Romagnolo Superiore (AES). In particular in the study area there is the AES; it consists of a unit with alluvial deposits of proximal alluvial fan and terraced deposits, between the ages of Middle Pleistocene and Holocene.

In the study outcrop, finally, the surface deposits separated on the basis of lithologic, textural and geometric characteristics.These deposits include: actual alluvial deposits (b1); slope deposits (a3); active and quiescent landslide deposits (a1).

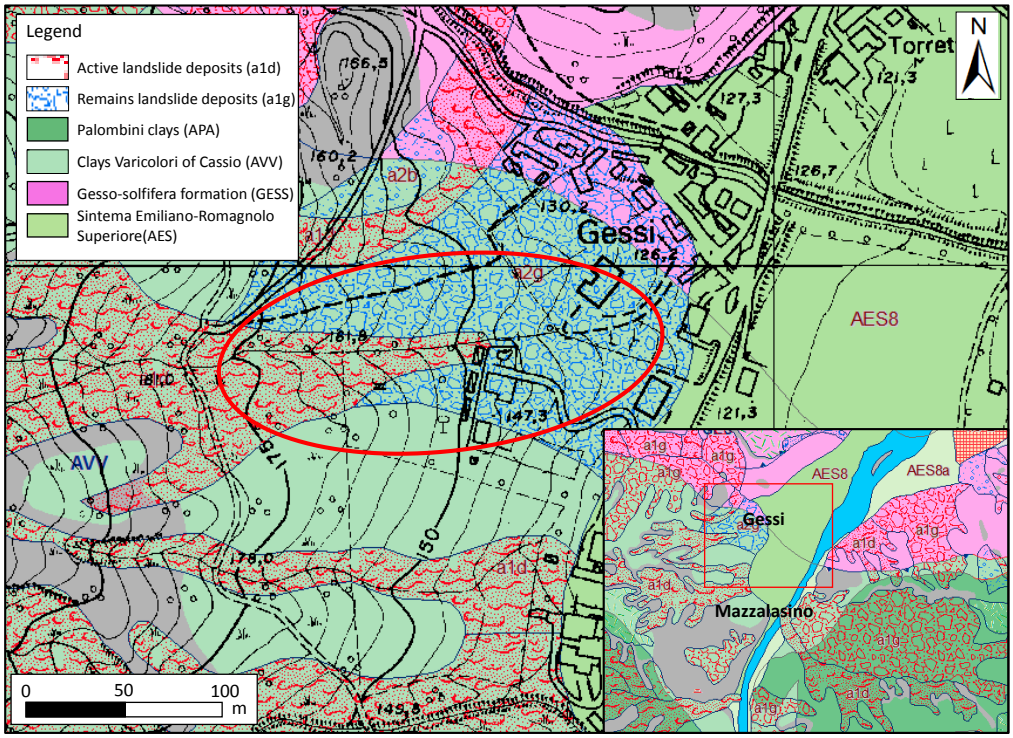

Fig. 47. Geological map of the study area.

6.2.10 Geotechnical characterization

In order to perform a geotechnical characterization of the involved materials was collected two soil samples at depth of about 10-50 cm (Fig. 48). The first samples located in the deposit area at the beginning of the channelled section the second at the landslide toe, those one were subjected to laboratory tests as index properties, grain size analysis, measurement of Atterberg limits and direct shear test. In addition, three geotechnical tests in situ were carried out with the aim to collect further information about the soil at the actual boundary conditions. In particular, two permeability measures with Constant Compact Head Permeameter (Amoozemeter) and one measure of shear strength with the Borehole Shear Test (BST) (Fig. 48).

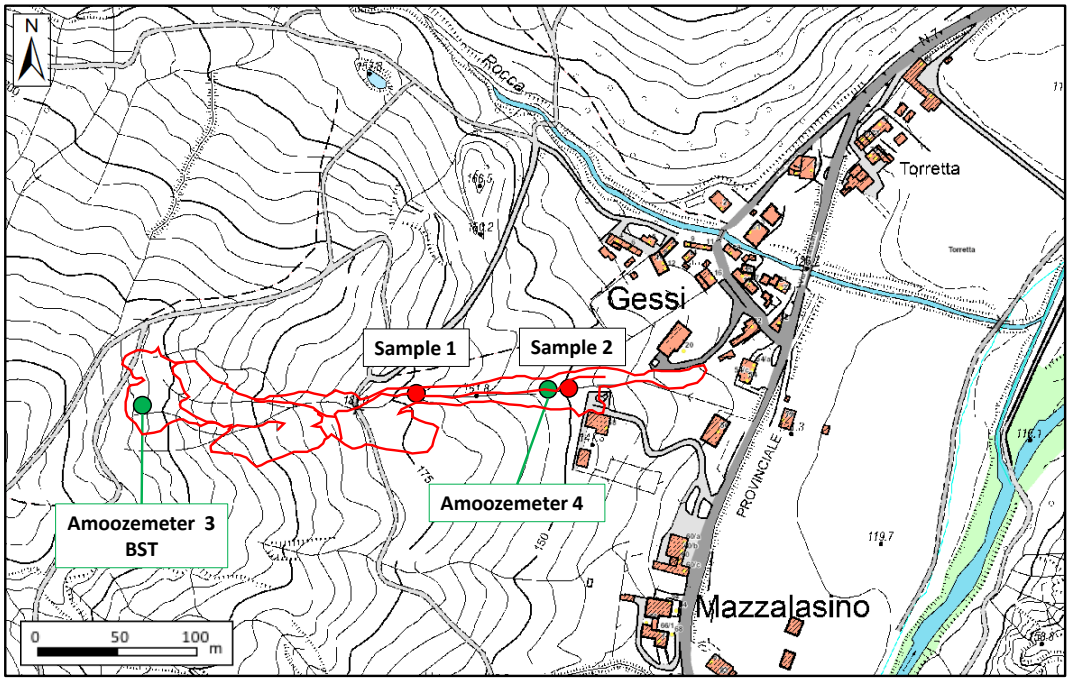

Fig. 48. The location of soil samples (in red) and of the geotechnical field investigation (in green).

The samples are mainly silty soils with a plasticity index ranging from 8 to 11 and were classified as CL and ML, following the Unified Soil Classification System (USCS, Wagner, 1957) classification (Table 11).

Table 11. Geotechnical parameters result

	Sample 1	**Sample 2**
USCS classification	CL	ML
Porosity (ρ %)	40.1	39.7
Void ratio (e -)	0.67	0.7
Total unit weigth (γ kN/m^3)	20.2	19.9
Water content (W %)	29.7	29.7
Liquid Limit (W_L %)	34	23
Plastic Limit (W_P %)	23	25

According to the classification of Hungr et al., 2014, it is possible distinguish the geotechnical material. In this case it is possible to analyze the W_L and W_P to understand the type of material involved in the mass movement. Considering the Plasticity index I_p =11 for the sample 1 and I_p = 8 for the sample 2 the material have a low plasticity and a Liquidity index I_L of about 0.6 and 0.5, respectively. The material can be considered between a "mud" and "debris", a unsorted material composed by a mixture of sand, gravel and cobbles with varying proportions of silt and clay. The water content can vary during the motion, due to the mixing with the surface water

(Hungr et al. 2014). In addition, according to the classification of Varnes' (1978) debris is all material containing than 20% coarse sizes (average diameter greater than 2 mm).

The test to find the friction angle and cohesion of material as conducted on the soil sample and in situ with the BST instrument. Direct shear tests were performed using normal stresses ranging between 40, and 80 kPa,

In the Borehole Shear Test (BST), the shear head of instrument is inserted into a 7 cm diameter borehole to the chosen test depth. A normal stress is then applied to push apart two serrated stainless steel plates, pressing them laterally against the sidewalls of a borehole. Then is important wait the soil consolidation at the first applied normal stress, (5 minutes for cohesionless soil and about 10 to 20 minutes for cohesive soil) after the shear head is pulled upward to measure the shear strength of the soil in contact with the plates. These operations are repeated four to five times using an increase of normal stress range from 20 to 80 kPA, according to the in situ characteristics. The results of two tests are show in Table 12; it is possible not a good agreement between laboratory and field shear tests.

Table 12. Results direct and borehole shear tests.

	Friction angle (ϕ °)	**Cohesion (c kPa)**
Sample 1	30.1	2
Sample 2	29.8	5
BST	33.8	0

The permeability tests are carried out with Amoozemeter a Constant Compact Head Permeameter used measurement of the saturated permeability of undersaturated soils. The test takes place preparing a borehole and filling it with water. The water level in the borehole is adjusted by raising or lowering the "adjustable bubble tube". When the water level has stabilized in the borehole, the exact depth of water is recorded as the "initial water level". After the water level is marked and the clock time recorded. Readings are repeated periodically every 30 to 120 s for sand and 60 to 120 min for clay. Periodic measurements of time and water-level marks are continued until the outflow and stabilizes at least three consecutive readings are approximately the same. The final water level in the borehole is recorded. More detail are in the works of Boersma (1965), Bouwer and Jackson (1974), Amoozegar and Warrick (1986), Philip (1985), Stephens et al. (1987), Amoozegar (1989a, 1992), and Amoozegar and Wilson (1999).

The results for two tests site are show in the Fig. 49a, b, the permeability is 2.19 X 10^{-6} and 5.19 X 10^{-7} m/s.

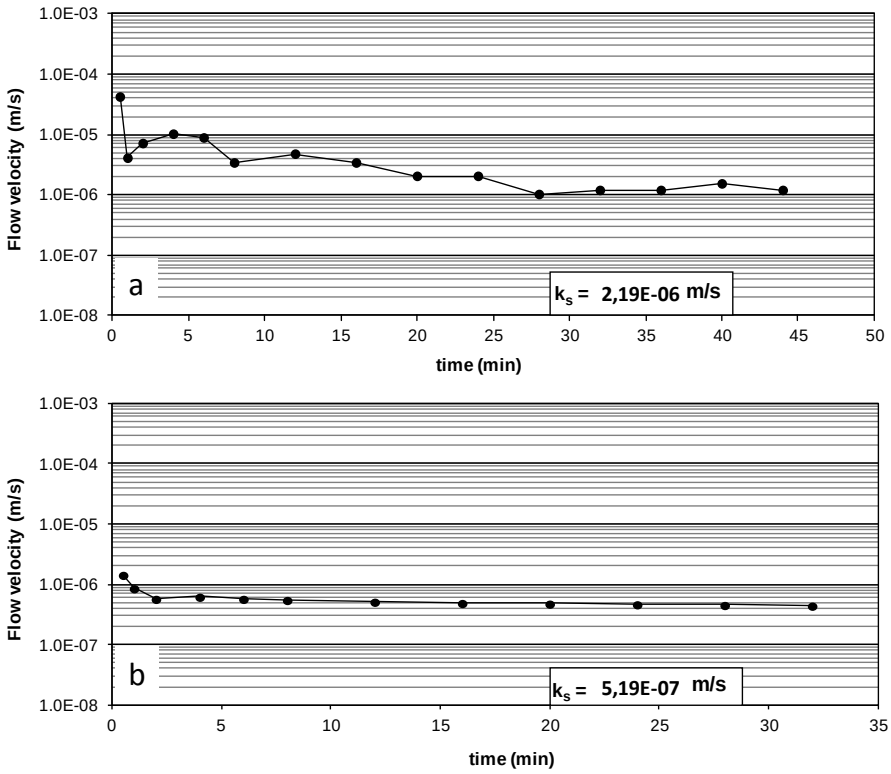

Fig. 49. Results of Amiizmeter test a) test site 3 and b) test site 4.

6.2.11 Velocity analysis

The flow velocity was estimated along the cross sections showed in Fig. 50, by mean of two methods (described in the paragraph 5.1.3): the superelevation of the debris surface in channel belt (Chow, 1959) and the Poiseuille equation (Hungr et al. 1984).

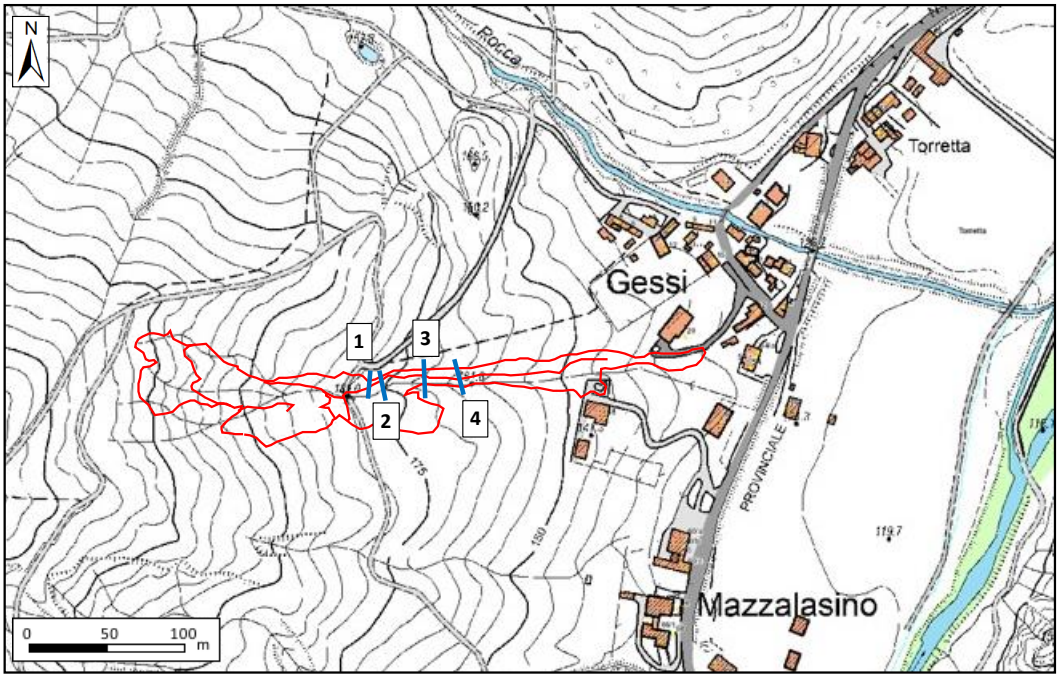

Fig. 50. Localization of cross-section for the velocity empirical evaluation of the flow.

The flow's curvature radius of the central streamline was calculated where debris slide arrive at the channel and become a debris flow, in this points the flow travels around a bends (cross-sections 1 and 2, Table 13). The curvature radius of the channel was obtained from a graphical processing using a 1:500 topographic map. On the other hand in the cross-sections 3 and 4 (Table 14), the velocity estimation was based on Poiseuille equation suitable for the straight sections, considering the dynamic viscosity (v) value equal to 3 as indicated by Hungr et al. (1984) and the constant based on the cross-sectional shape of the channel (l) equal to 3. In the next chapter the values were also compared with the results of the numerical model velocity in the same cross-section.

Table 13. Flow velocity obtained by Chow (1959).

Cross-section	g (m/s^2)	R_c (m)	Δh (m)	w(m)	**v (m/s)**
1	9.81	17.1	0.5	3.1	5.20
2	9.81	18.8	0.5	3.6	5.00

Table 14. Flow velocity obtained by Poiseuille equation (Hungr et al. 1984).

Cross-section	γ (kN/m^3)	δ (°)	H (m)	I (-)	ν (kPa)	**v (m/s)**
3	20	12	2.8	3	3	3.62
4	20	12	3	3	3	4.15

6.2.12 Laser scanning survey

The laser scanning investigation was performed during two field surveys, in data April 1st, 2015 and April 16th 2015, by means of a long range 3D Terrestrial Laser Imaging Sensor (RIEGL LMS-Z420i device), which is able to determine the position of up to 12,000 points per second, with a maximum angular resolution of 0.008°, and an accuracy of ± 10 mm from a maximum distance of 800 m (Giglie et al. 2014).

In order to completely cover the intervention areas and avoid the shadow areas, surveys from four different scan positions were performed (Fig. 51a).

Some laser cylindrical reflectors were placed on the slopes, and their coordinates defined by performing a differential Global Positioning System (GPS) survey. These tie points have been used subsequently to align the point clouds. This operation is always needed for correctly geo-referencing the point cloud on a chosen reference system and to merge two or more scans of the same object realized from different points of view.

In data 22nd April, 2015 another further GPS survey was carried out, in order to reconstruct the exact geometry of the landslide body, define the source area and identify the fractures of the land that could constitute the edges of further potential detachment areas.

The data obtained from the survey laser scanners have been processed with RiscanPro 1.7.9 software. The operations to obtain an HDDEM are described in the chapter 4.2.3. Due to the presence of buildings and dense vegetation, enough reliable information of some of the landslide areas were not acquired, in particular of the toe portion. Therefore it was necessary to integrate the relief of the CTR in scale 1: 10.000, performing a Digital Elevation Model (DEM) based on the filtered data from the laser scanner survey. The model was then sectioned horizontally obtaining the contour lines, which were finally attached to those of the existing CTR (Fig. 51b).

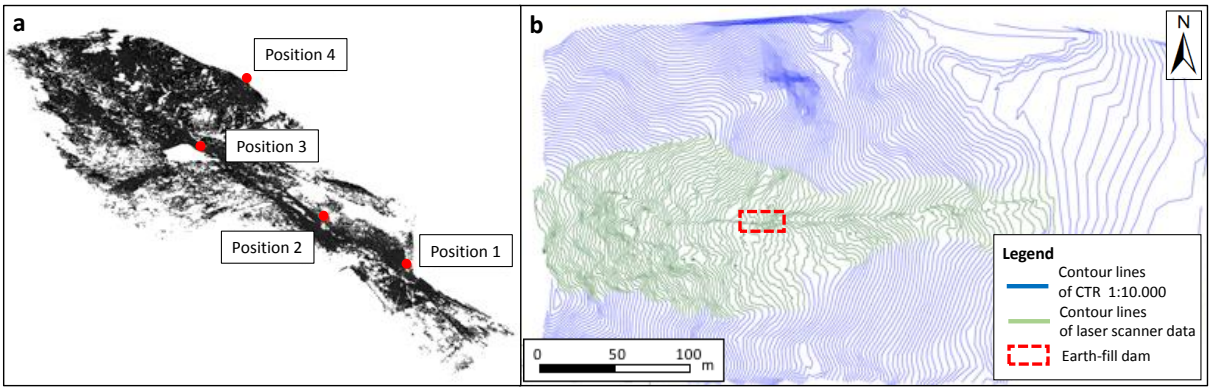

Fig. 51. a) Four different scan positions and b) laser scanner data integrated with the CTR (1:10.000).

In the period in which the data processing operations were carried out, some safety work on the landslide area were executed. These works have provided, in an initial phase, the execution of an earth-fill dam (Fig. 52) with the aim to prevent the excessive expansion of possible future landslides and to channel the flow towards existing channel. One last GPS survey, in date 9th September, 2015 was carried out to detect the geometry and location of the earth-fill dam which has been implemented in the digital terrain model, in order to obtain the current representation of the slope at the actual post landslide conditions.

Fig. 52. Earth-fill dam, built during safetying operations in landslide area (the position is shown in Fig. 51).

6.2.13 Gessi-Mazzalasino landslide back analysis

The calibration procedure is based on trial and error back-analysis in order to identify the most suitable rheological parameters to modelled the Gessi - Mazzalasino landslide event of March 27th 2015. To perform the back analysis both DAN-W and DAN3D were used.

For the back analysis a Digital Elevation Model (DEM) at 5 m grid node was created using a CTR 1:5000. This DEM has been integrated with the channel section derived from laser scanner survey due to the low resolution of CTR, which changed the real event dynamic and it has been smoothed with a Gaussian filter 3x3. In accordance with the landslide scenario, described above, a total volume of 10000 m^3 was assumed in accord with field investigations and the rest within the area. Using an approximate uniform source thickness of 6 m.

For DAN-W simulation a profile line crossing all landslide start from 228 m a.s.l. and stop at 130 m a.s.l. at the landslide toe, was considered (Fig. 53).

The entire phenomenon was divided in two main materials that represent different phases of the motion of the flow. Indeed, the event starting as a debris slide and transforming into debris flow at about 180 m a.s.l., where the flow is channelled. The Voellmy rheological model was choose, found in previous back analysis of similar events (Hungr and Evans 1996). Two basal shear resistances were chosen according to the landslide dynamic, the first rheology material has been used on the source area until the channelled sector (between 226 m and 173 m a.s.l.), the second was assumed in the channelled sector until the landslide toe (between 173 m and 131 m a.s.l.). The Voellmy resistance parameters were adjusted by trial and error to achieve the best simulation in terms of the flow velocity, observes thickness of deposits and the distance covered by the debris.

The best results from back-analysis provide a value for frictional coefficient of f=0.19 for first material and a value of f=0.15 for the second, while the turbulence term of ξ=250.00 m/s^2 remain constant throughout the event (Fig. 53).

Internal friction angle controls the longitudinal stress in the flowing landslide mass (Savage and Hutter, 1989) and it was set at 30° for simulations, according to the value obtained to laboratory and field test. The volume weight was set at 20 kN/m^3. The entrainment of the material from the path was not considered because the field investigations indicate that entrainment quantities were not very significant.

The analysis with DAN-W and DAN-3D give comparable but not exact results but these show a good agreement between simulation results and data field obtained by a first GPS survey, both in the average thickness and in the planar extension of the deposits. The landslide arrive at the flat area located in the middle of the slope, where the most of mobilized material is deposited up to 2 m of thickness, after moves in the impluvium until reaching, after 190 seconds, the inhabited area.

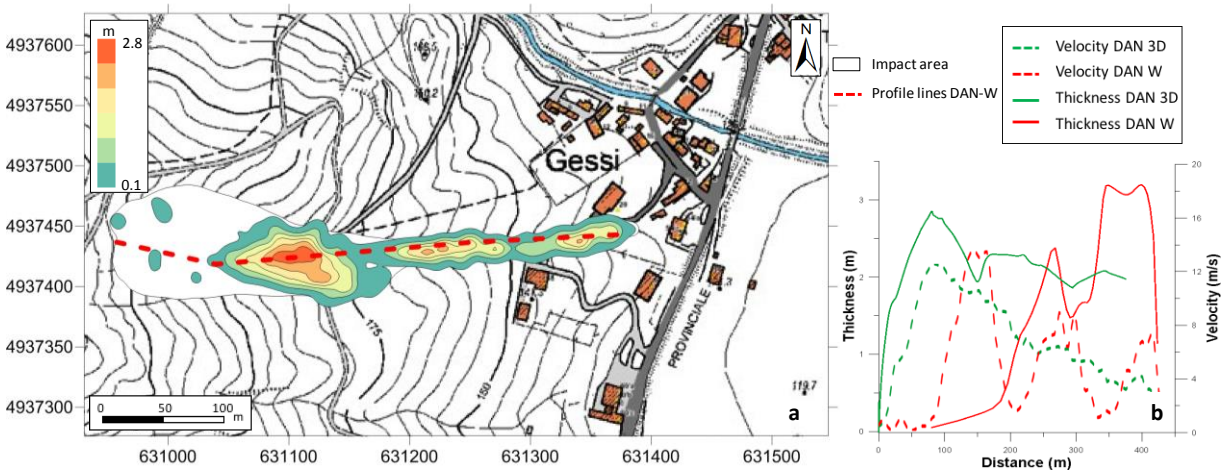

Fig. 53. Results of back analysis a) DAN-3D deposit thickness and impact area b) comparison between the DAN-W and DAN-3D.

The flow velocity obtained with models along the four cross-sections (Fig. 50) results higher than the velocity obtained by the empirical relationship in the first three section, while are very similar in the distal part (Table 15). These differences derive from the assumptions made during the simulation phase that make difficult to model both the kinematical and the depositional parameters of the flow, where our attention was mainly focused on.

Table 15. Empirical and numerical modelling velocity results.

Cross-sections	v (m/s) (Jonson and Rondine, 1984)	v (m/s) (Hungr et al. 1984)	v (m/s) (DAN-W and DAN-3D)
1	5.2	-	7.1
2	5.0	-	6.9
3	-	3.6	5.1
4	-	4.1	4.6

According to the model results, the flow would reach maximum speeds of about 8-12 m/s, in the upper part then has slowed down entering in the impluvium and stopped when the slope

decreased. These results are in agreement with the testimonies of local residents, who evaluated approximately the flow velocity, in the last meters, around values of the order of 0.5-1 m/s.

6.2.14 Empirical prediction methods

There are several empirical methods which connect four geometric parameters of characterization of landslides to predict the runout distance for forecast analysis; in particular in this case study were used three methods presented by Corominas (1996), Rickenmann (1999) and Hunter and Fell (2003), they correlate the flow's angle of reach with the volume:

[66] $log_{10}\left(\frac{H}{L}\right) = Blog_{10}V + A$ *(Corominas, 1996)*

[67] $L=1.9\ V^{0.16}\ H^{0.83}$ *(Rickenmann, 1999)*

[68] $\frac{H}{L} = 0.69tan\alpha_2 + 0.085$ *(Hunter and Fell, 2003)*

Where α_2 is the slope inclination while *A* and *B* are coefficients depending on the landslide types.

The results obtained, summarized in Table 16 show differences between the methods used to evaluate the run out distance and the comparison with the model and field investigations results.

Table 16. Runout distance calculated with empirical methods and calculated by numerical model and field investigations.

	A (-)	B (-)	V(m^3)	α_2 (°)	H (m)	**L (m)**
Corominas (1996)	-214	-0.07	10000	-	100	**234**
Rickenmann (1999)	-	-	10000	-	100	**299**
Hunter and Fell (2003)	-	-	-	12	100	**324**
DAN-3D	-	-	-	-	-	**205**

The results show that the worst case scenario, in terms of maximum distance of propagation, is proposed by Hunter and Fell (2003), with the runout distance of about 324 m, the other mathematical relations show lower values. This distance of Corominas (1996), of about 234 m is in good agreement with DAN-3D results.

Rickenmann (1999) and Hunter and Fell (2003) relationships provide a runout distance greater than those predicted by numerical model.

All the results provided by the empirical relationships and numerical model, still indicate that the landslide stops near the inhabited area and do not constitute a safety hazard of the population.

6.2.15 Forecast analysis

In order to evaluate the characteristics of new potential landslides in the area, another numerical simulation with DAN-3D was performed.

For this analysis, a new digital elevation model acquired by a laser scanner survey (TLS technique) was used (Fig. 51). This one represents the topography of the slope after the landslide in HRDEM. The model was smoothed with a 50 cm filter and resample into a 2 × 2 m grid, in order to eliminate the roughness obtained from the survey and marked during the elaborations. The simulation was carried out using the parameters found in the back analysis. For the forecast event was considered the same source area and volume of the past event of about 10000 m^3, assumed through field surveys. This volume portion was removed from HRDEM in order to obtain a representation of the topography surface.

The results show that, thanks to the safety work, the landslide impact area results to be smaller than that 2015 event. There should be no damage to downstream homes and all the mobilized mass stops at the beginning of impluvium, after 70 seconds. The maximum thickness of about 2.8 m is reached in the flat area at the middle of the slope with a maximum velocity of about 12 m/s (Fig. 54).

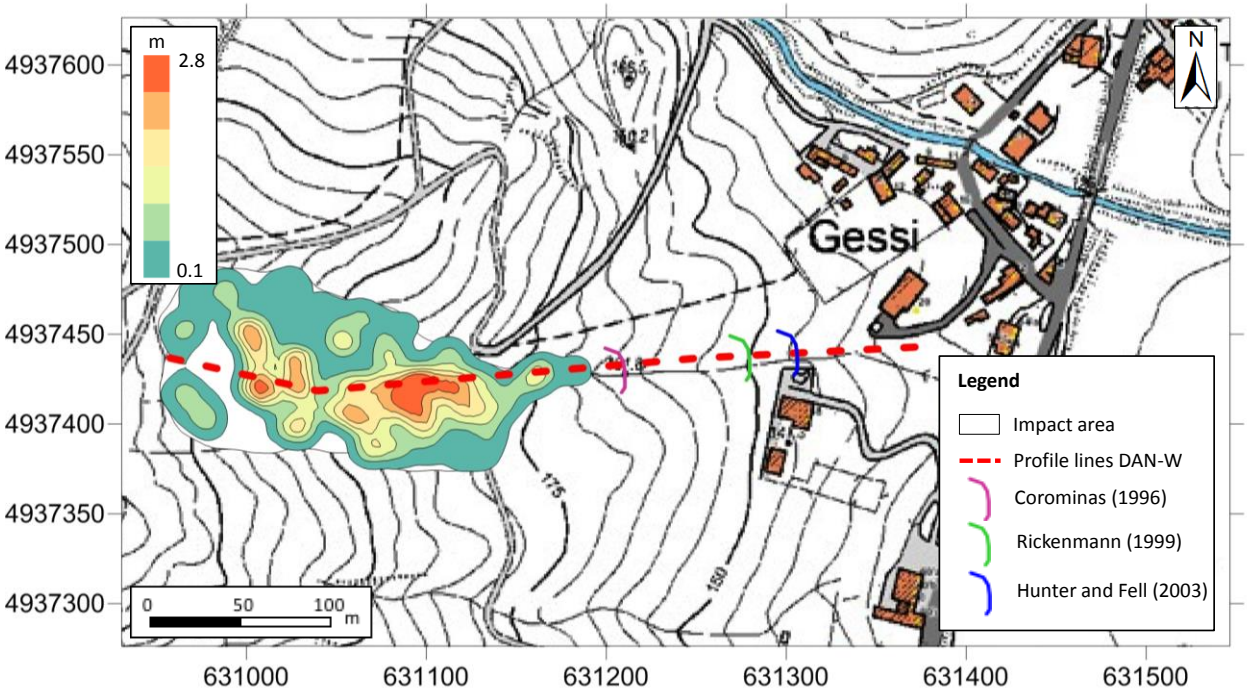

Fig. 54. Result of forecast simulation and comparison between the maximum runout distances obtained from both empirical and numerical methods.

6.2.16 Conclusion

The March 27th, 2015 a debris slide event detached from the upper part of Gessi-Mazzalasino village. The event was characterized by means of some geotechnical analysis and LiDAR surveys. In order to obtain more information about landslide runout the flow velocity was calculated along four cross sections, by mean of the superelevation of the debris surface in channel belt method (Chow, 1959) and the Poiseuille equation method. The latter, parameters with the field surveys data and runuot empirical equations were used to model the 2015 event by means of DAN-W and DAN-3D numerical codes and their results were discussed.

The runout simulation was obtained applying the Voellmy rheology to each of the two materials in which the path of the landslide was subdivided. The rheological parameters have been modified by trial and error procedure in order to obtain the best simulation of the 2015 event back analysis. Finally the models of DAN-W and DAN-3D were compared and there are able to reproduce with high accuracy: the debris flow impact area, the deposit thickness and the velocity of the debris slide. In order to assess the Gessi-Mazzalasino village exposure to possible future debris flow events, based on the back analysis results, a forecast analysis was performed. This analysis was carried out by means of DAN-3D simulations, considering the new topography acquired with TLS LiDAR survey (RIEGL LMS-Z420i device) and a source area and volume

calculated by field investigation, like the past event. The forecast event produce an impact maps area useful to evaluating the future scenario could be affect the Gessi-Mazzalasino village.

The obtained results show that the integration of the modelling technique with geomorphologic characteristics acquired by field investigations, together with the LiDAR surveys, can be a very useful tool for the scientific community and local administrations in order to manage the problem related to landslide events.

6.3 Santa Trada landslide

The landslide of Santa Trada is located in Santa Trada of Cannitello, in the municipality of Villa San Giovanni (RC) and affects a portion of the NW slope of Poggio Pignatelli (or Pignatello), on the left bank of the Santa Trada torrent (or Santa Trara). The slope has an inclination of 25 - 30° upslope with an increase up to 40° downslope. The study site is located about 3.5 km SW of Sicily, and about 4.5 km NE of Villa San Giovanni, near the Viaduct of Santa Trada of the motorway A3 Salerno-Reggio Calabria (Fig. 55).

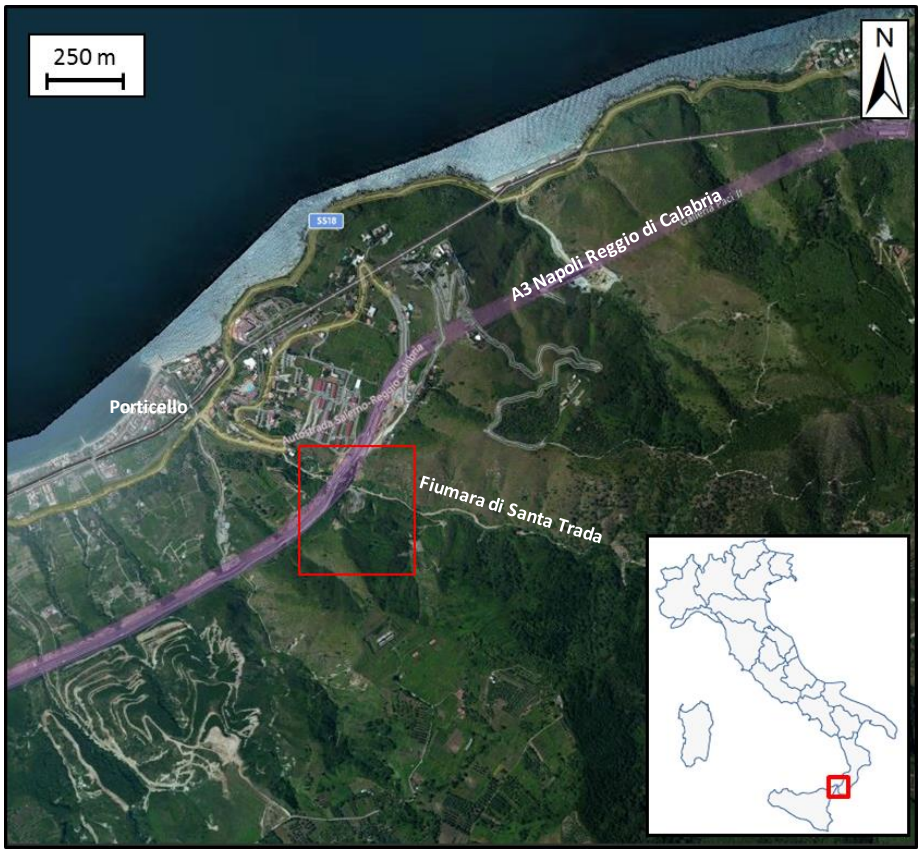

Fig. 55. Location and satellite image of the study area.

The Santa Trada landslide is classified ad a rock/debris slide (Hungr et al. 2001) has a total volume of about $10x10^3$ m^3 and put at high risk the motorway (Fig. 56c), namely the A3 branch located in the Calabria Region (Southern Italy) and the village below. In particular, on January 30th, 2009 after a period of heavy and persistent rainfall, a small portion of a slope located on the left side of the Santa Trada Creek Valley, involved in a rock/debris slide. The landslide started at approximately 140 m a.s.l., covering an area of about 4150 m^2 and is only a portion of the total rock mass instability that affects the slope. As show in Fig. 56a and b, near the source area there is the evidence of two main fractures cutting the depth of deposits. The first situated

at an altitude of about 190 m a.s.l. and the second located at an altitude of about 180 m a.s.l., delimiting largest unstable area. The slope portion detached during the 2009 event have a thickness of about 1 m, while considering geomorphology analysis and the recent geological field investigations the thickness of the portion delimitated by the second fractures (at 180 m a.s.l) is estimated between 3 and 5 m. Nevertheless, in a further analysis by Bozzano et al. (2012), the total source thickness considered for rock mass involved in gravity induced deformation, starting from 190 m a.s.l. is of about 23 m.

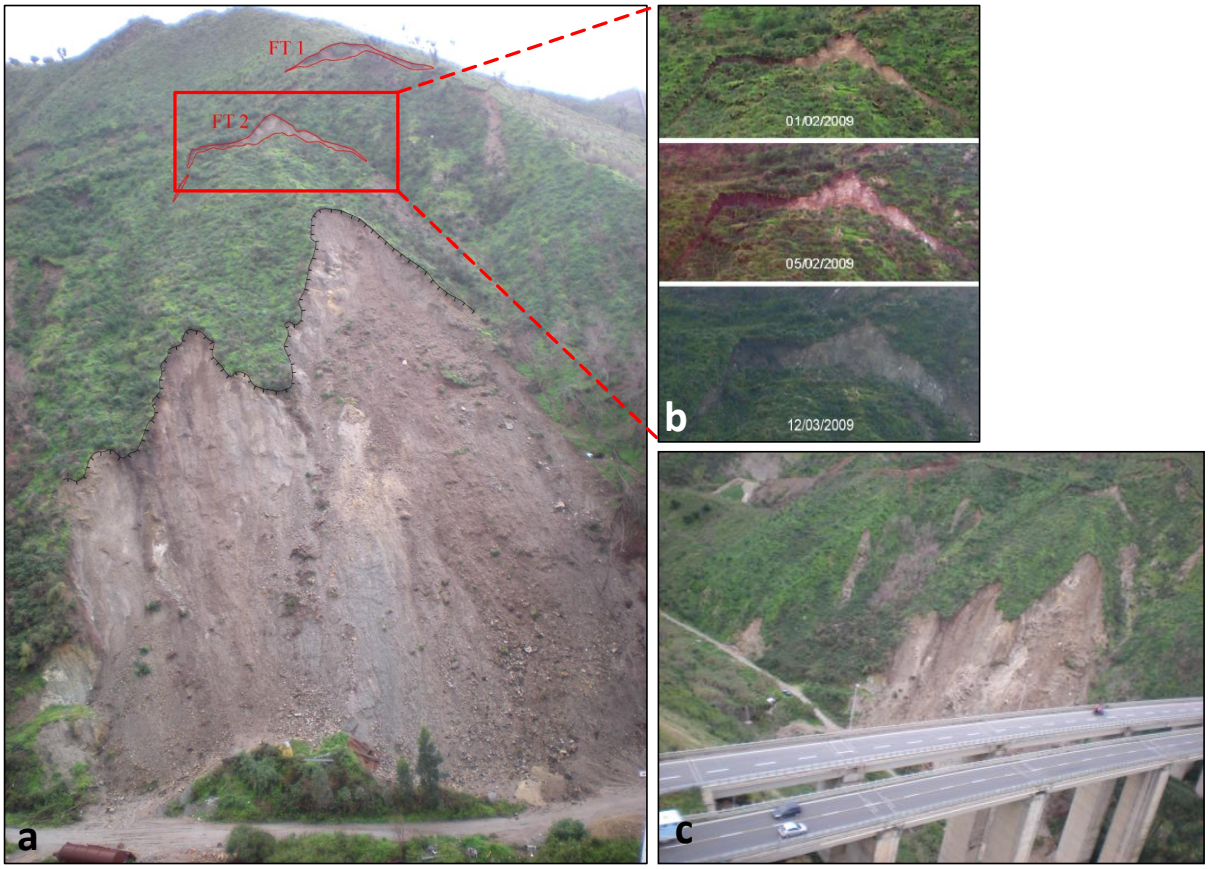

Fig. 56. Pictures of Santa Trada lanslide, in red the two fractures.

The gravitational instability of Santa Trada can be account as a mass rock creep, subjected to a gravitationally unstable state for a long period and strongly dependent on the visco-plastic features of the highly jointed gneiss. As Bozzano et al. (2012) say, the deformations of the rock mass are strictly related to the multi-stage evolution of the Santa Trada River Valley and to the anthropogenic stress release due to the quarry activity modified the strain rate of the rock mass. In fact, although no historical data of this landslide are available, in the official maps of the "Hydrogeological Setting Plan" (PAI – Piano di As- setto Idrogeologico) and of the "Inventory

of landslides in Italy" (IFFI – Inventario dei Fenomeni Franosi in Italia) several landslides landslide have been mapped in this area.

The landslide of the 30th January, 2009 was triggered due to the intense rainfall events that occurred during the 3 months before. Data recorded by the meteorological station located close to the study area, in the village of Scilla (RC), show that the cumulative rainfall measured in the month of December 2008 and January 2009 reached approximate 146.0 mm and 188.6 mm, respectively. These values are over the seasonal average and causes the soil saturation, worsening the already critical hydrogeological condition (Del Ventisette et al. 2011).

6.3.1 Geological setting

From a geological point of view the territory of Calabria is the connection between the Southern Apennines and the chain Sicilian-Maghrebian. This arc performance is due to the convergence between the Euro-Asian and African plate. The arc Calabro Peloritano is the innermost element of the chain and consists of several tectonic units on a Paleozoic crystalline basement. The latter emerges along the Tyrrhenian coast together with Miocene and Pliocene covers, plunging towards the SE and tiltate by St. Euphemia and Novigrad faults (Ferranti et al., 2008).

In the study area outcrops gneiss ascribed to the Ercinic substratum of the Calabrian arc and part of the Aspromonte metamorphic unit (Lentini et al., 2000; Carbone et al., 2008). These metamorphic rocks are characterised by a predominant isotropic, granular texture, including biotitic micas, plagioclasic minerals and rounded xenoliths. The area is also characterised by too many hierarchical terrace marine orders. These are composed of reddish-brown gravels and sands with a dip angle of less than 10°. They are transgressive on the Ercinic metamorphic substratum, as demonstrated by an about one meter-thick pebbly level that can be observed at their base (Fig. 57).

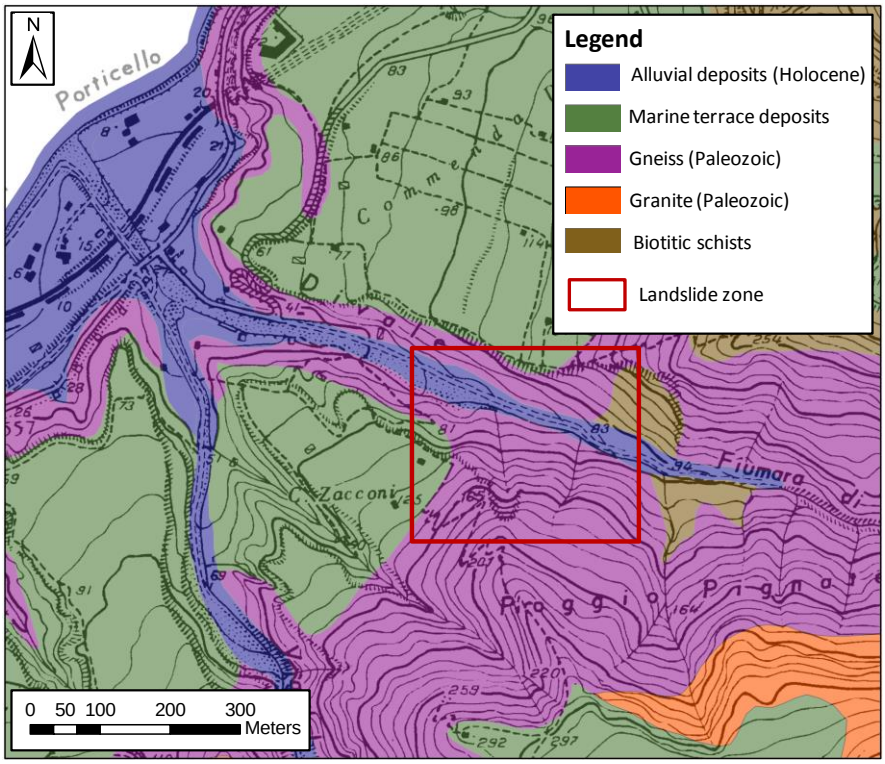

Fig. 57. Geological map of the study area.

6.3.2 Santa Trada GB-InSAR

The GB-InSAR was installed in front of the slope, on the motorway (Fig. 58), on 31 January 2009 and on 1 February, just 48 h after the occurrence of the landslide, the monitoring campaign started. The images are used to perform interferometric measurements and to derive displacement maps. Considering that radar interferometry provides only the displacement component along the radar line of sight (LOS), the viewpoint of the radar was selected so that its LOS was as parallel as possible to the expected direction of the landslide motion. The GB-InSAR, implemented by the Ellegi-LiSALab s.r.l. company, is composed of a continuous-wave step-frequency (CW-SF) transceiver, a 2.0 m long linear rail and two antennas that move on it at steps of few mm, therefore permitting the realization of synthetic aperture. The microwave transmitter produces, step-by-step, continuous waves at discrete frequency values, sweeping the bandwidth from 17.0 to 17.2 GHz (Ku band). Fig. 59 shows the image resolution grid generated with the acquisition parameters used for monitoring and the measurement parameters used by the installed system for monitoring the Trada Santa landslide.

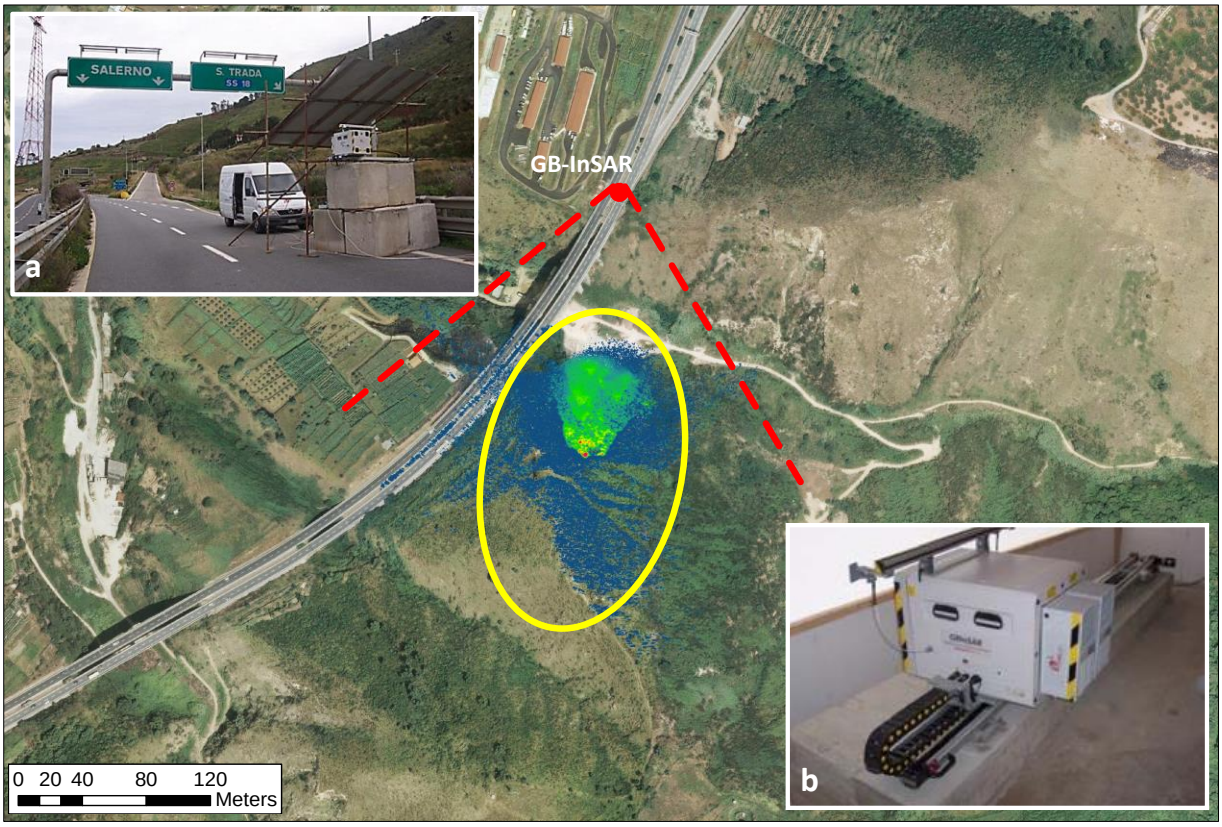

Fig. 58. Localization of the Santa Trada landslide and the radar image on ortophoto, a) the GB-InSAR position on A3 motorway and b) the GB-InSAR instrument.

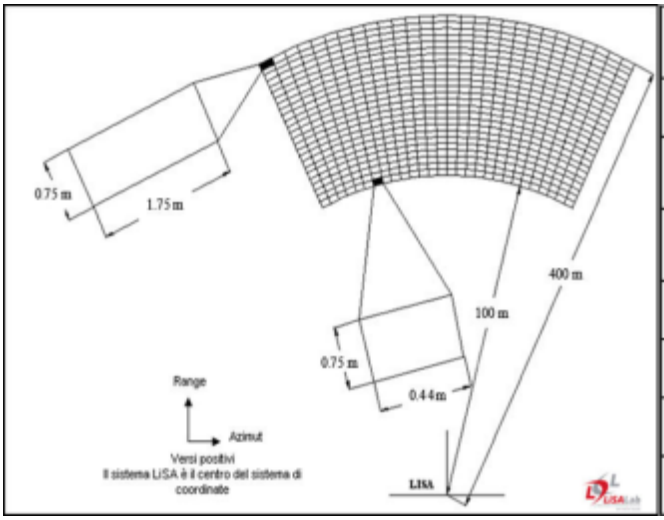

Central frequency	17.1 GHz
Bandwidth	200 MHz
Length of synthetic aperture	2 m
Minimum distance from the target	100 m
Maximum distance from the target	400 m
Range resolution	0.75 m
Azimuth resolution at 100 m	0.44 m
Azimuth resolution at 400 m	1.75 m

Fig. 59. Resolution grid size used during the monitoring campaign of Santa Trada.

Images can be acquired with a minimum of 6 min delay. Processed GB-InSAR data are sent for daily dispatching procedures aimed at monitoring the onset of deformation of the concerned area. The usefulness of the GB-InSAR system was not only limited to its capability of fully characterizing the landslide in spatial terms; it also permitted the operators to follow, during the whole campaign, the evolution of the mass movement and to study its kinematic behaviour,

which is fundamental in order to assess the risk scenarios' temporal evolution. The campaign lasted until 24 April when the emergency phase was declared finished.

The radar data used are the displacement maps 24h (acquired with rolling procedure); these maps allow to assessment the daily cinematic variations. To understand the area affected by movement and evaluate the magnitude of involved material is necessary overlapping radar images and optical image; this also allows us to suppose the possible risk scenarios. The displacement maps concerning to the monitoring period, highlight how the area affected by the major displacements is bounded by the second fracture (Fig. 56) and covers an area of about 6000 m. During the whole monitoring period several acceleration and deceleration phases were clearly detectable (Fig. 60):

- in the first 24 hours of monitoring it has been recorded a maximum speed of about 10 mm/h in proximity of the first fracture. Is also evident a second zone characterized by high located movements on the right side of the image (to the W). This area, from the typical form of a detrital cone, presents a speed of about 7 mm/h (Fig. 60a);
- starting on 3 February, the western sector of the landslide decreases its activity, while the eastern portion (left image) has an acceleration and records a displacement of about 200 mm in 24 hours, corresponding to a velocity of about 8 mm/h. Also the upper part of the landslide undergoes acceleration, reaching a speed of about 12 mm/h. The eastern sector of activities culminates on February 4 with the collapse of a small landslide inside the main body (Fig. 60b);
- on 12 February is recorded an acceleration that affects both the nearby portion of the first fracture (which records velocity of about 10 mm / h) and the two bottom areas, the eastern one (12 mm / h) and the West (> 13 mm / h; Fig. 60c);
- A peak velocity occurs from March 6th and lasts for about a week. In this case the activity mainly affects the eastern sector of the lower part of the landslide (Fig. 60d).

Thereafter until to 24 April, the date of the end of the monitoring, the landslide has been characterized by a general decrease of its speed, except for two brief acceleration peaks between 13 and 15 March and on 21 and 22 March they have affected the sector to the west and the eastern sector, respectively.

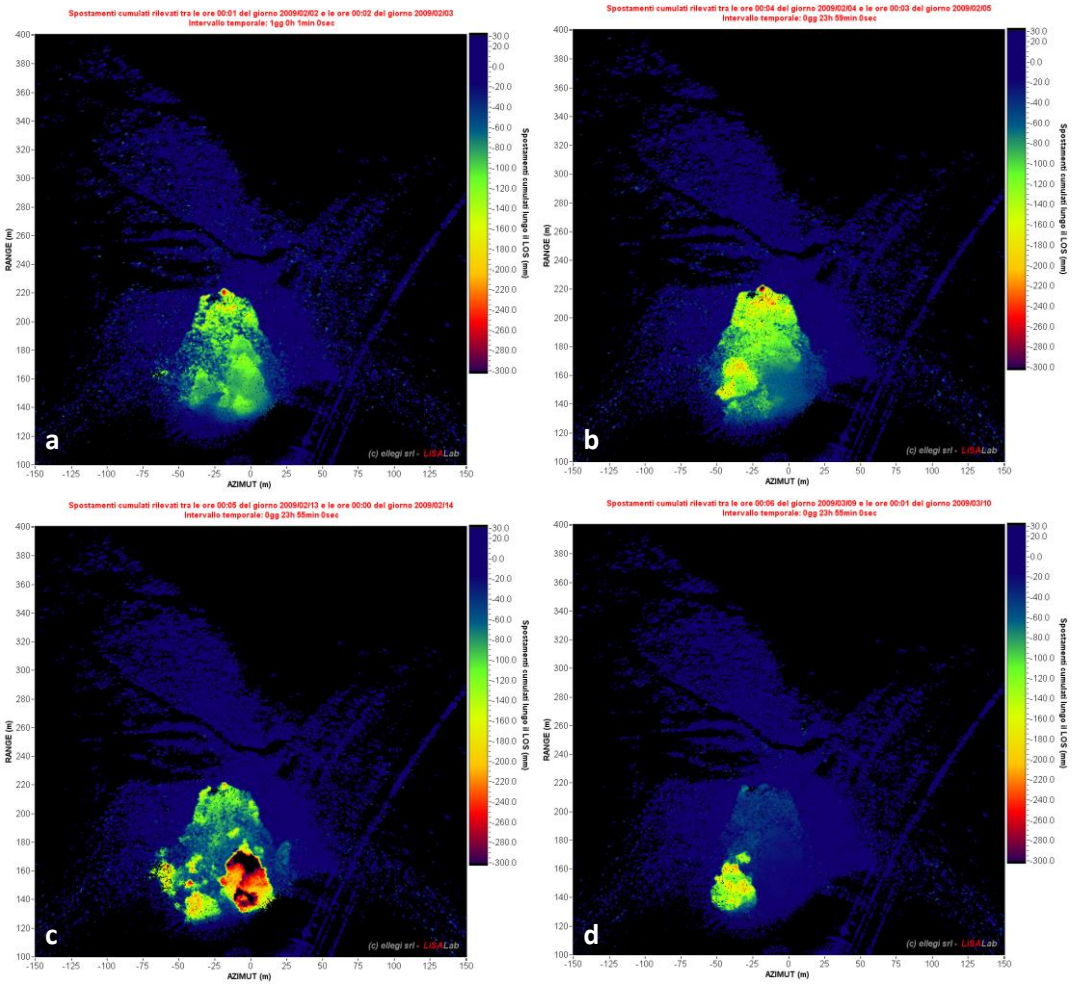

Fig. 60. Displacement maps with full scale at -300 mm, a) on a time interval of 24 hours and 1 minutes, from 00:01 on February 2nd, 2009 at 0:02 of the February 3rd, 2009, b) on a time interval of 23 hours and 59 minutes, from 00:04 on February 4th, 2009 at 0:03 of the February 5th, 2009, c) on a time interval of 24 hours, from 00:05 on February 13th, 2009 at 0:00 of the February 14th, 2009, d) on a time interval of 24 hours, from 00:06 on March 9th,2009 at 0:01 of the March 14th, 2009.

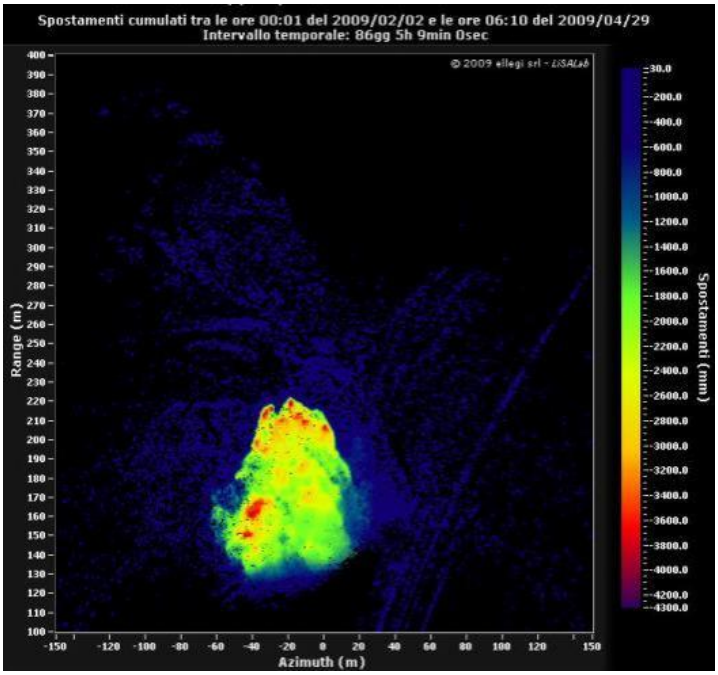

Fig. 61. Displacement map with full scale at -4300 mm to an interval of 86 days 5 hours and 9 minutes, from 00:01 on February 2nd, 2009 at 06:10 to April 29th, 2009.

According to interferometric data collected during the GB-InSAR monitoring campaign, the unstable area as an extension of nearly 6000 m^2 and a volume estimated of about 18.000 – 30000 m^3 (Fig. 61).

6.3.3 Santa Trada landslide back analysis

Numerical simulations of the 2009 event have been performed using DAN-W (Hungr, 1995) and DAN-3D dynamic models (McDougall and Hungr, 2004). A previous analysis was carried out used the model DAN-W and after, the rheological parameters found were applied to modelling with DAN-3D. As showed in the previews work of Revellino et al. (2013), DAN-W is very useful friendly and allows to easy adjusting the rheological parameters that may be implemented in DAN-3D to obtain the landslide path area.

For Santa Trada landslide the geometry path was reconstructed on a 1:5.000 scale DTM produced by Calabria 2007-2008 flight and resampled through bicubic interpolation method with mesh square 5x5 m. The profile line is located in the centre of the landslide as showed in Fig. 62 The source area of the modelled was made considering the description of the event by Del Ventisette et al. (2011), with the initial starting at 140 m a.s.l. and assuming to have a uniform thickness of 1 m, measured perpendicular to the slope. The profile line has a length of about 100 m with a maximum width of about 90 m.

The rheological relationship selected for the present analysis is the frictional model with a bulk basal friction angle $\phi_b = 35°$, chosen by trial and error procedure starting from the results found in literature for rockslide with comparable material and slope characteristics (Hungr and Evans, 1996; Pirulli, 2004; Willenberg, 2009).

The result of DAN-W back analysis is shown in Fig. 62b. The final flow profiles are plotted after 30 s when the landslide stops at the end of the slope. The velocity profiles are shown both for the front and the tail of the landslide reached a maximum peak of about 16 m/s. The outcomes of this analysis are also summarized in Table 17, in which models results are compared, including impact area and thickness of deposits. As in the field estimations the simulated deposit thicknesses is lower than 3 m and the landslide stop at the toe of the slope without causing damage to the viaduct.

The rheological frictional model found with DAN-W has also been used for the simulation with DAN-3D numerical modelling. This requires three sets of data files: the topography of the unfiled slope, the initial source mass, and the maximum depth of the material that can be entrained within a prescribed "entrainment zone" along the path.

The path file was obtain using DTM produced by Calabria 2007-2008 flight (1:5000 scale) taken before the event and filtered using a Gaussian smoothing (3×3). The source file was adjusted considering the thickness of 1 m, in order to estimate the starting volume of about 4250 m^3. No erosion has been considered.

As shown in Table 17, the value of frictional angle 35° produced the best final results. The Fig. 62 shows the results plotted at the end of simulation and the comparison between DAN-W and DAN-3D results.

Table 17. Summary of the input used and the main outcomes and comparing results.

	Landslide event of 2009	
	DAN-W	**DAN-3D**
Number of blocks/particles	50	2000
Unit weigth g (kN/m^3)	26.4	26.4
Friction angle, ϕ_i (°)	55	55
Bulk basal friction angle, ϕ_b (°)	35	35
Start Volume (m^3)	4250	4250
Impact area (m^2)	5500	6000
Peak velocity (m/s)	14	18
Max deposits thickness (m)	2.3	3.4

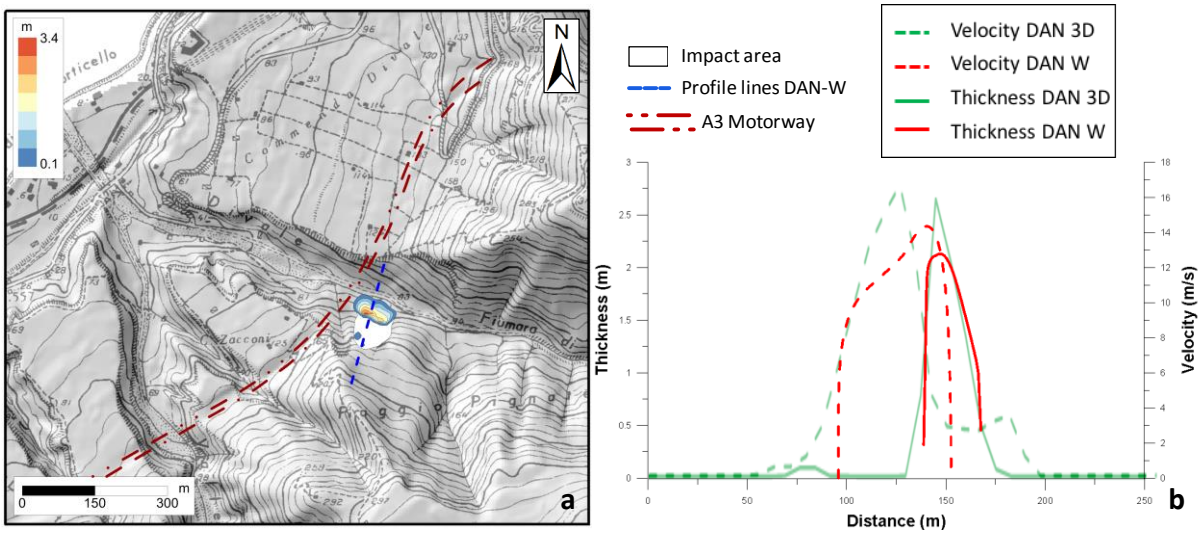

Fig. 62. The back analysis results of 2009 event, a) DAN-3D deposits thickness and impact area; b) comparison between the DAN-W and DAN-3D.

6.3.4 Model forecast

To understand the landslide runout evolution an analysis of radar data is conducted using the MATLAB code (describe in the Paragraph 5.2.1) in this case study 24h displacement maps was used to choose some new source areas which could be involved in future mass movements. Furthermore, it identifies the frequency with which the movements take place within the area considered. In this case was analysed 81 displacement maps acquired during the monitoring period between the February 2nd, 2009 and April 24th, 2009. The results show that the more critical area is delimited to the second fracture located at 180 m a.s.l with an extension of 6.000 m^2.

The analysis of the frequency map of displacement (Fig. 63) shows that there are only two small areas which during the monitoring period recorded repeatedly movement. By the analysis of the cumulative displacement maps it is possible, therefore to determine, two different scenarios of risk:

- the landslide could be reactivated starting from second fracture at 180 m a.s.l and collapse as a whole;
- the landslide could be developed in a series of small collapse.

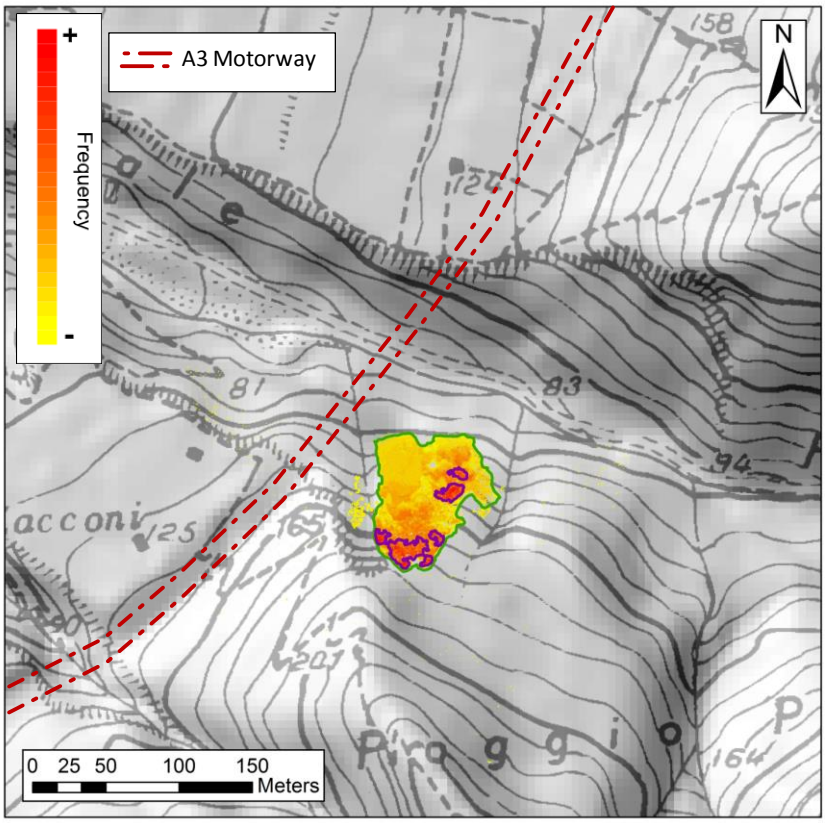

Fig. 63. Frquency map calculeted by MATLAB code from cumulative desplacements maps of GB-InSAR, in green the new source volume considered from data of less fequency of desplacemnt during the monitoring period, in purple the areas representing the major frequency of desplacement during the monitoring period

Another area choose in the forecast event analysis was choice considering the triggering back analysis carried out by the FLAC 6.0 in the work of Bozzano et al. (2012). They described the results of back analysis of the Santa Trada landslide of January 30th, 2009 and the hypothetical sliding surface that involves the entire slope starting from the first fracture located at 190 m a.s.l..

The forecast analysis was carried out only with DAN-3D numerical modelling. The path file was obtained modifying the DTM produced by Calabria 2007-2008 flight (1:5000 scales) by removing the thickness involved in the event in 2009 and filtering it using a Gaussian smoothing (3×3). Five scenarios were investigated based on the results of radar displacements maps analyses and the results suggested by Bozzano et al. (2012) (Table 18).

Table 18. Summary of the of five scenarios outcomes.

	DAN-3D Bulk basal friction angle, ϕ_b=35°				
Outputs	*Scenario 1*	*Scenario 2*	*Scenario 3*	*Scenario 4*	*Scenario 5*
Final volume (m^3)	18000	30000	2250	3800	230000
Impact area (m^2)	14800	18000	8300	9500	43700
Peak velocity (m/s)	17	17	25	28	40
Duration of the motion (s)	50	50	80	69	250
Max runout (m)	160	170	131	135	200
Max deposits thickness (m)	6.4	8	2.5	3.8	19

In the first case (*scenario 1*), has been used the total area show by radar images with a source deposits thickness of 3 m (Del Ventisette et al., 2011) and a volume of about 18000 m^3. The result is showed in Fig. 64a. The model forecasts that most of the slide volume enters the lower channel and affects the motorway pillars stopping by the latter, after 50 seconds. The maximum deposits thickness is 3.4 m. The front travels at a maximum velocity of 17 m/s.

In the second case (*scenario 2*) has been used the total area show by radar images with a source deposits thickness of 5 m (Del Ventisette et al., 2011) the result is shows in Fig. 64b.

In this case the volume involved in the instability movement is about 30000 m^3 the slide reaches the Santa Trada creek and moves under the motorway bridge with a maximum velocity of 17 m/s and a maximum thickness of 8 m.

In *scenario 3* and *4* has been considered the partial area interested by more frequent displacements, also in this case two source thickness are choice 3 and 5 m with a volume of 2250 m^3 and 3800 m^3, respectively. The result shows that the slide stop after few seconds at the end of the slope in the Santa Trada creek without reach the motorway bridge pillars (Fig. 64c,d).

From a thorough analysis of results is possible to note that during the monitoring periods the areas reporting the most displacements, are usually small portion of the landslide and their runout distance often doesn't represent a risk factor. More dangerous are the areas that at least

once recorded a significant moments, these areas usually are the widest and the involved volume that may constitute a real risk factor.

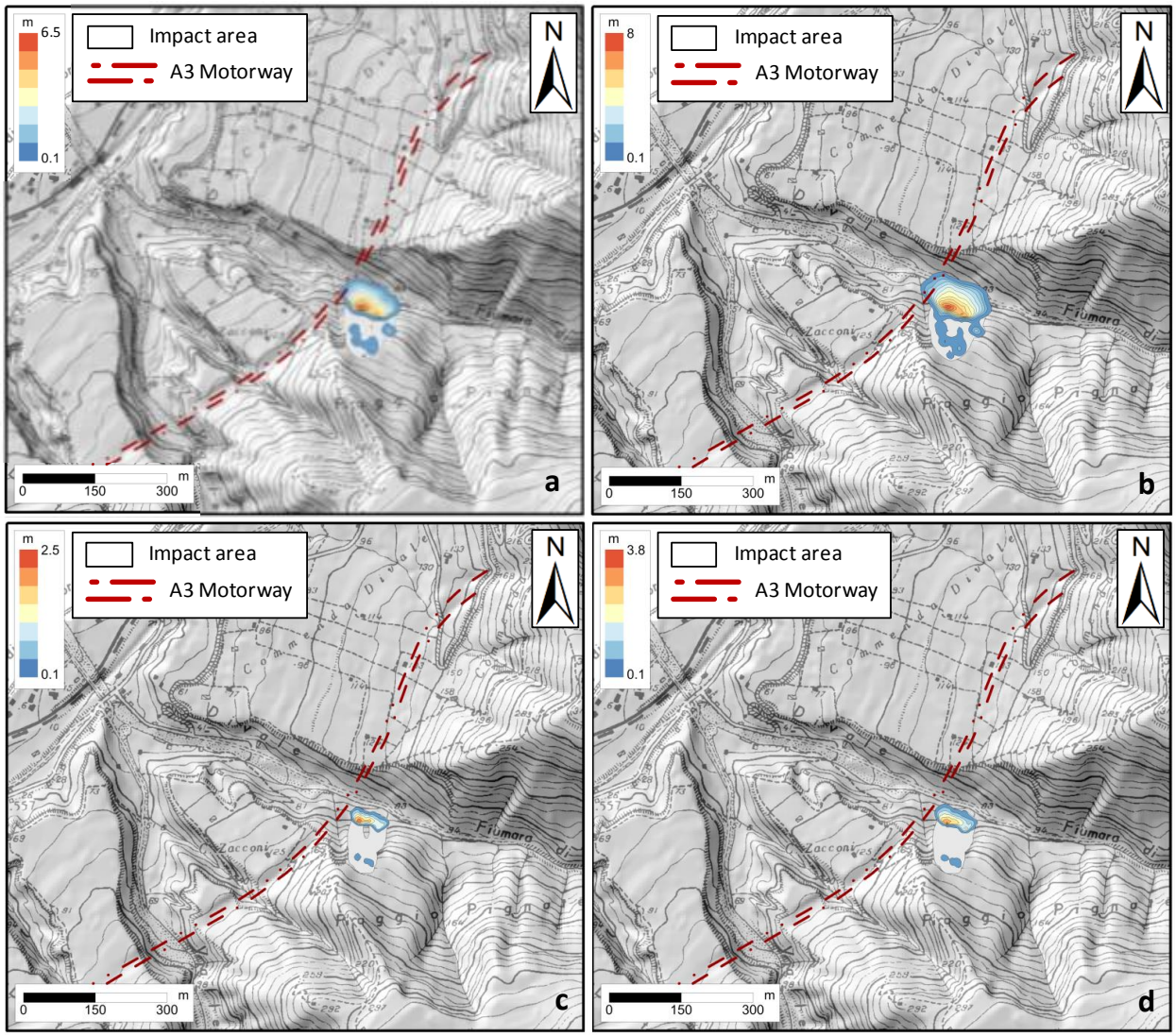

Fig. 64. Four forescat analysis results, considerig the more or less frequent despalacement area calculated by MATLAB code on GB-InSAR cumulative desplacemnts maps, a) less frequet with source thickness of 3m, b) less frequent with source thickness of 5m, c) more frequet with source thickness of 3m, d) more frequent with source thickness of 5m.

The last case (*scenario 5*) represents the event supposed by FLAC 6.0 back analyses. According to Bozzano et al. (2012) surveys the failure surface of the whole rock mass involved gravity-induced deformation is located at about 23 m depth whit a total volume involved of approximately 230000 m^3. The impact area of the flow is very wide, not only the flow enters in the lower channel and affects the motorway pillars crossing over, but it involves the close NW side too. A movement of this portion, which already has some instability and fracture, should be

of interest to the stretch of the A3 motorway near the Santa Trada viaduct. The thickness of material involved in this sector appears to be modest of approximately 1 m. Some monitoring analysis are just conducted by Department of Earth Science of University of Florence using the GB-InSAR data, highlight the dangers of this side.

The maximum simulated deposits thickness is 19 m with maximum velocity of 40 m/s (Fig. 65).

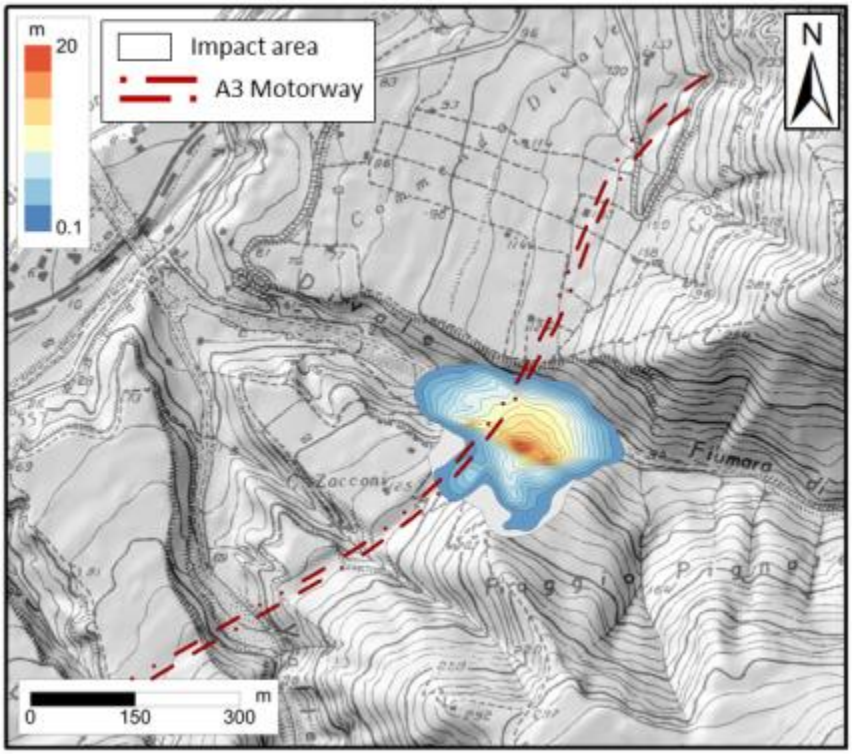

Fig. 65. Result of forecast analysis of *scenario 5, considering a source area and volume by Bozzano et al. (2011).*

6.3.5 Conclusion

On 30th January 2009 due to the intense rainfall a rock/debris slide occurred near Santa Trada, threatening the pillars of a viaduct of the A3 motorway. In order to characterize the rock mass instability some field and geotechnical surveys were carried out, together with GB-InSAR monitoring to asses possible risk scenarios. The field surveys allow us to find the main 2009 roks/debris slide geometric parameters and source area and volume, useful for back analysis. Both DAN-W and DAN-3D models successfully simulate the landslide propagation dynamics by using the frictional rheological relationship. The combined of two models could improve the practice efficiency of the modelling (Revellino et al., 2013). The frictional rheological model was chosen based on literature values of basal friction angle back calculated for rock/debris slide with similar volumes, material and characteristics. The results are in good agreement with the event runout and velocity.

The rheological model found for 2009 event back analysis was used for the forecast analysis.

The analysis on GB-InSAR cumulative displacements maps with MATLAB code have been possible to delimitate the areas affected by movements and to identify some temporal phases characterized by different activity levels. The frequency of occurred map allows us to delimited two different areas affected by more or less frequent displacements. These latter areas were interpolated with two different source deposits thickness found by Del Ventisette et al. (2011) to forecast new risk scenarios. Finally, the scenarios predicted by Bozzano et al., (2012) was modelled, which use the landslide triggering model FLAC for back analysis to found an hypothetical sliding surface that involves the entire slope starting at 190 m a.s.l at the height of the second identified fracture.

Most of the assessed forecast scenarios indicate a significant risk for the A3 motorway pillars.

Also in this case study, the integration between runout numerical modelling and GB-InSAR monitoring data may be a valid technique in order to assess the risk scenarios for rapid shallow landslide emergency.

7. Discussion of Results

The prediction of rapid shallow landslides motion is one of the most important issues for assessing and mitigating risk scenarios and hazard zonation. It can provide valuable management for land use and the development of mitigation strategy. With this aim in this thesis has been developed an integrated procedure for the forecasting of shallow landslide ruonout to be used for civil protection purposes.

The innovative procedure combining LiDAR and GB-InSAR remote sensing techniques with landslide runout numerical modelling was applied to four case studies. A first phase understands the landslide dynamic and collecting the main geotechnical and geomorphological features for each case studied. A full landslide description including pre- and post-event topography data, where they are available, information about location and volume of the source area, velocity, deposit thickness, runout distance and impact area, derived from field investigation, available in the literature or analyzed with the use of empirical equations and remote sensing data. The HRDEMs proceed by LiDAR data is a very useful tool in DAN-3D back analysis allowing the simulation of flow across complex 3-D terrain without the need to input a pre-defined slide path. The availability of LiDAR HRDEMs pre- and post-event is also a valid tool to analyze mass movement events and to reconstruct erosion and deposition, obtaining a clear description of the whole process (example in paragraph 6.2). This phase is an important support for back analysis, to calibrate the rheological parameters of numerical modeling.

In Table 19 are summarized the remote sensing techniques used for each case study and the rheological parameters obtained from back analysis for different types of landslides.

Table 19. Summary of techniques used and the back analysis results for the four study cases investigated.

Case studies	**Mechanisms**	**Combining techniques**	**DAN Rheological models**			
			Frictional	*Voellmy*		
Stromboli	Gi-PDC	ALS L LiDAR		f=0.19 ξ=1000 m/s^2		
Monte Rotolon	Debris flow	ALS LiDAR GB-InSAR	-	f=0.16 ξ=500 m/s^2	f=0.12 ξ=500 m/s^2	f=0.01 ξ=1000 m/s^2
Gessi-Mazzalasino	Debris slide	TLS LiDAR	-	f=0.19 ξ=250 m/s2	f=0.15 ξ=250 m/s2	-
Santa Trada	Rock/debris slide	GB-InSAR	ϕ_b=35°	-	-	-

The goodness of simulation result of DAN-W and DAN-3D numerical models has just been tested in many works (Hungr and Evans, 1996; McDougall, 2006). In this thesis the goodness of results has been tested comparing the field or derived from empirical equations data with the numerical modelling estimation. In particular, for each case studied the runout distance has represented the main parameters for model calibration. Furthermore, other calibration parameters have been used in different case studies such as: deposits thickness, velocity and duration of the motion. In the Monte Rotolon debris flow and Gessi-Mazzalasino debris slide case studies, the velocity estimations by empirical equations, have been a valuable parameter to test the goodness of the numerical simulation, in particular the velocity obtained by the model was compare with the one calculated at the same cross-sections location. In the graph (Fig. 66) are shown that model results are in good agreement with estimated velocities, only in the Monte Rotolon debris flow case study, the velocity predict by dynamic analysis near the toe of the source area is much greater than those estimated by empirical equations, due to the entrainment coefficient insert in this part of the model. Another calibration parameter has been the deposits thickness along the landslide path, in particular in the Fig. 67, it is possible note the comparison between the measured thickness values in field investigations and those predicted by numerical simulations, for three case studies: Stromboli gi-PDC (Zone A), Monte Rotolon debris flow and Gessi-Mazzalasino debris slide.

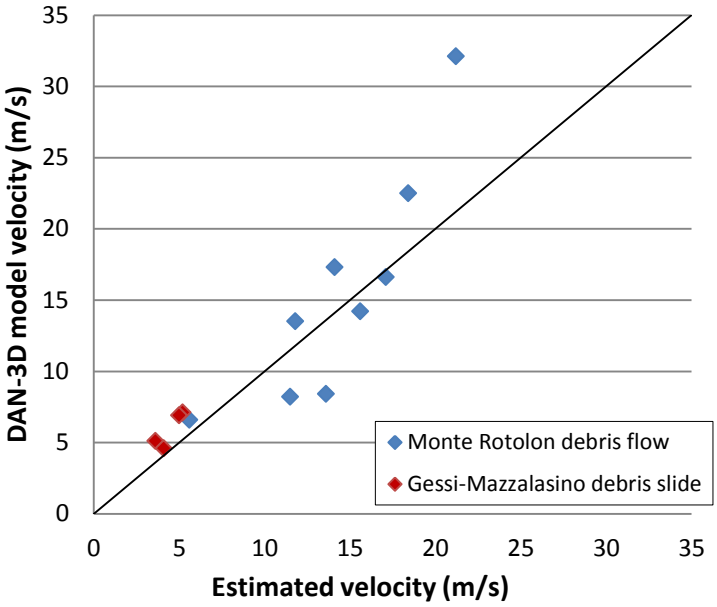

Fig. 66. Comparison of modelled and estimated velocities at cross-sections for Monte Rotolon debris flow (blue) and Gessi-Mazzalasino debris slide (red).

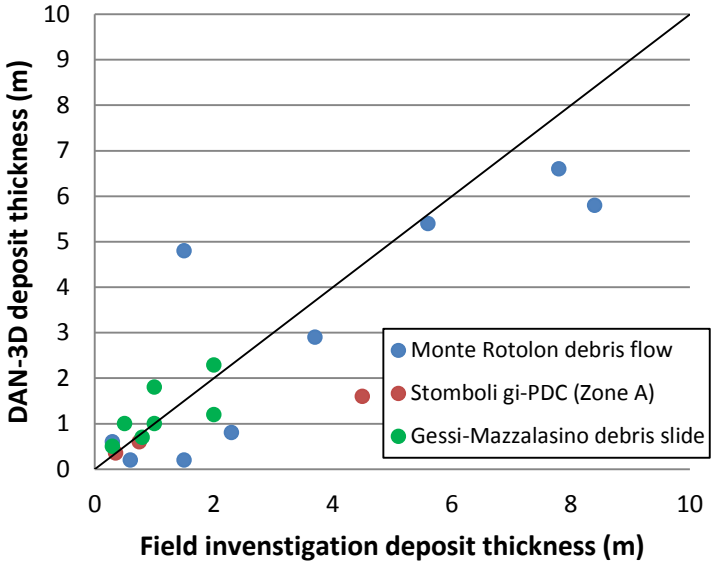

Fig. 67. Comparison of modelled and field estimated deposit thickness, for Stromboli gi-PDC (red), Monte Rotolon debris flow (blue) and Gessi-Mazzalasino debris slide (green).

A second phase of the procedure is the forecast analysis. An advanced system was carried out in order to evaluate risk of possible future landslide events. This includes the combination of the runout modelling analysis together with LiDAR and GB-InSAR data to identify the post-topography path, new possible landslide reactivation zones (source areas), and new volumes of

event. This working method could represent a standard procedure in case of areas prone to different types of shallow landslides.

A first difficult task is represented by the identification of new source areas, in this work these areas were detected with high precision through the integrated analysis of the radar displacement maps and field investigations. In particular, where GB-InSAR displacement monitoring is available, the use of MATLAB code can be a valuable tool to identify new possible source area.

A second difficult task is to obtain a new event volume; in this work are proposed three possible solutions. The first method is the field investigations, conducted on study areas in order to determine the presence of areas prone to detachment and identify the deposits thickness that may be involved in any future events (Gessi-Mazzalasino debris slide), or identify the occurrence of surface fractures (Santa Trada rock/debris slide). The second is based on a statistical analysis, performed on source area thickness of past events (Monte Rotolon debris flow), considering the same involved materials and the same triggering mechanism. Finally, the latter method is based on thickness found by numerical models of landslide triggering, as finite difference program FLAC (Itasca 2005), that performs the mobilized volume with slope stability analysis identifying the rupture surface (Santa Trada rock/debris slide). Nevertheless, the accuracy of the proposed methods lies in the skill of expert operators in the choice of reliable volumes of possible future events.

A final discussion can be done on the results obtained examining the frequency of GB-InSAR displacement recorded and the size of the landslide, in particular the volume involved and the impact area obtained from simulated forecast events.

This relationship can be associated with magnitude-cumulative frequency (MCF) relationships of landslides studied by many authors as: Whitehouse and Griffths (1983), Hovius et al. (1997), Pelletier et al. (1997) and Hungr et al. (1999). The most famous example is the Gutenberg-Richter relationship for earthquakes (Gutenberg and Richter 1954).

This shows that the logarithm of the number *N* of earthquakes exceeding a given magnitude *M* in a region is linearly related to the magnitude:

$$[69] \quad LogN = A + bM$$

where *A* and *b* are constants. As *M* is measured on a logarithmic scale, this relationship is a straight line on a log-log scale.

In the two case studies, the Monte Rotolon debris flow and the Santa Trada rock/debris slide, the distribution between frequency of displacement occurrence (the MATLAB code computes how many times each pixel has recorded a significant displacement during the monitoring period) and landslide source volume is a power-law type; in log-log scale. The relationship is inverse, the volume or the impact areas increases when frequency of displacement occurrence decreases. The monitored areas which recorded several times cumulative displacements, during the selected monitoring period, always match smaller source areas involving lower volumes (Fig. 68). In the same way behaves the final impact area of the simulated forecast events (Fig. 69).

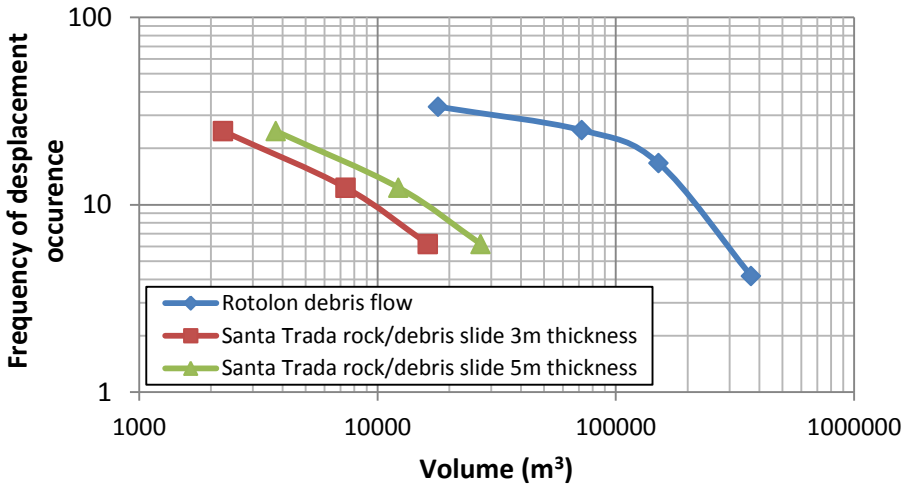

Fig. 68. Volume – frequency of desplacements occurrence for Monte Rotolon debris flow case study and Santa Trada rock/debris slide case study.

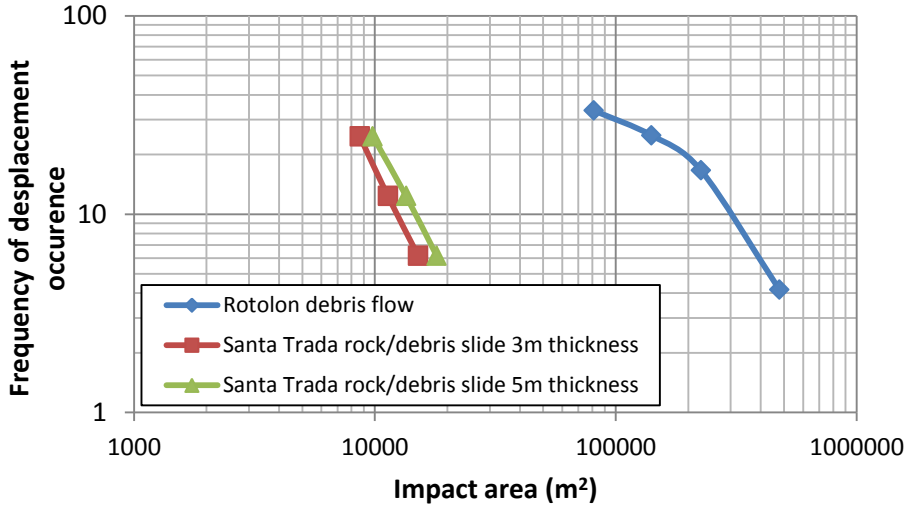

Fig. 69. Impact area – frequency of desplacements occurrence for Monte Rotolon debris flow case study and Santa Trada rock/debris slide case study.

The limitation and error for this type of analysis concerns, mainly the reconstruction of parameters on which is based the numerical modelling calibration. Some parameters depend by reliability of the field observation such as: the deposits thickness estimations, the geotechnical parameters measured (affected by the instrumental errors). Also the velocity evaluation based on field survey of run up or superelevation provide estimates of maximum velocities at points, contains certain errors because the flow may have been travelling faster at another location along the path without leaving an observable record.

The continuum numerical models schematize the real dynamics of landslide, many models use a theory of "apparent" fluids in which the rheological properties of the model flowing body simulates the behavior of the real landslide, and include some different methods to calculate the landslide erosion and material properties. For DAN-W and DAN-3D the assumptions described in models introduction (paragraph 3.3), provide the simplicity of the models and the possibility of choice among different rheologies, some of which are particularly simple. The limitations and errors for this type of software concern also the construction of the source and the path files for the model, which must be reconstructed with highest accuracy. The importance to have the pre- and post-topography by HRDEMs recorder by LiDAR data allow us to obtain a good landslide path and magnitude of the event. The new procedure described in this thesis use the combination with remote sensing data and so the errors evaluation includes, also, the instrument limitations and accuracy such as: the distance of acquisition, the reflectivity of the observed scene, the incident angle of the radar or laser signal.

The methods proposed to calculate the new source areas and volume of possible future landslide events represent a new procedure to implemented in fast and expert assessment in Civil Protection evaluation.

The obtained results show that the combination of the modelling technique together with the GB-InSAR derived displacement maps can be a very useful tool for the scientific community and local administrations in order to manage the problem related to shallow rapid landslide events. This working method could represent a standard procedure in case of areas prone to different type rapid mass movement, in case of LiDAR surveys or GB-InSAR displacement monitoring. Nevertheless, the accuracy of the proposed method lies in the skill of expert operators in the choice of reliable volumes of possible future debris flow events.

8. Reference

Abellán, A., Jaboyedoff, M., Oppikofer, T., Vilaplana, J.M. (2009). Detection of millimetric deformation using a terrestrial laser scanner: experiment and application to a rockfall event. *Nat. Hazards Earth Syst.*, *9*(2), 365-372.

Abellan, A., Vilaplana, J.M., Calvet, J., Blanchard, J. (2010). Detection and spatial prediction of rockfalls by means of terrestrial laser scanning modelling. Geomorphology., 119,162-171.

Abbruzzese, D. (1935). Sulla catastrofica esplosione dello Stromboli dell'11 settembre 1930. Gioenia Proc. Soc. Na.t Sci., 1, 1-13.

Agliardi, F., Crosta, G., Zanchi, A., Ravazzi, C. (2009). Onset and timing of deep-seated gravitational slope deformations in the eastern Alps, Italy. Geomorphology., 103, 113-129.

Altieri, V., Colombo, P., Dal Prà, A. (1994). Studio per la Valutazione delle condizioni di stabilità dei versanti e del fondovalle del bacino idrografico del Torrente Rotolon nell'Alta Valle dell'Agno in Comune di Recoaro Terme (Vicenza). Relazione Geologico – Geotecnica. Regione del Veneto Segreteria Regionale per il Territorio – Dipartimento Lavori Pubblici – Venezia 97 [in italian].

Amoozegar, A. (1989). A compact constant-head permeameter for measuring saturated hydraulic conductivity of the vadose zone. Soil Sci. Soc. Am. J., 53, 1356-1361.

Amoozegar, A., Warrick. A.W. (1986). Hydraulic conductivity of saturated soils. Field methods. In Methods of Soil Analysis, part 1, Madison, Wis.: Am. Soc. Agron, ed. A. Klute, 735-770.

Amoozegar, A., Wilson, G.V. (1999). Methods for measuring hydraulic conductivity and drainable porosity. Am. Soc. Agron., Agron. Monogr., 38, 1149-1205.

Apuani, T., Corazzato, C., Cancelli, A., Tibaldi, A. (2005b). Stability of a collapsing volcano (Stromboli, Italy): limit equilibrium analysis and numerical modelling. J. Volcanol. Geoth. Res., 144(1-4), 191-210.

Ardizzone, F., Cardinali, M., Galli, M., Guzzetti, F., Reichenbach, P. (2007). Identification and mapping of recent rainfall-induced landslides using elevation data collected by airborne Lidar. Nat. Hazard. Earth Sys., 7(6), 637-650.

Asmar, B.N., Langston, P.A., Matchett, A.J., Walters, J.K. (2003). Energy monitoring in distinct element models of particle systems. Adv. Powder Technol., *14*(1), 43-69.

Ayotte, D., Hungr, O. (2000). Calibration of a runout prediction model for debris-flows and avalanches. In Proceedings of the 2nd International Conference on Debris-Flow Hazards

Mitigation: Mechanics, Prediction, and Assessment, Taipei, Taiwan. Edited by GF Wieczorek and ND Naeser. AA Balkema, Rotterdam, 505-514.

Bagnold, R.A. (1954). Experiments on a gravity-free dispersion of large solid spheres in a Newtonian fluid under shear. *In Proceedings* of the Royal Society of London A: Mathematical, Physical and Engineering Sciences. The Royal Society, 225(1160), 49-63.

Baltsavias, E.P. (1999). Airbone laser scanning: basic relations and formulas. ISPRS J Photogramm Remote Sens., 54, 199-214.

Barbieri, G., De Zanche, V., Di Lallo, E., Mietto, P., Sabatini, U.D., Sedea, R. (1980). Carta geologica dell'area di Recoaro. Mem. Sc. Geol. XXXIV Padova 23-52 [in Italian].

Barberi, F., Rosi, M., Sodi, A. (1993). Volcanic hazard assessment at Stromboli based on review of historical data. Acta. Vulcanol., 3, 173-187.

Bardi, F., Frodella, W., Ciampalini, A., Bianchini, S., Del Ventisette, C., Gigli, G., Fanti, R., Moretti, S., Basile, G., Casagli, N. (2014). Integration between ground based and satellite SAR data in landslide mapping: The San Fratello case study. Geomorphology, 223, 45-60.

Beguería, S., Van Asch, T.W., Malet, J.P., Gröndahl, S. (2009). A GIS-based numerical model for simulating the kinematics of mud and debris flows over complex terrain.

Benz, W. (1990). Smooth particle hydrodinamics: a review. In: Buchler, J. R. (Ed.). The Numerical Modelling of Nonlinear Stellar Pulsation: Kluwer Accademic, Dordrecht, 269-288.

Bertagnini, A., Di Roberto, A., Pompilio, M. (2011). Paroxysmal activity at Stromboli: lessons from the past. Bull. Volcanol., 73(9), 1229-1243.

Berti, M., Simoni, A. (2007). Prediction of debris flow inundation areas using empirical mobility relationships. Geomorphology, 90(1), 144-161.

Bingham, E.C., Green, H. (1919). Paint, a plastic material and not a viscous liquid; the measurement of its mobility and yield value. In Proc. Am. Soc. Test. Mater, 19, 640-664.

Bjerrum, C.J., Dorsey, R.J. (1995). Tectonic controls on deposition of Middle Jurassic strata in a retroarc foreland basin, Utah-Idaho trough, western interior, United States. Tectonics, *14*(4), 962-978.

Blight, G.E. (1997). Origin and formation of residual soils. Mechanics of Residual Soil, 1-15.

Bossi, G., Crema, S., Frigerio, S., Mantovani, M., Marcato, G., Pasuto, A., Schenato, L., Cavalli, M. (2015). The Rotolon catchment early-warning system. *Edited by* G. Lollino, M. Arattano, M. Rinaldi O. Giustolisi, J.C. Marechal and G.E. Grant. In Engineering Geology for Society and Territory. Springer International Publishing, 3, 91-95.

Bossi, G., Cavalli, M., Crema, S., Frigerio, S., Quan Luna, B., Mantovani, M., Marcato, G., Schenato, L., Pasuto, A. (2015b). Multi-temporal LiDAR-DTMs as a tool for modelling a complex landslide: a case study in the Rotolon catchment (eastern Italian Alps). Nat. Hazards Earth Sys., 15(4), 715–722.

Bozzano, F., Martino, S., Montagna, A., Prestininzi, A. (2012). Back analysis of a rock landslide to infer rheological parameters. Eng. Geol., 131, 45-56.

Bouwer, H., Jackson, R.D. (1974). Determining soil properties. In Drainage for agriculture, Agronomy ed J. van Schilfgaarde, 17, 611-672.

Braga, G.P., Castellarin, A., Corsi, M., de Vecchi, G.P., Gatto, G.O., Largaiolli, T., ... Zirpoli, G. (1968b). F 36 Schio alla scala 1: 100. 000. Ist. Ital. Arti Grafiche, Bergamo.

Brayshaw, D., Hassan, M.A. (2009). Debris flow initiation and sediment recharge in gullies. Geomorphology, 109(3), 122-131.

Calder, E.S., Cole, P.D., Dade, W., Druitt, T.H., Hoblitt, R.P., Huppert, H.E., Ritchie, L., Sparks, R.S.J., Young, S.R. (1999). Mobility of pyroclastic flows and surges at the Soufriere Hills Volcano, Montserrat. Geophys. Res. Letts., 26(5), 537-540.

Calvari, S., Intrieri, E., Di Traglia, F., Bonaccorso, A., Casagli, N., Cristaldi, A. (2016). Monitoring crater-wall collapse at active volcanoes: a study of the 12 January 2013 event at Stromboli. Bull. of Volcanol., *78*(5), 1-16.

Campbell, C.S., (1989). Self-lubrication for long runout landslides. J. Geol., 653-665.

Carbone, S., Messina, A., Lentini, F., (2008). Note Illustrative della carta geologica d'Italia alla scala 1:50.000: Foglio 601. Dipartimento Difesa del Suolo, Servizio Geologico d'Italia. S.EL.CA. Firenze, 170.

Carter, W., Shrestha, R., Tuell, D., Bloomquist, D., Sartori, M. (2001). Airborne laser swath mapping shines new light on earth's topography. Eos, Trans, Am. Geophys. Union., 82(46), 549, 550-555.

Casagli, N., Catani, F., Del Ventisette, C., Luzi, G. (2010). Monitoring, prediction, and early warning using ground-based radar interferometry. Landslides, 7(3), 291-301.

Castellarin, A., Corsi, M., De Vecchi, G. P., Gatto, G. O., Largaiolli, T., Mozzi, G., … Zirpoli, G. (1968a). Note illustrative della Carta Geologica d'Italia alla scala 1: 100.000, Foglio 36 Schio. Serv. Geol. D'Italia. Roma, 94.

Chandler, J. (1999). TECHNICAL COMMUNICATIONS-Effective Application of Automated Digital Photogrammetry for Geomorphological Research. Earth Surf. Proc. Land., *24*(1), 51-64.

Charbonnier, S.J., Gertisser, R. (2012). Evaluation of geophysical mass flow models using the 2006 block-and-ash flows of Merapi Volcano, Java, Indonesia: towards a short-term hazard assessment tool. J. Volcanol. Geoth. Res., 231, 87-108.

Chen, H., Lee, C.F. (2003). A dynamic model for rainfall-induced landslides on natural slopes. Geomorphology, *51*(4), 269-288.

Chen, J.C., Jan, C.D., Lee, M.H. (2007). Probabilistic analysis of landslide potential of an inclined uniform soil layer of infinite length: theorem. Envirron geol., *51*(7), 1239-1248.

Chow, V.T. (1959). Open-Channel Hydraulics. McGraw-Hill, New York, 465.

Christen, M., Kowalski, J., Bartelt, P. (2010). RAMMS: numerical simulation of dense snow avalanches in three-dimensional terrain. Cold Reg.Sci. Technol., 6*3*(1), 1-14.

Cleary, P.W., Prakash, M. (2004). Discrete-element modelling and smoothed particle hydrodynamics: potential in the environmental sciences. Philosophical translation-royal society of London series a mathematical physical and engineering science, *362*, 2003-2030.

Colesanti, C., Ferretti, A., Novali, F., Prati, C., Rocca, F. (2003). SAR monitoring of progressive and seasonal ground deformation using the permanent scatterers technique. IEEE Trans. Geosci. Remote Sens., 41(7), 1685-1701.

Corominas, J. (1996). The angle of reach as a mobility index for small and large landslides. Can. Geotech. J., *33*(2), 260-271.

Corominas, J., Van Westen, C., Frattini, P., Cascini, L., Malet, J.P., Fotopoulou, S., Catani, F., Van Den Eeckhaut, M., Mavrouli, O., Agliardi, F., Pitilakis, K., Winter, M.G., Pastor, M., Ferlisi, S.,Tofani, V., Herva´s, J., Smith, J.T. (2014). Recommendations for the quantitative analysis of landslide risk. Bull. Eng. Geol. Environ., 73(2), 209-263.

Coussot, P. (1992). Rheology of debris flow-Study of concentrated suspensions (Doctoral dissertation, Ph. D. thesis, INPG, Grenoble, France).

Coussot, P., Meunier, M. (1996). Recognition, classification and mechanical description of debris flows. Earth Sci. Rev., 40(3), 209-227.

Crosta, G.B., Imposimato, S., Roddeman, D.G. (2003). Numerical modelling of large landslides stability and runout. Nat. Hazards Earth Sys., 3(6), 523-538.

Crosta, G.B., Chen, H., Frattini, P. (2006). Forecasting hazard scenarios and implications for the evaluation of countermeasure efficiency for large debris avalanches. Eng. Geol., 83(1), 236-253.

Cruden, D.M. (1991). A simple definition of a landslide. Bull. Eng. Geol Env., 43(1), 27-29.

Cruden, D. M., Varnes, D. J. (1993). Landslides: Investigation and Mitigation. Transportation Research Board Special Report 247, 36-75.

Cruden, D. M., Varnes, D. J. (1996). Landslide types and processes. In Landslides: Investigation and Mitigation, Special Report 247, 36-75. Washington: Transportation Research Board.

Cundall, P.A., Strack, O.D. (1979). A discrete numerical model for granular assemblies. Geotechnique, 29(1), 47-65.

D'Agostino, V. (1996). Analisi quantitativa e qualitativa del trasporto solido torrentizio nei bacini montani de Trentino Orientale [quantitative and qualitative analysis of sediment transport in torrents of mountainous catchments of eastern Trentino], Scritti dedicati a Giovanni Tournon, Associazione Idrotecnica Italiana, Sezione Liguria Piemonte e Valle d'Aosta (in Italian).

Dade, W.B., Huppert, H.E. (1998). Long runout rockfalls. Geology, 26, 803-806.

Daido, A. (1971). On the occurrence of mud-debris flow.

Davies, K.D., Quearry, M.W., Bonis, S.B. (1978). Glowing avalanches from the 1974 eruption of the volcano Fuego, Guatemala. Geol. Soc. Am. Bull., 89, 369-384.

Davies, T.R.H. (1986). Large debris flows: a macro-viscous phenomenon. Acta. Mechanica., 63(1-4), 161-178.

Dent, J.D., Lang, T.E. (1980). Modeling of snow flow. J. Glaciol., 26(94), 131-140.

Dent, J.D., Lang, T.E. (1983). A biviscous modified Bingham model of snow avalanche motion. Annals Glaciol., 4, 42-46.

De Fino, M., La Volpe, L., Falsaperla, S., Frazzetta, G., Neri, G., Francalanci, L., Rosi, M., Sbrana A. (1988). The Stromboli eruption of December 6, 1985–April 25, 1986: Volcanological, petrological and seismological data. Rend. Soc. Ital. Mineral. Petrol. 43, 1021-1038.

Di Roberto, A., Bertagnini, A., Pompilio, M., Bisson, M. (2014). Pyroclastic density currents at Stromboli volcano (Aeolian Islands, Italy): a case study of the 1930 eruption. Bull. Volcanol., 76(6), 1-14.

Di Traglia, F., Intrieri, E., Nolesini, T., Bardi, F., Del Ventisette, C., Ferrigno, F., Frangioni, S., Frodella, W., Gigli, G., Lotti, A., Tacconi Stefanelli, C., Tanteri, L., Leva, D., Casagli, N. (2014). The ground-based InSAR monitoring system at Stromboli volcano: linking changes in displacement rate and intensity of persistent volcanic activity. Bull. Volcanol., 76, 1-18.

De Zanche, V., Mietto, P. (1981). Review of the Triassic sequence of Recoaro (Italy) and related problems.

Del Ventisette, C., Intrieri, E., Luzi, G., Casagli, N., Fanti, R., Leva, D. (2011). Using ground based radar interferometry during emergency: the case of the A3 motorway (Calabria Region, Italy) threatened by a landslide. Nat. Hazards Earth Syst. Sci, 11(9), 2483-2495.

Eberhardt, E., Stead, D., Coggan, J. S. (2004). Numerical analysis of initiation and progressive failure in natural rock slopes—the 1991 Randa rockslide. Int. J. Rock Mech. Min. Scie., *41*(1), 69-87.

Evans, S.G., Clague, J.J. (1988). Catastrophic rock avalanches in glacial environments. In Proceedings of the 5th International Symposium on Landslides. Lausanne Switzerland, 2, 1153-1158.

Ferranti, L., Monaco, C., Antonioli, F., Maschio, L., Kershaw, S., Verrubbi, V. (2007). The contribution of regional uplift and coseismic slip to the vertical crustal motion in the Messina Straits, southern Italy: Evidence from raised Late Holocene shorelines. J. Geophys. Res., 112, B06401.

Fidolini, F., Pazzi, V., Frodella, W., Morelli, S., Fanti, R. (2015). Geomorphological characterization, monitoring and modeling of the Monte Rotolon complex landslide (Recoaro Terme, Italy). Edited by G. Lollino, D. Giordan, G. B. Crosta, J. Corominas, R. Azzam, J. Wasowski and N. Sciarra. In Engineering Geology for Society and Territory. Springer International Publishing, 2, 1311-1315.

Frodella, W., Morelli, S., Fidolini, F., Pazzi, V., Fanti, R. (2014). Geomorphology of the Rotolon landslide (Veneto Region, Italy). J. Maps, 10(3), 394-401.

Frodella, W., Fidolini, F., Morelli, S., Pazzi, V. (2015). Application of infrared thermography for landslide mapping: The rotolon DSGDS case study. Rend. Online Soc. Geol. Ita., 35, 144-147.

Fröhlich, C., Mettenleiter, M. (2004). Terrestrial laser scanning–new perspectives in 3D surveying. International archives of photogrammetry, remote sensing and spatial information sciences, 36(Part 8), W2.

Fruneau, B., Achache, J., Delacourt, C. (1996). Observation and modelling of the Saint-Etienne-de-Tinée landslide using SAR interferometry. Tectonophysic*s*, 265(3), 181-190.

Gigli, G., Morelli, S., Fornera, S., Casagli, N. (2014). Terrestrial laser scanner and geomechanical surveys for the rapid evaluation of rock fall susceptibility scenarios. Landslides, 11(1), 1-14.

Gingold, R.A., Monaghan, J.J.(1977). Smoothed particles hydrodynamics: theory and application to non-spherical stars. Mon. Not. R. Astro. Soc., 181, 375-389.

Gomarasca, M. A. (2004). Elementi di geomatica. Associazione Italiana di Telerilevamento, Milano, 618.

Gordon, S., Lichti, D., Stewart, M. (2001). Application of a high-resolution, ground-based laser scanner for deformation measurements. In: Proceedings of the 10th international FIG symposium on deformation measurements, Orange, California, USA, 19–22 March 2001, 23-32.

Gray, J.M.N.T., Wieland, M., Hutter, K. (1999). Gravity-driven free surface flow of granular avalanches over complex basal topography. In *Proceedings* of the Royal Society of London A: Mathematical, Physical and Engineering Sciences. The Royal Society., 455(1985), 1841-1874.

Greve, R., Koch, T., Hutter, K. (1994). Unconned flow of granular avalanches along a partly curved surface. I. Theory. Proc. R. Soc. Lond. A., 445, 399-413.

Griswold, J. P., Iverson, R. M. (2008). Mobility statistics and automated hazard mapping for debris flows and rock avalanches. US Department of the Interior, US Geological Survey.

Gutenberg, B., and Richter, C.F. 1954. Seismicity of the earth. 2nd ed. Princeton University Press, Princeton, N.J.

Hampel, R. (1977), Geschiebewirtschaft in Wildbächen, Wildbach und Lawinenverbau 41(1), 3-34 (in German).

Happel, J., Brenner, H. (1965). Low Reynolds Number Hydrodynamics with Special Application to Particulate Media: John Happel, Howard Brenner. Prentice-Hall.

Haugerud, R.A., Harding, D.J., Johnson, S.Y., Harless, J.L., Weaver, C.S., Sherrod, B.L. (2003). High-resolution lidar topography of the Puget Lowland, Washington—A Bonanza for earth science. GSA Today 13:4–10

Hayashi, J.N. Self, S. (1992). A Comparison of Pyroclastic Flow and Debris Avalanche Mobility. J. Geophys. Res., 97B6, 9063-9071.

Hazlett, R.W., Buesch, D., Anderson, J.L., Elan, R., Scandone, R. (1991). Geology, failure conditions, and implications of seismogenic avalanches of the 1944 eruption at Vesuvius, Italy. J. Volcanol. Geoth. Res., 47(3-4), 249-264.

Heim, A. (1932). Bergsturz und Menschenleben. Fretz and Wasmuth Verlag, Zurich, 218.

Hendron, A.J., Patton, F.D. (1985). The Vaiont slide, a geotechnical analysis based on new geologic observations of the failure surface. US Army Corps of Engineers Technical Report GL-85-5 (2 volumes).

Herschel, W.H., Bulkley, R. (1926). Konsistenzmessungen von Gummi-Benzollosungen, Kolloid Z. 39, 291-300.

Hovius, N., Stark, C. P., Allen, P. A. (1997). Sediment flux from a mountain belt derived by landslide mapping. Geology, 25(3), 231-234.

Hsü, K.J. (1975). Catastrophic debris streams (sturzstroms) generated by rockfalls. Geological Soc. Amer. Bull., 86(1), 129-140.

Hungr, O., Morgenstern, N.R. (1984). Experiments on the flow behaviour of granular materials at high velocity in an open channel. Geotechnique, 34(3).

Hungr, O. (1990). Mobility of rock avalanches: report of the National Research Institute of Earth Science and Disaster Prevention, Japan, 46, 11-20.

Hungr, O. (1995). A model for the runout analysis of rapid flow slides, debris flows, and avalanches. Can. Geotech. J., 32(4), 610-623.

Hungr, O., Evans, S.G. (1996). Rock avalanche runout prediction using a dynamic model. In Proceedings of the 7th International Symposium on Landslides, Trondheim, Norway, 1, 233-238.

Hungr, O., Evans, S. G., & Hazzard, J. (1999). Magnitude and frequency of rock falls and rock slides along the main transportation corridors of southwestern British Columbia. Can. Geotech. J., 36(2), 224-238.

Hungr, O. (2000). Analysis of debris flow surges using the theory of uniformly progressive flow. Earth Surf. Pro. Land., *25*(5), 483-495.

Hungr, O., Evans, S.G., Bovis, M.J., Hutchinson, J.N. (2001). A review of the classification of landslides of the flow type. Environ. Eng. Geosc., VII(3), 1-18.

Hungr, O., Dawson, R.F., Kent, A., Campbell, D., Morgenstern, N.R. (2002). Rapid flow slides of coal-mine waste in British Columbia, Canada. Rev. Eng. Geol., 15, 191-208.

Hungr, O., Evans, S.G. (2004a) Entrainment of debris in rock avalanches: an analysis of a long run-out mechanism. Geol. Soc. Amer. Bull., 116(9-10), 1240-1252.

Hungr, O., Corominas, J., Eberhardt, E. (2005). Estimating landslide motion mechanisms, travel distance and velocity. In Landslide Risk Management. O. Hungr, R. Fell, R. Couture and E. Eberhardt (Eds.). Taylor and Francis, London, 99-128.

Hungr, O., McDougall, S. (2009). Two numerical models for landslide dynamic analysis. Comput. Geosci., 35(5), 978-992.

Hungr, O., Leroueil, S., Picarelli, L. (2012). Varnes classification of landslide types, un update. Proc. 11th Int. Symp. Landslides, Banff, Canada. Taylor & Francis Group, London, 1, 47- 58.

Hungr, O., Leroueil, S., Picarelli, L. (2014). The Varnes classification of landslide types, an update. Landslides, 11.2, 167-194.

Hunter, G., Fell, R. (2003). Travel distance angle for" rapid" landslides in constructed and natural soil slopes. Can. Geotech. J., 40(6), 1123-1141.

Hutchinson, J.N. (1988). General report: Morphological and geotechnical parameters of landslides in relation to geology and hydrogeology. Proc. 5th Int. Symp. Landslides, Lausanne, Switzerland, Balkema, Rotterdam, 1, 3-35.

Hutter, K., Savage, S. B. (1988). Avalanche dynamics: the motion of a finite mass of gravel down a mountain side. *In Proceedings* of the 5th International Symposium on Landslides, July, 7-9.

Kelfoun, K., Druitt, T.H. (2005). Numerical modeling of the emplacement of Socompa rock avalanche, Chile. J. Geophys. Res. Sol. Ea., 110(B12), 1978-2012.

Kelfoun, K., Samaniego, P., Palacios, P., Barba, D. (2009). Testing the suitability of frictional behaviour for pyroclastic flow simulation by comparison with a well-constrained eruption at Tungurahua volcano (Ecuador). Bull. Volcanol., 71, 1057-1075.

Kelfoun, K. (2011). Suitability of simple rheological laws for the numerical simulation of dense pyroclastic flows and long-runout volcanic avalanches. J. Geophys. Res. Sol. Ea., 116 (B8).

Kraus, K., Pfeifer, N. (1998). Determination of terrain models in wooded areas with airborne laser scanner data. ISPRS J. Photog. remote Sens., *53*(4), 193-203.

Koch, T., Greve, R., Hutter, K. (1994). Unconfined flow of granular avalanches along a partly curved surface. II. Experiments and numerical computations. Proc. R. Soc. London, Ser. A 445, 415- 435.

Koerner, H.J. (1976). Reichweite und Geschwindigkeit von Bergsturzen und fleisschneelawinen. Rock Mech., 8, 225–256.

Kraus, K., Pfeifer, N. (1998). Determination of terrain models in wooded areas with airborne laser scanner data. ISPRS J. Photog. remote Sens., *53*(4), 193-203.

Kronfellner-Kraus, G. (1984). Extreme Feststofffrachten und Grabenbildungen von Wildbächen [extreme sediment loads and erosion of torrents], Proc. Int. Symp. Interpraevent, Villach, Austria,Bd. 2, 109–118 [in German].

Kronfellner-Kraus, G. (1987). Zur Anwendung der Schätzformel fuer extreme Wildbach-Feststofffrachten im Süden und Osten Oesterreichs [on the application of the formula to

estimate extreme sediment loads in torrents of southern and eastern Austria], Wildbach- und Lawinenverbau 51(106), 187-200 [in German].

Kwan, J., Sun, H.W. (2007). Benchmarking exersise on landslide mobility modelling-runout anayses using 3dDMM. In *Preceding* the 2007 International Forum on landslide disaster management, 2, 945-966.

Ingensand, H. (2006). Metrological aspects in terrestrial laser-scanning technology. *In Proceedings* of the 3rd IAG/12th FIG Symposium, Baden, Austria.

Itasca, F. (2005). Fast lagrangian analysis of continua in 3 dimensions. *Online Manual*.

Iverson, R.M. (1997). The physics of debris flows. Rev. geoph., *35*(3), 245-296.

Iverson, R.M., Schilling, S.P., Vallance, J.W. (1998). Objective delineation of lahar-inundation hazard zones. Geol. Soc. Amer. Bull., 110(8), 972-984.

Iverson, R.M., Denlinger, R.P. (2001). Flow of variably fluidized granular masses across three-dimensional terrain: 1. Coulomb mixture theory. J. Geoph. Res.: Solid Earth, 106(B1), 537-552.

Iverson, R M. (2005). Debris-flow mechanics. In Debris-flow hazards and related phenomena Springer Berlin Heidelberg, 105-134.

Jaboyedoff, M., Pedrazzini, A., Horton, P., Loye, A., Surace, I. (2008a). Preliminary slope mass movements susceptibility mapping using LIDAR DEM. *In Proceedings* of 61th Canadian geotechnical conference, 419-426.

Jaboyedoff, M., Oppikofer, T., Locat, A., Locat, J., Turmel, D., Robitaille, D., Demers, D., Locat, P. (2009a). Use of ground-based LIDAR for the analysis of retrogressive landslides in sensitive clay and of rotational landslides in river banks. Can. Geotech. J., 46, 1379-1390.

Jaboyedoff, M., Oppikofer, T., Abellán, A., Derron, M.H., Loye, A., Metzger, R., Pedrazzini, A. (2012). Use of LIDAR in landslide investigations: a review. Nat. Hazards, 61(1), 5-28.

Jakob M., Stein, D., Ulmi, M. (2011). Vulnerability of buildings to debris flow impact. Nat. Hazards, 60, 241-261.

Jakob, M. (2005). A size classification for debris flows. Eng. Geol., 79(3), 151-161.

Johnson, K.L. (1970). The correlation of indentation experiments. J. Mech. Phys. Solids., 18, 115-126.

Johnson, A.M., Rodine, J.R. (1984). Debris flows. In: D. Brunsden and D.B. Prior (Editors), Slope Instability. Wiley, Chichester, 257-361.

Laigle, D., Coussot, P. (1997). Numerical modeling of mudflows. *J. Hydra. Eng.*, *123*(7), 617-623.

Laigle, D., Hector, A.F., Hübl, J., Rickenmann, D. (2003). Comparison of numerical simulation of muddy debris-flow spreading to records of real events.

Lane, S.N., James, T.D., Crowell, M.D. (2000). Application of digital photogrammetry to complex topography for geomorphological research. Photogram. Rec., *16*(95), 793-821.

Lang, T.E., Dawson, K.L., Martinelli, M. (1979). Application of numerical transient fluid dynamics to snow avalanche flow, part I, development of computer program AVALANCH. J. Glacial., 22, 107-I15.

Legros, F. (2002). The mobility of long-runout landslides. Eng. Geol., 63(3), 301-331.

Lentini, F., Catalano, S., Carbone, S. (2000). Carta Geologica della Provincia di Messina. Assessorato Territorio-Servizio geologico, SELCA, Firenze.

Lichti, D.D. (2007). Error modelling, calibration and analysis of an am-cw terrestrial laser scanner system. ISPRS J. Photogram. Remote Sens., 61(5), 307-324.

Lim, M., Petley, D.N., Rosser, N.J., Allison, R.J., Long, A.J., Pybus, D. (2005). Combined digital photogrammetry and time-of-flight laser scanning for monitoring cliff evolution. Photogram. Rec., 20(110), 109-129.

Lorenzini, G., Mazza, N. (Eds.). (2004). Debris flow: Phenomenology and rheological modelling. Wit Press.

Lube, G., Cronin, S.J., Platz, T., Freundt, A., Procter, J.N., Henderson, C., Sheridan, M.F. (2007). Flow and deposition of pyroclastic granular flows: A type example from the 1975 Ngauruhoe eruption, New Zealand. J. Volcanol. Geoth. Res., 161(3), 165-186.

Lucy, L.B. (1977). A numerical approach to the testing of the fission hypothesis. Astron. J., 82(12), 1013-1024.

Manetti, L., Steinmann, G. (2007). 3DeMoN ROBOVEC—integration of a new measuring instrument in an existing generic remote monitoring platform. In: 7th international symposium on field measurements in geomechanics, September 2007, Boston, MA, USA, 24-27.

Mantovani, F., Soeters, R., Van Westen, C.J. (1996). Remote sensing techniques for landslide studies and hazard zonation in Europe. Geomorphology, *15*(3), 213-225.

McKinnon, M., Hungr, O., McDougall, S.D (2008). Dynamic analyses of Canadian landslides. In *Proceedings* of the Fourth Canadian Conference on GeoHazards: From Causes to Management, 20-24.

McDougall, S.D., Hungr, O. (2003). Objectives for the development of an integrated three-dimensional continuum model for the analysis of landslide runout. *In Proceedings* of the 3rd International Conference on Debris-Flow Hazards Mitigation: Mechanics, Prediction and Assessment. Edited by D. Rickenmann and CL Chen. Millpress, Rotterdam, The Netherlands, 481-490.

McDougall, S., Hungr, O. (2004). A model for the analysis of rapid landslide motion across three-dimensional terrain. Can. Geotech. J., 41(6), 1084-1097.

McDougall, S. (2006). A new continuum dynamic model for the analysis of extremely rapid landslide motion across complex 3D terrain (Doctoral dissertation, University of British Columbia).

Medina, V., Hürlimann, M., Bateman, A. (2008). Application of FLATModel, a 2D finite volume code, to debris flows in the northeastern part of the Iberian Peninsula. Landslides, *5*(1), 127-142.

Melosh, H.J. (1979). Acoustic fluidization: A new geologic process?. J. Geophys. Res.- Sol. Ea., 84(B13), 7513-7520.

Mitchell, R.J., Markell, A.R. (1974). Flowsliding in sensitive soils. Can. Geotech. J., 11(1), 11-31.

Miyabuchi, Y., Ikebe, S.I., Watanabe, K. (2005). The July 10, 2003 and the January 14, 2004 ash emissions from a hot water pool of the Nakadake crater, Aso volcano, Japan. Bull. Volcanol. Soc. Jpn., 50, 227-241.

Miyabuchi, Y., Watanabe, K., Egawa, Y. (2006). Bomb-rich basaltic pyroclastic flow deposit from Nakadake, Aso Volcano, southwestern Japan. J. Volcanol. Geoth. Res., 155(1-2), 90-103.

Miyazawa, N., Tanishima, T., Sunada, K., Oishi, S. (2003). Debris-flow capturing effect of grid type steel-made sabo dam using 3D distinct element method. *In:* Rickenmann, D., Chen, C.-l. (Eds.), *Proceedings* of the Third International Conference on Debris Flow Hazard Mitigation: Mechanics, Prediction, and Assessment, Davos. Millpress, Rotterdam, Netherlands, 527-538.

Mizuyama, T., Kobashi, S., Ou, G. (1992). Prediction of debris flow peak discharge. *In Proceedings* of the International Symposium Interpraevent, Bern, Switzerland, 4, 99-108.

Monaghan, J.J. (1989). On the problem of penetration in particle methods. J. Comput. Phys., 82, 1-15.

Monaghan, J.J. (1992). Smoothed particle hydrodynamics. Ann. Rev. Astron. Astrophys., 30, 543-574.

Morelli, S., Garduño Monroi, V.H., Gigli, G., Falorni, G., Arreygue Rocha, E., Casagli, N. (2010). The Tancitaro debris avalanche: characterization, propagation and modelling. J. Volcanol. Geoth. Res., 193, 93-105.

Nairn, I.A., Self, S. (1978). Esplosive eruptions and pyroclastic avalanches from Ngauruhoe in February 1975. J. Volcanol. Geoth. Res., 3(1-2), 39-60.

Nave, R., Ricci, T., Barberi, F., Davis, M., Isaia, R. (2010). Preception of volcanic risk in Italy: Etn, Vesuvio and Campi Flegrei. In Cities on Volcanoes 6 Conference.

Nicoletti, P. G., Sorriso-Valvo, M. (1991). Geomorphic controls of the shape and mobility of rock avalanches. Geol. Soc. Amer. Bull., 103(10), 1365-1373.

Nocentini, M., Tofani, V., Gigli, G., Fidolini, F., Casagli, N. (2015). Modeling debris flows in volcanic terrains for hazard mapping: the case study of Ischia Island (Italy). Landslides, 12(5), 831-846.

Norini, G., De Beni, E., Andronico, D., Polacci, M., Burton, M., Zucca, F. (2009). The 16 November 2006 flank collapse of the south-east crater at Mount Etna, Italy: Study of the deposit and hazard assessment. J. Geophys. Res.- Sol. Ea., 114(B2), 1978-2012.

O'Brien, W.J., Showalter, J.J. (1993). Effects of current velocity and suspended debris on the drift feeding of Arctic grayling. Transactions of the American Fisheries Society, 122(4), 609-615.

Oppikofer, T., Jaboyedoff, M., Keusen, H.R. (2008). Collapse at the eastern Eiger flank in the Swiss Alps. Nat. Geosci. 1, 531-535.

Ostwald, W., 1925, Concerning the function rate of the viscosity of dispersion systems: IV: Kolloid-Zeitschrift, 36, 248-250.

Pastor, M., Haddad, B., Sorbino, G., Cuomo, S., Drempetic, V. (2009). A depth-integrated, coupled SPH model for flow-like landslides and related phenomena. Int. J. num. anal. methods geomech., 33(2), 143-172.

Patra, A.K., Bauer, A.C., Nichita, C.C., EPitman, E.B., Sheridan, M.F., Bursik, M., Rupp, B., Webber, A., Stinton, A.J., Namikawa, L.M., Renschler, C.S. (2005). Parallel adaptive numerical simulation of dry avalanches over natural terrain. J. Volcanol. Geotherm. Res., 139(1–2): 89-102.

Pelletier, J. D., Malamud, B. D., Blodgett, T., & Turcotte, D. L. (1997). Scale-invariance of soil moisture variability and its implications for the frequency-size distribution of landslides. Eng. Geol, *48*(3), 255-268.

Petrascheck, A., Kienholz, H. (2003). Hazard assessment and mapping of mountain risks in Switzerland. Debris-flow hazard mitigation: mechanics, prediction and assessment. Millpress, Rotterdam.

Petrie, G., Toth, C.K. (2008). I. Introduction to laser ranging, profiling and scanning, II. Airbone and spaceborne laser profiles and scanners, III. Terrestrial laser scanners (chapters 1 to 3). In: Shan J, Toth CK (eds) Topographic laser ranging and scanning: principles and processing, CRC Press, Taylor & Francis.

Philip, J.R. (1985). Approximate analysis of the borehole permeameter in unsaturated soil. Water Resour. Res., 21(4), 1025-1033.

Picarelli, L., Olivares, L., Comegna, L., Damiano, E. (2008). Mechanical aspects of flow-like movements in granular and fine grained soils. Rock Mech. Rock Eng., 41(1), 179-197.

Pierson, T.C. (1986). Flow behavior of channelized debris flows, Mount St. Helens, Washington. Hillslope processes, 269-296.

Pierson, T.C., Costa, J.E. (1987). A rheologic classification of subaerial sediment-water flows. Rev. in Eng. Geol., 7, 1-12.

Pierson, T.C., Janda, R.J. (1994). Volcanic mixed avalanches: a distinct eruption-triggered mass-flow process at snow-clad volcanoes. Geol. Soc. Am. Bull., 106(10), 1351-1358.

Pioli, L., Rosi, M., Calvari, S., Spampinato, L., Renzulli, A., Di Roberto, A. (2008). The eruptive activity of 28 and 29 December 2002, The Stromboli volcano an integrated study of the 2002-2003 eruption. Washington, USA: American Geophysical Union, 105-115.

Pirulli, M., Scavia, C., Mangeney-Castelnau, A. (2004). Sviluppo di un modello basato sulla meccanica del continuo per lo studio della propagazione di valanghe di roccia. Incontro Annuale dei Ricercatori di Geotecnica (IARG).

Pirulli, M. (2005). Numerical modelling of landslide runout. A continuum mechanics approach (Doctoral dissertation, Politecnico di Torino).

Pirulli, M., Mangeney, A. (2008). Results of back-analysis of the propagation of rock avalanches as a function of the assumed rheology. Rock Mech. Rock Eng., 41(1), 59-84.

Pistolesi, M., Rosi, M., Pioli, L., Renzulli, A., Bertagnini, A., Andronico D. (2008). The paroxysmal event and its deposits. In Calvari, S., S. Inguaggiato, G. Puglisi, M. Ripepe, M. Rosi, The Stromboli volcano an integrated study of the 2002-2003 eruption. Washington, USA: American Geophysical Union, 317-330.

Pitman, E.B., Nichita, C.C., Patra, A., Bauer, A., Sheridan, M., Bursik, M. (2003). Computing granular avalanches and landslides. Phys. Fluids (1994-present), 15(12), 3638-3646.

Ponte, G. (1948). Attività straordinaria dello Stromboli. Ann. Geophys., 1(2), 200-202.

Prochaska, A., Santi, P., Higgins, J., and Cannon, S. (2008). A study of methods to estimate debris flow velocity, Landslides, 5(4), 431-444.

Procter, J.N., Cronin, S.J., Platz, T., Patra, A., Dalbey, K., Sheridan, M., Neall, V. (2010). Mapping block-and-ash flow hazards based on Titan 2D simulations: a case study from Mt. Taranaki, NZ. Nat. Hazards, 53(3), 483-501.

Revellino, P., Hungr, O., Guadagno, F.M., Evans, S.G. (2004). Velocity and runout prediction of destructive debris flows and debris avalanches in pyroclastic deposits, Campania Region, Italy. Env. Geol., 45(3), 295-311.

Revellino, P., Guerriero, L., Grelle, G., Hungr, O., Fiorillo, F., Esposito, L., Guadagno, F. M. (2013). Initiation and propagation of the 2005 debris avalanche at Nocera Inferiore (Southern Italy). Ita. J. Geosc., 132(3), 366-379.

Riccò, A. (1907). Sull'attività dello Stromboli dal 1891 in poi. Boll. Sismol. Soc. Ital., 12, 205.

Rickenmann, D., Zimmermann, M. (1993). The 1987 debris flows in Switzerland: documentation and analysis. Geomorphology, 8(2-3), 175-189.

Rickenmann, D. (1994). An alternative equation for the mean velocity in gravel-bed rivers and mountain torrents. In Proceedings of the ASCE National Conference on Hydraulic Engineering, 1, 672-676.

Rickenmann, D. (1999). Empirical relationships for debris flows. Nat. Hazards, 19(1), 47-77.

Rickenmann, D. (2005). Runout prediction methods. In Debris-flow hazards and related phenomena. Springer Berlin Heidelberg, 305-324.

Rittmann, A. (1931). Der Ausbruch des Stromboli am 11. September 1930. Z Vulkanologie 14, 47-77.

Rosi, M., Bertagnini, A., Landi, P. (2000). Onset of the persistent activity at Stromboli volcano (Italy). Bull. Volcanol., 62(4-5), 294-300.

Rosi, M., Bertagnini, A., Harris, A.J.L., Pioli, L., Pistolesi, M., Ripepe, M. (2006). A case history of paroxysmal explosion at Stromboli: timing and dynamics of the April 5, 2003 event. Earth Planet. Sci. Lett., 243(3), 594-606.

Rosi, M., Pistolesi, M., Bertagnini, A., Landi, P., Pompilio, M., Di Roberto, A. (2013). Stromboli Volcano, Aeolian Islands (Italy): present eruptive activity and hazard. Accepted, in: Lucchi,

F., A. Peccerillo, J. Keller, C.A. Tranne, and P.L. Rossi (Eds.), Geol. Soc. London Mem., Geology of the Aeolian Islands (Italy).

Sassa, K. (1988). Motion of landslides and debris flows: prediction of hazard area: report for Grant-in-aid for Scientific Research by Japanese Ministry on Education. Sci. Cult., (61480062), 1-82.

Savage, S.B., Hutter, K. (1989). The motion of a finite mass of granular material down a rough incline. J. fluid mech., 199, 177-215.

Savage, S. B., Hutter, K. (1991). The dynamics of avalanches of granular materials from initiation to runout. Part I: Analysis. Acta. Mechanica, 86(1-4), 201-223.

Scheidl, C., Rickenmann, D. (2010). Empirical prediction of debris-flow mobility and deposition on fans. Earth Surf. Pro. Land., 35(2), 157-173.

Schilling, S.P. (1998). LAHARZ; GIS programs for automated mapping of lahar-inundation hazard zones (No. 98-638). US Geological Survey; Information Services [distributor].

Schneuwly-Bollschweiler, M., Stoffel, M., Rudolf-Miklau, F. (2012). Dating torrential processes on fans and cones: methods and their application for hazard and risk assessment. Springer Science & Business Media, Berlin, Heidelberg, New York, 47.

Shan, J., Toth, C.K. (2009). Topographic laser scanning and ranging. Principles and processing.

Skempton, A.W. (1953). Discussion in soil stability problems in road engineering. Proc. of the Institution of Civil Engineers, 2, 219-280.

Slob, S., Hack, H., Turner, A.K. (2002). An approach to automate discontinuity measurements of rock faces using laser scanning techniques. In: Dinid da Gama C, Riberia e Sousa L (eds) Proceedings of ISRM *EUROCK 2002.*

Slob, S., Hack, R. (2004). 3D terrestrial laser scanning as a new field measurement and monitoring technique. In: Engineering geology for infrastructure planning in Europe: a European perspective, Lectures Notes in Earth Sciences, Springer, Berlin/Heidelberg, 104, 179-189

Sosio, R., Crosta, G.B., Hungr, O. (2008). Complete dynamic modelling calibration for the Thurwieser rock avalanche (Italian Central Alps). Eng. Geol., 100, 11-26.

Sosio, R., Crosta, G.B., Hungr, O. (2012). Numerical modelling of debris avalanche propagation from collapse of volcanic edifices. Landslide, 9, 315-334.

Sosio, R., Crosta, G.B., Chen, J.H., Hungr, O. (2012b). Modelling rock avalanche propagation onto glaciers. Quat. Sci. Rev., 47, 23-40.

Sovilla, B., Burlando P., Bartelt P. (2006). Field experiments and numerical modeling of mass entrainment in snow avalanches, J. Geophys. Res., 111.

Squarzoni, C., Delacourt, C., Allemand, P. (2003). Nine years of spatial and temporal evolution of the La Valette landslide observed by SAR interferometry. Eng. Geol., 68(1), 53-66.

Stead, D., Eberhardt, E., Coggan, J.S. (2006). Developments in the characterization of complex rock slope deformation and failure using numerical modelling techniques. Eng. Geol., 83(1), 217-235.

Sulpizio, R., Bonasia, R., Dellino, P., Mele, D., Di Vito, M.A., La Volpe, L. (2010). The Pomici di Avellino eruption of Somma–Vesuvius (3.9 ka BP). Part II: sedimentology and physical volcanology of pyroclastic density current deposits. Bull. Volcanol., 72(5), 559-577.

Takahashi, T. (1991). Debris flow. International association for hydraulic research monograph. A.A. Balkema, Rotterdam, TheNetherlands.

Takahashi, T., Tsujimoto, H. (2000). A mechanical model for Merapi-type pyroclastic flow. J. Volcanol. Geoth. Res., 98(1), 91-115.

Takei, A. (1980). Interdependence of sediment budget between individual torrents and a river-system, Proc. Int. Symp. Interpraevent, Villach, Austria, Bd., 2, 35–48.

Tarchi, D., Ohlmer, E., Sieber, A. (1997). Monitoring of structural changes by radar interferometry. J. Res. Nondestructive Eval., 9(4), 213-225.

Tarchi, D., Casagli, N., Fanti, R., Leva, D., Luzi, G., Pasuto, A., Pieraccini, M., Silvano, S. (2003). Landslide monitoring by using ground-based SAR interferometry: an example of application to the Tessina landslide in Italy. Eng. Geol., 68(1): 15-30.

Taylor, G.R., Hearn, G.J. (2000). Landslide hazard assessment and mitigation: a Hong Kong case study. In Second International Congress on Debris Flows Hazard Mitigation: mechanics, prediction and assessment, 461-469.

Terzaghi, K. (1950). Geologic aspects of soft ground tunnelling. In: Trask, J. (Ed.), Applied Sedimentation. John Wiley, New York (Chapter 11).

Terzaghi, K., Peck, R.B. (1967). "Soil Mechanics in Engineering Practice" 2nd ed. John Wiley and Sons, New York.

Teza, G., Galgaro, A., Zaltron, N., Genevois, R. (2007). Terrestrial laser scanner to detect landslide displacement fields: a new approach. Int. J. Remote Sens., 28, 3425-3446.

Thomas, D.G. (1963). Transport characteristics of suspensions VII. Relation of hindered-settling floc characteristics to rheological parameters. AIChE J., 9(3), 310-316.

Trivelli, G. (1991). Storia del territorio e delle genti di Recoaro. Comune di Recoaro Terme. Istituto Geografico De Agostini [in italian].

Ui, T., Matsuwo, N., Sumita, M., Fujinawa, A. (1999). Generation of block-and-ash flows during the 1990–1995 eruption of Unzen Volcano, Japan. J. Volcanol. Geoth. Res., 89, 123-137.

Varnes, D.J. (1954). Landslide types and processes. In Eckel, E.B. (ed.), Landslides and Engineering Practice, Special Report 28: Highway Research Board, National Academy of Sciences, Washington, DC., 20-47.

Varnes, D.J. (1978). Slope movement: types and processes. In Landslides: Analysis and Control, Report Washington: Transportation Research Board, 176, 11-33.

Voellmy, A. (1955). Uber die Zerstorunskraft von Lawinen (On breaking force of avalanches). Schweizerische Bauzeitung, 73, 212-285 [in German].

Wagner, A.A. (1957). The use of the Unified Soil Classification System by the Bureau of Reclamation: Proceedings, 4th International Conference on Soil Mechanics and Foundation Engineering (London), 1, 125.

Wehr, A., Lohr, U. (1999). Airborne laser scanning–an introduction and overview. ISPRS J. Photogramm. Remote Sens.,54, 68-82.

Whitehouse, I. E., Griffiths, G. A. (1983). Frequency and hazard of large rock avalanches in the central Southern Alps, New Zealand. Geology, 11(6), 331-334.

Widiwijayanti, C., Voight, B., Hidayat, D., Schilling, S.P. (2009). Objective rapid delineation of areas at risk from block-and-ash pyroclastic flows and surges. Bull. Volcanol., 71(6), 687-703.

Willenberg, H., Eberhardt, E., Loew, S., McDougall, S., Hungr, O. (2009). Hazard assessment and runout analysis for an unstable rock slope above an industrial site in the Riviera valley, Switzerland. Landslides, 6(2), 111-119.

Working Party on World Landslide Inventory, (1990). A suggested method for reporting a landslide, Bulletin IAEG, No, 41, 5-12.

Zanchetta, G., Sulpizio, R., Pareschi, M.T., Leoni, F.M., Santacroce, R. (2004). Characteristics of May 5^6, 1998 volcaniclastic debris flows in the Sarno area (Campania, southern Italy): relationships to structural damage and hazard zonation. J. Volcano. Geoth. Res., 133(1), 377-393.

Zeller, J. (1985). Feststoffmessung in kleinen Gebirgseinzugsgebieten [Sediment measurement in small mountainous catchments], Wasser, Energie, Luft 77 (7/8), 246–251 [in German].

Zimmermann, R., Fichtner, W. (1997). Low-power logic styles: CMOS versus pass-transistor logic. IEEE J. Solid State Circuits, 32(7), 1079-1090.

Zischinsky U. (1969) - Uber sackungen. Rock Mech., 1(1): 30-52.

9. Publications

- Salvatici T., Di Roberto A., Di Traglia F., Bisson M., Morelli S., Fidolini F., Bertagnini A., Pompilio M., Hungr O., Casagli N. (2016). From hot rocks to glowing avalanches: Numerical modelling of gravity-induced pyroclastic density currents and hazard maps at the Stromboli volcano (Italy). Geomorphology, 273, 93-106.
- Morelli S., Salvatici T., Nolesini T., Di Traglia F., Del Ventisette C., Casagli N., Di Roberto A., Bisson M., Pompilio M., Bertagnini A. (2016). Analogue and numerical modeling of the Stromboli hot avalanches. Landslides and Engineered Slopes. Experience, Theory and Practice, Vol. 3, pp. 1493-1500.
- Salvatici T., Morelli T., Di Traglia F., Di Roberto A. Runout modelling of gravity-induced pyroclastic density currents at Stromboli volcano (Italy). Rend. Online Soc. Geol. It., Bologna. (In press).
- Salvatici T., Morelli S., Pazzi V., Frodella W., Fanti R. Debris flow source area forecasting and simulated impact assestment in the Rotolon creek valley (northern Italy). Journal of Mountain Science. (Proof).

Geomorphology 273 (2016) 93–106

Contents lists available at ScienceDirect

Geomorphology

journal homepage: www.elsevier.com/locate/geomorph

Invited review

From hot rocks to glowing avalanches: Numerical modelling of gravity-induced pyroclastic density currents and hazard maps at the Stromboli volcano (Italy)

Teresa Salvatici [a,*], Alessio Di Roberto [b], Federico Di Traglia [a], Marina Bisson [b], Stefano Morelli [a], Francesco Fidolini [a], Antonella Bertagnini [b], Massimo Pompilio [b], Oldrich Hungr [c], Nicola Casagli [a]

[a] Dipartimento di Scienze della Terra, Università di Firenze, Via La Pira 4, 50121 Firenze, Italy
[b] Istituto Nazionale di Geofisica e Vulcanologia, Sezione di Pisa, Via della Faggiola 32, 56126 Pisa, Italy
[c] Department of Earth, Ocean and Atmospheric Sciences, University of British Columbia, Vancouver Campus, V6T 1Z4 Vancouver, Canada

ARTICLE INFO

Article history:
Received 30 October 2015
Received in revised form 1 August 2016
Accepted 5 August 2016
Available online 7 August 2016

Keywords:
Pyroclastic density currents
Geophysical flows modelling
Stromboli volcano
Hazard maps

ABSTRACT

Gravity-induced pyroclastic density currents (PDCs) can be produced by the collapse of volcanic crater rims or due to the gravitational instability of materials deposited in proximal areas during explosive activity. These types of PDCs, which are also known as "glowing avalanches", have been directly observed, and their deposits have been widely identified on the flanks of several volcanoes that are fed by mafic to intermediate magmas. In this research, the suitability of landslide numerical models for simulating gravity-induced PDCs to provide hazard assessments was tested. This work also presents the results of a back-analysis of three events that occurred in 1906, 1930 and 1944 at the Stromboli volcano by applying a depth-averaged 3D numerical code named DAN-3D. The model assumes a frictional internal rheology and a variable basal rheology (i.e., frictional, Voellmy and plastic). The numerical modelling was able to reproduce the gravity-induced PDCs' extension and deposit thicknesses to an order of magnitude of that reported in the literature. The best results when compared with field data were obtained using a Voellmy model with a frictional coefficient of $f = 0.19$ and a turbulence parameter $\xi = 1000\ m\ s^{-1}$. The results highlight the suitability of this numerical code, which is generally used for landslides, to reproduce the destructive potential of these events in volcanic environments and to obtain information on hazards connected with explosive-related, mass-wasting phenomena in Stromboli Island and at volcanic systems characterized by similar phenomena.

Contents

1. Introduction . . . 94
2. Eruptive activity and pyroclastic flows at the Stromboli volcano . . . 94
   2.1. Gravity-induced PDCs in 1906, 1930 and 1944 . . . 94
   2.2. Description of the deposits . . . 95
3. Methods . . . 96
   3.1. Model description . . . 96
   3.2. Model calibration and input data for simulation . . . 98
4. Results . . . 99
5. Discussion . . . 101
   5.1. Evaluation of modelling results . . . 101
   5.2. Implications for hazards . . . 103
6. Conclusions . . . 104
Acknowledgements . . . 105
References . . . 105

* Corresponding author.
E-mail address: teresa.salvatici@unifi.it (T. Salvatici).

http://dx.doi.org/10.1016/j.geomorph.2016.08.011

1. Introduction

Glowing avalanches generated from the collapse of the unstable portion of a volcanic crater's rim or the gravitational instability of materials deposited during explosive activity can be defined as gravity-induced pyroclastic density currents (PDCs). They have been directly observed and their deposits have been identified on the flanks of several volcanoes fed by mafic to intermediate magmas (Davies et al., 1978; Nairn and Self, 1978; Hazlett et al., 1991; Arrighi et al., 2001; Alvarado and Soto, 2002; Calvari and Pinkerton, 2002; Cole et al., 2005; Yasui and Koyaguchi, 2004; Yamamoto et al., 2005; Miyabuchi et al., 2006; Behncke et al., 2008; Di Roberto et al., 2014; Di Traglia et al., 2014; Calvari et al., 2016). Such gravity-induced PDCs have small volumes (10^4–10^7 m^3) but are emplaced at very high temperatures and can travel far from the source (Davies et al., 1978; Nairn and Self, 1978; Hazlett et al., 1991; Yamamoto et al., 2005; Miyabuchi et al., 2006; Di Roberto et al., 2014). Small volume PDCs are potentially dangerous for communities close to the volcanoes and tourists. Runouts longer than 8 km from the source have been reported for gravity-induced PDCs that presumably resulted from the avalanching of pyroclastic materials accumulated on slopes steeper than the angle of repose at Shin-Fuji volcano, Japan (Yamamoto et al., 2005) and for those that emerged from notches in the crater rim during the 1974 eruption of the Fuego volcano, Guatemala (Davies et al., 1978). Similar "gravity-induced" processes have been hypothesized for the formation of the glowing avalanches generated during the 1975 eruption at Ngauruhoe volcano, New Zealand (Nairn and Self, 1978; Lube et al., 2007) and for the PDCs of Asama volcano, Japan (Aramaki and Takahashi, 1992; Yasui and Koyaguchi, 2004) and Tungurahua volcano, Ecuador (Kelfoun et al., 2009). On 11 February 2014, a large volume of unstable and hot rocks detached from the lower-eastern flank of Etna's New Southeast Crater, Italy, and caused a PDC, travelling approximately 3 km on the eastern flank of the volcano and reaching the bottom of Valle del Bove at an average speed of >60 km h^{-1} (Bonforte and Guglielmino, 2015; De Beni et al., 2015). In addition, there are more hazards connected with small-volume gravity-induced PDCs. To improve hazard assessments from all types of PDCs, it is necessary to expand the understanding of PDCs and evaluate their possible impacts on human activities.

In this research, the suitability of landslide numerical models for simulating and assessing hazards related to gravity-induced PDCs was tested. The results of a back-analysis of three events of "glowing avalanches" at the Stromboli volcano are presented. The DAN-3D depth-averaged 3D numerical code, developed by McDougall and Hungr (2004) and Hungr and McDougall (2009), was applied. As case studies, three gravity-induced PDCs in 1906, 1930 and 1944 were selected. In relation to the 1930 event, detailed descriptions were compiled by Rittmann (1931) and Abbruzzese (1935) shortly after the eruption, from which crucial parameters such as the total runout distance, velocity, thickness and distribution of the deposits were deduced. Additional data on the flow dynamics and distributions of the deposits have been reported by Di Roberto et al. (2014).

The findings were also used to assess whether the inhabited areas of Stromboli (Stromboli and Ginostra villages) could be affected if one of the events is repeated in the future with dynamics similar to that in historical times and to evaluate the potential associated damage. The methodology used here may be applied to other volcanoes and, perhaps to other geological contexts, giving implications for hazard assessments in areas prone to mass-flows.

2. Eruptive activity and pyroclastic flows at the Stromboli volcano

Stromboli is the northernmost volcanic island of the Aeolian archipelago, in the southern Tyrrhenian Sea (Fig. 1). The island is the subaerial part of a rather regular volcanic edifice that rises to 924 m above sea level (a.s.l.) from a base that lies at a water depth between 1300 and 2300 m. Volcanic activity on Stromboli has been continuous since the III–VII centuries A.D. and consists of mild- to low-energy intermittent explosions (Strombolian activity), which are occasionally interrupted by effusive events and violent explosions that are commonly called paroxysms (Barberi et al., 1993; Rosi et al., 2000). The active vents are located in the crater terrace at approximately 750 m a.s.l. on the upper part of the Sciara del Fuoco (SdF), which is a horseshoe-shaped depression on the NW uninhabited flank of the volcano (Fig. 1).

At the Stromboli volcano, the formation of mass flows of hot pyroclasts has been reported several times. The flows occurred as a direct result of explosive and effusive volcanic activities such as those on 6 December 1985, (De Fino et al., 1988), 5 April 2003, (Rosi et al., 2006, accepted for publication; Pistolesi et al., 2008) and 12 January 2013 (Di Traglia et al., 2014; Calvari et al., 2016) or of the sliding of incandescent pyroclastic fall deposits accumulated over steep slopes such as during the 1930 and 1944 paroxysms (Di Roberto et al., 2014) and the eruptive activity of 28 and 29 December 2002 (Pioli et al., 2008). Gravity-induced PDCs usually occur in the SdF depression and therefore do not represent a serious threat to the population of Stromboli (Barberi et al., 1993; Rosi et al., accepted for publication). However, in 1906, 1930 and 1944, gravity-induced PDCs occurred outside the SdF, and in the latter two cases they reached the coast of the island. In particular, the 1930 PDCs reached the village of Stromboli on the NE part of the island, causing extensive damage and four casualties (Rittmann, 1931).

2.1. Gravity-induced PDCs in 1906, 1930 and 1944

Little information was reported on the PDCs on 15 July 1906 and 20 August 1944. Riccò (1907) reported that during the late afternoon of 15 July 1906 a very large eruption of incandescent material hit the area of Forgia Vecchia on the ESE side of the island (Fig. 1) and was preceded by a loud and long-lasting rumble. A column of incandescent material flowed in the direction of the village of Ginostra, WSW from the vent, burning the vegetation. Similarly, Ponte (1948) described that on 20 August 1944 a large amount of incandescent material consisting of large blocks and ash that had accumulated on the summit of the volcano and on the Forgia Vecchia flowed downslope, reached the shore and formed a ca. 100-m-long delta in the sea. The delta was rapidly eroded by the action of sea waves.

The event during the 1930 paroxysm is the best described. It was triggered by the sliding of an approximately 1 m-thick source deposit with an estimated volume of at least 45,000 m^3 and consisting of metre-sized spatters, decimetre-sized bombs, lapilli, and ash (Rittmann, 1931; Abbruzzese, 1935). That deposit had accumulated over an area of >60,000 m^2 on the steep cliff side of Chiappe Lisce (Fig. 1) approximately 1 h before the initiation of the gravity-induced PDC event (Rittmann, 1931) during an extremely violent paroxysm; this paroxysm was possibly the most violent event known to date in the recent history of Stromboli (Bertagnini et al., 2011). The initiation mechanism can be classified as a "rock irregular slide", which is defined as the "sliding of a rock mass on an irregular rupture surface consisting of a number of randomly oriented joints, separated by segments of intact rock" (Hungr et al., 2014). The failure mechanism of this type of landslide is generally complex and difficult to describe and often includes elements of toppling (Hungr et al., 2014). At Stromboli, the inclination of some slopes exceeds the internal friction angle of the pyroclastic materials, but this condition is not sufficient to induce "rock irregular slide" events (Nolesini et al., 2013). Instead, the sliding processes are induced by the accumulation of pyroclastic materials, which produces a loading effect (overloading) on the summit of the volcano (Nolesini et al., 2013). This mechanism was also proposed for the generation of the glowing avalanches at Mt. Vesuvius during the 1944 eruption (Hazlett et al., 1991). Analogue modelling by Nolesini et al. (2013) revealed that the accumulation of material (representing either lava or spatter

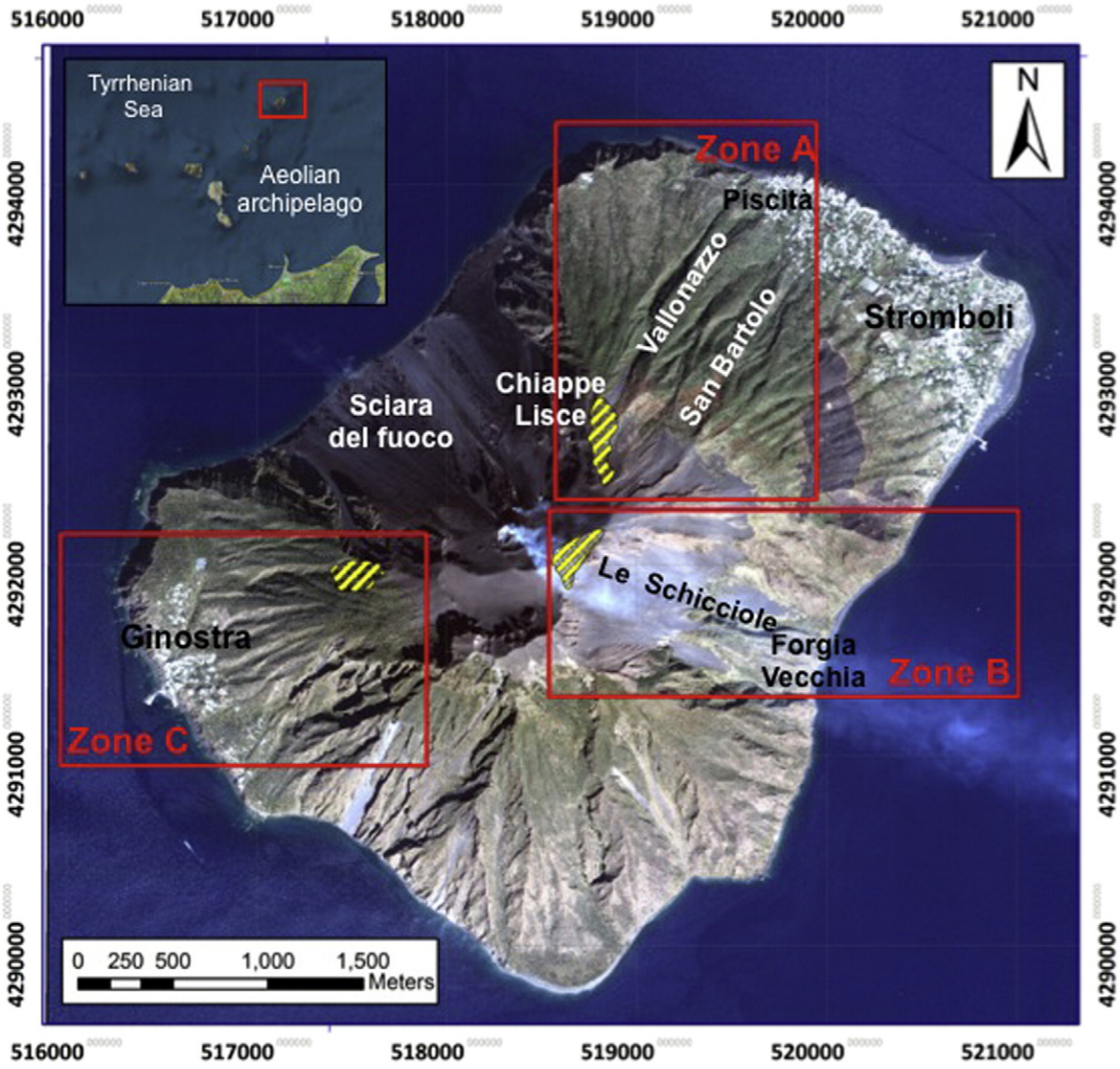

Fig. 1. Orthoimage of the study area, Stromboli volcano with the primary toponyms (from the QuickBird Satellite Sensor). The three red rectangular areas cover the volcanic sectors involved in the gravity-induced PDCs of 1930 (zone A), 1944 (zone B) and 1906 (zone C). These zones were used for numerical modelling with DAN-3D. The source areas of the three events are shown by yellow hatches.

agglutinates) overcomes slope stability, generates complex systems of landslides and increases the volume of material involved in the sliding processes.

The phenomenon begins with instability in the lower part of the slope on which material accumulates which results in a remobilization of the deposited material in a landslide (Fig. 2a). This mechanism for generating gravity-induced PDCs is consistent with the model proposed by Ui et al. (1999) and Takahashi and Tsujimoto (2000) for the dome collapse-induced block and ash flows (Merapi-type) during the 1991–1995 eruption of Unzen Volcano, Japan.

Failures of crater-rims or pyroclastic piles develop into rockslides, dry gravel/debris flows or avalanches (Hazlett et al., 1991; Cole et al., 2005; Di Traglia et al., 2014), which have been described as the "extremely rapid, massive, flow-like motion of fragmented rock from a large rock slide or rock fall" (Hungr et al., 2014). Rockslides attain a degree of mobility that far exceeds what would be expected from a frictional flow of dry, angular, broken rock, and the mobility is increased with the volume of an event (Heim, 1932; Hayashi and Self, 1992; Dade and Huppert, 1998; Calder et al., 1999).

2.2. Description of the deposits

The deposits related to the 1930 event, including grain-size and componentry were described in Di Roberto et al. (2014). The deposits of the 1930 paroxysms comprise of 1) a spatter bomb deposit and 2) a fallout deposit. Spatter deposits crop out on both sides of the Sciara del Fuoco down to 120 m a.s.l. in an area that extends to some hundreds metres apart from both margins of the depression. Below 400 m a.s.l., the deposit consists of up to 4 m^2-sized, single to agglutinated, ribbon to convoluted spatter bombs up to 50 cm in length, which often laterally pass to alignments of flattened pumice and scoria bombs with centimetres to decimetres sizes. Moving upslope on the volcano, the spatter deposit becomes more and more continuous, and above 400 m a.s.l., it crops out as a decimetre-thick, nearly continuous accumulation.

At the base of the spatter deposit, a pyroclastic fallout deposit of coarse ash to medium lapilli ($Md\Phi = 0.8–2.5$) occurs, with thickness of a few to ca. 20 cm and consists of fresh, light coloured pumice, glassy black scoriae, and variable amounts of lithic fragments.

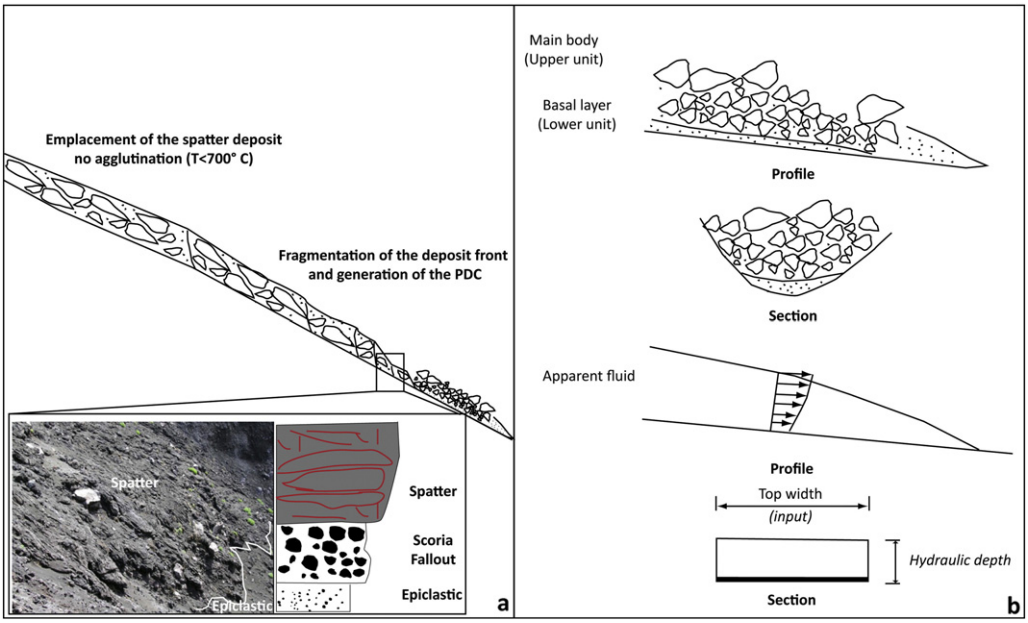

Fig. 2. The model approach a) Generation of gravity-induced PDCs at the Stromboli volcano through the sliding of spatter blankets accumulated during paroxysmal explosions. b) "Equivalent-fluid" simplified approach for the simulation of mass flow motion used in DAN-3D (Hungr, 1995; Hungr and McDougall, 2009). The momentum equations evaluate the internal frictional rheology, which is governed by an internal friction angle and by a basal rheology that is chosen by the operator according to one of seven rheological functions: frictional, plastic, Newtonian, turbulent, Bingham, Coulomb frictional and Voellmy.

The most complete outcrop of the 1930 PDC occurs at the opening of the S. Bartolo Valley, at approximately 420 m a.s.l. The thickness of the PDC deposits there is >4.5 m, and the base is not exposed. The deposit rapidly thins downslope, and 75 m away from the main outcrop it is ca. 2 m-thick. This order of magnitude of the thickness (approximately 1.5 m) remains to the end of the Vallonazzo where the PDC stopped.

The PDC deposit consists of two main units. The lower unit is a ~10 to 20 cm-thick, well-sorted medium ash, with $\sigma\phi = 1.27$ (sorting, with ϕ is the negative log base 2 of the grain diameter), $Md\phi = 1.63$ (median diameter) and $F1 = 72.20$ (wt.% of material, <1 mm). Lower unit often exhibits parallel to low-angle cross-laminations and short alignments of centimetric lapilli. The components include juvenile scoriae and pumices, which constitute 73 vol.% and show subrounded shapes and incipient surficial abrasion. Lithics, which represent 27 vol.% of the deposit, are concentrated mainly in the finest grain sizes and consist of reddish, holocrystalline subvolcanic rocks; orange-coloured, palagonitized or altered glassy scoriae; and loose magmatic crystals (plagioclase, clinopyroxene and olivine).

The upper unit ($\sigma\phi = 5.09$, $Md\phi = -0.79$, and $F1 = 31.19$) is constituted by metre-sized lithic blocks and bombs, multi decimetre to centimetre-sized juvenile scoriae, and pumices supported by a poorly sorted, massive, coarse ash matrix. The larger blocks are often aligned in the direction of flow and are concentrated on the uppermost part of the deposit.

3. Methods

3.1. Model description

In accordance with the failure mechanism and motion of the Stromboli PDCs, the suitability of the DAN-3D depth-averaged numerical code (McDougall and Hungr, 2004; Hungr and McDougall, 2009) was tested. The code is commonly used in landslide modelling to simulate and assess hazards related to gravity-induced flows. In addition, DAN-3D has been commonly and effectively used for the simulation of volcanic debris avalanches (Morelli et al., 2010; Sosio et al., 2012a) and other landslides in which the dominant process is represented by grain collisions (McDougall and Hungr, 2004; Sosio et al., 2008; Hungr and McDougall, 2009; Sosio et al., 2012b). The numerical code assumes a simplified "equivalent-fluid" approach for the simulation of mass-flow motion (Fig. 2b; Hungr, 1995; Hungr and McDougall, 2009). Starting from the theory of Savage and Hutter (1989); Hungr (1995) proposed

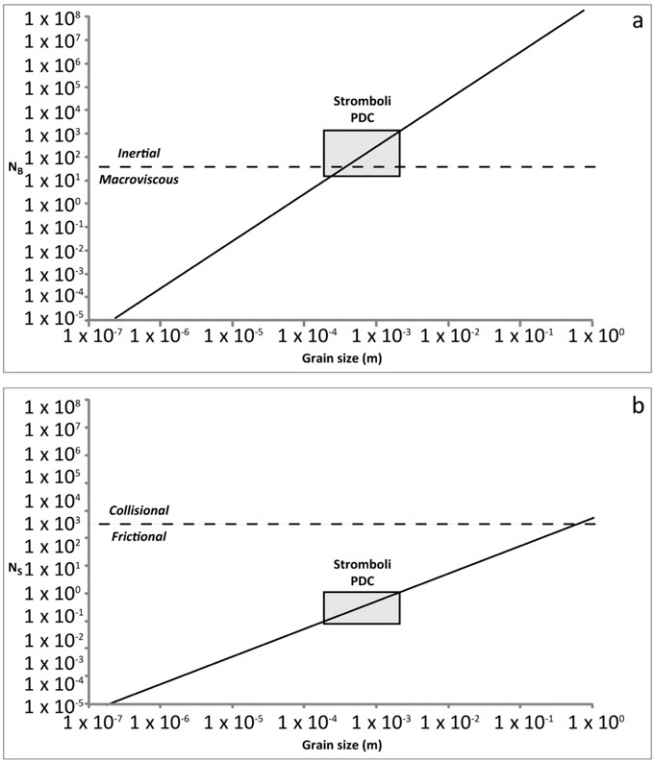

Fig. 3. The numbers to understand the dynamic regime of granular flows a) Bagnold number and b) Savage number estimations for the 1930 Stromboli gravity-induced PDC, based on grain-size data reported by Di Roberto et al. (2014). Although the PDC was at the inertial and macroviscous border for the Bagnold number, the Savage number estimation revealed a frictional behaviour that supports the assumption of internal frictional behaviour used in the DAN-3D model.

Table 1
Main characteristics of the three events. Zones A, B, and C are from Rittmann (1931), Abbruzzese (1935) and Di Roberto et al. (2014).

	Zone A	Zone B	Zone C
Eruption	1930	1944	1906
Date	Sept 11	Jun 15 (uncertain)	Aug 20
Area of interest	NE flank	WSW flank	ESE flank
Source elevation (m a.s.l.)	790	920	600
Volume source (m^3)	42,000	35,000	33,000
Entrainment (Mm^3)	Unspecified	Unspecified	Unspecified
Travel distance (km)	1.6	1.5	–
Thickness (m)	0.1–4	0.1–0.6	–
Velocity ($m\ s^{-1}$)	15–20	–	–
H/L (height/run out distance)	<0.4	<0.5	–

a semi-empirical approach in which the heterogeneous flowing material was modelled as a hypothetical material governed by two simple rheological relationships, one for the base and the other for the inner part, which may differ from each other. The idea of the separation of internal and basal friction mechanisms has its roots in the depth-integrated solutions of classical fluid dynamics, where a variety of viscous or turbulent relationships can be used to determine basal friction forces of a flowing sheet of fluid, whereas the internal stress distribution is assumed to be hydrostatic (e.g., Chow, 1959; Savage and Hutter, 1989; Hungr and McDougall, 2009).

Many published papers have confirmed the validity of Coulomb's (1776) model of rate-independent frictional deformation in modelling PDCs as granular materials (Iverson and Denlinger, 2001; Widiwijayanti et al., 2009; Procter et al., 2010; Sulpizio et al., 2010a; Charbonnier and Gertisser, 2012). The assumption of a frictional internal rheology is based on the dynamic regime of granular flows that can be expressed by two major non-dimensional numbers: the Bagnold number (N_B) and the Savage number (N_S). The former characterizes the relative importance of the interstitial fluid to the transport of momentum and can be formulated as (Bagnold, 1954; Iverson and Denlinger, 2001; Bursik et al., 2005):

$$N_b = \left(\frac{C_s}{C_*^{1/3} C_s^{1/3}}\right)^{1/2} \frac{\rho_s \gamma d^2}{\mu} \tag{1}$$

where C_s is the volumetric particle concentration in the flow (=0.5, as suggested by Iverson and Denlinger, 2001), C is the particle density at maximum packing (=0.7; Iverson and Denlinger, 2001), ρ_S is the particle density ($\rho_S = 1.08 \times 10^3\ kg\ m^{-3}$; Apuani et al., 2005a), γ is the strain rate (=10; Iverson and Denlinger, 2001), d is the typical particle diameter (in the range measured by Di Roberto et al., 2014, see Section 2.2), and μ is the dynamic viscosity of the interstitial fluid ($=3.5 \times 10^{-5}$, Iverson and Denlinger, 2001). The bracketed term in (1) shows the influence of the grain concentration C_s on the stress regime. For $N_B \le 40$, the material is in the macroviscous regime, in which the interstitial fluid plays a significant role in momentum transfer, but probably only under extreme unusual circumstances (very fine-rich flows), where the bulk behaviour of a volcanic granular flow would be macroviscous (Bursik et al., 2005). Otherwise, for $N_B \ge 450$, the flow behaviour is supposed to be inertial, i.e., momentum transport is by interparticle interactions (Bursik et al., 2005).

The Savage number, which characterizes the relative importance of momentum transfer by interparticle collisions to that by inter-particle friction, can be expressed as

$$N_s = \frac{\rho_s \gamma^2 d^2}{(\rho_s - \rho) g z}, \tag{2}$$

where ρ is the density of the interstitial fluid (=6; Iverson and Denlinger, 2001), g is the gravitational acceleration, and z is a slope perpendicular coordinate measured from the flow surface down. Approximately, N_S represents the ratio of grain collision stresses to Coulomb friction produced by grain contact stresses (Iverson and Denlinger, 2001). The collisional regime ($N_S \ge 0.1$) characterizes flows where grain collisions may be important to momentum transfer, and shear stress depends on strain rate, as in a fluid (diluted granular flows; e.g., Bursik et al., 2005). Otherwise, the flow is in the frictional regime (Bursik et al., 2005). The presence of intergranular pore-fluid pressure influences Coulomb friction in deforming granular masses, but only if high fluid pressures produce complete mixture fluidization, simulating the condition $\rho_S = \rho$ (Bagnold, 1954; Iverson and Denlinger, 2001). However, regardless of the shear rate or degree of dilatation, the Coulomb equation adequately describes bulk intergranular shear stresses produced in response to the slope-parallel member of the mixture weight (Iverson and Denlinger, 2001).

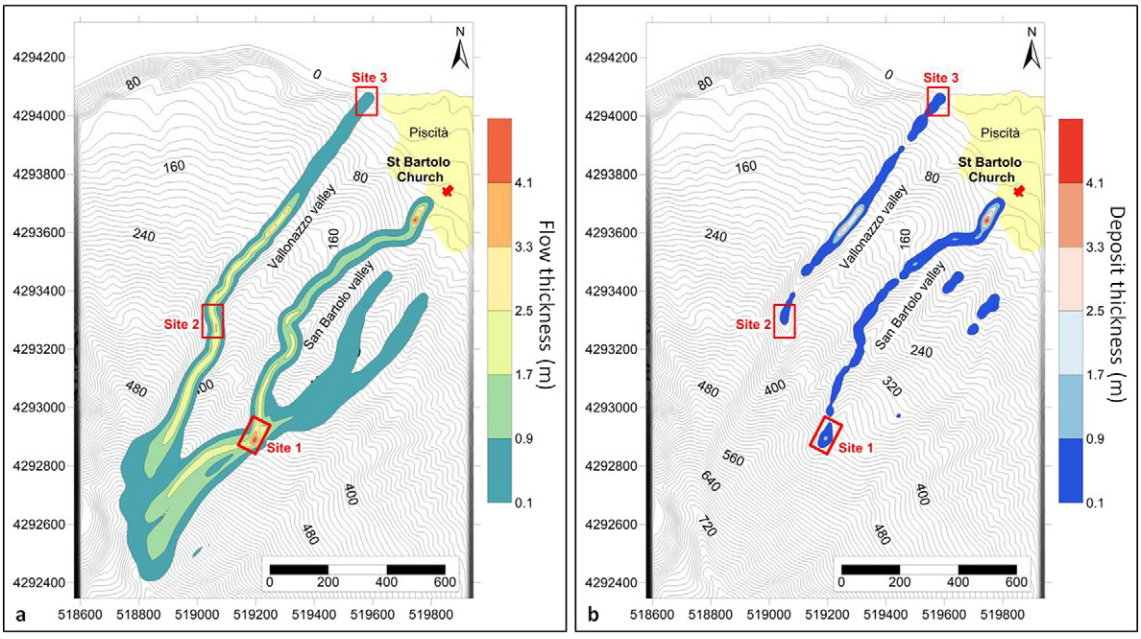

Fig. 4. Results of the DAN-3D simulation with the non-modified input thickness: a) flow thickness and b) deposit thickness after an interval of 135 s for zone A (1930-like event).

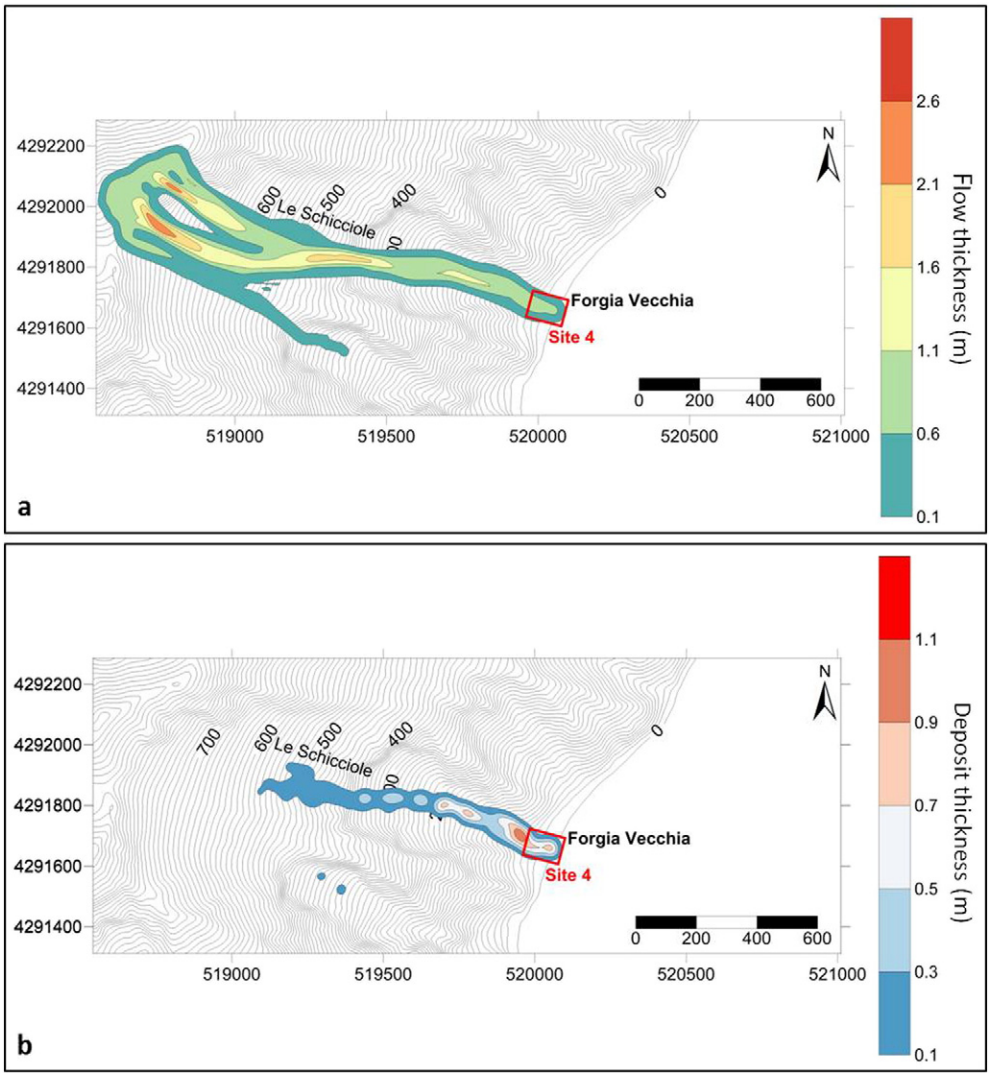

Fig. 5. Results of the DAN-3D simulation with the non-modified input thickness: a) flow thickness and b) deposit thickness after an interval of 88 s for zone B (1944-like event).

Based on the grain-size data reported in Di Roberto et al. (2014), the Stromboli gravity-induced PDCs fall on the border between the macroviscous and inertial regime (Fig. 3a) and in the frictional regime field (Fig. 3b).

DAN-3D uses the Lagrangian numerical method to solve the depth-average integrated St. Venant equations adapted from Smoothed Particle Hydrodynamics (SPH) (Monaghan, 1989, 1992; Benz, 1990). The model is divided into an internal frictional rheology that is governed by an internal friction angle and a basal rheology that is chosen by the operator according to one of seven rheological kernels implemented in the numerical code (Hungr, 1995): frictional, plastic, Newtonian, turbulent, Bingham, power law and Voellmy. A detailed description of the model was reported by Hungr and McDougall (2009).

3.2. Model calibration and input data for simulation

Simulations were performed on three areas corresponding to those affected by the gravity-induced PDCs of 1930 (zone A), 1944 (zone B) and the area possibly affected in the 1906 event (zone C) (Fig. 1). Zone A was used as a test area because information on the distributions and thickness of deposits, the velocity of the 1930 glowing avalanche, the event duration and the total travel distance are known from the literature (Rittmann, 1931; Abbruzzese, 1935; Di Roberto et al., 2014).

The materials involved in 1906 and 1944 gravity-induced PDCs were assumed to be similar to that of 1930 (for example, see Bertagnini et al., 2011). Thus, the parameters obtained for zone A were used to calibrate the model by back-analysis and to find the input rheological parameters that were later applied to the simulations in zones B and C. The main characteristics of the three events under consideration are shown in Table 1.

The modelling was performed on a high resolution (50 cm) Digital Elevation Model (DEM) of the current volcanic flank. The DEM was obtained by elaborating the 3D data (8 points m^{-2}) acquired during the airborne laser scanning survey on 04 May 2012 to 18 May 2012 carried out by the BLOM Compagnia Generale Ripreseaeree S.P.A. (www.blomasa.com).

The construction period and resolution of the DEM are important issues when testing the accuracy of any terrain-dependent model, and, in this case, the exact reconstruction of the pre-event topography is difficult. We used the current topography assuming that it well approximates the topography before the avalanche. Most of the materials deposited by the pyroclastic flow have been eroded, and only limited portions are preserved in sheltered areas, and, therefore, the topography is largely unchanged compared to that of 1930. Because DAN-3D does not work correctly with path grids that are excessively detailed, the path grid file was resampled to a spatial resolution of 5 m and repeatedly filtered using Gaussian smoothing (3 × 3). The use of the

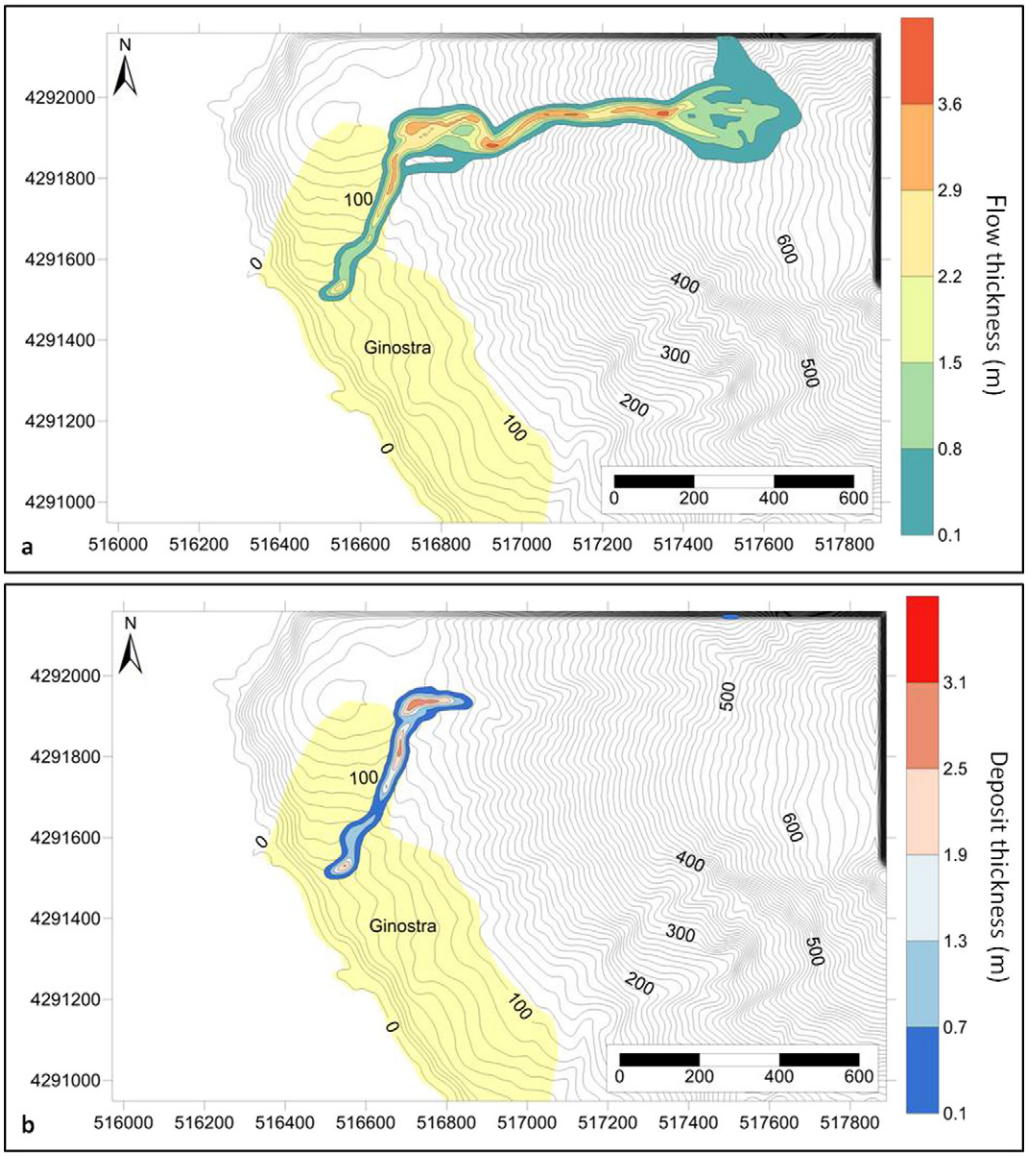

Fig. 6. Results of the DAN-3D simulation with the non-modified input thickness: a) flow thickness and b) deposit thickness after an interval of 180 s for zone C (1906-like event).

Smoothed Particle Hydrodynamics (SPH) numerical technique allowed the slide materials to spread, branch and join without problems due to the mesh and flow boundaries (McDougall and Hungr, 2003).

The area where accumulations of spatter and fallout deposits were observed (Rittmann, 1931) was assumed to be the source area of the 1930 gravity-induced PDC, whereas for the 1906 and 1944 eruptions, the source areas were identified as the regions upslope of the flow path where the slope exceeds 29° (Di Roberto et al., 2014). This value is usually assumed to be the lowermost value of the angle of repose for dry pyroclastic deposits (Apuani et al., 2005b; Miyabuchi et al., 2005). The initial value of 1 m for the thickness of the sliding material was defined according to the observations by Rittmann (1931) regarding the material accumulated on the summit of the volcano shortly before the 1930 PDC. The value was then applied to the other two events. The source volumes reconstructed using those areas and material thicknesses are reported in Table 1.

Erosion was not considered because a very low degree of substrate erosion and entrainment was observed in the field and defined by a sedimentological study of the 1930 event deposits (Di Roberto et al., 2014).

Because DAN-3D does not implement a routine for automatically stopping the simulation, we decided to interrupt the simulation when the flow reached sea level. If the flow never reached the coastline, the simulation was manually stopped when the flow velocity decreased to zero.

Finally, to provide a useful contribution to the assessment of hazards associated with gravity-induced PDCs at Stromboli, a further set of simulations with doubled thicknesses of the source deposits was also performed (double volume). The corresponding potential event could be considered a worst-case scenario for the inhabited areas of Stromboli Island.

4. Results

The simulations relative to the 1930 PDC were performed with frictional, plastic and Voellmy rheologies by a trial-and-error procedure (Morelli et al., 2010; Sosio et al., 2012a, 2012b). This method was used to obtain values of the runout, velocity, and duration of the flow that will match those derived from the literature and the available field data. The simulation that best reproduced the path, extension, and thickness order of magnitude of the 1930 gravity-induced PDC deposit (zone A) was obtained using a Voellmy rheological model with a frictional coefficient of $f = 0.19$, a turbulence parameter $\xi = 1000\ \mathrm{m\ s^{-2}}$, a unit weight of 14.71 and an internal friction angle of $\phi_i = 20°$ (Apuani et al., 2005b). That rheology

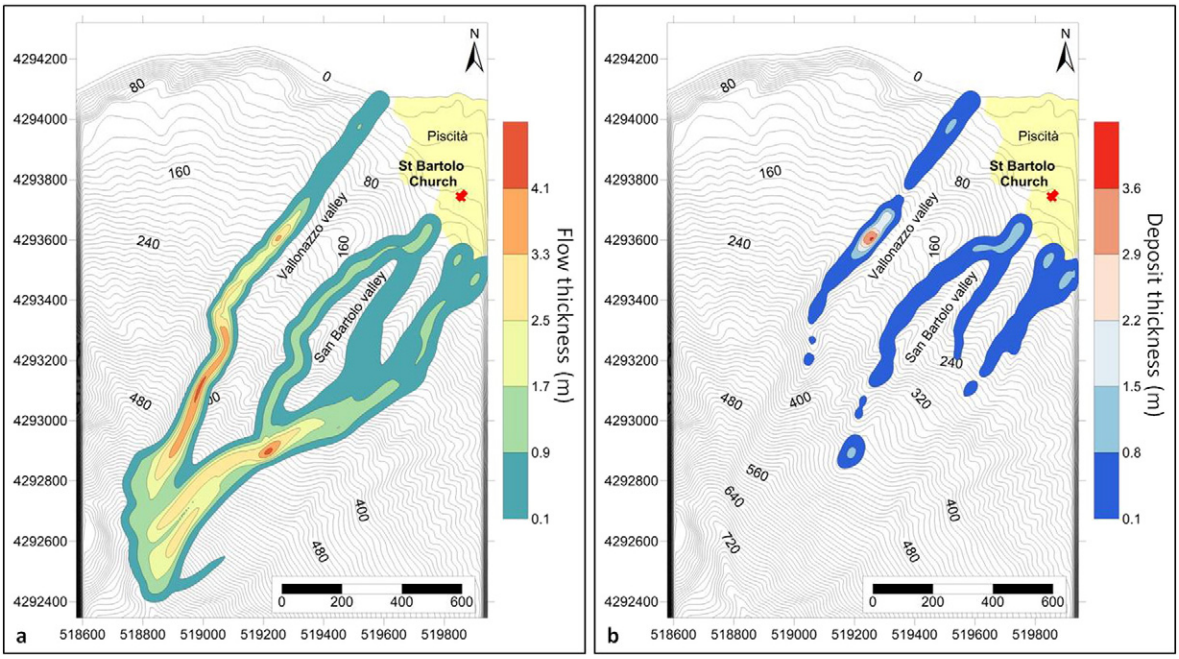

Fig. 7. Results of the DAN-3D simulation using a double input thickness: a) flow thickness and b) deposit thickness after an interval of 90 s for zone A (1930-like event).

matched the frictional and turbulent behaviours and allowed a better description of the complex dynamics of the avalanche and its long travel distance.

Simulations using the Voellmy rheological model displayed a strong topographic control, which allowed the 1930-like gravity-induced PDCs to flow inside the Vallonazzo valley with little overbank deposition. The Voellmy rheology differs from the simple Coulomb-type friction law by the presence of a turbulent component in addition to the frictional component ξ (Sosio et al., 2012a, 2012b). This component aids the flow resistance, which depends on the square of the velocity, by incorporating a coefficient that is used to represent the effects of turbulence and/or collisions (Kelfoun et al., 2010). The main parameters used during the back-analysis to constrain the model results were the flow length, impact area along the valley and the runout time. Historical accounts and field data (Abbruzzese, 1935) revealed that during the 1930 event "… flows of incandescent material were sliding into the S. Bartolo and Piscità (Vallonazzo) valleys. The first one stopped within tens of metres from the church of S. Bartolo (where the slope change from 25° to 15°), whereas the second one reached the sea". The simulation using the Voellmy rheological model was able to reproduce the two main gravity-induced PDCs reported in the literature (Rittmann, 1931; Abbruzzese, 1935; Di Roberto et al., 2014); the first flow extended along the Vallonazzo valley and reached the sea close to Piscità after 135 s, and the second flow moved in the San Bartolo valley and stopped near the church of San Bartolo after approximately 120 s (Fig. 4a).

The Voellmy rheological model also simulated the 1930 PDC deposits' thicknesses, matching the order of magnitude of those measured in the field by Di Roberto et al. (2014). At approximately 418 m a.s.l. in the San Bartolo valley (Site 1 of Di Roberto et al., 2014; Fig. 4b) the measured thickness was approximately 4.5 m, and the simulated thickness was 1.6 m. In the NE rim of the Vallonazzo valley, at approximately 370 m a.s.l. (Site 2 of Di Roberto et al., 2014; Fig. 4b), the measured and simulated thicknesses were comparable and had accuracies of 30–40 cm, whereas close to the outlet of Vallonazzo valley (Site 3 of Di Roberto et al., 2014; Fig. 4b), the measured thickness was approximately 100 cm, and the simulated thickness was 60 cm. The areas hit by the gravity-induced PDC and covered by the deposit were 3.6×10^5 and 0.8×10^5 m^2, respectively.

Comparatively, the frictional basal rheologies with friction angles between 20°–25° and shear strength between 2 and 5 kPa) basal allowed the simulation of 1930-like gravity-induced PDCs. The low topographic control produced over-estimates of lateral spread and velocity of the flow, whereas the thickness was under-estimated. Similar results were obtained by Sosio et al. (2012a), who modelled volcanic debris avalanches using DAN-3D. Frictional rheology assumes that emplacement is controlled by path topography. Deposition is strongly slope-dependent, and material therefore flows at any gradient greater than the basal friction angle (Sosio et al., 2012a). The plastic basal rheology (yield stress fluid) depends on the shear stress applied to its basal level, regardless of its thickness and velocity (Kelfoun, 2011), which does not allow for strong topographic control like the 1930 gravity-induced PDC.

The rheological parameters obtained using this procedure for the 1930 PDC were then used in the simulation of the gravity-induced PDCs events in zones B (in 1944) and C (in 1906). The results for zone B show that the flow moved into the "Le Schicciole" valley (Forgia Vecchia) and reached the sea in 88 s. In this case, the simulated deposit thickness of 60 cm matched the field measurement (Fig. 5; Di Roberto et al., 2014). The areas impacted by the PDC and covered by the deposit in zone B were 3.1×10^5 and 0.8×10^5 m^2, respectively.

The simulation in zone C showed that the flow never reached the sea (Fig. 6). After an initial phase of spreading on the flat area above the village of Ginostra, the flow channelized inside the village and stopped after approximately 180 s. In this case, no data in the literature describe the flow dynamics and runout or the deposit's thickness, and a direct comparison between the results of the simulation and field evidence was impossible. In zone C, the areas impacted by the PDC and covered by the deposit were 1.5×10^5 and 0.3×10^5 m^2, respectively.

A second set of simulations was performed in the same areas. In these simulations we arbitrarily used a source deposit with double thickness compared to previous simulations, i.e. a double volume of materials involved in the flow. A paroxysm able to emplace a thickness of deposit double respect to those emplaced in 1930 possibly represents the worst scenario for the generation of a gravity-

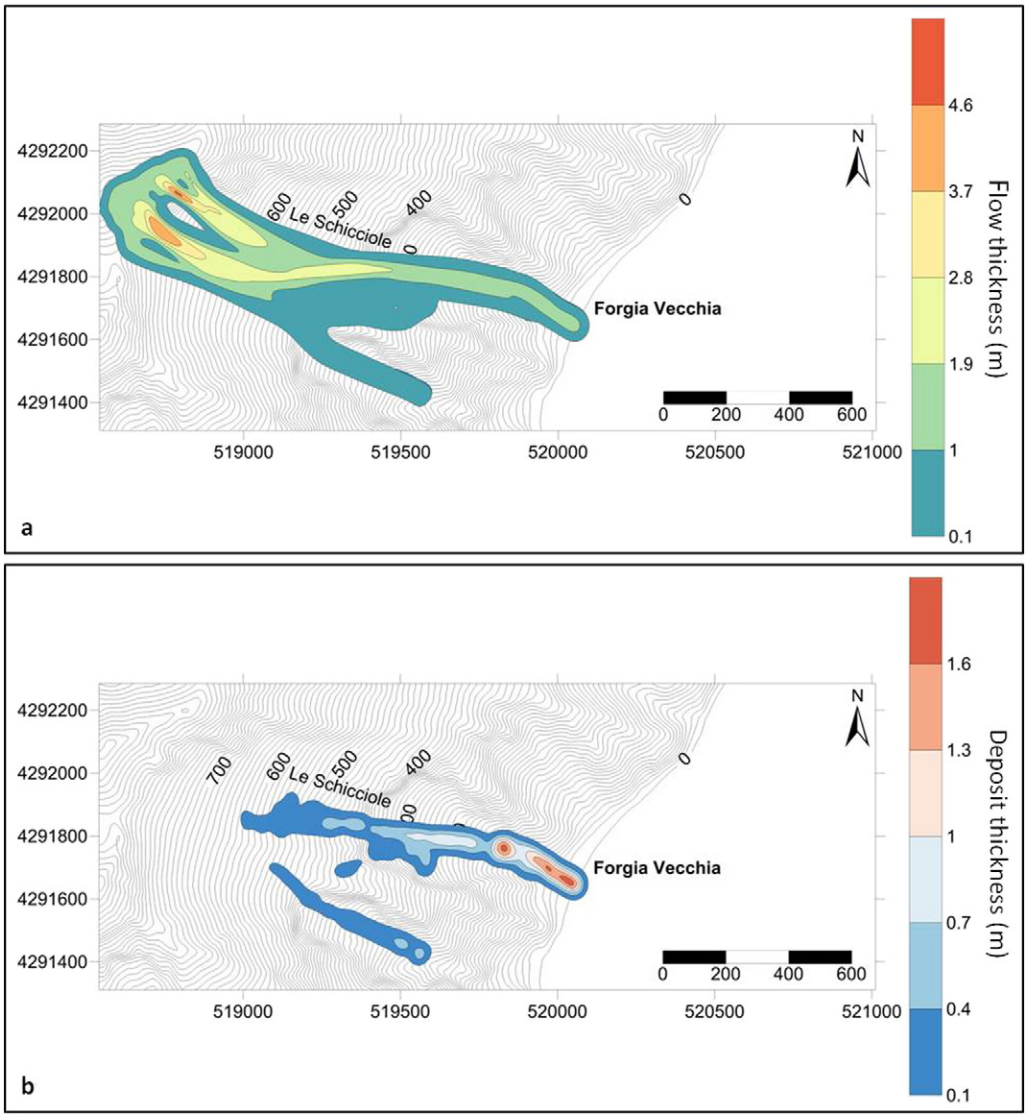

Fig. 8. Results of the DAN-3D simulation with a double input thickness: a) flow thickness and b) deposit thickness after an interval of 70 s for zone B (1944-like event).

induced PDC on the Stromboli volcano. The results show that areas impacted by double volume PDCs are larger than those affected during the first simulation. In particular, in zone A, the flow reached the Piscità locality after approximately 90 s and moved into the San Bartolo valley and adjacent valleys, depositing material along its path. The deposits were more distributed and reached a maximum thickness of 3.8 m in the Vallonazzo valley (Fig. 7). The areas impacted by the gravity-induced PDC and covered by the deposit in the simulation with the double initial thickness were 5.6×10^5 and 1.3×10^5 m^2, respectively.

The simulation in zone B showed that deposition still occurred in the "Le Schicciole" valley (Forgia Vecchia), but it also occurred in the adjacent valley. In this case, the flow front reached the coastline after approximately 70 s (Fig. 8). The areas impacted by the gravity-induced PDC and covered by the deposit in the simulation with a double initial thickness in zone B were 4.1×10^5 and 1.6×10^5 m^2, respectively.

In zone C, the flow ran through Ginostra village and reached sea level after approximately 100 s, with little lateral expansion in the urbanized areas. The deposit's maximum thickness was 4.4 m (Fig. 9). The areas impacted by the PDC and covered by the deposit according to the simulation with the double initial thickness were 1.9×10^5 and 0.5×10^5 m^2, respectively.

In the simulation with double volume, the travel times of the flows in areas A, B and C decreased by 30%, 20% and 44%, respectively. The increase in volume caused consistent increase in the flow velocity and a greater impact force of the flow.

5. Discussion

5.1. Evaluation of modelling results

The best-fit rheologies (internal friction and basal friction/turbulent) well explained the 1930 PDC deposits, especially in the upper part of the deposit, which consists of a "blocks/bombs-and-ash-flow" (Miyabuchi et al., 2006) with metre to centimetre-sized clasts supported by a poorly sorted, massive, coarse ash matrix. This deposit is similar to the small-volume block-and-ash flows and rockfalls during the Soufriere Hills eruption (Cole et al., 2002) and the small-volume PDCs during the 1975 eruption at Ngauruhoe (Nairn and Self, 1978), which were interpreted as inertial granular flows (Lube et al., 2007). The lower unit consists of tens of cm-thick, well-sorted, medium ash deposit that often exhibit parallel to low-angle cross-laminations and short alignments of centimetric lapilli, which are in good agreement with the basal friction + turbulent rheology described by the Voellmy rheological model.

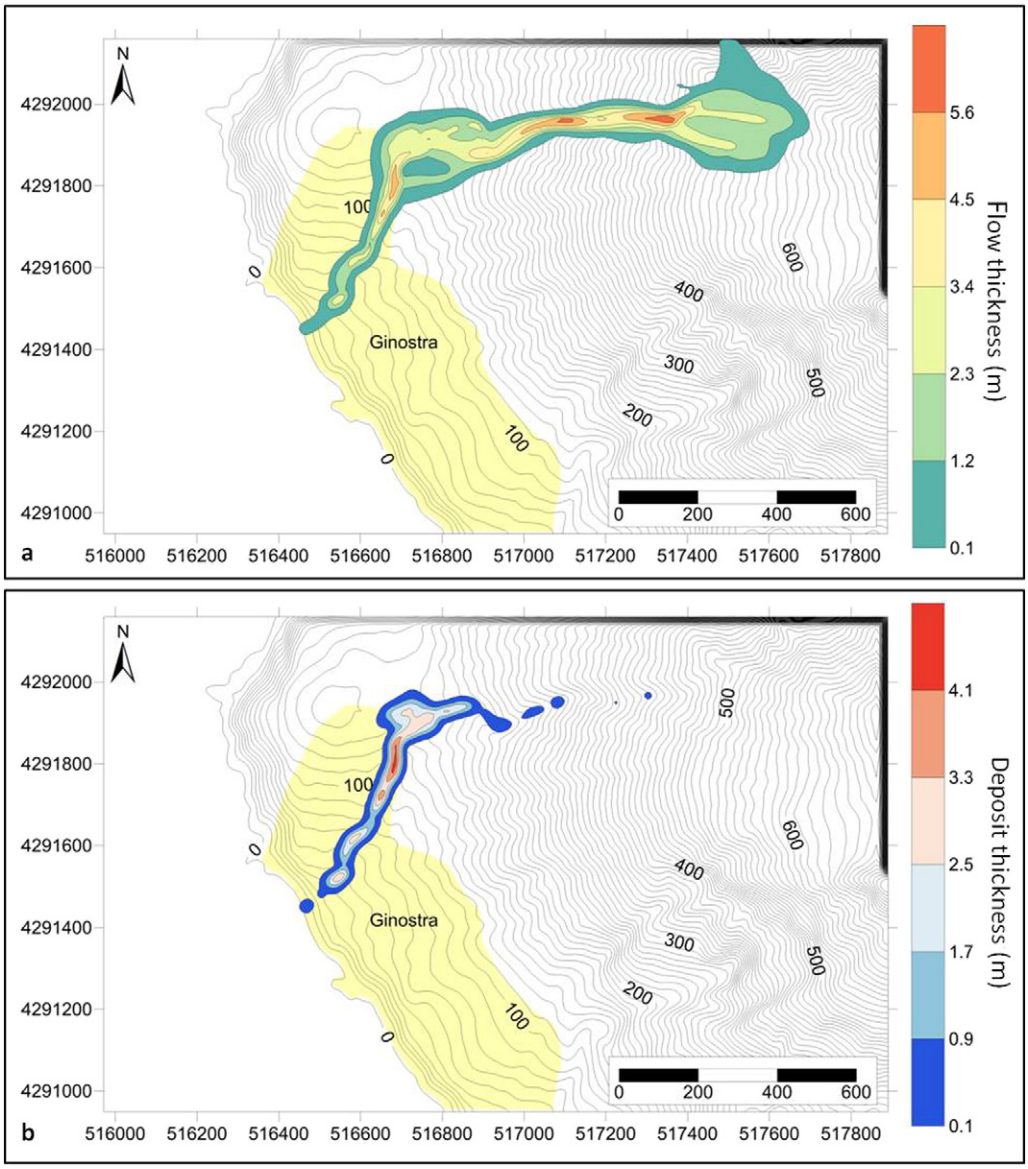

Fig. 9. Results of the DAN-3D simulation with a double input thickness: a) flow thickness and b) deposit thickness after an interval of 100 s for zone C (1906-like event).

Since the work of Hayashi and Self (1992), the assumption of a pure frictional internal rheology has been questioned based on observations of high mobility PDCs and volcanic debris avalanches. Long run-out rockfalls, debris avalanches and PDCs exhibit horizontal runout distances (L) that can be 5–20 times the vertical fall height (H), depending on the magnitude of the event. Several explanations for the scale dependence of H/L have been offered (Hungr, 1990), including mechanical fluidization (Hayashi and Self, 1992), acoustic fluidization (Melosh, 1979), and self-lubrication (Campbell, 1989). In particular, self-lubrification implies that most of the flowing mass moves over a thin, dilute layer of very agitated particles, where the energy dissipation is much smaller than in the mechanical fluidization (Hayashi and Self, 1992). Because this assumption was confirmed by the presence of a basal layer in the PDCs' deposits and the similarity of the basic physical processes that characterize dry granular avalanches and granular-flow dominated volcaniclastic flows (dense PDCs and debris avalanches), numerical codes that separate internal and basal frictions (i.e., Titan2D; Patra et al., 2005) have been increasingly used for reproducing past flows and hazard mapping (Saucedo et al., 2005; Norini et al., 2009; Widiwijayanti et al., 2009; Procter et al., 2010; Sulpizio et al., 2010b; Charbonnier and Gertisser, 2012).

DAN-3D was previously used by Morelli et al. (2010) and Sosio et al. (2012a) to constrain the flow parameters of large volcanic debris avalanches. Good results were obtained using DAN-3D for the large volume mass flows as well as the small-volume mass-flows investigated in this study. DAN-3D can be successfully used for modelling mass granular flows that are dominated by grain-collisions.

The main limitation of DAN-3D is the unchangeable internal rheology. Motion and field-based observations of dense PDCs and volcanic debris avalanche deposits have sometimes been explained using a plastic rheology (constant retarding stress or a Bingham rheology with no viscosity), in which the shear stress is constant regardless of the thickness or velocity of the flow (Dade and Huppert, 1998). Kelfoun and Druitt (2005) and Kelfoun et al. (2009, 2011) showed that the plastic rheology allows the morphology, lithology distribution and extension of volcanic debris avalanches and PDCs, even if Bingham behaviour with a minor viscous response cannot be excluded.

Charbonnier and Gertisser (2012) compared the hazard mapping of PDCs using both Titan2D (internal-basal frictional rheology) and VolcFlow (constant retarding stress). Their results evidenced the main limitation of using internal-basal frictional rheology for reproducing

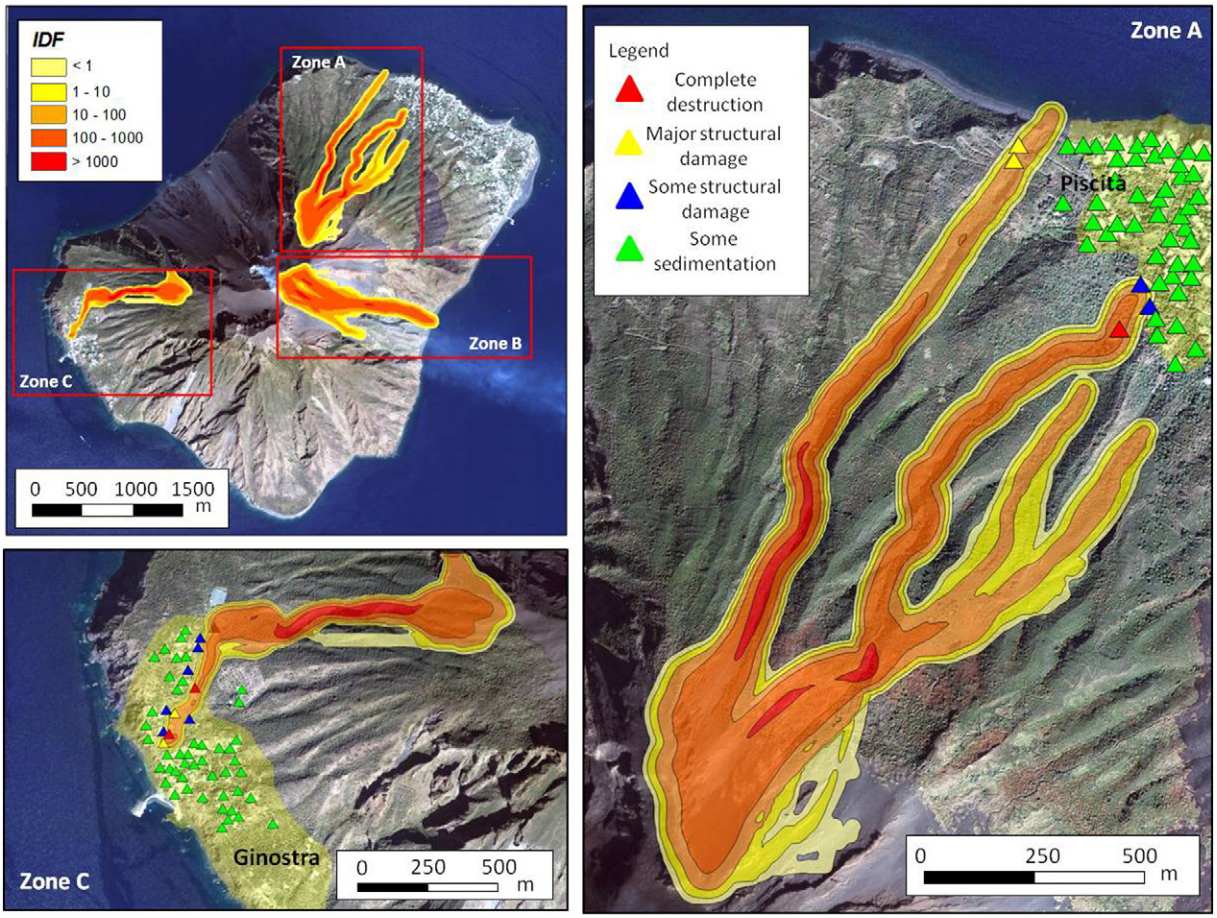

Fig. 10. Hazard evaluation for gravity-induced PDCs with the non-modified input thickness, showing the potential intensity index (I_{DF}) and the effect on buildings in the village of Stromboli, Piscità (zone A) and in the village of Ginostra (zone C).

PDC velocities and travel times. Using a constant retarding stress, the resulting simulations reproduced the morphologies and distributions of the natural deposits as well as the times of emplacement and velocities of the PDCs. Further investigations of the suitability of different internal rheologies will be performed.

5.2. Implications for hazards

The hazards at Stromboli can be related to different volcanic phenomena that include: ballistic fallout, tephra fallout, column-collapse or gravity-induced pyroclastic density currents, shockwaves, wildfires, lava flows and landslides and resultant tsunamis (Barberi et al., 1993; Rosi et al., accepted for publication). Hazardous volcanic events related to persistent activity are grouped into two categories: (1) moderately hazardous, relatively frequent events (1–2 per year), which include the fallout of heavy materials onto pathways and shelters generally used by guides and tourists and the ignition of wildfires; and (2) highly hazardous, medium frequency phenomena (a few events per century), which potentially can affect settled areas and include falling blocks that reach settled areas, PDCs, widespread wildfires and small tsunamis (Rosi et al., accepted for publication).

As mentioned, gravity-induced PDCs are usually confined to the Sciara del Fuoco depression and are produced by the remobilization of significant thicknesses of tephra on steep slopes during paroxysmal explosions, the collapse of the crater rims or by lava breaking off the sides and fronts of advancing lava flows (Pioli et al., 2008; Rosi et al., accepted for publication; Di Roberto et al., 2014; Di Traglia et al., 2014). Otherwise, small-volume gravity-induced PDCs were produced on the ESE side of the island in 1944, and on the inhabited NE part of the island in 1930 where they caused four casualties.

Hazard maps at the Stromboli volcano have been proposed by Barberi et al. (1993); Nave et al. (2010) and Rosi et al. (accepted for publication) and mainly focused on ballistic ejection and tsunamis, whereas threats associated with gravity-induced PDCs have not been examined in detail. This study represents the first contribution to a hazard assessment related to gravity-induced PDCs on Stromboli Island.

The potential damage from PDCs interacting with buildings in the villages of Stromboli and Ginostra was evaluated using the method proposed by Jakob et al. (2011), which has been applied to the evaluation of debris flow impacts. The method determines the potential building damage using an intensity index (I_{DF}; a sort of impact force):

$$I_{DF} = dv^2 \tag{4}$$

where d is the maximum expected flow depth, and v is the maximum flow velocity.

The dynamic pressure (P_{dyn}) used to estimate the potential impact of PDCs is defined as (Valentine, 1998):

$$P_{dyn} = 0.5\rho v^2 \tag{5}$$

where ρ is the flow density. Otherwise, in the dynamic pressure calculation, the particle concentrations, and the flow density are not always constrained. For the intensity index used here, only parameters derived from the modelling results were used; therefore, no other assumptions were made.

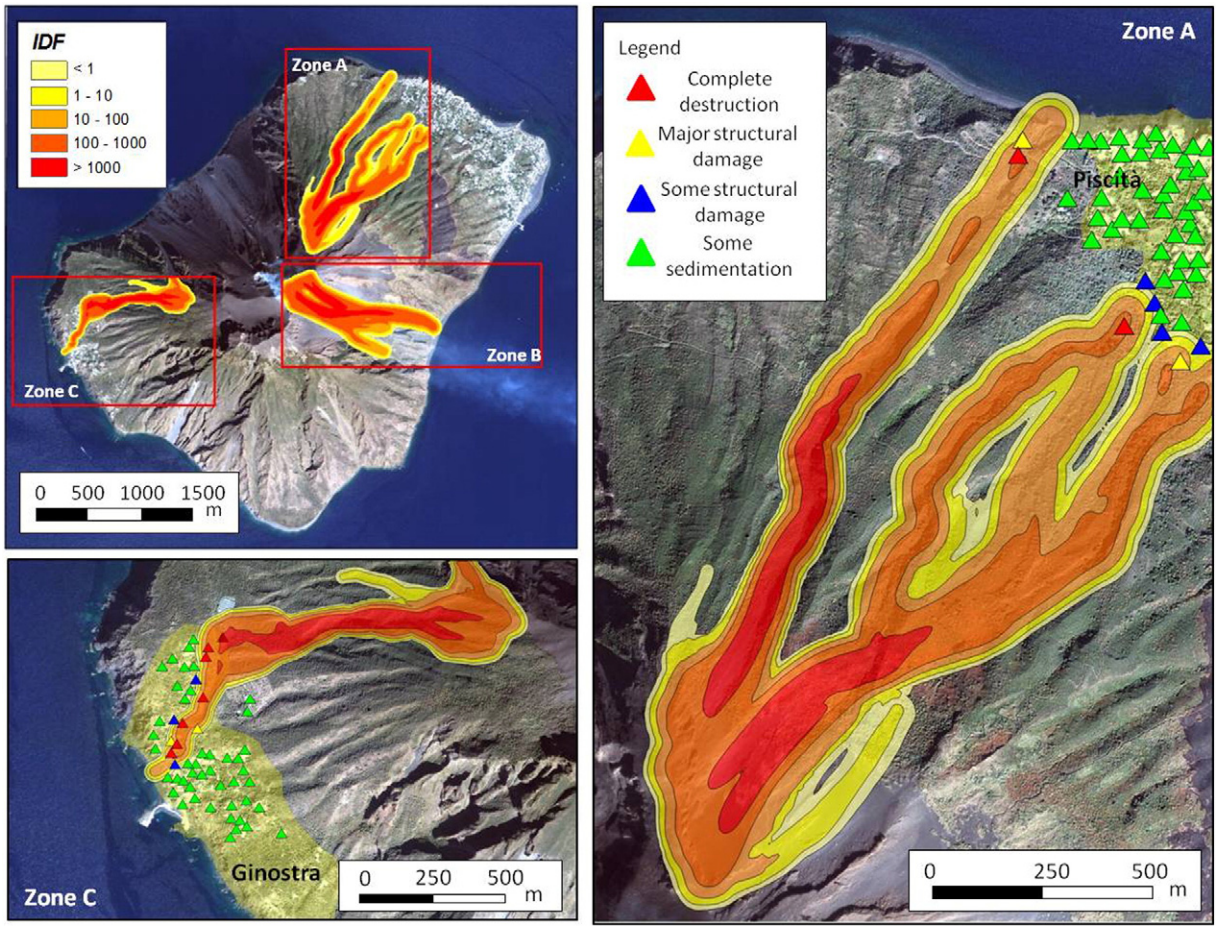

Fig. 11. Hazard evaluation for gravity-induced PDCs, with a double input thickness, showing the potential intensity index (I_{DF}) and the effect on buildings in the village of Stromboli, Piscità (zone A) and in the village of Ginostra (zone C).

The potential building damage was then estimated by classifying the calculated I_{DF} index, using the four classes proposed by Jakob et al. (2011), which range from some sedimentation (I) to complete destruction (IV). This classification is derived from back-analyses using building damage data from several case studies (Jakob et al., 2011; Corominas et al., 2014).

The modelling results in zone A were employed to evaluate the potential hazard in the Piscità zone of the village of Stromboli (Fig. 10). The simulations showed serious threats due to the flows channelled into the St. Bartolo and Vallonazzo valleys. The first flow could destroy and inflict structural damage to buildings in the village near the St. Bartolo Church, whereas the second flow could inflict major structural damage on two edifices on the Vallonazzo rims. The simulation carried out for zone C also revealed a potential hazard in the village of Ginostra (Fig. 10). The simulated path of the gravity-induced PDC, which travelled from the southwestern part of the summit area, could interact with the present-day urbanization of the village and result in some structural damage or the complete destruction of several buildings in the central part of Ginostra.

The simulations with double initial thicknesses of the sliding masses in zones A and C show that in the case of gravity-induced PDCs, the areas with higher I_{DF} would greatly increase (Fig. 11). This implies that the greater spatter accumulation in the upper part of the island is related to directed paroxysmal explosions, which could produce serious threats to the inhabited areas of the island. Zone B is free of human settlement and was not considered for this type of evaluation.

The results of the simulations with a double initial thicknesses suggest that the performance of DAN-3D for simulating events primarily depends on calibration using field-based data such as deposit distributions (locations and areas of initial piles) and volumes (single or multiple volumes), and direct observations (i.e., travel times).

6. Conclusions

Gravity-induced PDCs are well known for their ability to travel long distances, and understanding their mobility is therefore critical for evaluating areas at risk (Davies et al., 1978). Gravity-induced PDCs at the Stromboli volcano were analysed using the DAN-3D numerical code developed by McDougall and Hungr (2004) and Hungr and McDougall (2009) to reproduce the 1930 PDC extension and thickness reported in the literature. The best-fit results were obtained using a Voellmy model with a frictional coefficient $f = 0.19$ and a turbulence parameter $\xi = 1000\ \mathrm{m\ s^{-2}}$.

Hazard maps can be generated using DAN-3D. The potential damage from the gravity-induced PDCs was evaluated using the intensity index (I_{DF}) proposed by Jakob et al. (2011). The results showed that gravity-induced PDCs represent a serious threat and can potentially produce destruction and structural damage in all the inhabited areas of the Island of Stromboli. Moreover, the flow speed, number of impacted buildings, and the area with high I_{DF} values increase as the volumes of gravity-induced PDCs increase. Further investigations on the effects of this type of mass-wasting phenomena entering the sea are necessary to evaluate the tsunamigenic potential of the Stromboli gravity-induced PDCs.

DAN-3D has been used to constrain the flow parameters of large volcanic debris avalanches (Morelli et al., 2010, Sosio et al., 2012a) and the large-volume end-members of gravity-induced mass-flows in volcanic areas. The results obtained using DAN-3D for both small mass-flows

(this work) and the previously reported large mass-flows allow us to conclude that the model can be used for granular flows with various sizes, and can also be applied to other volcanoes prone to mass flows.

Acknowledgements

This work has been partially financed by the "Presidenza del Consiglio dei Ministri – Dipartimento della Protezione Civile" (Presidency of the Council of Ministers, Department of Civil Protection, Italy) in the framework of the InGrID and InGrID2015 research agreements between the Presidency of the Council of Ministers, Department of Civil Protection, and the Department of Earth Sciences, University of Firenze. This publication, however, does not reflect the position or official policies of the Department of Civil Protection. Karim Kelfoun, Jonathan Procter and an anonymous reviewer are thanked for their helpful comments, which have improved this manuscript, and we are grateful for valuable guidance from the editor, Takashi Oguchi.

References

Abbruzzese, D., 1935. Sulla catastrofica esplosione dello Stromboli dell'11 settembre 1930. Gioenia Proc. Soc. Nat. Sci 1, 1–13.

Alvarado, G.E., Soto, G.J., 2002. Pyroclastic flow generated by crater- wall collapse and outpouring of the lava pool of Arenal Volcano, Costa Rica. Bull. Volcanol. 63 (8), 557–568. http://dx.doi.org/10.1007/s00445-001-0179-9.

Apuani, T., Corazzato, C., Cancelli, A., Tibaldi, A., 2005a. Physical and mechanical properties of rock masses at Stromboli: a dataset for volcano instability evaluation. Bull. Eng. Geol. Environ. 64 (4), 419–431. http://dx.doi.org/10.1007/s10064-005-0007-0.

Apuani, T., Corazzato, C., Cancelli, A., Tibaldi, A., 2005b. Stability of a collapsing volcano (Stromboli, Italy): limit equilibrium analysis and numerical modelling. J. Volcanol. Geotherm. Res. 144 (1–4), 191–210. http://dx.doi.org/10.1016/j.jvolgeores.2004.11.028.

Aramaki, S., Takahashi, M., 1992. Geology and petrology of Asama Volcano. Field Workshop Guidebook to Asama and Kusatsu-Shirane Volcanoes, Japan. IAVCEI Commission on Explosive Volcanism.

Arrighi, S., Principe, C., Rosi, M., 2001. Violent strombolian and subplinian eruptions at Vesuvius during post-1931 activity. Bull. Volcanol. 63 (2–3), 126–150 (Doi: 10.1007ls004450100130).

Bagnold, R.A., 1954. Experiments on a gravity-free dispersion of large solid spheres in a Newtonian fluid under shear. Proceedings of the Royal Society of London A: Mathematical, Physical and Engineering Sciences. The Royal Society vol. 225(1160), pp. 49–63. http://dx.doi.org/10.1098/rspa.1954.0186.

Barberi, F., Rosi, M., Sodi, A., 1993. Volcanic hazard assessment at Stromboli based on review of historical data. Acta Vulcanol. 3, 173–187.

Behncke, B., Calvari, S., Giammanco, S., Neri, M., Pinkerton, H., 2008. Pyroclastic density currents resulting from the interaction of basaltic magma with hydrothermally altered rock: an example from the 2006 summit eruptions of Mount Etna, Italy. Bull. Volcanol. 70 (10), 1249–1268. http://dx.doi.org/10.1007/s00445-008-0200-7.

Benz, W., 1990. Smooth particle hydrodinamics: a review. In: Buchler, J.R. (Ed.), The Numerical Modelling of Nonlinear Stellar Pulsation. Kluwer Accademic, Dordrecht, pp. 269–288.

Bertagnini, A., Di Roberto, A., Pompilio, M., 2011. Paroxysmal activity at Stromboli: lessons from the past. Bull. Volcanol. 73 (9), 1229–1243. http://dx.doi.org/10.1007/s00445-011-0470-3.

Bonforte, A., Guglielmino, F., 2015. Very shallow dyke intrusion and potential slope failure imaged by ground deformation: the 28 December 2014 eruption on Mount Etna. Geophys. Res. Lett. 42 (8), 2727–2733.

Bursik, M., Patra, A., Pitman, E.B., Nichita, C., Macias, J.L., Saucedo, R., Girina, O., 2005. Advances in studies of dense volcanic granular flows. Rep. Prog. Phys. 68 (2), 271.

Calder, E.S., Cole, P.D., Dade, W., Druitt, T.H., Hoblitt, R.P., Huppert, H.E., Ritchie, L., Sparks, R.S.J., Young, S.R., 1999. Mobility of pyroclastic flows and surges at the Soufriere Hills Volcano, Montserrat. Geophys. Res. Lett. 26 (5), 537–540.

Calvari, S., Pinkerton, H., 2002. Instabilities in the summit region of Mount Etna during the 1999 eruption. Bull. Volcanol. 63, 526–535. http://dx.doi.org/10.1007/s004450100171.

Calvari, S., Intrieri, E., Di Traglia, F., Bonaccorso, A., Casagli, N., Cristaldi, A., 2016. Monitoring crater-wall collapse at active volcanoes: a study of the 12 January 2013 event at Stromboli. Bull. Volcanol. 78 (5), 1–16. http://dx.doi.org/10.1007/s00445-016-1033-4.

Campbell, C.S., 1989. Self-lubrication for long runout landslides. J. Geol. 653-665.

Charbonnier, S.J., Gertisser, R., 2012. Evaluation of geophysical mass flow models using the 2006 block-and-ash flows of Merapi Volcano, Java, Indonesia: towards a short-term hazard assessment tool. J. Volcanol. Geotherm. Res. 231, 87–108.

Chow, V.T., 1959. Open-channel Hydraulics. vol. 680. McGraw-Hill, New York.

Cole, P.D., Calder, E.S., Sparks, R.S.J., Clarke, A.B., Druitt, T.H., Young, S.R., Herd, R.A., Harford, C.L., Norton, G.E., 2002. Deposits from dome-collapse and fountain-collapse pyroclastic flows at Soufriere Hills Volcano. Montserrat. In: Druitt, T.H., Kokelaar, B.P. (Eds.), The Eruption of Soufriere Hills Volcano, Montserrat, From 1995 to 1999. Geological Society, London. Memoirs vol. 21, pp. 231–262.

Cole, P.D., Fernandez, E., Duarte, E., Duncan, A.M., 2005. Explosive activity and generation mechanisms of pyroclastic flows at Arenal volcano, Costa Rica between 1987 and 2001. Bull. Volcanol. 67 (8), 695–716. http://dx.doi.org/10.1007/s00445-004-0402-6.

Corominas, J., Van Westen, C., Frattini, P., Cascini, L., Malet, J.P., Fotopoulou, S., Catani, F., Van Den Eeckhaut, M., Mavrouli, O., Agliardi, F., Pitilakis, K., Winter, M.G., Pastor, M., Ferlisi, S., Tofani, V., Herva's, J., Smith, J.T., 2014. Recommendations for the quantitative analysis of landslide risk. Bull. Eng. Geol. Environ. 73 (2), 209–263.

Coulomb, C.A., 1776. Sur une application des regles maximis et minimis a quelques problems de statique, relatives a l'architec-ture. Acad. Sci. Paris Mem. Math. Phys. 7, 343–382.

Dade, W.B., Huppert, H.E., 1998. Long runout rockfalls. Geology 26, 803–806.

Davies, K.D., Quearry, M.W., Bonis, S.B., 1978. Glowing avalanches from the 1974 eruption of the volcano Fuego, Guatemala. Geol. Soc. Am. Bull. 89, 369–384. http://dx.doi.org/10.1130/0016-7606(1978)89<369:GAFTEO>2.0.CO;2.

De Beni, E., Behncke, B., Branca, S., Nicolosi, I., Carluccio, R., Caracciolo, F.A., Chiappini, M., 2015. The continuing story of Etna's New Southeast Crater (2012–2014): evolution and volume calculations based on field surveys and aerophotogrammetry. J. Volcanol. Geotherm. Res. 303, 175–186.

De Fino, M., La Volpe, L., Falsaperla, S., Frazzetta, G., Neri, G., Francalanci, L., Rosi, M., Sbrana, A., 1988. The Stromboli eruption of December 6, 1985–April 25, 1986: volcanological, petrological and seismological data. Rend. Soc. Ital. Mineral. Petrol. 43, 1021–1038.

Di Roberto, A., Bertagnini, A., Pompilio, M., Bisson, M., 2014. Pyroclastic density currents at Stromboli volcano (Aeolian Islands, Italy): a case study of the 1930 eruption. Bull. Volcanol. 76 (6), 1–14. http://dx.doi.org/10.1007/s00445-014-0827-5.

Di Traglia, F., Intrieri, E., Nolesini, T., Bardi, F., Del Ventisette, C., Ferrigno, F., Frangioni, S., Frodella, W., Gigli, G., Lotti, A., Tacconi Stefanelli, C., Tanteri, L., Leva, D., Casagli, N., 2014. The ground-based InSAR monitoring system at Stromboli volcano: linking changes in displacement rate and intensity of persistent volcanic activity. Bull. Volcanol. 76, 1–18. http://dx.doi.org/10.1007/s00445-013-0786-2.

Hayashi, J.N., Self, S., 1992. A comparison of pyroclastic flow and debris avalanche mobility. J. Geophys. Res. 97B6, 9063–9071.

Hazlett, R.W., Buesch, D., Anderson, J.L., Elan, R., Scandone, R., 1991. Geology, failure conditions, and implications of seismogenic avalanches of the 1944 eruption at Vesuvius, Italy. J. Volcanol. Geotherm. Res. 47 (3–4), 249–264. http://dx.doi.org/10.1016/0377-0273(91)90004-J.

Heim, A., 1932. Bergsturz und Menschenleben. Zurich, Fretz und Wasmuth. English Translation by N.A. Skermer 1989 Landslide and Human Lives. BiTech Publusher, Vancouver B.C.

Hungr, O., 1990. Mobility of rock avalanches: report of the National Research Institute of Earth Science and Disaster Prevention, Japan. 46, 11–20.

Hungr, O., 1995. A model for the runout analysis of rapid flow slides, debris flows, and avalanches. Can. Geotech. J. 32, 610–623.

Hungr, O., McDougall, S., 2009. Two numerical models for landslide dynamic analysis. Comput. Geosci. 35 (5), 978–992. http://dx.doi.org/10.1016/j.cageo.2007.12.003.

Hungr, O., Leroueil, S., Picarelli, L., 2014. The Varnes classification of landslide types, an update. Landslides 11, 167–194.

Iverson, R.M., Denlinger, R.P., 2001. Flow of variably fluidized granular masses across three-dimensional terrain: 1. Coulomb mixture theory. J. Geophys. Res. Solid Earth 106 (B1), 537–552. http://dx.doi.org/10.1029/2000JB900329.

Jakob, M., Stein, D., Ulmi, M., 2011. Vulnerability of buildings to debris flow impact. Nat. Hazards 60, 241–261. http://dx.doi.org/10.1007/s11069-011-0007-2.

Kelfoun, K., 2011. Suitability of simple rheological laws for the numerical simulation of dense pyroclastic flows and long-runout volcanic avalanches. J. Geophys. Res. Solid Earth 116 (B8).

Kelfoun, K., Druitt, T.H., 2005. Numerical modeling of the emplacement of Socompa rock avalanche, Chile. J. Geophys. Res. Solid Earth 110 (B12), 1978–2012.

Kelfoun, K., Samaniego, P., Palacios, P., Barba, D., 2009. Testing the suitability of frictional behaviour for pyroclastic flow simulation by comparison with a well-constrained eruption at Tungurahua volcano (Ecuador). Bull. Volcanol. 71, 1057–1075.

Kelfoun, K., Giachetti, T., Labazuy, P., 2010. Landslide-generated tsunamis at Réunion Island. J. Geophys. Res. Earth Surf. 115 (F4). http://dx.doi.org/10.1029/2009JF001381.

Lube, G., Cronin, S.J., Platz, T., Freundt, A., Procter, J.N., Henderson, C., Sheridan, M.F., 2007. Flow and deposition of pyroclastic granular flows: a type example from the 1975 Ngauruhoe eruption, New Zealand. J. Volcanol. Geotherm. Res. 161 (3), 165–186. http://dx.doi.org/10.1016/j.jvolgeores.2006.12.003.

McDougall, S., Hungr, O., 2003. Objectives for the development of an integrated three-dimensional continuum model for the analysis of landslide runout. In: Rickenmann, D., Chen, C.L. (Eds.), Proceedings of the 3rd Inter-national Conference on Debris-flow Hazards Mitigation: Mechanics, Prediction and Assessment. Millpress, Rotterdam, The Netherlands, pp. 481–490.

McDougall, S., Hungr, O., 2004. A model for the analysis of rapid landslide motion across three-dimensional terrain. Can. Geotech. J. 41 (6), 1084–1097. http://dx.doi.org/10.1139/T04-052.

Melosh, H.J., 1979. Acoustic fluidization: a new geologic process? J. Geophys. Res. Solid Earth 84 (B13), 7513–7520. http://dx.doi.org/10.1029/JB084iB13p07513.

Miyabuchi, Y., Ikebe, S.I., Watanabe, K., 2005. The July 10, 2003 and the January 14, 2004 ash emissions from a hot water pool of the Nakadake crater, Aso volcano, Japan. Bull. Volcanol. Soc. Jpn. 50, 227–241.

Miyabuchi, Y., Watanabe, K., Egawa, Y., 2006. Bomb-rich basaltic pyroclastic flow deposit from Nakadake, Aso Volcano, southwestern Japan. J. Volcanol. Geotherm. Res. 155 (1–2), 90–103. http://dx.doi.org/10.1016/j.jvolgeores.2006.02.007.

Monaghan, J.J., 1989. On the problem of penetration in particle methods. J. Comput. Phys. 82, 1–15.

Monaghan, J.J., 1992. Smoothed particle hydrodynamics. Annu. Rev. Astron. Astrophys. 30, 543–574.

Morelli, S., Garduño Monroi, V.H., Gigli, G., Falorni, G., Arreygue Rocha, E., Casagli, N., 2010. The Tancitaro debris avalanche: characterization, propagation and modelling.

J. Volcanol. Geotherm. Res. 193, 93–105. http://dx.doi.org/10.1016/j.jvolgeores.2010.03.008.
Nairn, I.A., Self, S., 1978. Explosive eruptions and pyroclastic avalanches from Ngauruhoe in February 1975. J. Volcanol. Geotherm. Res. 3 (1–2), 39–60.
Nave, R., Ricci, T., Barberi, F., Davis, M., Isaia, R., 2010. Perception of volcanic risk in Italy: Etn, Vesuvio and Campi Flegrei. Cities on Volcanoes 6 Conference.
Nolesini, T., Di Traglia, F., Del Ventisette, C., Moretti, S., Casagli, N., 2013. Deformations and slope instability on Stromboli volcano: integration of GBInSAR data and analog modelling. Geomorphology 180, 242–254.
Norini, G., De Beni, E., Andronico, D., Polacci, M., Burton, M., Zucca, F., 2009. The 16 November 2006 flank collapse of the south-east crater at Mount Etna, Italy: study of the deposit and hazard assessment. J. Geophys. Res. Solid Earth 114 (B2) 1978–2012.
Patra, A.K., Bauer, A.C., Nichita, C.C., EPitman, E.B., Sheridan, M.F., Bursik, M., Rupp, B., Webber, A., Stinton, A.J., Namikawa, L.M., Renschler, C.S., 2005. Parallel adaptive numerical simulation of dry avalanches over natural terrain. J. Volcanol. Geotherm. Res. 139 (1–2), 89–102. http://dx.doi.org/10.1007/s11069-009-9440-x.
Pioli, L., Rosi, M., Calvari, S., Spampinato, L., Renzulli, A., Di Roberto, A., 2008. The Eruptive Activity of 28 and 29 December 2002, the Stromboli Volcano an Integrated Study of the 2002–2003 Eruption. American Geophysical Union, Washington, USA, pp. 105–115 http://dx.doi.org/10.1029/182GM10.
Pistolesi, M., Rosi, M., Pioli, L., Renzulli, A., Bertagnini, A., Andronico, D., 2008. The paroxysmal event and its deposits. In: Calvari, S., Inguaggiato, S., Puglisi, G., Ripepe, M., Rosi, M. (Eds.), The Stromboli Volcano an Integrated Study of the 2002–2003 Eruption. American Geophysical Union, Washington, USA, pp. 317–330.
Ponte, G., 1948. Attività straordinaria dello Stromboli. Ann. Geophys. 1 (2), 200–202.
Procter, J.N., Cronin, S.J., Platz, T., Patra, A., Dalbey, K., Sheridan, M., Neall, V., 2010. Mapping block-and-ash flow hazards based on Titan 2D simulations: a case study from Mt. Taranaki, NZ. Nat. Hazards 53 (3), 483–501.
Riccò, A., 1907. Sull'attività dello Stromboli dal 1891 in poi. Boll. Soc. Sismol. Ital. 12, 205.
Rittmann, A., 1931. Der Ausbruch des Stromboli am 11. September 1930. Z Vulkanologie 14, 47–77.
Rosi, M., Bertagnini, A., Landi, P., 2000. Onset of the persistent activity at Stromboli volcano (Italy). Bull. Volcanol. 62 (4–5), 294–300.
Rosi, M., Bertagnini, A., Harris, A.J.L., Pioli, L., Pistolesi, M., Ripepe, M., 2006. A case history of paroxysmal explosion at Stromboli: timing and dynamics of the April 5, 2003 event. Earth Planet. Sci. Lett. 243 (3), 594–606. http://dx.doi.org/10.1016/j.epsl.2006.01.035.
Rosi, M., Pistolesi, M., Bertagnini, A., Landi, P., Pompilio, M., Di Roberto, A., 2013. Stromboli Volcano, Aeolian Islands (Italy): present eruptive activity and hazard. In: Lucchi, F., Peccerillo, A., Keller, J., Tranne, C.A., Rossi, P.L. (Eds.), Geol. Soc. London Mem., Geology of the Aeolian Islands (Italy) (accepted for publication).
Saucedo, R., Macıas, J.L., Sheridan, M.F., Bursik, M.I., Komorowski, J.C., 2005. Modelling of pyroclastic flows of Colima Volcano, Mexico: implications for hazard assessment. J. Volcanol. Geotherm. Res. 139, 103–115. http://dx.doi.org/10.1016/j.jvolgeores.2004.06.019.
Savage, S.B., Hutter, K., 1989. The motion of a finite mass of granular material down a rough incline. J. Fluid Mech. 199, 177–215.
Sosio, R., Crosta, G.B., Hungr, O., 2008. Complete dynamic modelling calibration for the Thurwieser rock avalanche (Italian Central Alps). Eng. Geol. 100, 11–26. http://dx.doi.org/10.1016/j.enggeo.2008.02.012.
Sosio, R., Crosta, G.B., Hungr, O., 2012a. Numerical modelling of debris avalanche propagation from collapse of volcanic edifices. Landslides 9, 315–334. http://dx.doi.org/10.1007/s10346-011-0302-8.
Sosio, R., Crosta, G.B., Chen, J.H., Hungr, O., 2012b. Modelling rock avalanche propagation onto glaciers. Quat. Sci. Rev. 47, 23–40.
Sulpizio, R., Bonasia, R., Dellino, P., Mele, D., Di Vito, M.A., La Volpe, L., 2010a. The Pomici di Avellino eruption of Somma–Vesuvius (3.9 ka BP). Part II: sedimentology and physical volcanology of pyroclastic density current deposits. Bull. Volcanol. 72 (5), 559–577. http://dx.doi.org/10.1007/s00445-009-0340-4.
Sulpizio, R., Capra, L., Sarocchi, D., Saucedo, R., Gavilanes-Ruiz, J.C., Varley, N.R., 2010b. Predicting the block-and-ash flow inundation areas at Volcán de Colima (Colima, Mexico) based on the present day (February 2010) status. J. Volcanol. Geotherm. Res. 193 (1), 49–66.
Takahashi, T., Tsujimoto, H., 2000. A mechanical model for Merapi-type pyroclastic flow. J. Volcanol. Geotherm. Res. 98 (1), 91–115. http://dx.doi.org/10.1016/S0377-0273(99)00193-6.
Ui, T., Matsuwo, N., Sumita, M., Fujinawa, A., 1999. Generation of block-and-ash flows during the 1990–1995 eruption of Unzen Volcano, Japan. J. Volcanol. Geotherm. Res. 89, 123–137. http://dx.doi.org/10.1016/S0377-0273(98)00128-0.
Valentine, G.A., 1998. Damage to structures by pyroclastic flows and surges, inferred from nuclear weapons effects. J. Volcanol. Geotherm. Res. 87 (1), 117–140.
Widiwijayanti, C., Voight, B., Hidayat, D., Schilling, S.P., 2009. Objective rapid delineation of areas at risk from block-and-ash pyroclastic flows and surges. Bull. Volcanol. 71 (6), 687–703. http://dx.doi.org/10.1007/s00445-008-0254-6.
Yamamoto, T., Takada, A., Ishizuka, Y., Miyaji, N., Tajima, Y., 2005. Basaltic pyroclastic flows of Fuji volcano, Japan: characteristics of the deposits and their origin. Bull. Volcanol. 67 (7), 622–633. http://dx.doi.org/10.1007/s00445-004-0398-y.
Yasui, M., Koyaguchi, T., 2004. Sequence and eruptive style of the 1783 eruption of Asama Volcano, central Japan: a case study of an andesitic explosive eruption generating fountain-fed lava flow, pumice fall, scoria flow and forming a cone. Bull. Volcanol. 66 (3), 243–262.

Landslides and Engineered Slopes. Experience, Theory and Practice – Aversa et al. (Eds)

Analogue and numerical modeling of the Stromboli hot avalanches

S. Morelli, T. Salvatici, T. Nolesini, F. Di Traglia, C. Del Ventisette & N. Casagli
Dipartimento di Scienze della Terra, Università di Firenze, Firenze, Italy

A. Di Roberto, M. Bisson, M. Pompilio & A. Bertagnini
Istituto Nazionale di Geofisica e Vulcanologia, Sezione di Pisa, Pisa, Italy

ABSTRACT: Hot avalanches at Stromboli volcano were investigated by means analogue and numerical modeling. Analogue experiments were performed with the aim of understanding the effects of different trigger mechanisms of slope instability while the runout of Stromboli hot rock avalanches was modeled using two numerical codes DAN-W (2D version) and DAN-3D. The accumulation experiments demonstrate that the accretion of a portion of the slope alters the flank stability and triggers small landslides. Numerical models were able to reproduce the extension and the order of magnitude of the thickness of the hot avalanches reported in the literature. The best results of DAN-3D and DAN-W models on the 1930 hot avalanche were obtained using a Voellmy model with a frictional coefficient f = 0.19 and a turbulence parameter ξ = 1000 m/s.. The obtained results allowed to produce a hazard evaluation for the explosive-related, mass-wasting phenomena in the inhabited areas of Stromboli Island.

1 INTRODUCTION

Hot avalanches deposits, originated from the sliding of the crater rim or the gravitational instabilities of material accumulated during explosive eruptions, are widely identified on the flanks of several volcanoes worldwide (Davies et al., 1978; Nairn and Self, 1978; Hazlett et al., 1991; Arrighi et al., 2001; Cole et al., 2005; Yamamoto et al. 2005; Behncke et al., 2008; Di Roberto et al. 2014; Di Traglia et al., 2014). Such kind of events usually occurs on edifices fed by mafic to intermediate magmas and have small volumes (10^4–10^7 m^3) but emplace at very high temperatures and can travel far from the source at very high speed. These features make them potentially dangerous for communities that live and concentrate their socio-economic activities close to the volcanoes and for the high number of tourists attending them each year for recreational activities.

Analogue experiments were conducted with the aim to understand the triggering mechanism and the evolution of landslides along the Sciara del Fuoco, a horse-sharpened depression on the northwest flank of the Stromboli volcano. To simulate the brittle behavior of the volcanic material along the Sciara del Fuoco slope we used analogue materials reported in Nolesini et al. (2013): i) quartz Fontainebleau's sand; ii) uniform sand; iii) Sciara del Fuoco volcaniclastic material; iv) silty-sand. The analogue models reveal that the accumulation of material in the summit part of the slope reproduced the effect of spatter or lava loading on the volcano flanks and were able to induce landslides.

With the purpose of testing the suitability of landslide numerical models in simulating and assessing the hazard related to hot avalanches, the results of the back analysis of three events of avalanches occurred at Stromboli volcano are also presented. They were performed using 2D and 3D numerical codes called DAN-W and DAN-3D respectively (Hungr 1995, McDougall and Hungr, 2004; Hungr and McDougall, 2009). In this work, the bidimensional simulation was joined to a more complex one (3D) in order to test if also the simplest mathematical approach maintains high levels of reliability in case of strictly channeled events like those investigated. As case studies, three flows occurred on 1906, 1930 and 1944 were selected. Back analysis was undertaken through the use of DAN-3D and DAN-W codes, considering the 1930 event as test case. In fact, for this event, detailed descriptions are available from many authors. Rittmann (1931) and Abbruzzese (1935) gathered many data shortly after the eruption and in particular they deduced the total runout distance, velocity, thickness and distribution of deposits. More recently, Di Roberto et al. (2014) provide additional data on flow dynamics and distribution of deposits.

The simulations were able to reproduce the extension and the order of magnitude of the deposit thickness of events reported in the literature (Rittmann, 1931; Abbruzzese, 1935; Di Roberto et al., 2014). The outcomes were also used

to assess whether and how the inhabited areas of Stromboli (Stromboli and Ginostra villages) can be struck if one of these events would repeat in the future with similar dynamics of the historical episodes.

2 STUDY AREA: THE STROMBOLI VOLCANO

Stromboli is a volcanic island of the Aeolian archipelago (Tyrrhenian Sea southern Italy) (Fig. 1). The island is the subaerial part of volcanic edifice, characterized by a rather regular conical shape, rising up to 924 m above sea level (a.s.l.) from a base that lies between 2300 m and 1300 m of water depth. The volcanic activity of Stromboli has been continuous since the 8th century AD and mainly consists in low energy intermittent explosions (Strombolian activity) occasionally interrupted by effusive events and by violent explosions regularly called paroxysms (Barberi et al., 1993; Rosi et al., 2013). The active vents are located in the crater terrace, at about 750 m in the upper part of the Sciara del Fuoco (SdF), a horseshoe-shaped depression that occupies the NW flank of the volcano (Fig. 1). At Stromboli volcano, the formation of mass flows of hot pyroclasts have been observed and reported several times. These occur directly as a result of the explosive and effusive volcanic activity and usually spread within the SdF thus not representing a serious menace for the population of Stromboli (Barberi et al., 1993; Rosi et al., 2013). However, at least in 1930, 1944 and possibly in 1906, the hot avalanches occurred outside the SdF and in the first two cases they reached the coastline. In particular, the 1930 event reached the village of Stromboli on the NE part of the island causing extensive damages and four fatalities (Rittmann, 1931).

Few data are reported on the hot avalanches occurred on 15 July 1906 and 20 August 1944 and the main information can be obtained by the writing of Riccò (1907) and Ponte (1948) respectively. On the other hand, the best-described event is undoubtedly that occurred during the 1930 paroxysm thanks to some distinguished post-event studies supported by more recent investigations on deposits. This hot avalanche was triggered by the sliding of an approximately 1 m-thick deposit, corresponding to an estimated volume of at least 75,000 m^3, and consisting of meter-sized spatter, decimeter-sized bombs, lapilli, and ash (Rittmann, 1931; Abbruzzese, 1935). This deposit accumulated over an area of more than 60,000 m^2 on the steep cliff side of Chiappe Lisce about one hour before the landslide event (Rittmann, 1931) during an extremely violent paroxysm (Bertagnini et al., 2011). The description of the 1930 deposits,

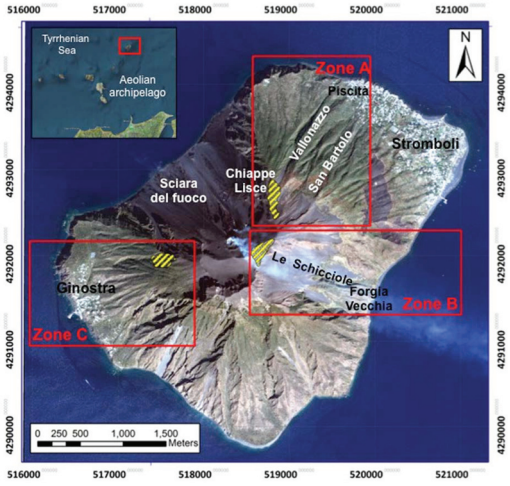

Figure 1. Study area: Stromboli volcano with the main toponyms (by QuickBird Satellite Sensor). The three red rectangular areas cover the volcano sector involved in the event of 1930 (zone A), 1944 (zone B) and 1906 (zone C). These zones are used for numerical modeling with DAN-3D. In yellow the three events source areas.

including grain-size and nature of main components is reported by Di Roberto et al. (2014).

3 MATERIALS AND METHODS

3.1 *Analogue modeling*

Analogue experiments were performed with the aim of understanding the effects of the triggering mechanism of slope instability and constraining the geometry of the induced deformations. Experiments were conducted to consider the accumulation of material on the slope. For this study 20 different models were completed using different materials (Nolesini et al., 2013). Much of the Sciara del Fuoco is inaccessible due to continuous ejection of products from the frequent explosions and frequent falling rocks. The samples taken in the marginal position of Sciara del Fuoco are considered representative of the deep position.

Data on grain size and the structure of volcaniclastic materials of Stromboli volcano are reported in Apuani et al. (2005), Rotonda et al. (2009) and Nolesini et al. (2013). To simulate the brittle behavior of Sciara del Fuoco material, four different analogue materials reported in Nolesini et al. (2013) were used: i) quartz Fontainebleau's sand; ii) uniform sand; iii) Sciara del Fuoco volcaniclastic material; iv) silty-sand.

Nolesini et al. (2013) observed that the Stromboli Sciara del Fuoco material is quite different

from the other types of analyzed granular materials, due to the large heterogeneity and, specifically, to the presence of fine material, resulting in a high internal friction angle of the Stromboli material. The brittle behavior of rocks can be expressed by the Mohr-Coulomb criterion of failure ($\tau=\mu\sigma(1-\lambda)+c$; where τ and σ are the shear and normal stress on the sliding surface, μ is the internal friction coefficient, λ is the Hubbert—Rubey coefficient of fluid pressure and c is the cohesion). Since cohesion has the dimensions of a stress, it should share a similar scaling ratio. In the same way the internal friction coefficient must have similar values both in models and in nature. The models were suitably scaled such that 1 cm in the model represents 100 m in nature, involving a geometrical length ratio

$l^*=lmod=lnat=10^{-4}$.

Considering the length ratio, the gravity ratio ($g^* = 1$; the models where performed in the natural gravity field) and the density ratio $\rho^* \approx 0.5$, the stress σ^* acting on the model is 5×10^{-5} Pa. The Plexiglas tank is $25 \times 30 \times 50$ cm, and these dimensions limit the boundary effects due to confinement. The modeling material was sieved on a slope with an inclination that varied between 45° and 25°. During the deposition of the material, a colorful reference level was used as a marker, and a final grid 5×5 cm was put on the last sand layer to better observe the deformations. The tank was then situated in a horizontal position, and the experiment was started. All of the models were developed in the Earth Science Department Laboratory of the University of Firenze.

3.2 *Numerical modeling*

Considering the sliding processes associated to this kind of event, the motion of Stromboli hot avalanches was modeled using DAN-W (for two-dimensional analyses) and DAN-3D (for three-dimensional analyses) numerical models (McDougall & Hungr, 2004; Hungr & McDougall, 2009), that are commonly used for the simulation of volcanic debris avalanches (Morelli et al., 2010; Sosio et al., 2012b) and other landslides in which grain collisions are dominant factors (McDougall & Hungr, 2004; Sosio et al., 2008; Hungr & McDougall, 2009; Sosio et al., 2012a). These numerical codes both assume a simplified approach for the simulation of mass flow motion that is considered an "equivalent-fluid" (McDougall & Hungr, 2004; Hungr & McDougall, 2009). DAN-W and DAN-3D use the Lagrangian numerical method to solve the depth-averaged St. Venant equations (Monaghan, 1989; 1992; Benz, 1990). The momentum equations evaluate an internal frictional rheology, governed by an internal friction angle and by a basal rheology, chosen by the modeler according to one of the eight rheological kernel provided by the numerical code (Hungr, 1995). In DAN-3D and in DAN-W it is possible to use eight different rheological functions: frictional, plastic, Newtonian, turbulent, Voellmy, Bingham, Coulomb frictional, and power law.

Simulations were performed on three areas roughly corresponding to those affected by the hot avalanches of 1930 (zone A), 1944 (zone B), and the area possibly involved in the 1906 event (zone C). The zone A was used as calibration area, since the data about the deposits distribution (areal spread, thickness and travel distance), the velocity of the flow and the temporal duration are available from previous studies (Rittmann, 1931; Abbruzzese, 1935; Di Roberto et al., 2014).

In performing these analyses, all the materials involved in 1906 and 1944 hot avalanches were assumed similar to those of 1930 (Bertagnini et al., 2011). Subsequently, the parameters obtained for 1930 event (zone A) were used to calibrate the model by back analysis and to find the input rheological parameters used later in the zone B and C. The main characteristics of the three considered events are listed in Table 1.

Three input files are necessary to run the simulation: i) path topography; ii) source of landslide depth and iii) erosion depth. The first file is the landscape which includes the total sliding surface (obtained in a post-event scenery) and it is represented by a Digital Elevation Model (DEM) at very high resolution (50 cm cell size). This DEM was obtained elaborating the 3D data acquired during the airborne laser scanning survey carried out in 2012 by the BLOM company (www.blomasa.com) using a Leica ADS80 device (vertical accuracy ± 10/20 cm and horizontal accuracy ± 25 cm).

Table 1. Main characteristics of the three studied events: zone A, B, and C.

	Zone A	Zone B	Zone C
Eruption date	11/09/*1930*	15/06/*1944* (doubtful day)	20/08/*1906*
Interested area	NE flank	WSW flank	ESE flank
Source Elevation (m a.s.l.)	790	920	600
Volume source (m^3)	42000	35000	33000
Travel distance (km)	1.6	1.5	-
Thickness (m)	0.1-4	0.1-0.6	-
Velocity (m/s)	15-20	-	-

The source depth file corresponds to the thickness of the sliding mass before the collapse. This file, stored as grid, was defined considering the area where the accumulation of spatter and fall-out deposits was observed during the 1930 paroxysm (Rittmann, 1931; Bertagnini et al., 2011; Di Roberto et al., 2014) or argued for the 1906 and 1944 eruptions (e.g. considering where topographies exceeds 29°; for more details see Apuani et al., 2005). From the source data file, the software computes the area covered by the critical mass and the volume of slide material contained in each cell of the global reference grid. The initial value of 1 m for the thickness of the sliding material was established according to the descriptions of Rittmann (1931) about the material accumulated on the summit of the volcano and involved in the collapse.

The erosion depth file distinguishes the entrainment area and it is stored as grid. For our simulation the erosion rate and the entrainment ratio are both zero and the volume of the landslide does not change during the runout. This is clearly suggested by the 1930 hot avalanche deposits observed on the field by Di Roberto et al. (2014).

For the elaborations constrains imposed by DAN-3D all grids were resampled to spatial resolution of 5 meters before inserting them in the calculation code. The preparation of grids used as input data for DAN-3D was done by means of ESRI ArcGIS(TM) and Golden Software SURFER(TM).

The duration of a simulation depends on three main parameters: a) the size of the global reference grid, b) the length of the time step and c) the number of the used particles. DAN-3D allows the user to change the smoothing length constant and the number of particles (McDougall, 2006). For our simulations, 2000 particles and smoothing length constant B = 4 were used. Since this modeling software does not implement a routine for the automatic stop, the simulation was suspended in Zone A and B when the flow reached the coastline. In the case in which the flow never reached the sea level (Zone C) the simulation was manually blocked 180 seconds after that the flow stopped. Two input files are necessary for the two-dimensional processing: path and top. The path file is represented by the topographic profile of the slope along which the mass moves, and the top file defines the thickness of the source area along the selected longitudinal section profile (initial sliding mass geometry). The width of the landslide can be also specified only for the pseudo-three-dimensional visualization. The hot avalanche initial mass was split in 50 equally-spaced boundary blocks with constant volume and shape factor 1 which indicates a rectangular cross-section of the channel in which the material moved. In DAN-W the simulation automatically stops when the flow arrives at the end of the established path profile or when the mass stops. The topographic and geometrical input data (path and top files) were directly extrapolated by the results obtained with DAN-3D. In fact, the 2D analysis was performed along profiles representing the lines connecting the source regions with the most distal extension of the deposits previously modeled with the 3D tool. For the zone A two separate models were performed along the two principal line of flow described by Abruzzese (1935): one in Vallonazzo valley and the other in San Bartolo valley. Through the results of DAN-3D it was possible to calculate the volumes channeled in the two valleys: 26000 m^3 and 16000 m^3 respectively. While for the zones B and C only one line profile was chosen for each case with a calculated slide volume of 29000 m^3 and 34000 m^3 respectively.

4 RESULTS

4.1 *Analogue models*

In total, 20 different experiments were conducted. All models were constructed in a series of progressive steps, starting from a simplified model and moving toward a more realistic representation. The rheological properties of the sand were tested at different slope angles over the range of 35° to 40°, and the best angle to approximate the Sciara del Fuoco condition, according to the data, is 35° (Fig. 2). An increase in the thickness of the deposited material always leads to frequent landslides. The material inserted in the model breaks the slope stability, generates a complex system of landslides and increases the volume of material involved in the sliding processes. The succession of phenomena is derived from instability in the lower part of the slope where landslide material progressively accumulates.

This lower part achieves a state of equilibrium each time until the arrival of new material from the upper portion, which determines a remobilization of the previous material in a larger landslide (Fig. 2). The addition of material to the slope, creates a greater tension at a single point, changes the slope equilibrium and is the origin of the material sliding down the slope.Accumulation corresponds to the continuous deposition of material (spatter or lava) and to an increase in the thickness of the slope.

The analogue models reveal that the internal friction angles alone are not able to generate the slope instability. The accumulation experiments demonstrate that the accretion of a portion of

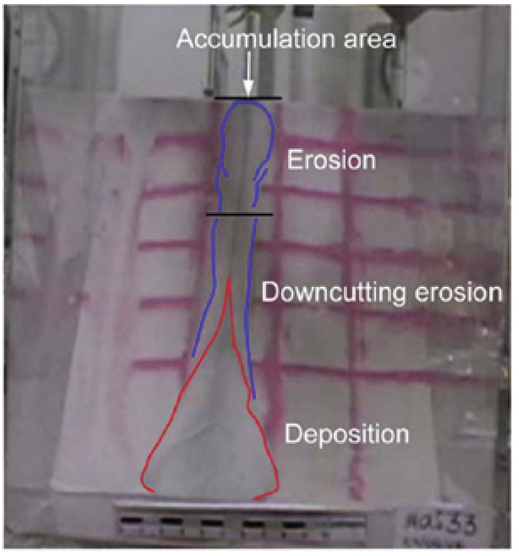

Figure 2. Initial model set-up. Each series is built into a plexiglass box on an inclined plane. The inclination of the plane change between 25° and 45°. The material, mobilized by the first landslide movement, remains in the lower part of the model and creates a potentially unstable area which generates the second landslide movement. Afterward, a series of progressive landslides were triggered and were all localized approximately 10 cm up the slope (from Nolesini et al., 2013).

the slope alters the flank instability and triggers small landslides. Breaking the equilibrium that exists in the slope forms a successive series of landslides that propagate upwards along the slope.

4.2 *Numerical models*

In the back analysis with DAN-3D relative to the 1930 hot avalanche the main rheological parameters within each rheological function were varied using a trial-and-error procedure. For example, we started varying the basal friction angle for the Frictional rheology and the frictional coefficient and turbulence parameter in the Voellmy rheology (1955). This was executed in order to obtain values of runout, velocity and duration of the flow matching as much as possible those deriving from the literature and from the more recent studies. The best results for the simulation of the 1930 hot avalanche (Figs. 3a, b) were obtained using a Voellmy rheological model with a frictional coefficient $f = 0.19$ and a turbulence parameter $\xi = 1000$ m/s. The flow length is the main parameter used during the back analysis to constrain the model Historical accounts and field data revealed that during the 1930 event incandescent flows moved into the S. Bartolo and Piscità (Vallonazzo) valleys. The first one stopped few meters from the church of S. Bartolo, while the second one had a major impulse and arrived at the coastline (Abbruzzese, 1935; Rittmann, 1931; Di Roberto et al., 2014).

The simulation was able to reproduce the behavior of these two main flows with a first event along the Vallonazzo valley reaching the sea level at the urbanized area of Piscità after 135 seconds and a second one in the San Bartolo valley stopping close to the San Bartolo church, after about 120 seconds. The model successfully simulated also the 1930 event deposits' thicknesses, matching the order of magnitude of those measured by Di Roberto et al. (2014) during their field survey. In the San Bartolo valley, at about 780 m a.s.l. the measured thickness is about 4.5 m, versus a simulated thickness of 1.6 m. In the NE rim of Vallonazzo valley at about 300 m a.s.l, the measured and simulated thicknesses are instead fully comparable and attain 30–40 cm, whereas close to the outlet of Vallonazzo valley, the measured thickness is about 100 cm and the simulated thickness is 60 cm. The areas impacted by the avalanche and covered by the deposit are, for both impluviums as a whole, 3.6×10^5 m^2 and 0.8×10^5 m^2, respectively. The outcomes of DAN-W code along the considered sections of this area show a good correspondence with the 3D simulation (Fig. 3).

The rheological parameters obtained with this procedure for 1930 hot avalanche were then used in the simulation of the events occurred in zones B (1944) and C (1906). The simulation results in the zone B show that the flow moves in "Le Schicciole" valley and reaches the sea in 88 seconds. In this case, the simulated thickness of 60 cm well matches the field measurement (Di Roberto et al., 2014). The area impacted by the avalanche and covered by the deposit in zone B are 3.1×10^5 m^2 and 0.8×10^5 m^2, respectively. The 2D simulation also obtained similar results. The simulation in the zone C shows that the flow never reaches the sea level. After an initial spreading into a flat area above the village of Ginostra, the flow moves (compactly canalized and with a significant change of direction) inside the village and stops after about 180 seconds. In this case, no records that describe the flow dynamics, the runout or the thickness of the deposits exist. Thus, any direct comparison between simulation results and field evidences is not possible. In zone C, the areas impacted by the avalanche and covered by the deposit are, for both impluviums as a whole, 1.5×10^5 m^2 and 0.3×10^5 m^2, respectively. Also in this case, DAN-W results show a very good correlation with the DAN-3D simulations.

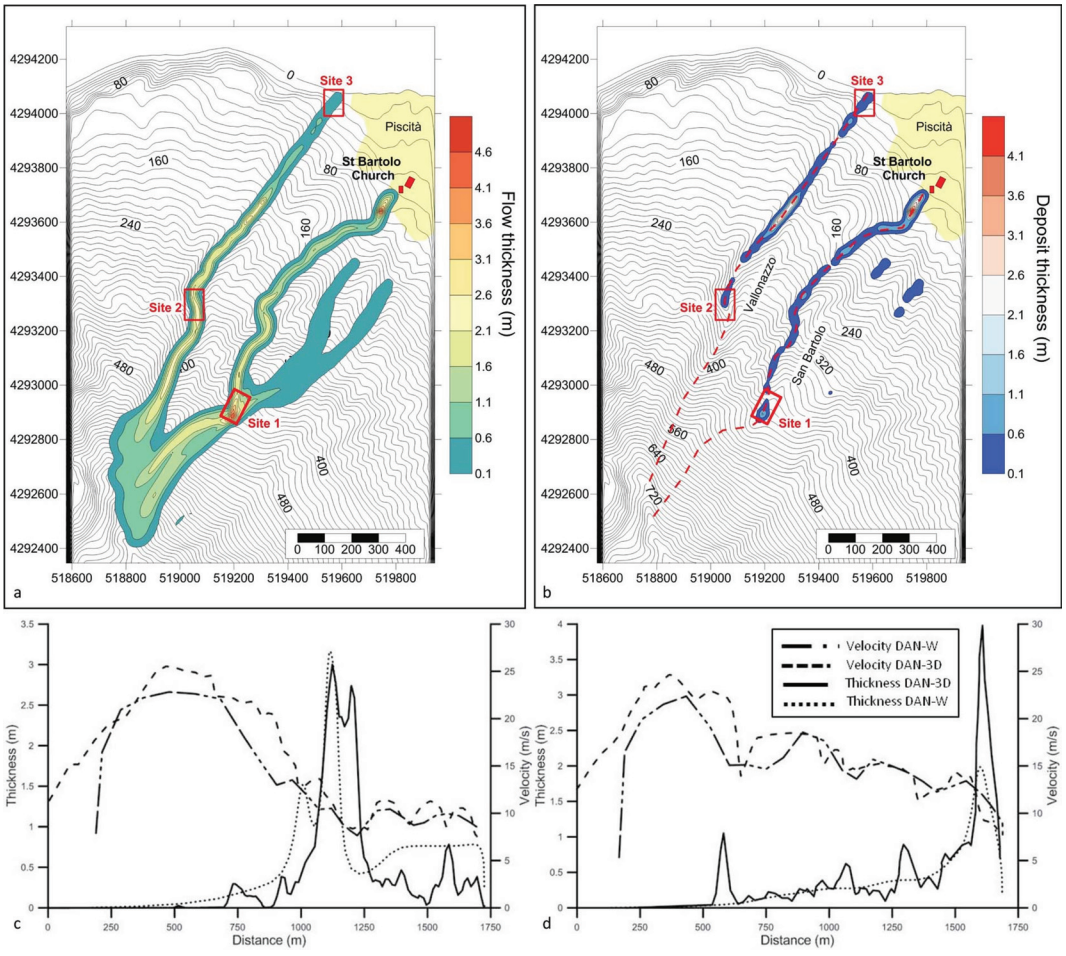

Figure 3. Results of DAN-3D simulation of a) flow thickness and b) deposit thickness for the zone A (1930-like event); comparison between the DAN-W and DAN-3D for the c) Vallonazzo and d) San Bartolo valleys.

5 DISCUSSION

Hot avalanches are able to travel long distances with destructive consequences. So, the evaluation of their mobility is important for the assessment of the areas at risk in future events. The morphometric parameters that best describe their mobility are: the height of vertical drop (H), the runout distance (L), the volume (V) and the covered area (A). Hayashi and Self (1992), Calder et al. (1999) and Saucedo et al. (2005) used different relationships between these four above mentioned parameters to explain the mobility of hot avalanches. In particular, Hayashi and Self (1992) asserted that different material properties rather than different emplacement mechanisms appear to be the best explanation in the Log (V) versus Log (H/L) plot (Fig. 4a). If the historical data of hot avalanches and volcanic avalanches are compared, the plot shows an inverse correlation with coincident regression lines for the two types of deposits, implying that the material properties are similar for both phenomena.

The main difference is represented by the position in the graph. In fact, by plotting the data of hot avalanches found by Calder et al. (1999) and Saucedo et al. (2005), it is easily noticeable that they usually have smaller volumes and higher H/L ratios than volcanic avalanches. This is in good agreement with the general results obtained from the work of Corominas (1996). The H/L ratios resulting from the analysis of the hot avalanches of Stromboli are 0.42, 0.57 and 0.39 for A, B and C zones respectively (Fig. 4b).

Further analysis of the mobility of Stromboli hot avalanches was performed considering the parameter $A/V^{2/3}$ used by Calder et al. (1999)

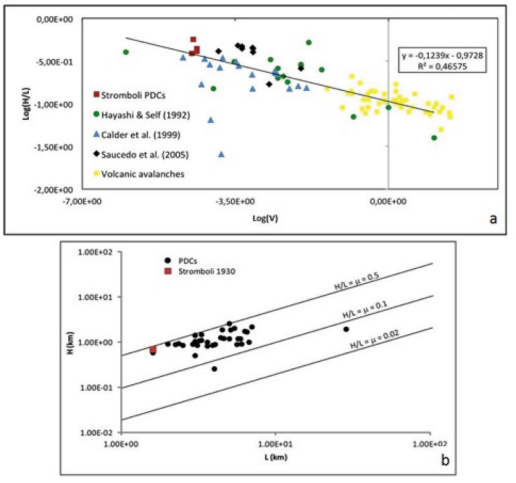

Figure 4. a) Log(V) vs Log(H/L), b) H/L ratio of the Stromboli hot avalanches (called here PDCs) compared with world-wide events (data from Hayashi and Self, 1992; Calder et al., 1999; Suacedo et al., 2005).

to discriminate between the mobility of hot avalanches at Soufriere Hills Volcano (Montserrat). The Stromboli events show that the $A/V^{2/3}$ factor varies between 60 (zone A) and 117 (zone B), being comparable to what measured by Calder et al. (1999) for small volume hot avalanches.

6 CONCLUSIVE REMARKS

Hot avalanches at Stromboli volcano were analyzed by means of analogue models for the triggering mechanism evaluation. Then DAN-W and DAN-3D numerical codes were used to investigate the behavior evaluation of the collapsed material during the runout using as test case the 1906, 1944 and 1930 events. The main outcomes can be summarized as follow:

- DAN-3D was able to reproduce the extension and the order of magnitude of the thickness of two hot avalanches reported in the literature;
- the best modeling results on the 1930 hot avalanche were obtained using a Voellmy model with frictional coefficient of $f = 0.19$ and a turbulence parameter $\xi = 1000$ m/s;
- the outcomes of DAN-W code along the considered sections show a very good correspondence with the 3D simulation;
- the suitability of analogue modeling to understand the triggering mechanism and the evolution of landslide along the Sciara del Fuoco depression has been verified; moreover the best analogue modeling results are obtained with 35° inclination slope and reveal that the internal friction angles alone are not able to generate the slope instability. The accumulation of material on the slope (lava, spatter) trigger little landslides, developing in retrogressive landslide;
- H/L index values resulting from the analysis of the Stromboli hot avalanches are respectively 0.42, 0.57 and 0.39 for the three zones, and are in good agreement with the inverse trend in reduction of H/L with increase of landslides volumes (V) and H/L values less of 0.6 for landslides volumes below 10^{-4} km^3 (Corominas 1996);
- the estimated $A/V^{2/3}$ factor for Stromboli hot avalanches varies between 60 and 117, being comparable with that of small volume events generated by column collapse (Calder et al., 1999).

REFERENCES

Abbruzzese, D. 1935. Sulla catastrofica esplosione dello Stromboli dell'11 settembre 1930. *Gioenia Proc. Soc. Nat. Sci.*, 1, 1–13.

Apuani, T., Corazzato, C., Cancelli, A. & Tibaldi A. 2005. Physical and mechanical properties of rock masses at Stromboli: a dataset for volcano instability evaluation. *Bull Eng. Geol. Environ.*, 64(4), 419–431, doi: 10.1007/s10064–005–0007–0.

Arrighi, S., Principe, C., & Rosi, M. 2001. Violent strombolian and subplinian eruptions at Vesuvius during post-1931 activity. *Bull. Volcanol.*, 63(2–3), 126–150, doi: 10.1007ls004450100130.

Barberi, F., Rosi, M. & Sodi, A. 1993. Volcanic hazard assessment at Stromboli based on review of historical data. *Acta. Vulcanol.*, 3, 173–187.

Behncke, B., Calvari, S., Giammanco, S., Neri, M. & Pinkerton, H. 2008. Pyroclastic density currents resulting from the interaction of basaltic magma with hydrothermally altered rock: an example from the 2006summit eruptions of Mount Etna, Italy. *Bull. Volcanol.*, 70(10), 1249–1268, doi: 10.1007/s00445-008-0200-7.

Benz, W. 1990. Smooth particle hydrodinamics: a review. In: Buchler, J. R. (ed.). *The Numerical Modelling of Nonlinear Stellar Pulsation*. Kluwer Accademic, Dordrecht, 269–288.

Bertagnini, A., Di Roberto, A. & Pompilio, M. 2011. Paroxysmal activity at Stromboli: lessons from the past. *Bull. Volcanol.*, 73(9), 1229–1243, doi: 10.1007/s00445-011-0470-3.

Calder, E.S., Cole, P.D., Dade, W., Druitt, T.H., Hoblitt, R.P., Huppert, H.E., Ritchie, L., Sparks, R.S.J. & Young, S.R. 1999. Mobility of pyroclastic flows and surges at the Soufriere Hills Volcano, Montserrat. *Geophys. Res. Letts.*, 26(5), 537–540.

Cole, P.D., Fernandez, E., Duarte, E., & Duncan, A.M. 2005. Explosive activity and generation mechanisms of pyroclastic flows at Arenal volcano, Costa Rica between 1987 and 2001. *Bull. Volcanol.,* 67(8), 695–716.

Corominas, J. 1996. The angle of reach as a mobility index for small and large landslide. *Can. Geotech. J.*, 33, 260–271.

Davies, K.D., Quearry, M.W. & Bonis, S.B. 1978. Glowing avalanches from the 1974 eruption of the volcano Fuego, Guatemala. *Geol. Soc. Am. Bull.*, 89, 369–384. doi:10.1130/0016-7606(1978)89 < 369:GAFTEO > 2.0.CO;2.

Di Roberto, A., Bertagnini, A., Pompilio, M. & Bisson, M. 2014. Pyroclastic density currents at Stromboli volcano (Aeolian Islands, Italy): a case study of the 1930 eruption. *Bull. Volcanol.*, 76(6), 1–14, doi: 10.1007/s00445-014-0827-5.

Di Traglia, F., Intrieri, E., Nolesini, T., et al. 2014. The ground-based InSAR monitoring system at Stromboli volcano: linking changes in displacement rate and intensity of persistent volcanic activity. *Bull. Volcanol.*, 76, 1–18, doi: 10.1007/s00445-013-0786-2.

Hayashi, J.N. & Self, S. 1992. A Comparison of Pyroclastic Flow and Debris Avalanche Mobility. *J. Geophys Res.*, 97B6, 9063-9071.

Hazlett, R.W., Buesch, D., Anderson, J.L. Elan, R. & Scandone, R. 1991. Geology, failure conditions, and implications of seismogenic avalanches of the 1944 eruption at Vesuvius, Italy. *J. Volcanol. Geoth. Res.*, 47(3–4), 249–264, doi: 10.1016/0377-0273(91)90004-J.

Hungr, O. & McDougall, S. 2009. Two numerical models for landslide dynamic analysis. *Computers & Geosciences*, 35(5), 978–992, doi: 10.1016/j.cageo.2007.12.003.

Hungr, O. 1995. A model for the runout analysis of rapid flow slides, debris flows, and avalanches. *Can. Geotech. J.*, 32, 610–623.

Mc Dougall, S. 2006. *A new continuum dynamic model for the analysis of extreme rapid landslide motion across complex 3D terrain*. Unpublished Ph.D Dissertation, Department of Earth and Ocean Sciences, University of British Columbia, 253.

McDougall, S. & Hungr, O. 2004. A model for the analysis of rapid landslide motion across three-dimensional terrain. *Canad. Geotech. J.*, 41(6), 1084–1097, doi: 10.1139/T04–052.

Monaghan, J.J. 1989. On the problem of penetration in particle methods. *J. Comput. Phys*. 82, 1–15.

Monaghan, J.J. 1992. Smoothed particle hydrodynamics. *Ann. Rev. Astron. Astrophys*. 30, 543–574.

Morelli, S., Garduño Monroi, V.H., Gigli, G., Falorni, G., Arreygue Rocha, E. & Casagli, N. 2010. The Tancitaro debris avalanche: characterization, propagation and modeling. *J. Volcanol. Geoth. Res.*, 193, 93–105, doi: 10.1016/j.jvolgeores.2010.03.008.

Nairn, I.A. & Self, S. 1978. Esplosive eruptions and pyroclastic avalanches from Ngauruhoe in February 1975. *J. Volcanol. and Geoth. Res.*, 3(1–2), 39–60.

Nolesini, T., Di Traglia, F., Del Ventisette, C., Moretti, S. & Casagli, N. 2013. Deformations and slope instability on Stromboli volcano: Integration of GBInSAR data and analog modeling. *Geomorphology*, 180, 242–254.

Ponte, G. 1948. Attività straordinaria dello Stromboli. *Annals of Geophysics*, 1(2), 200–202.

Riccò, A. 1907. Sull'attività dello Stromboli dal 1891 in poi. *Boll Soc Sismol Ital*, 12, 183–205.

Rittmann, A. 1931. Der Ausbruch des Stromboli am 11. September 1930. *Z Vulkanologie* 14, 47–77.

Rosi, M., M. Pistolesi, A. Bertagnini, P. Landi, Pompilio, M. & Di Roberto, A. 2013. Stromboli Volcano, Aeolian Islands (Italy): present eruptive activity and hazard. *Geological Society, London, Memoirs*, 37(1), 473–490.

Rotonda, T., Tommasi, P., & Boldini, D. 2009. Geomechanical characterization of the volcaniclastic material involved in the 2002 landslides at Stromboli. *Journal of geotechnical and geoenvironmental engineering*, 136(2), 389–401.

Saucedo, R., Macıas, J.L., Sheridan, M.F., Bursik, M.I & Komorowski, J.C. 2005. Modeling of pyroclastic flows of Colima Volcano, Mexico: implications for hazard assessment. *J. Volcanol. Geoth. Res.*, 139, 103–115.

Sosio, R., Crosta, G.B. & Hungr, O. 2012b. Numerical modeling of debris avalanche propagation from collapse of volcanic edifices. *Landslides* 9, 315–334, doi: 10.1007/s10346-011-0302-8.

Sosio, R., Crosta, G.B., & Hungr, O. 2008. Complete dynamic modelling calibration for the Thurwieser rock avalanche (Italian Central Alps). *Engineering Geology* 100, 11–26, doi: 10.1016/j.enggeo.2008.02.012.

Sosio, R., Crosta, G.B., Chen, J.H. & Hungr, O. 2012a. Modelling rock avalanche propagation onto glaciers. *Quaternary Science Reviews*, 47, 23–40.

Voellmy, A. 1955. Über die Zerstörunskraft von Lawinen. *Schweizerische Bauzeitung*, 73, 212–285. (in German)

Yamamoto, T., Takada, A., Ishizuka, Y. Miyaji, N. & Tajima, Y. 2005. Basaltic pyroclastic flows of Fuji volcano, Japan: characteristics of the deposits and their origin. *Bull. Volcanol.*, 67(7), 622–633, doi: 10.1007/s00445-004-0398-y.

Rend. Online Soc. Geol. It., Vol. 41 (2016), pp. 195-198, 3 figs. (doi: 10.3301/ROL.2016.127)

Runout modelling of gravity-induced pyroclastic density currents at Stromboli volcano (Italy)

Teresa Salvatici ([a]), Stefano Morelli ([a]) Federico Di Traglia ([a]) & Alessio Di Roberto ([b])

([a]) Department di Science della Terra, Università di Firenze, Via La Pira 4, 50121, Firenze (Italy), Firenze, Italy. E-mail: Teresa.salvatici@unifi.it
([b]) Istituto Nazionale di Geofisica e Vulcanologia, Sezione di Pisa, Via della Faggiola 32, 56126, Pisa (Italy)

Document type: Short note.
Manuscript history: received 17 December 2015; received in revised form 24 February 2016; accepted 29 March 2016; editorial responsibility and handling by Margherita C. Spreafico.

ABSTRACT

Gravity-induced pyroclastic density currents (PDCs) at Stromboli volcano were investigated by means numerical and empirical modelling. With the aim of testing the suitability of landslide numerical model DAN-3D and empirical models are used related to gravity-induced PDCs, in particular this work presents the results of the back analysis of three events occurred on 1906, 1930 and 1944 at Stromboli volcano. These two methods were able to reproduce the extension and the order of magnitude of the thickness of the PDCs reported in the literature. The best results of DAN-3D models were obtained using a Voellmy model with frictional coefficient of f = 0.19 and a turbulence parameter ξ = 1000 m/s. The mobility terms, find with the numerical model, are compared with empirical data of literature of the similar events.

KEY WORDS: Pyroclastic density currents, DAN-3D, empirical methods.

INTRODUCTION

Gravity-induced pyroclastic density currents (PDCs) have been observed directly and their deposits have been widely identified on the flanks of several volcanoes (Davies et al., 1978; Di Roberto et al. 2014; Di Traglia et al., 2014). Such kind of events usually occurs on edifices fed by mafic to intermediate magmas and have small volumes (10^4-10^7 m^3) but emplace at very high temperatures and can travel far from the source at very high speed. These features make them potentially dangerous for communities that live and concentrate their socio-economic activities close to the volcanoes and for the high number of tourists attending them each year for their recreational activities.

With the aim of testing the suitability of landslide numerical and empirical models in simulating and assessing the impact area related to the gravity induced PDCs, the results of the back analysis of three events occurred at Stromboli volcano are presented. They were performed use both 3D numerical codes called DAN-3D (Hungr & McDougall, 2009) both empirical methods to test and compare the mobility of this particular PDCs with the other kinds of pyroclastic density current. As case studies, three flows occurred on 1906, 1930 and 1944 at Stromboli volcano, were selected. The Back analysis was undertaken through the use of DAN-3D, considering the 1930 event as test case. In fact, for this event detailed descriptions are available from many authors. Rittmann (1931) and Abbruzzese (1935) gathered a lot of data shortly after the eruption and in particular they deduced the total runout distance, velocity, thickness and distribution of deposits. More recently Di Roberto et al. (2014) provide additional data on flow dynamics and distribution of deposits. The simulations were able to reproduce the extension and the order of magnitude of the deposit thickness of events reported in the literature (Rittmann, 1931; Abbruzzese, 1935; Di Roberto et al., 2014).

TESTING AREA

Stromboli is a volcanic island of the Aeolian archipelago (Tyrrhenian Sea, southern Italy). The island is the subaerial part of stratovolcano, distinguished by a rather regular conical edifice, rising up to 924 m above sea level (a.s.l.) from a base that lies between 2300 m and 1300 m of water depth. The volcanic activity of Stromboli has been continuous since the third-seventh centuries and mainly consists in low energy intermittent explosions (Strombolian activity) occasionally interrupted by effusive events and by violent explosions regularly called paroxysms (Barberi et al., 1993).

The active vents are located in the crater terrace, at about 750 m in the upper part of the Sciara del Fuoco (SdF), a horseshoe-shaped depression that occupies the NW flank of the volcano (fig. 1).

NUMERICAL MODELLING

Considering the sliding processes associated to this kind of event the motion of Stromboli gravity-induced PDCs were modelled using a DAN-3D numerical model (Hungr & McDougall, 2009). This numerical code assumes a simplified approach of "equivalent-fluid" for the simulation of mass flow motion (Hungr & McDougall, 2009). The model uses the Lagrangian numerical method to solve the depth-average integrated St. Venant equations, adapted from smoothed particle hydrodynamics (SPH). The momentum equations evaluate an internal frictional rheology, governed by an

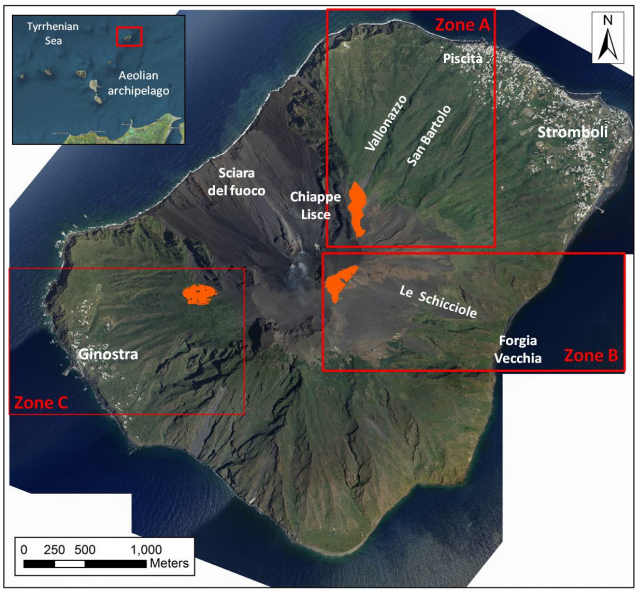

Fig. 1 - Testing area: Stromboli volcano with the main toponyms. The three red rectangular areas cover the volcano sector involved in the PDC of 1930 (zone A), 1944 (zone B) and 1906 (zone C). These zones are used for numerical modelling with DAN-3D. In orange the three events source areas.

internal friction angle and by a basal rheology, chosen by the modeller according to one of the eight rheological kernels: frictional, plastic, Newtonian, turbulent, Voellmy, Bingham, Coulomb frictional and power law.

Simulations were performed on three areas roughly corresponding to those affected by gravity-induced PDCs of 1930 (zone A), 1944 (zone B) and the area possibly involved in the 1906 event (zone C). The zone A was used as testing area, since the data about the deposits distribution (areal spread, thickness and travel distance), the velocity of the flow and the temporal duration are available from previous studies (Rittmann, 1931; Abbruzzese, 1935; Di Roberto et al., 2014).

In performing these analyses all the materials involved in 1906 and 1944 events were assumed similar to those of 1930.

Subsequently, the parameters obtained for 1930 event (zone A) were used to calibrate the model by back analysis and to find the input rheological parameters used later in the zone B and C.

EMPIRICAL METHODS

Gravity-induced PDCs are well known for their ability to travel long distances, so their mobility is critical to evaluate the areas at risk from future events (Davis et al., 1978). Many authors have found empirical correlations using morphometric parameters like, the total height of vertical drop (H), the runout distance (L), the volume (V) and the inundated area (A). In particular Hayashi & Self, (1992) compared the historical data of PDCs and volcanic avalanches in a plot of Log (V) versus Log (H/L). Another important mobility index is H/L, where H is the potential energy and L the runout distance, this ratio was considered by several authors (Corominas, 1996; Di Roberto et al., 2014; Alvarado & Soto, 2002; Davies et al., 1978).

Further analysis of the mobility of Stromboli gravity-induced PDCs was performed considering the parameter A/V2/3 suggested by Dade & Huppert, (1998) for the runout of rockfalls and used later by Calder et al., (1999) to discriminate between the mobility of PDCs at Soufriere Hills Volcano (Montserrat).

RESULTS

NUMERICAL MODEL

In the back analysis with DAN-3D relative to the 1930 event the best results for the simulation was obtained using a Voellmy rheological model with a frictional coefficient f = 0.19 and a turbulence parameter ξ = 1000 m/s. These rheological parameters are found using a trial-and-error procedure in order to obtain values of runout distance, deposit thickness, velocity and duration of the flow, in accord with the historical accounts and field data described by Rittmann, (1931), Abbruzzese, (1935) and Di Roberto et al., (2014). They claim that during the 1930 event incandescent flows moved into the S. Bartolo and Piscità (Vallonazzo) valleys. The first one stopped few meters from the church of S. Bartolo after 120 seconds, while the second one had a major impulse and arrived at the coastline after 135 seconds. Furthermore the model successfully simulated the 1930 event deposits' thicknesses, matching the order of magnitude of those measured by Di Roberto et al., (2014) during their field survey. In the San Bartolo valley, at about 780 m a.s.l. the measured thickness is about 4.5 m, versus a simulated thickness of 1.6 m. In the NE rim of Vallonazzo valley at about 300 m a.s.l, the measured and simulated thicknesses are instead fully comparable and attain 30-40 cm, whereas close to the outlet of Vallonazzo valley, the measured thickness is about 100 cm and the simulated thickness is 60 cm. The area impacted by the avalanche and covered by the deposit are, for both impluviums on the whole, 3.6 x 105 m2 and 0.8 x 105 m2, respectively (fig. 2).

The rheological parameters obtained with this procedure for 1930 PDCs event are then used in the simulation of the events occurred in zones B (1944) and C (1906). The simulation results in the zone B show that the flow moves in "Le Schicciole" valley and reaches the sea in 88 seconds. The simulated thickness of 60 cm well matches the field measurement (Di Roberto et al., 2014). The area impacted by the avalanche and covered by the deposit in zone B are 3.1 x 105 m2 and 0.8 x 105 m2, respectively (fig. 2).

The simulation in the zone C shows that the flow never reaches the sea level. After an initial spreading into a flat area above the village of Ginostra, the flow moves (compactly canalized and with a significant change of direction) inside the village and stops after about 180 seconds. In this case, any direct comparison between simulation results and field evidences is not possible. In zone C, the area impacted by the avalanche and covered by the deposit are 1.5 x 105 m2 and 0.3 x 105 m2, respectively (fig. 2).

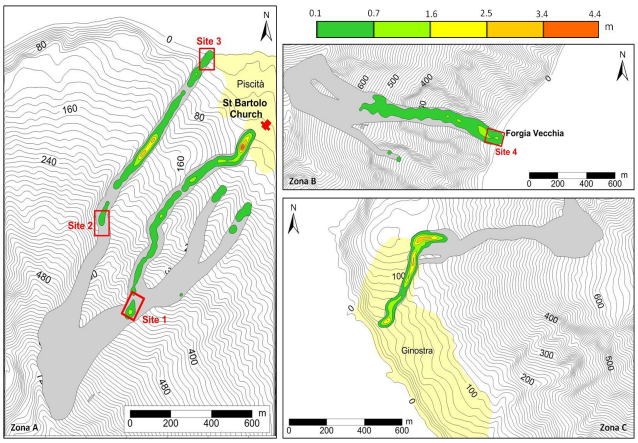

Fig. 2 - Results of DAN-3D simulation of flow thickness (grey color) and deposit thickness for the zone A (1930-like event), zone B (1944-like event) and zone C (1906-like event).

EMPIRICAL METHODS

The result obtained with the analysis of geometric and morphometric parameters of Stromboli gravity-induced PDCs show a good correspondence with the results obtained in the literature. In particular, studying the plot with data of PDCs found by Calder et al., (1999), Saucedo et al., (2005) and Hayashi & Self, (1992) is possible to observe that the major difference of PDCs with volcanic avalanches is represented by the position in the graph. In fact the PDCs commonly have smaller volumes and higher H/L ratios than volcanic avalanches. This is in good agreement with the general results obtained from the work of Corominas, (1996). This author shows a general inverse trend in reduction of H/L with increase of landslides volumes (V) and H/L values less of 0.6 for landslides volumes below 10-4 km3.

Using DAN-3D numerical model it is possible to get the travel angle, that is the angle of the line connecting the centre of gravity of the slide source and the deposit mass. The tangent of this angle expresses H/L (Morelli et al., 2010).

The H/L ratios resulting from the analysis with DAN-3D of the Stromboli events are 0.42, 0.57 and 0.39 for A, B and C zones respectively. This result indicates that the tree events are classified as tips of PDCs with small volumes and with an H/L value in good agreement with the general mobility trend found in literature (fig. 3a, b).

The results of analysis on A/V2/3 factor of the Stromboli gravity-induced PDCs deposits show that the factor varies between 60 (zone A) and 117 (zone B), being comparable to what measured by Calder et al., (1999) at Soufriere Hills Volcano for small volume PDCs (fig. 3c, d).

CONCLUSIONS

Gravity-induced PDCs at Stromboli volcano were analyzed through the use of DAN-3D numerical code developed by

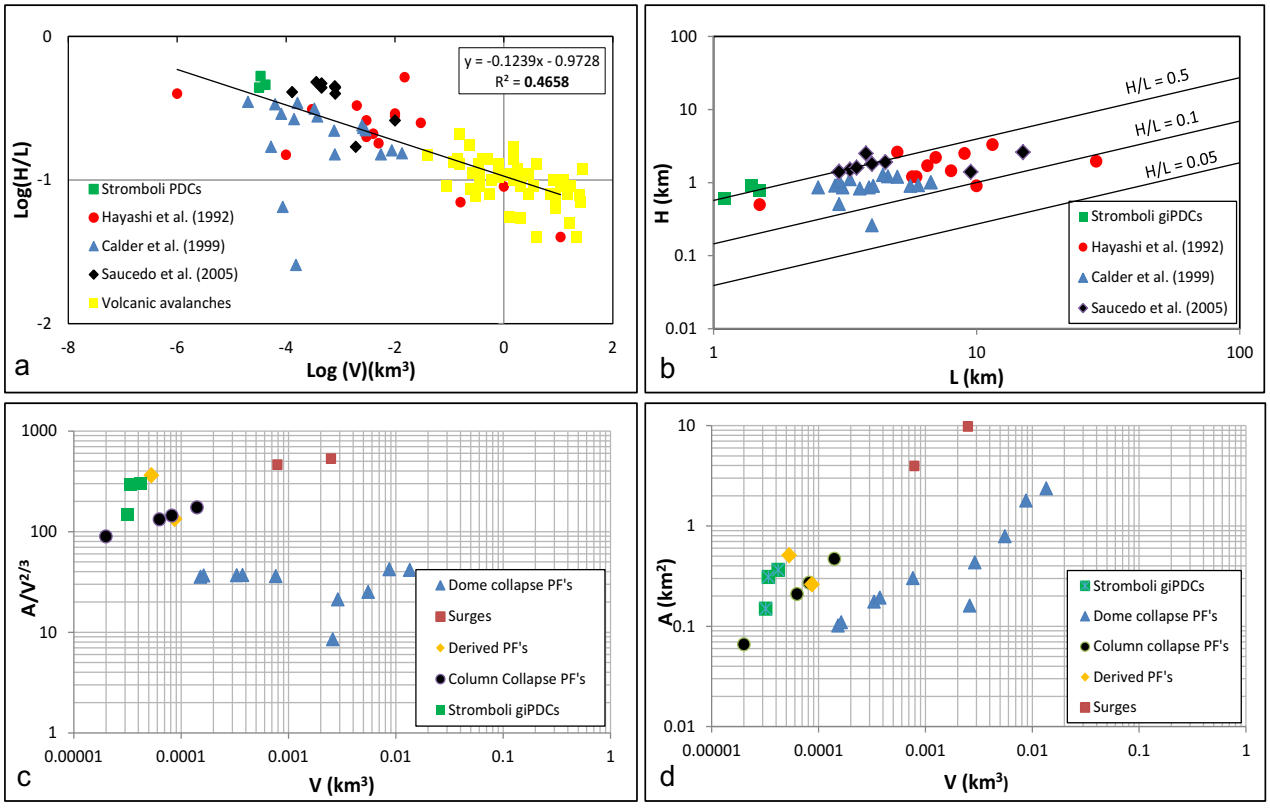

Fig. 3 - a) Log(V) vs Log(H/L), b) H/L ratio of the Stromboli gravity-induced PDCs compared with world-wide PDCs, c) $A/V^{2/3}$ vs V , d) A vs V of the Stromboli gravity-induced PDCs compared with different kinds of PDCs (data from Hayashi and Self, 1992; Calder et al., 1999; Suacedo et al., 2005).

Hungr & McDougall, (2009) and of empirical methods, using as test case the 1906, 1944 and 1930 PDC events. The main outcomes of the simulations show that DAN-3D was able to reproduce the extension and the order of magnitude of the thickness of the events reported in the literature. With a trial-and-error procedure on the model of 1930 events, was possible to set the Voellmy rheology with frictional coefficient of f = 0.19 and a turbulence parameter ξ = 1000 m/s. The results obtained with the empirical method show a good correspondence between the tree gravity-induced PDCs of Stromboli volcano with the PDCs reported in literature.

ACKNOWLEDGMENTS

This work has been partially financed by the "*Presidenza del Consiglio dei Ministri – Dipartimento della Protezione Civile*" (Presidency of the Council of Ministers - Department of Civil Protection) within the framework of the InGrID and InGrID2015 research agreements between the Presidency of the Council of Ministers - Department of Civil Protection and the Department of Earth Sciences - University of Firenze; this publication, however, does not reflect the position and the official policies of the Department of Civil Protection.

REFERENCES

Abbruzzese D. (1935) - Sulla catastrofica esplosione dello Stromboli dell'11 settembre 1930. Gioenia Proc. Soc. Nat. Sci., 1, 1-13.

Alvarado G. E. & Soto G. J. (2002) - Pyroclastic flow generated by crater-wall collapse and outpouring of the lava pool of Arenal Volcano, Costa Rica. Bull. Volcanol., 63, 8, 557-568.

Barberi F., Rosi M. & Sodi A. (1993) - Volcanic hazard assessment at Stromboli based on review of historical data. Acta. Vulcanol., 3, 173-187.

Calder E.S., Cole P.D., Dade W., Druitt T.H., Hoblitt R.P., Huppert H.E., Ritchie L., Sparks R.S.J. & Young S.R., (1999) - Mobility of pyroclastic flows and surges at the Soufriere Hills Volcano, Montserrat. Geophys. Res. Letts., 26, 5, 537-540.

Corominas J. (1996) - The angle of reach as a mobility index for small and large landslide. Can. Geotech. J., 33, 260-271.

Dade W.B. & Huppert H.E. (1998) - Long runout rockfalls. Geology, 26, 803-806.

Davies K.D., Quearry M.W. & Bonis S.B. (1978) - Glowing avalanches from the 1974 eruption of the volcano Fuego, Guatemala. Geol. Soc. Am. Bull., 89, 369–384.

Di Roberto A., Bertagnini A., Pompilio M. & Bisson M. (2014) - Pyroclastic density currents at Stromboli volcano (Aeolian Islands, Italy): a case study of the 1930 eruption. Bull. Volcanol., 76, 6, 1-14.

Di Traglia F., Intrieri E., Nolesini T., Bardi F., Del Ventisette C., Ferrigno F. & Stefanelli, C. T. (2014) - The ground-based InSAR monitoring system at Stromboli volcano: linking changes in displacement rate and intensity of persistent volcanic activity. Bulletin of volcanology, 76(2), 1-18.

Hayashi J. N. & Self S. (1992) - A Comparison of Pyroclastic Flow and Debris Avalanche Mobility. J. Geophys Res., 97B6, 9063-9071.

Hungr O. & McDougall S. (2009) - Two numerical models for landslide dynamic analysis. Computers & Geosciences, 35, 5, 978-992.

Morelli S., Monroy V. H. G., Gigli G., Falorni G., Rocha E. A. & Casagli N. (2010) - The Tancitaro debris avalanche: characterization, propagation and modeling. Journal of Volcanology and Geothermal Research, 193, 1, 93-105.

Rittmann A. (1931) - Der Ausbruch des Stromboli am 11. September 1930. Z. Vulkanologie 14, 47-77.

Saucedo R., Macıas J. L., Sheridan M. F., Bursik M. I. & Komorowski J. C. (2005) - Modeling of pyroclastic flows of Colima Volcano, Mexico: implications for hazard assessment. J. Volcan Geoth. Res., 139, 103-115, doi: 10.1016/j.jvolgeores.2004.06.019.

DEBRIS FLOW HAZARD ASSESSMENT BY MEANS OF NUMERICAL SIMULATIONS: IMPLICATIONS FOR THE ROTOLON CREEK VALLEY (NORTHERN ITALY)

ABSTRACT

On 4th November 2010, a debris flow detached from a large debris cover accumulated above the lowermost portion of the Rotolon landslide (Vicentine Pre-Alps, NE Italy) and channelized in the valley below within the Rotolon Creek riverbed. Such event evolved into a highly mobile and sudden debris flow, damaging some hydraulic works and putting at high risk four villages located along the creek banks. A monitoring campaign was carried out by means of a ground based radar interferometer (GB-InSAR) to evaluate any residual displacement risk in the affected area and in the undisturbed neighbouring materials. Moreover, starting from the current slope condition, a landslide runout numerical modelling was performed by means of DAN-3D code to assess the impacted areas, flow velocity, and deposit distribution of the simulated events. The rheological parameters necessary for an accurate modelling were obtained through the back analysis of the 2010 debris flow event. Back analysis was calibrated with all of the available terrain data coming from field surveys and ancillary documents, such as topographic, geomorphological and geological maps, with pre- and post-event LiDAR derived DTMs, and with orthophotos. Finally, to identify new possible future debris flow source areas as input data for the new modelling, all the obtained terrain data were reanalysed and integrated with the GB-InSAR displacement maps; consequently, new simulations were made to forecast future events. The results show that the integration of the selected modelling technique with ancillary data and radar displacement maps can be a very useful tool for managing problems related to debris flow events in the examined area.

KEY WORDS: debris flow, DAN-3D, GB-InSAR, numerical modelling, DSGSD.

1 INTRODUCTION

Debris flows are water-laden collapsing masses of soil and fragmented rock encompassing a wide range of characteristics and varying widely in magnitude (Jakob 2005), composition (Coussot and Meunier 1996), and initiation process (Coe et al. 2008). Some of these phenomena start in low-order streams, both in riverbeds and overbank deposits, because of the intense runoff, or to overland flow, mobilizing sediment without slope instability phenomena (Brayshaw and Hassan 2009). Other debris flow types are related to slope failures that rush down mountainsides, subsequently funnelling into stream channels and forming thick deposits on valley floors (Iverson 1997). The latter type in particular is usually associated with intense erosion along their path, which can lead to a substantial increase in volume, runout distance, and disruptive energy. All these aspects may eventually cause severe damage to infrastructure and endanger people, especially in populated mountainous areas, where most human activities are concentrated in valley floors (Pazzi et al. 2016), coinciding with debris flow impact areas (i.e., the area impacted by the flow during its descent, which has the maximum flow areal spreading since the beginning of the run).

For this reason, the prediction of landslide runout and its effect is essential in landslide risk assessment. The main quantitative methods, useful to obtain it, can be classified as either empirical or analytical. Empirical methods operate on observational data correlations to calculate the extent of the runout zone (Hsü 1975; Corominas 1996). Analytical methods try to predict the motion of the landslide mass from initiation to deposition, providing estimates of hazard extent and intensity (Savage and Hutter 1989; Iverson 1997). The latter models perform the time-wise numerical solution of the equations of motion and advance the location of the simulated landslide incrementally, computing the spatial distribution of landslide hazard intensity parameters, such as flow velocity and depth (Hungr 1995).

The latter approach was applied to the Rotolon creek valley (Little Dolomites chain, NE Italy) which hosts populations from ancient times and it is historically prone to landslide processes (Trivelli et al. 1991). These gravitational instabilities are induced by the local geological and geomorphological features, such as very steep slopes characterized by highly fractured and weathered rocks. Following a period of heavy and persistent rainfall, on 4th November 2010, a debris flow detached from the debris cover of the lowermost portion of the Rotolon landslide debris cover, channelizing into the Rotolon creek riverbed, mixing with water, and evolving into a highly mobile debris flow with a travel distance of approximately 4 km. This event damaged several hydraulic works, such as weirs, fords, and bank protections, putting at high risk the infrastructures (e.g., bridges and roads alongside the watercourse) and especially four villages situated along the creek banks (Maltaure, Turcati, Parlati and Recoaro Terme) (Frodella et al. 2014). On 8th December 2010, a GB-InSAR monitoring campaign was carried out to assess the landslide residual displacements and support the local authorities for the emergency management (Fidolini et al. 2015). In this framework, a landslide geomorphological mapping was performed (Frodella et al. 2014, 2015), together with the design and implementation of an early warning system, and a landslide trigger/runout analysis (Frigerio et al. 2014; Bossi et al. 2015a, 2015b). In this work, a back analysis of the 2010 event was carried out using a 3D numerical code called DAN-3D (McDougall and Hungr 2004; Hungr and McDougall 2009), refining the analysis carried out by Bossi et al. (2015b) and integrating information coming from different disciplines, comprising geomorphology, hydraulics, and geotechnical data. DAN-3D was chosen because it was developed for the simulation of extremely rapid shallow landslides movements, even in complex topographies (McDougall and Hungr 2004, Salvatici et al. 2016a, b). Moreover, the DAN-3D code was considered for the studied debris flow since it is based on the "equivalent fluid" theory, which is capable of simulating entrainment and corresponding rheology changes (Hungr 1995).

Furthermore, the DAN-3D simulated results were validated by means of two essential comparisons between i) the flow geometrical parameters obtained by the pre- and post-landslide event high resolution DTMs (2 m grid resolution) and ii) the modelled flow velocities along selected cross-sections, with the ones estimated from the empirical equations of Chow (1957), Mizuyama et al. (1992), and Rickenmann (1999) (Figure 1a). Finally, a forecast analysis was carried out to evaluate possible future debris flow events. This analysis required to find a new possible landslide source area and volumes, to use the post-event DTM as topography, and to use the rheological parameters of back analysis. The more difficult task is usually represented by the identification of new possible landslide reactivation zones (i.e., source areas). In this work, such area was detected with high precision through the integrated analysis of the radar displacement maps (Fidolini et al. 2015) and the geomorphological field evidence (Frodella et al. 2014; 2015). Starting from this source area, new simulations were performed, taking into account the 2010 event back analysis rheological parameters and the new possible landslide detachments, whose volumes were calculated by means of a statistical analysis of the 2010 source area thickness.

2 STUDY AREA

The study area is located in the western sector of the Veneto region (Northern Italy), in the Vicentine Pre-alps, on the south-eastern flank of the Little Dolomites chain, which are part of the Agno river basin (Figure 1a). The Rotolon landslide affects limestone and dolomitic formations belonging to the South Alpine Domain (early Triassic-early Jurassic) (Barbieri et al. 1980; Figure 1b), covering an area of approximately 626,000 m^2 and developing from approximately 1700 m to 1100 m a.s.l. (Frodella et al. 2014, 2015; Fidolini et al. 2015). For its areal extension, morpho-structural characteristics (presence of trenches, counter-slope scarps, sub-horizontal fractures in correspondence with the landslide toe, accessory instability phenomena, and kinematic very slow displacement of large fractured rock masses

(Agliardi et al. 2009), this landslide presents the features of a "*Sackung*"-type Deep Seated Gravitational Slope Deformation (DSGSD), according to Zischinsky (1969).

The landslide area can be divided into two sectors: i) an upper Detachment sector and ii) a lower Dismantling sector (Frodella et al. 2014). The Detachment sector has a mean slope of approximately 30° and is located nearby the landslide crown: it is characterized by tensional fractures, trenches and crests and largely comprises colluvial, rockfall and rock avalanche materials, with very coarse and heterometric clasts and scattered boulders. The Dismantling sector has a slope mean angle of approximately 34° and is characterized by mainly cobble-sized blocks and scattered boulders in coarse sandy matrix, coming from the Detachment sector rock slopes. This area is particularly prone to debris flow, as documented by recent bibliographies (Trivelli 1991; Altieri et al. 1994; Bossi et al. 2015b) and historical documentation available since 1573 (Schneuwly-Bollschweiler et al. 2012). The 2010 debris flow event started along the right bank sector of the Rotolon landslide detrital cover, at approximately 1400 m a.s.l., and settled at approximately 550 m a.s.l., with an adopt height of approximately 850 m. The collapsed material, characterized by a volume of approximately 320,000 m^3 (Bossi et al. 2015b) spread along 4 km, was formed by very coarse and heterometric clasts, ranging from cobbles to boulders with scattered blocks (decimetric to decametric in size) in a coarse sandy matrix.

3 ANALYTICAL METHODS

3.1 DAN-3D numerical model

Many dynamic models exist; particularly, the DAN-3D numerical code (McDougall and Hungr 2004; Hungr and McDougall 2009) was selected to model the 4th November 2010 debris flow event. The model uses the Lagrangian numerical method to solve the depth-average integrated Saint-Venant equations, adapted from Smoothed Particle Hydrodynamics (SPH). This numerical code assumes a simplified approach of "equivalent-fluid" (Hungr 1995) with an internal frictional rheology, governed by an internal friction angle and a basal rheology. The latter was chosen by using some implemented rheological kernel: i) frictional; ii) Bingham; iii) Voellmy; iv) Newtonian and v) plastic. These kernels are usually selected based on an empirical calibration procedure, in which a case study is subjected to trial-and-error back analysis. The choice of the rheology leads to different results: for example, a frictional model produces relatively high velocities and forward-tapering deposits, while a Voellmy model predicts lower velocities and forward-bulging deposits (Hungr and Evans 1996). Furthermore, DAN-3D can simulate the entrainment while considering the "erosion rate" factor, defined as the ratio between the final slide volume, the initial slide volume and the length of the erodible zones. The model requires three input files: topography (path file), source area (source file), and number of materials used with different rheology and erosion (erosion file). According to the related recent bibliography (Yifru 2014; Nocentini et al. 2015; Schraml et al. 2015, Salvatici et al. 2016 a, b; Morelli et al. 2016) and examining the dynamic of the event through its deposit, the Voellmy rheological kernel was chosen for the entire stretch. This rheology assumes the resistance as the sum of a frictional and a turbulent term:

$$\tau = f\sigma_z + \frac{\rho g v_x^2}{\xi} \quad (1)$$

In this equation, *f* is the frictional component of resistance, which controls the runout distance, while ξ (m/s) is the turbulence parameter, which controls the flow velocity, introduced by Voellmy (1955); in landslide dynamics, it represents all possible sources of velocity-dependent resistance. ρ, *g* and *v* are the density, the gravity, and the velocity, respectively. The Voellmy model is useful because it requires only two parameters to calibrate. When the flow moves rapidly, the turbulent term controls the friction and the frictional term prevails when the flow moves slowly.

The pre-event topography was modified with post-event topography by subtracting the deposit thickness of the source area to obtain the perfect path file for the model. The source thickness was calculated by subtracting post- and pre-event 2-meter-high resolution DTMs and isolating the source area (Morelli et al. 2010). To perform simulation of the studied event, a constant rheology along its path was not considered. The landslide runout propagation, in fact, was divided into three parts, according to the most evident fluvial morphological variability: i) narrowing and enlargements; ii) hydraulic jumps and curvatures; iii) possible contributions from minor tributaries; and iv) the presence of several hydraulic works for flow control, such as weirs, fords, gabions, retaining walls and other bank protections. Subsequently, a forecast analysis was carried out to individuate risk scenarios. The new model was applied to the post-event topography, considering the rheological parameters obtained for the 2010 debris flow event back analysis and assuming a new possible events source area provided by the analysis of cumulative monthly displacement maps calculated from radar data.

3.2 Empirical flow velocity estimation

Most equations available in the literature estimate the translation velocity of the frontal part or the maximum (mean cross-sectional) velocity along the debris flow surge (Hungr et al. 1984). To validate the back analysis, the flow velocity assessment represents a useful parameter. In the latter framework, the velocity of the Rotolon event was estimated using two different equations:

- the back-calculation method of the Forced Vortex Equation for super-elevation, which requires an estimate of the bend's radius of curvature (Chow 1959; Hungr et al. 1984; Revellino et al. 2004; Zanchetta et al. 2004; Prochaska et al. 2008):

$$v = \left(\frac{\mathrm{gR_c\Delta h}}{\mathrm{w}}\right)^{0.5} \quad (2)$$

  where g is the acceleration of gravity, Δh is the super-elevation of the debris wave in the channel bends, w is the channel width and R_c is the curvature radius. The radius of curvature can be calculated in the field using the relation between the two cross-section arc lengths and their angular (azimuth) difference or taken from the topographic map. The equation assumes that flow is subcritical, the radius of curvature is equal for all streamlines, and every streamline's velocity is equal to the mean flow velocity (Pierson and Scott 1985).

- the method of velocity prediction, based on the maximum discharge (Rickenmann 1999, Zanchetta et al. 2004):

$$v = 2.1{Q_p}^{0.33}S^{0.33} \quad (3)$$

  where Q_p is the maximum discharge and S is the channel bed slope.

The flow's radius of curvature was calculated where debris flow travels around a bend (cross-sections 1b-4b, Figure 1a). It was obtained both from a graphical processing using a 1:5000 topographic map and from the application of the method of Prochaska et al. (2008) and its empirical equations. The super-elevation of debris flow (h in Table 2) in the channels bed was calculated from an integrate analysis between a 2010 November orthophoto, post-event DTM, and field observation. On the other hand, at each cross-section from 1a to 5a (Figure 1a), the velocity estimation was based on Rickenmann's (1999) flow equations, considering the approximate maximum discharge (Q_p), assessed using two empirical relationships between peak discharge and volume of the debris flow (Mizuyama et al. 1992; Rickenmann 1999) (Table 2).

3.3 Ground Based Interferometric Synthetic Radar (GB-InSAR)

GB-InSAR is a remote sensing technique widely used for ground displacements and slope movements monitoring with metric or sub-metric resolution and submillimetre accuracy (Rudolf et al. 1999; Tarchi et al. 2003; Antonello et al. 2004; Nolesini et al. 2013; Bardi et al. 2014; Frodella et al. 2016). This instrumentation provides a remotely sensed measurement of ground displacements from an installation point on a solid base facing the observed scenario. GB-InSAR radar systems generate an electromagnetic wave belonging to the microwave portion of the electromagnetic spectrum and measure the echo of scattering surfaces. The technique working principle is the evaluation of the phase difference, pixel by pixel, between two pairs of averaged sequential SAR images of the same scenario, constituting an interferogram (Bamler and Hartl 1998). From the obtained interferogram, considering the time spanning between two or more subsequent coherent SAR image acquisitions, it is possible to derive a map of the displacements along the sensor line of sight (LOS), with selectable sampling frequency. To monitor the source area of the 2010 landslide, a GB-InSAR system was located in the village of Maltaure, at an average distance of 3 km with respect to the debris flow source area and the surrounding debris cover (Figure 1b). The antenna moved along a 2.7 m rail, and the SAR image range resolution (spatial resolution along the direction perpendicular to the rail) was approximately 3 m, while the azimuth resolution (spatial resolution parallel to the synthetic aperture) was between 1.6 m and 9.3 m (with a 500 m and 2900 m sensor-target distance, respectively). The landslide monitoring activity was carried out from 8th December 2010 to 31st March 2013 (Fidolini et al. 2015) (Figure 2a). By comparing the landslide geomorphological field observations (Frodella et al. 2014, 2015) with the obtained GB-InSAR displacement maps, a potential source area of possible future debris flow was detected (Figure 2b). The radar displacement maps were elaborated in a MATLAB environment to automatically extract from the cumulated displacement maps all the areas affected by movements higher than a selected threshold value. The latter was automatically calculated by the MATLAB code as the minimum displacement among all the minimum displacement monthly values. The extracted areas were analysed in the ArcGIS™ and in Golden Software SURFER™ environments to obtain the new critical sector, which could be the potential source area of future possible events. This critical sector is characterized by the peak cumulative displacements recorded in the monitored area (Figure 2b), confirming that it is characterized by intense ground deformation and erosional processes. Furthermore, as confirmed by geomorphological evidence, the thermographic surveys, the rainfall temporal distribution and the modelled drainage pattern (Frodella et al. 2014, 2015), this abovementioned detected area is characterized by the presence of ephemeral creeks which contribute to the sub-surface water circulation. In addition, considering that this area, part of a DSGSD Dismantling sector, is made of a very permeable detrital cover with high slope angle sectors (mean value of 34°), it is usually assumed that in case of exceptional heavy rainfall (very concentrated events or accumulated waters for a long and uninterrupted period as occurred in November 2010) this area can be affected by debris sector detachments, which therefore trigger debris flows.

4 RESULTS AND DISCUSSION

4.1 Numerical model: back analysis

Knowledge of measurable characteristics of a real event, such as runout distance, geometric distribution of deposits, velocities, and time duration of the flow motion, is fundamental for landslide runout back analysis based on numerical models. In this case study, the morphometric results of simulations (i.e deposits distribution as areal spread, thickness, and travel distance) were calibrated using the difference between the pre- and post-event high-resolution DTMs (2x2 m cell resolution) of the studied valley with the support of field investigations (Figure 3). Whereas the flow velocity was calculated by empirical equations, as described in section 3.2. The best results of the back analysis DAN-3D simulation

were obtained using three types of materials (for materials, DAN-3D means the rheological properties) with different frictional coefficients (*f*) and turbulence parameters (ξ) (Table 1) in the Voellmy kernel. The considered model has an erosion rate of 1.1 x 10^{-4} (-) and a maximum erosion depth of 5 m only in the first material. These values were established by the volume analysis of Bossi et al. (2015). In summary, the main elements that, in our opinion, most influenced the flow dynamics (and therefore the choice of rheological parameters) are as follows: i) the high plano-altimetric changes in the riverbed and the consequent variability of hydraulic sections; ii) the presence of two weirs at approximately 940 m a.s.l. that intercept the natural distribution of sediments; iii) the presence of the confluence of an ephemeral tributary of the Rotolon Creek (Agno di Campogrosso Creek) located at approximately 900 m a.s.l. (Figure 1a), which, during periods of intense rainfalls, is characterized by a high river discharge contributing to the debris transport and fluidification (Bossi et al. 2015b); iv) the persistence of bank protections for a significant stretch upstream from the villages of Turcati and Maltaure; v) the presence of a narrowing section (i.e., a road bridge with a reinforced pylon in the middle of the riverbed) (Figure 1a). The exposed build-up of sediments around this bridge following the 2010 debris flow event suggested that its shape and dimension contributed to slowing down and stopping much of the coarser clast and boulder flow portions, while the remaining finer sediments flowed downstream along the creek bed for approximately two kilometres (Figure 2). Therefore, this bridge was considered a key element also for the terminal stages of the new simulations.

The parameters used in the Voellmy rheology successfully simulated the deposit thicknesses and the areal distribution of the 2010 event, matching positively the order of magnitude of those measured with the differences between pre- and post-event DTMs (Figure 4a). Particularly, the modelled flow in the sector upstream the Agno di Campogrosso confluence (Figure 4b) shows a good accordance with the maximum thickness of approximately 10 m reached by the debris flow (Figure 4a). The comparison between the debris flow thickness and DAN-3D results was weighed also in other key locations along the creek bed, especially with respect to the same cross-sections used for the velocity estimation (Figure 4). The maximum obtained thickness difference was approximately 1.5 m, as shown in cross-section 3a (Figure 4). The calculated debris flow impact area was approximately 245,000 m^2, while the area covered by the modelled deposits was 250,000 m^2. A good correlation was found between the deposited volume calculated through the difference of DTMs (DoD analysis) by Bossi et al. (2015b) and that found via DAN-3D modelling. The volume obtained by means of the DoD procedure was approximately 372,000 m^3, whereas the DAN-3D volume was approximately 371,000 m^3. A very good accordance was obtained between the modelled results and the DTM analysis; nevertheless, localized differences between the abovementioned results were generated, mainly due to the input data and particularly to the model path processing stages.

4.2 Velocity calculations

The resulting mean flow velocity estimations are shown in Table 2. Here, these values were also compared with the results of the numerical model velocity in the same cross-section (Figure 1a, Figure 5). This was possible because the DAN-3D code can calculate the maximum velocity at each point of the impact area. The velocities, calculated as the mean of maximum velocity for each cross-section using DAN-3D, were in good agreement with all the values obtained using the equations of Rickenmann (1999) and Mizuyama et al. (1992), ranging from 32.0 m/s (section 1a) to 6.6 m/s (section 4b, Table 3). By comparing the flow velocity profiles obtained through the abovementioned equations and the modelled results (Figure 6), it was possible to observe a similar trend along the overall debris flow travel distance, with an initial exponential deceleration and a decrease of mean velocity in the final section. Higher velocities were recorded in the first two sections (1a, 2a) falling within Material 1 (Table 1) of the runout model, where erosion occurs. The

major difference between the calculated and modelled velocities was evident in the upstream part of the debris flow sector, while in the middle and lower flow sectors, the obtained velocities showed similar values (sometimes almost coincident) (Table 3).

4.3 Assessment of back analysis accuracy

The goodness of the DAN-3D numerical models result has already been tested in many works (Hungr and Evans 1996; McDougall 2006). In this paper, it was investigated and verified by comparing simultaneously the numerical modelling outcomes with both field observations and derived data coming from empirical equations and maps processing. Particularly, the runout distance represents the main parameters for model calibration. Furthermore, other calibration parameters were used, such as deposits thickness and velocity along the landslide path. Figure 7a shows the comparison between the model velocity results and the calculated data. Here it is evident that the modelled velocities are in good agreement with the estimated ones. However, only on the slope just below the source area the velocity predicted by the dynamic analysis is much greater than those estimated by empirical equations because of the entrainment coefficient inserted in this part of the simulation. Moreover, in Figure 7b the comparison between the thicknesses values measured during the field investigations and those predicted by numerical simulations is exhibited. From this it emerges that the used model predicts the overall deposit thickness, as just observed in the cross-sections (Figure 1, Figure 5), with a range of accuracy of approximately 20%. Consequently, as regards the general rheological behaviour, the Voellmy kernel proved to be particularly suitable to reproduce the debris flow dynamics demonstrating a strong topographic control and providing good results in terms of velocity and distribution of deposits.

4.4 Possible event forecasting procedure

To assess the Rotolon valley exposure to possible future debris flow events, new DAN-3D simulations were carried out, combining the extension of the source area established by means of the displacement map analysis (Figure 2b) and the rheological parameters obtained by means of the 2010 event back analysis (Table 1). Usually, the estimate of a hypothetical volume potentially prone to collapse represents a difficult task, even in the case of accurate field measurements. Therefore, to overcome this problem, three credible volumes were estimated for the possible new source area extension (Figure 2b), starting from three different thickness values (average, modal and maximum) derived from a statistical analysis of the 2010 source area thicknesses. This method was applied while considering that the source debris materials of the new possible event have the same emplacement and thickness of the past event source area. The method considered the 2010 event deposits thickness frequency distribution histogram and used the statistical values to find new volumes (Figure 8). In this context, the three volume values calculated were as follows: i) modal (165,000 m^3), ii) average (304,000 m^3), and iii) maximum (894,000 m^3). The runout outcomes showed that using the modal and average values, the modelled debris flow in any case stops upstream of Turcati and Maltaure villages; the maximum deposit thicknesses were 8.0 m and 8.5 m, respectively (Figure 9a, b). On the other hand, using the maximum volume value, the resulting debris flow showed highly mobile and very rapid features and can reach the Recoaro Terme village, even overflowing the riverbanks, with dangerous implications for the inhabitants (Figure 9c). In this case, the maximum deposit thickness was approximately 9.5 m. The main difference between these simulations is the distribution of deposits and the different impact areas, which range from approximately 263,000 m^2 using the modal volume to approximately 1,000,000 m^2 using the maximum volume. Furthermore, a critical debris flow volume assessment was performed based on the possible future events capable of reaching the villages of Turcati and Maltaure. The obtained

critical volume was 373,000 m^3 (slightly more than the statistically calculated average value and less than half of the maximum value), while the average thickness of its source area was approximately 8.0 m (Figure 9d).

5 CONCLUSION

The 4th November 2010 debris flow event that detached from the Rotolon DSGSD detrital cover was modelled by means of DAN-3D numerical code, and its results were discussed. The runout simulation shows that amongst the available rheological kernels, the best rheology in the used model is the Voellmy-type. The latter was applied to each of the three materials, in which the path of the landslide was conventionally subdivided. After some attempts made by varying the rheological reference parameters, the 2010 event back analysis could reproduce with high accuracy: i) the debris flow impact area; ii) deposit thickness; iii) velocity; iv) the final flow erosion volume. To assess the Rotolon valley exposure to possible future debris flow events, based on the back analysis results, a forecasting analysis was performed. This analysis was obtained by means of DAN-3D simulations, considering a) the same input data of the back analysis; b) a new possible source area detected by means of GB-InSAR displacement data analysis; and c) different hypothesized thicknesses by means of statistical considerations based on the differences between the pre- and post-2010 debris flow event DTMs. These simulations produced impact area maps useful for evaluating the different future debris flow scenarios within the Rotolon valley. The obtained results show that the integration of the modelling technique with ancillary data (such as detailed geomorphological and topographic maps, location and characteristics of the hydraulic works along the creek bed), together with the GB-InSAR-derived displacement maps, can be a very useful tool for the scientific community and local administrations to manage the problem related to debris flow events in the examined area. This working method could represent a standard procedure in cases of areas prone to different types of debris flow in the case of GB-InSAR displacement monitoring. Nevertheless, the final reliability of the proposed method lies in the skill of expert operators regarding the choice of plausible volumes of possible future debris flow events.

ACKNOWLEDGMENTS

The GB-InSAR data were acquired in the framework of the monitoring activity carried out in the post-emergency management coordinated by the Italian Civil Protection Department. The available DTMs and aerial photos were acquired by means of aerial LiDAR surveys on behalf of the Veneto Soil Defense Regional Directorate on 21st October 2010 (pre-event) and 23rd November 2010 (post-event), respectively.

CONFLICT OF INTEREST

The authors declare that they do not have any conflict of interest.

REFERENCES

Agliardi F, Crosta GB, Zanchi A, et al. (2009) Onset and timing of deep-seated gravitational slope deformations in the eastern Alps, Italy. Geomorphology 103: 113-129. DOI:10.1016/j.geomorph.2007.09.015.

Altieri V, Colombo P, Dal Prà A (1994) Studio per la Valutazione delle condizioni di stabilità dei versanti e del fondovalle del bacino idrografico del Torrente Rotolon nell'Alta Valle dell'Agno in Comune di Recoaro Terme (Vicenza). Relazione Geologico – Geotecnica. Regione del Veneto Segreteria Regionale per il Territorio – Dipartimento Lavori Pubblici – Venezia 97. (In italian).

Antonello G, Casagli N, Farina P, et al. (2004). Ground-based SAR interferometry for monitoring mass movements. Landslides 1(1), 21-28. DOI:10.1007/s10346-003-0009-6.

Bamler R, Hartl P (1998) Synthetic aperture radar interferometry. Inverse Problems 14(4): R1.

Barbieri G, De Zanche V, Di Lallo E, et al. (1980) Carta geologica dell'area di Recoaro. Memorie Scietà Geologica XXXIV Padova. pp. 23-52. (In Italian).
Brayshaw D, Hassan MA (2009) Debris flow initiation and sediment recharge in gullies. Geomorphology 109(3): 122-131. DOI:10.1016/j.geomorph.2009.02.021.
Bardi F, Frodella W, Ciampalini A, et al. (2014) Integration between ground based and satellite SAR data in landslide mapping: The San Fratello case study. Geomorphology 223: 45-60.
Bossi G, Crema S, Frigerio S, et al. (2015a) The Rotolon catchment early-warning system. In Lollino G et al. (eds.), Engineering Geology for Society and Territory. Springer International Publishing 3: 91-95.
Bossi G, Cavalli M, Crema S, et al. (2015b) Multi-temporal LiDAR-DTMs as a tool for modelling a complex landslide: a case study in the Rotolon catchment (eastern Italian Alps). Natural Hazards and Earth System Science 15(4): 715-722. DOI:10.5194/nhess-15-715-2015.
Coe JA, Cannon SH, Sant PM (2008) Introduction to the special issue on debris flows initiated by runoff, erosion, and sediment entrainment in western North America. Geomorphology 96(3): 247-249. DOI:10.1016/j.geomorph.2007.05.001.
Corominas J (1996) The angle of reach as a mobility index for small and large landslides. Canadian Geotechnical Journal 33(2): 260-271.
Coussot P, Meunier M (1996) Recognition, classification and mechanical description of debris flows. Earth-Science Reviews 40(3): 209-227. DOI:10.1016/0012-8252(95)00065-8.
Chow VT (1959) Open-Channel Hydraulics. McGraw-Hill, New York. pp 465.
Evans SG, Clague JJ (1992) Glacier-related hazards and climatic change. In proceeding of the world at risk: Natural hazards and climate change, AIP Conference, Boston, Massachusetts (USA), 4-16 Jan 1992. pp 48-60.
McColl ST, Davies TRH, McSaveney MJ (2010) Glacier retreat and rock-slope stability: debunking debuttressing. Geologically active: delegate papers 11th Congress of the International Association for Engineering Geology and the Environment, Auckland, Aotearoa, New Zealand, 5-10 September 2010. pp 467-474.
Fidolini F, Pazzi V, Frodella W, et al. (2015) Geomorphological characterization, monitoring and modeling of the Monte Rotolon complex landslide (Recoaro Terme, Italy). In Lollino G (eds.), Engineering Geology for Society and Territory. Springer International Publishing. pp 1311-1315.
Frigerio S, Schenato L, Bossi G, et al. (2014) A web-based platform for automatic and continuous landslide monitoring: The Rotolon (Eastern Italian Alps) case study. Computers & Geosciences 63: 96-105.
Frodella W, Morelli S, Fidolini F, et al. (2014) Geomorphology of the Rotolon landslide (Veneto Region, Italy). Journal of Maps 10(3): 394-401. DOI:10.1080/17445647.2013.869666.
Frodella W, Fidolini F, Morelli S, et al. (2015) Application of infrared thermography for landslide mapping: The rotolon DSGDS case study. Rendiconti Online Società Geologica Italiana 35: 144-147.
Frodella W, Ciampalini A, Gigli G, et al. (2016) Synergic use of satellite and ground based remote sensing methods for monitoring the San Leo rock cliff (Northern Italy). Geomorphology 264: 80-94. DOI: 10.1016/j.geomorph.2016.04.008.
Hsü KJ (1975) Catastrophic debris streams (sturzstroms) generated by rockfalls. Geological Society of America Bulletin 86(1): 129-140.
Hungr O, Morgan GC, Kellerhals R (1984) Quantitative analysis of debris torrent hazard for design of remedial measures. Canadian Geotechnical Journal 21(4): 663-677. DOI: 10.1139/t84-073.
Hungr O (1995) A model for the runout analysis of rapid flow slides, debris flows, and avalanches. Canadian Geotechnical Journal 32(4): 610-623. DOI: 10.1139/t95-063.
Hungr O, Evans SG (1996) Rock avalanche runout prediction using a dynamic model. In Proceedings of the 7th International Symposium on Landslides Trondheim Norway: 17-21 June 1996. In Senneset K, Balkema AA (eds.), Rotterdam, The Netherlands. pp 233-238.
Hungr O, McDougall S (2009) Two numerical models for landslide dynamic analysis. Computers & Geosciences 35(5): 978-992. DOI:10.1016/j.cageo.2007.12.003
Iverson RM (1997) The physics of debris flows. Reviews of geophysics 35(3): 245-296. DOI:10.1029/97RG00426.
Jakob M (2005) A size classification for debris flows. Engineering geology 79(3): 151-161. DOI:10.1016/j.enggeo.2005.01.006.
McDougall S, Hungr O (2004) A model for the analysis of rapid landslide motion across three - dimensional terrain. Canadian Geotechnical Journal 41(6): 1084-1097. DOI: 10.1139/T04-052.
McDougall S (2006). A new continuum dynamic model for the analysis of extremely rapid landslide motion across complex 3D terrain. PhD thesis, University of British Columbia, Vancouver, British Columbia.
Mizuyama T, Kobashi S, Ou G (1992) Prediction of debris flow peak discharge. In Proceedings of the International Symposium Interpraevent, Bern, Switzerland. pp 99-108.
Morelli S, Salvatici T, Nolesini T, et al. (2016) Analogue and numerical modeling of the Stromboli hot avalanches. *In* Landslides and Engineered Slopes. Experience, Theory and Practice. Proceedings of the 12th International Symposium on Landslides: 12-19 June 2016, Napoli, Italy. Edited by S. Aversa, L. Cascini, L. Picarelli, C. Scavia, pp. 1493–1500. CRC Press, Napoli, Italy. DOI: 10.1201/b21520-184

Morelli S, Monroy VHG, Gigli G, et al. (2010) The Tancitaro debris avalanche: characterization, propagation and modeling. Journal of Volcanology and Geothermal Research, 193(1): 93-105.

Nocentini M, Tofani V, Gigli G, et al. (2015) Modeling debris flows in volcanic terrains for hazard mapping: the case study of Ischia Island (Italy). Landslides 12(5): 831-846. DOI:10.1007/s10346-014-0524-7.

Nolesini T, Di Traglia F, Del Ventisette C, et al. (2013) Deformations and slope instability on Stromboli volcano: Integration of GBInSAR data and analog modeling. Geomorphology 180-181: 242-254. DOI:10.1016/j.geomorph.2012.10.014

Pazzi V, Morelli S, Pratesi, et al. (2016). Assessing the safety of schools affected by geo-hydrologic hazards: The geohazard safety classification (GSC). International Journal of Disaster Risk Reduction, 15: 80-93. http://dx.doi.org/10.1016/j.ijdrr.2015.11.006

Pierson TC, Scott KM (1985) Downstream dilution of a lahar: transition from debris flow to hyperconcentrated streamflow. Water resources research 21(10): 1511-1524.

Prochaska A, Santi P, Higgins J, et al. (2008) A study of methods to estimate debris flow velocity, Landslides 5(4): 431–444. DOI:10.1007/s10346-008-0137-0.

Revellino P, Hungr O, Guadagno FM, et al. (2004) Velocity and runout prediction of destructive debris flows and debris avalanches in pyroclastic deposits, Campania Region, Italy. Environmental Geology 45(3): 295-311. DOI:10.1007/s00254-003-0885-z.

Rickenmann D (1999) Empirical relationships for debris flows. Natural Hazards 19(1): 47-77.

Rudolf H, Leva D, Tarchi D, et al. (1999) A mobile and versatile SAR system. In Proceeding of the Geoscience and Remote Sensing Symposium, 1999. IGARSS'99. IEEE 1999 International. pp 592-594.

Salvatici T, Di Roberto A, Di Traglia F, et al. (2016a) From hot rocks to glowing avalanches: Numerical modelling of gravity-induced pyroclastic density currents and hazard maps at the Stromboli volcano (Italy). Geomorphology 273: 93-106. DOI:10.1016/j.geomorph.2016.08.011.

Salvatici T, Morelli S, Di Traglia F (2016b) Runout modelling of gravity-induced pyroclastic density currents at Stromboli volcano (Italy). Rendiconti Online Soietà Geologica Italiana 41: 195-198. DOI: 10.3301/ROL.2016.127.

Savage SB, Hutter K (1989) The motion of a finite mass of granular material down a rough incline. Journal of fluid mechanics 199: 177-215. DOI: https://doi.org/10.1017/S0022112089000340.

Schneuwly-Bollschweiler M, Stoffel M, Rudolf-Miklau F (2012) Dating torrential processes on fans and cones: methods and their application for hazard and risk assessment. Springer Science & Business Media, Berlin, Heidelberg, New York, Vol. 47.

Schraml K, Thomschitz B, McArdell BW, et al. (2015) Modeling debris-flow runout patterns on two alpine fans with different dynamic simulation models. Natural Hazards and Earth System Sciences Discussions 3(2): 1397-1425. DOI:10.5194/nhess-15-1483-2015.

Tarchi D, Casagli N, Fanti R, et al. (2003) Landslide monitoring by using ground-based SAR interferometry: an example of application to the Tessina landslide in Italy. Engineering Geology 68(1): 15-30. DOI:10.1016/S0013-7952(02)00196-5.

Trivelli G (1991) Storia del territorio e delle genti di Recoaro. Comune di Recoaro Terme. Istituto Geografico De Agostini. (In Italian)

Voellmy A (1955) Uber die Zerstorunskraft von Lawinen (On breaking force of avalanches). Schweizerische Bauzeitung 73: 212–285 [in German].

Yifru AL (2014) Assessment of Rheological Models for Run-out Distance Modeling of Sensitive Clay Slides, Focusing on Voellmy Rheology. M.Sc. thesis, Norwegian University of Science and Technology.

Zanchetta G, Sulpizio R, Pareschi MT, et al. (2004) Characteristics of May 5^6, 1998 volcaniclastic debris flows in the Sarno area (Campania, southern Italy): relationships to structural damage and hazard zonation. Journal of volcanology and geothermal research 133(1): 377-393. DOI:10.1016/S0377-0273(03)00409-8.

Zischinsky U (1969) Uber sackungen. Rock Mechanics 1(1): 30-52.

Tables and caption list

Table 1 Parameters of each material with Voellmy rheology: friction (*f*) and turbulence (ξ).

	Range of altitude (m a.s.l.)	*f*	ξ (m/s^2)
Material 1	1420 - 920	0.18	500
Material 2	920 - 780	0.12	1000
Material 3	780 - 560	0.01	1000

Table 2 The parameters calculated at each mean velocity along cross-sections: S (°) is the slope, w (m) is the flow width, h (m) is the flow super-elevation, Qp_1 (m^3/s) and Qp_2 (m^3/s) are the Rickenmann (1999) and Mizuyama et al. (1992) velocity, respectively, and R (m) is the curvature radius.

	S (°) (slope)	w (m) (flow width)	h (m) (super-elevation of the flow)	Qp_1 (m^3/s) (Rickenmann 1999)	Qp_2 (m^3/s) (Mizuyama et al. 1992)	R (m) (radius of curvature)
Section 1a	14			4400	3000	
Section 2a	9			4400	3000	
Section 1b	9	35	2.7			236
Section 3a	7			4400	3000	
Section 4a	6			4400	3000	
Section 2b	9	10	0.6			125
Section 5a	4			4400	3000	
Section 3b	6	10	1			142
Section 4b	7	9	3.2			40

Table 3 Mean flow velocity measured with respect to selected cross-sections (for their map locations, refer to Figure 1a).

	v (m/s) (Chow, 1959)	v (m/s) (Rickenmann 1999)	v (m/s) (Mizuyama et al. 1992)	v (m/s) (DAN-3D, maximum velocity)
Section 1a		21.2	18.7	32.1
Section 2a		18.4	16.3	22.5
Section 1b	14.1			17.3
Section 3a		17.1	15	16.6
Section 4a		15.6	13.8	14.2
Section 2b	11.8			13.5
Section 5a		13.6	12	8.4
Section 3b	11.5			8.2
Section 4b	5.6			6.6

Figures and caption list

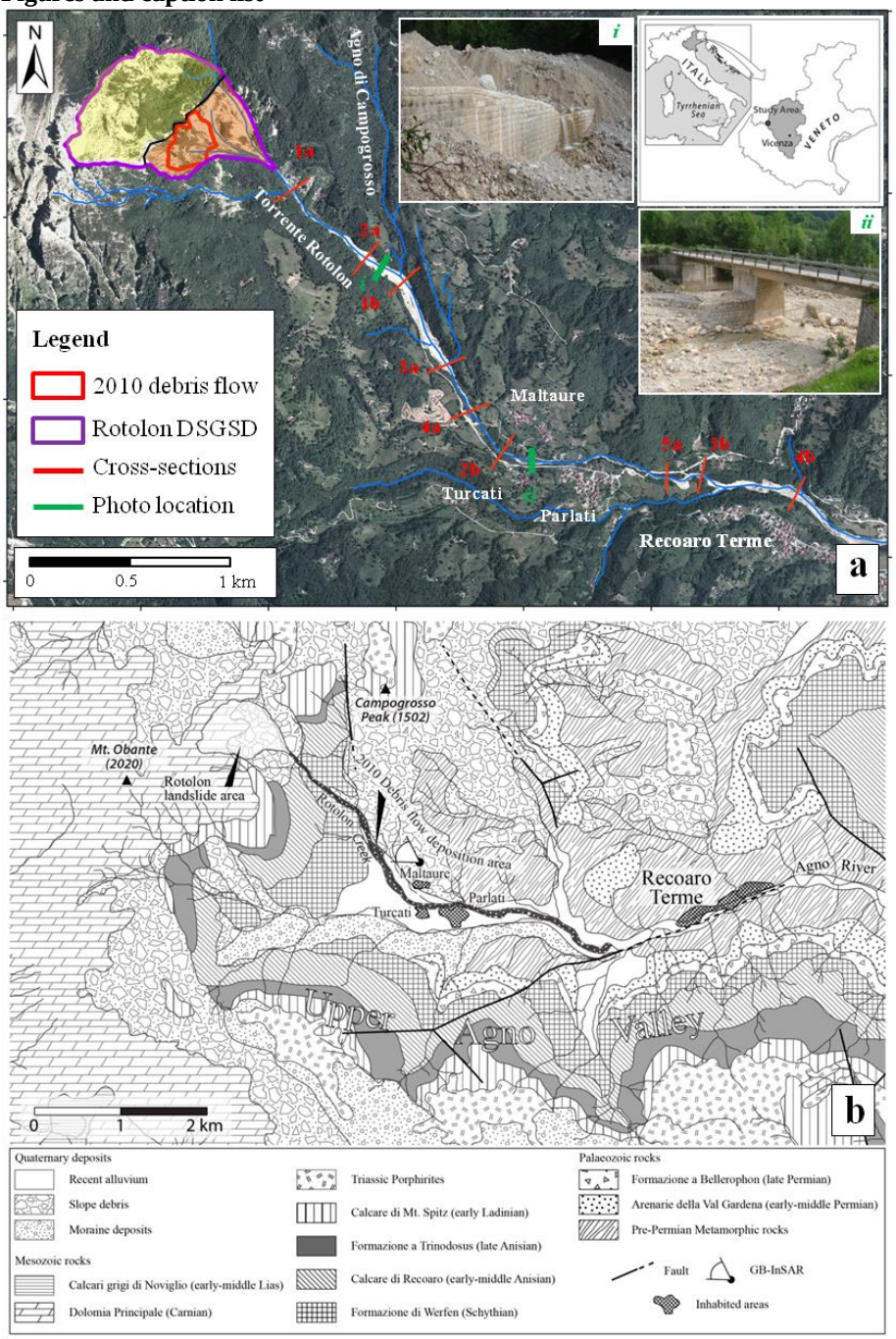

Figure 1 Overview of the study area: a) the Rotolon DSGSD landslide (violet line), with the local hydrographic network (blue lines) and all the main villages in the valley. The 4th November 2010 debris flow source area is highlighted in red. Yellow indicates the Detachment sector, orange indicates the Dismantling sector (according to

Fidolini et al. 2015), and the black line divides the two sectors. Numbered red lines are the analysed cross-sections. i) and ii) are two examples of the infrastructures located along the creek. b) Geological map with radar position (modified from Fidolini et al. 2015).

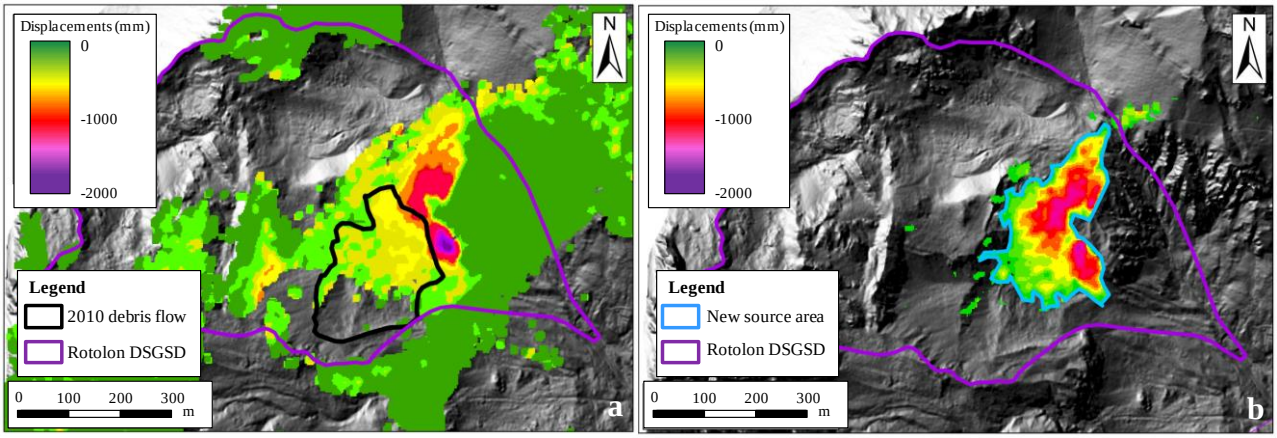

Figure 2 Cumulative displacement map recorded by GB-InSAR a) between December 2010 and March 2013 within the black outlined 2010 debris flow event source area; b) the MATLAB code elaboration and the new possible source area (shown in blue).

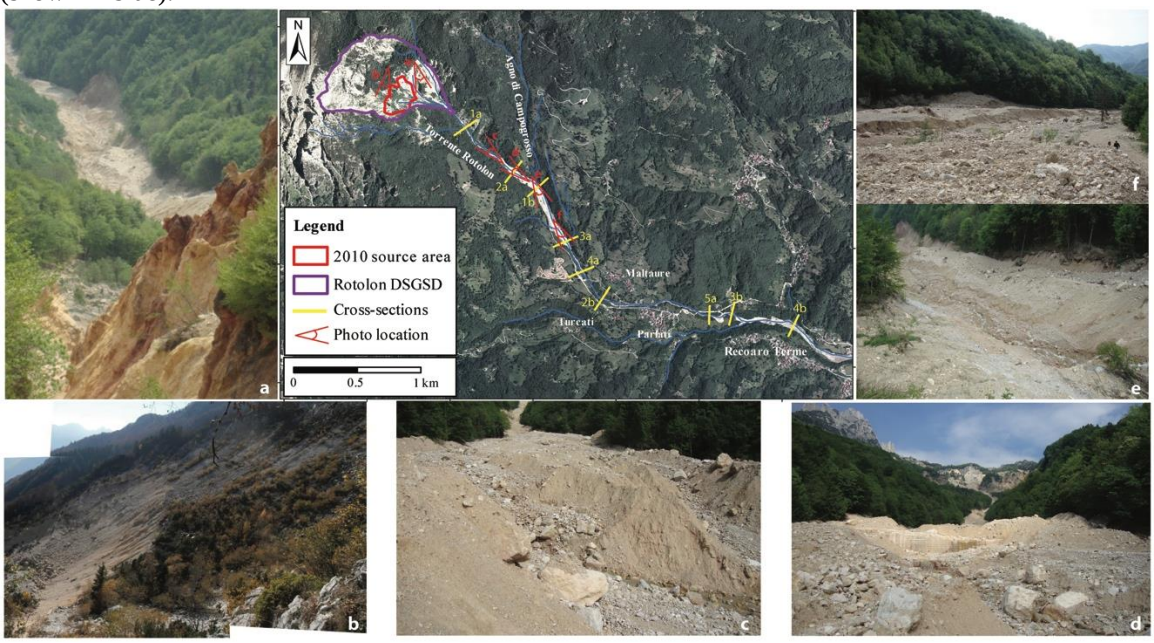

Figure 3 Location of photos acquired during field surveys following the 2010 landslide event: a) proximal deposit below the source area, b) residual source area, c, d, e, f) 2010 debris flow deposits in the valley upstream the urbanized area.

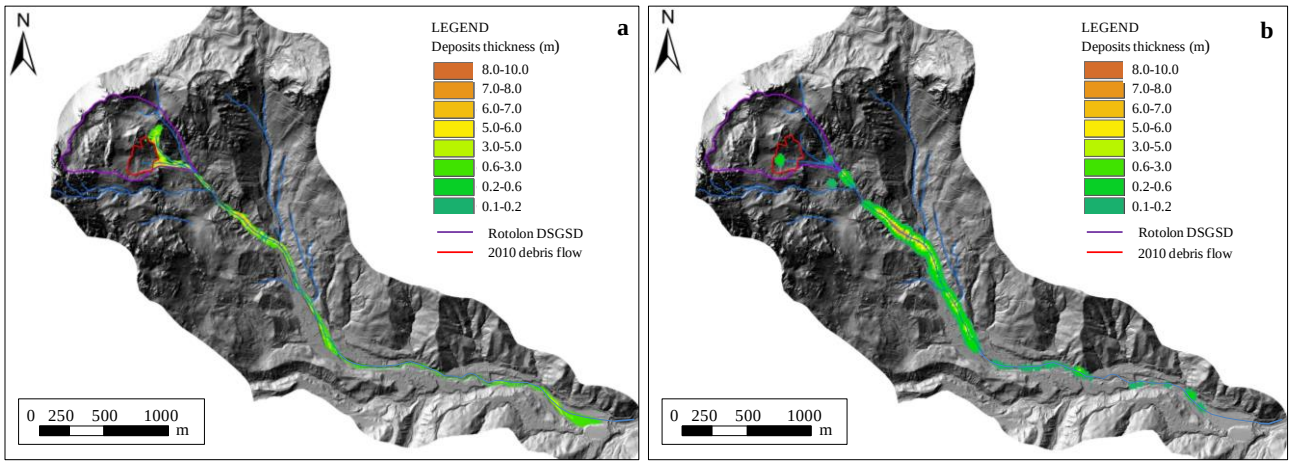

Figure 4 Comparison between a) the deposit thicknesses resulting from the deference of two DTMs (pre- and post-event), b) the deposit thicknesses resulting from the back analysis using DAN-3D. The violet line is the Rotolon landslide DSGSD and the red one is the source area of the 2010 debris flow.

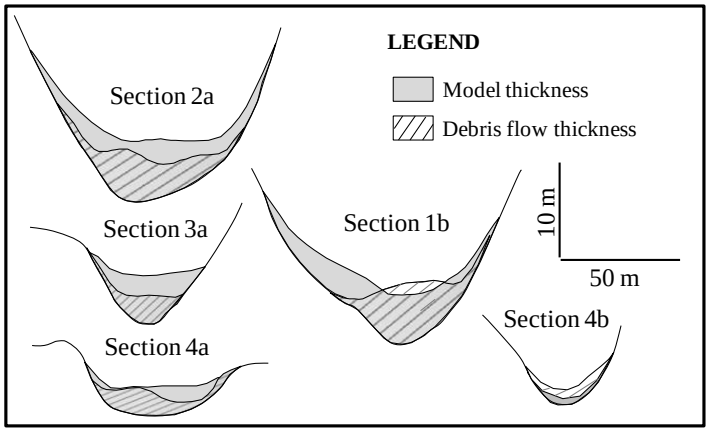

Figure 5 Comparison between deposit thicknesses along some cross-sections: striped grey area denotes the real debris flow thickness; grey area denotes the modelled thickness (for their map localization, refer to Figure 1a).

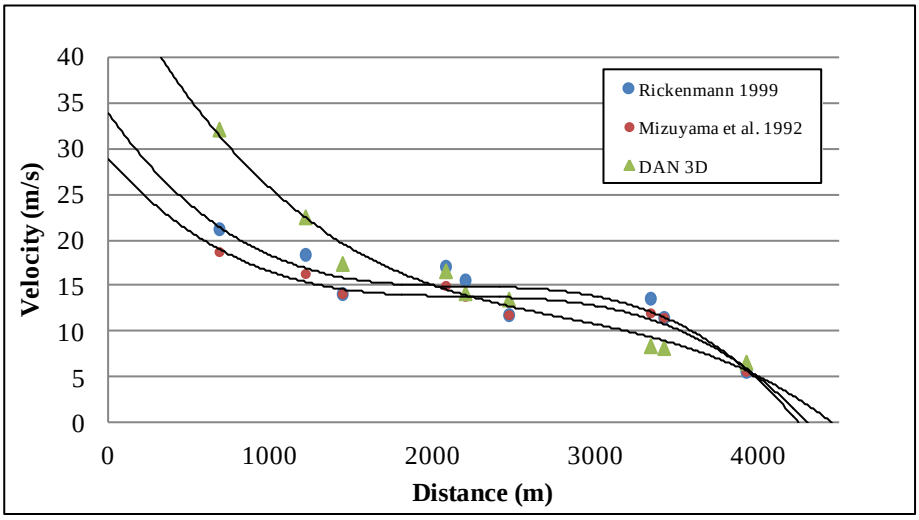

Figure 6 Velocity profiles calculated by using Rickenmann (1999) equations (blue line), Mizuyama et al. (1992) equation (red line) and DAN-3D simulation (green line).

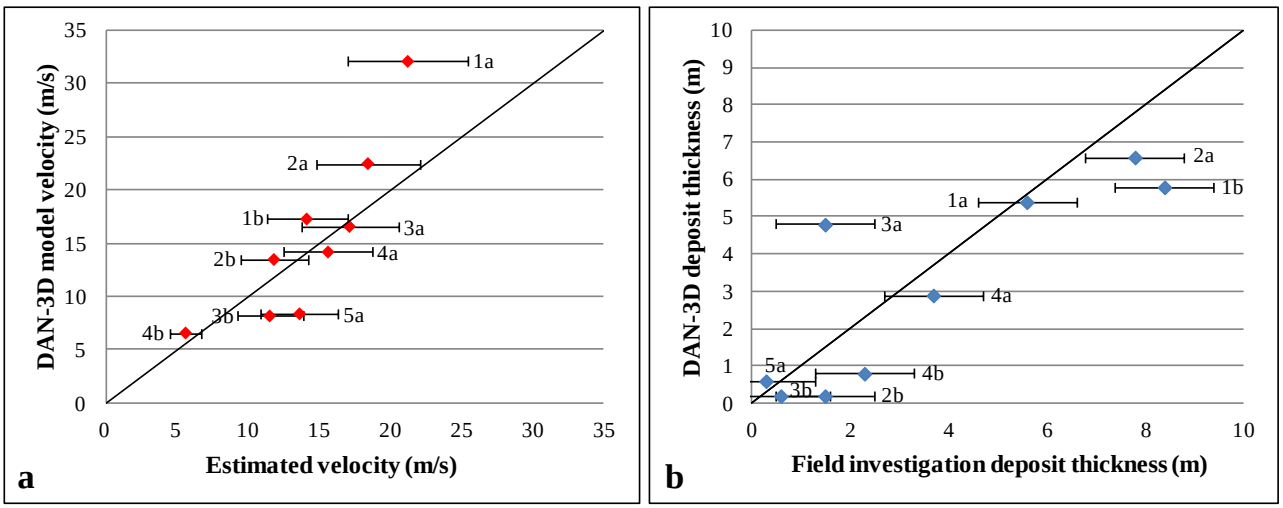

Figure 7 Comparison of modelled and estimated velocities and deposit thicknesses at each cross-section: a) comparison between DAN-3D and empirical equation velocity, b) between DAN-3D and field-estimated deposit thickness. The continuous black line indicates the theoretically perfect correlation.

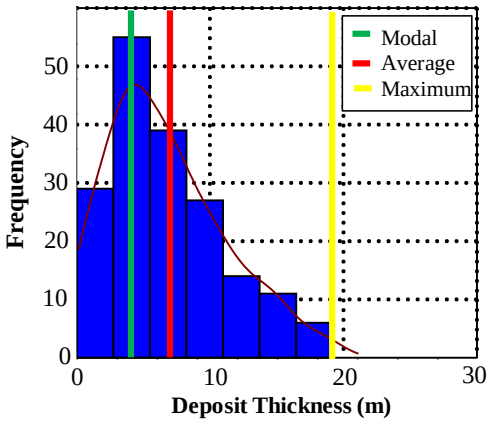

Figure 8 Statistical analysis of the deposit thicknesses of the 2010 event**.**

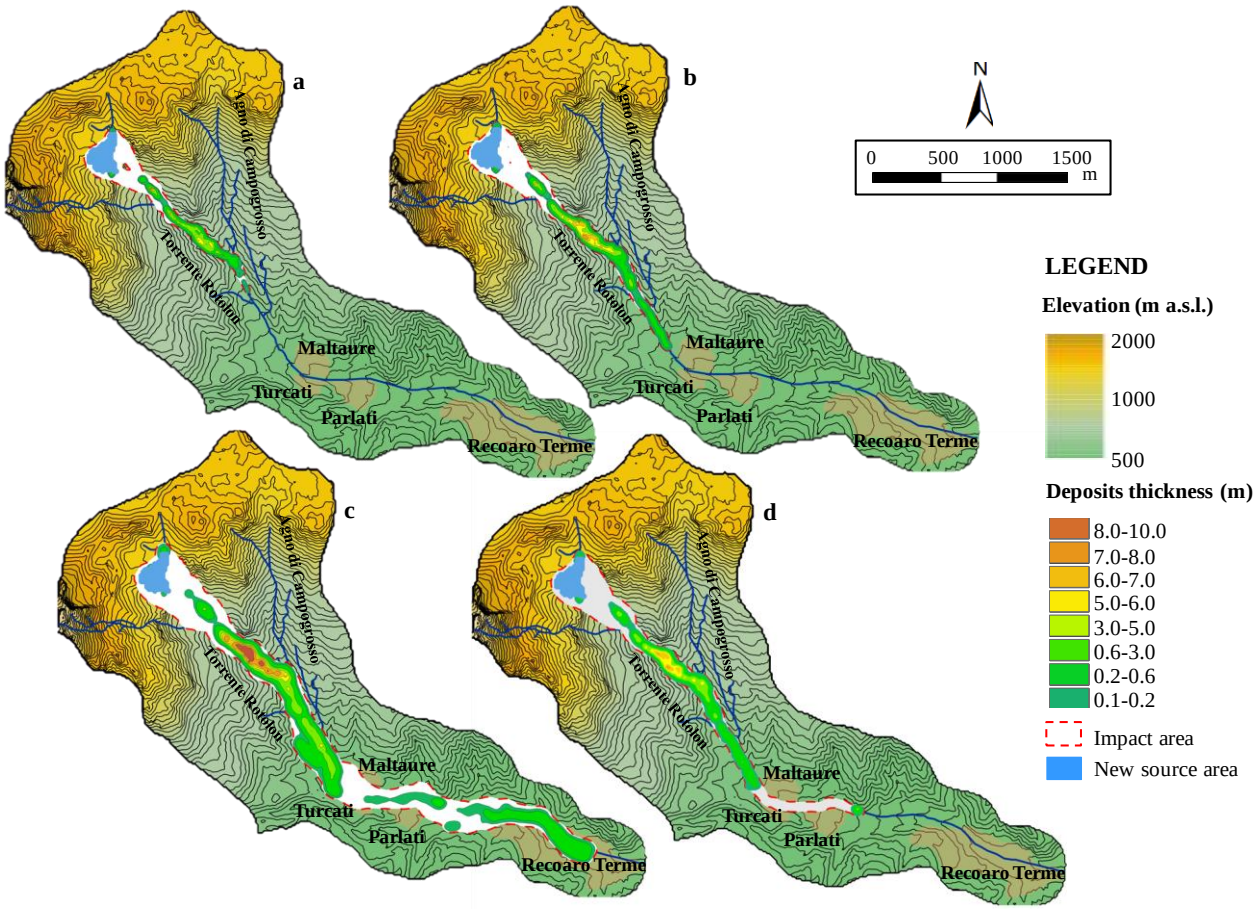

Figure 9 Forecast analysis of future possible events with different values of collapsing volumes: a) modal (165,000 m^3), b) average (304,000 m^3), c) maximum (894,000 m^3) and d) critical (373,000 m^3). The considered source area is the area shown in Figure 2, represented in blue. The red dashed area includes the impact area of the modelled debris flows: it contains variable deposit thicknesses (chromatic scale) and not covered areas (white sectors).